FLORIDA INTERNATIONAL UNIVERSITY

Miami, Florida

UNDERSTANDING EXOSOMAL EXTRACELLULAR VESICLES AND MORPHINE IN THE NEUROPATHOLOGY OF HUMAN IMMUNODEFICIENCY VIRUS AND DIFFERENTIAL ZIKA VIRUS STRAIN-ASSOCIATED PATHOLOGY

A dissertation submitted in partial fulfillment of

the requirements for the degree of

DOCTOR OF PHILOSOPHY

in

BIOMEDICAL SCIENCE

by

Allen Caobi

2022

To: Dean Juan C. Cendan
Herbert Wertheim College of Medicine

This dissertation, written by Allen Caobi, and entitled Understanding Exosomal Extracellular Vesicles and Morphine in the Neuropathology of Human Immunodeficiency Virus and Differential Zika Virus Strain-Associated Pathology, having been approved in respect to style and intellectual content, is referred to you for judgment.

We have read this dissertation and recommend that it be approved.

_____
Manuel Barbieri

_____
Nazira El-Hage

_____
Fatah Kashanchi

_____
Ajeet Kaushik

_____
Andrea D. Raymond, Major Professor

Date of Defense: April 1, 2022

The dissertation of Allen Caobi is approved.

_____
Dean Juan C. Cendan
Herbert Wertheim College of Medicine

_____
Andrés G. Gil
Vice President for Research and Economic Development
and Dean of the University Graduate School

Florida International University, 2022

ACKNOWLEDGMENTS

I would like to take this opportunity to thank the Department Chair, Dr. Nair, the Graduate Program Director, Dr. Agoulnik, and Dr. Barbieri whom without I would not have been granted the opportunity to learn, improve, and cultivate a better future for myself under this program. Dr. Raymond has been an endless source of both knowledge and patience and I am eternally grateful for her guidance, trust, and support throughout these years. The dissertation committee (Dr. Agudelo, Dr. Barbieri, Dr. El-Hage, Dr. Kashanchi, Dr. Kaushik, and Dr. Raymond) has been supportive and constructive in their suggestions and feedback throughout the years, providing critical commentary on experiment design and scope of the dissertation aims. I would also like to thank, Mickensonne Andre, Dr. Arti Vashit, Adriana Yndart, and Odalys De La Rosa for all of their assistance and input over the years. Furthermore, the entire Department of Immunology and Nanomedicine have been incredibly helpful and accommodating, and I am very grateful for all of the times I have had the opportunity to use any of their equipment, knowledge, or personnel. I would like to thank my family, for both their emotional and financial support, without I would not have been able to afford living in this city. Lastly, I am appreciative of having been awarded the Dissertation Year Fellowship in the summer of 2021, as it has permitted me to focus on finishing my dissertation without having to lose a substantial amount of time with a teaching assistantship on the final year.

ABSTRACT OF THE DISSERTATION

UNDERSTANDING EXOSOMAL EXTRACELLULAR VESICLES AND MORPHINE IN THE NEUROPATHOLOGY OF HUMAN IMMUNODEFICIENCY VIRUS AND DIFFERENTIAL ZIKA VIRUS STRAIN-ASSOCIATED PATHOLOGY

by

Allen Caobi

Florida International University, 2022

Miami, Florida

Professor Andrea D. Raymond, Major Professor

Exosomal Extracellular Vesicles (xEVs), integral to intercellular communication and regulation of immune responses, have functional effects based on their contents, which they transport to neighboring cells. However, in the context of infection, EV cargo can be modulated, by either infected or uninfected cells. We hypothesize that CNS-associated neuropathology, is partially, due to the cargo transported by the exosomes. We theorize that the cargo released from infected cell-derived xEVs may either facilitate or inhibit viral neuropathogenicity. Here we investigated xEVs in the case of two neurotropic viruses, Zika virus (ZIKV) and Human Immunodeficiency Virus (HIV). The hallmark characteristic of ZIKV-infection is fetal microcephaly, with unclear mechanisms. Findings from this study demonstrate that ZIKV pathogenic strain, FLR, induces differential gene expression and miRNA expression, relative to the non- 5 pathogenic Ugandan ZIKV strain, MR766, modulating inflammation and immune function. To understand the mechanisms of microcephaly we looked at exosomes that have crossed or

are released from infected placental cells. ZIKV-FLR infection of Human Villous Trophoblasts (HVTs), a placental cell, was infected using a Transwell placental barrier (PB) model to mimic exosome transfer across the PB, in addition to evaluating PB integrity and permeability. HVTs resulted in the release of EVs containing an enhanced concentration of hsa-mir-612, hsa-mir-873-5p, and hsa-mir-1305. hsa-mir-612 targets genes which disrupt signaling cascades and promote apoptosis. The ZIKV-Envelope protein (EP) was found to promote apoptosis. Overall findings suggest that NGF-differentiated neurons were more susceptible to ZIKV infection. 25-30% of people living with HIV (PLWH) develop neurocognitive impairment (NCI) despite successful viral suppression by Anti-Retroviral Therapy (ART). Opiate abuse is known to exacerbate HIV transmission and neuropathology. NCI disrupts the quality of life of PLWHs by disrupting executive functions, motor skills, and memory. The battery of psychological examinations to ascertain NCI status is often a cumbersome and arduous task. Neuroinflammation is implicated in NCI and given the role of xEVs in regulating inflammatory responses; we postulate that xEVs may contribute to NCI pathology, with EV-derived miRNA profiles functioning as a barcode identifying NCI status. The data shows that there is some differential expression of protein, dependent on NCI status (ANI/MCMD).

TABLE OF CONTENTS

CHAPTER	PAGE
CHAPTER 1	1
Exosomes	2
Isolation of EVs	7
Differential Centrifugation – the Gold Standard	7
Immunoaffinity	7
Density Gradient - OptiPrep™	8
Chromatography	9
Precipitation	9
Ultrafiltration	10
Nanoplasmon-Enhanced Scattering (nPES)	10
Lab-on-chip Exosome Isolation	11
EV content and characterization in health and disease	11
Exosomal Content and Characterization	12
Role of EVs in the Pathogenesis of Viral Infections	13
Picornaviridae and Togaviridae	13
Herpesviridae	14
Filoviridae	15
Paramyxoviridae	16
Orthomyxoviridae	17
Hepadnaviridae	18
Flaviviridae	20
ZIKA	21
EV-Mediated Restriction of ZIKV Pathogenesis	22
EV-Mediated Enhancement of ZIKV Neuropathology	24
Coronaviridae	26
Retroviridae	28
Human Immunodeficiency Virus type 1 (HIV-1)	28
HIV Phylogeny	33

HIV in the ART Era 35
HIV Epidemiology 39
Opiate Epidemics in the USA 42
HIV and Opiates 44
CNS infiltration by HIV-1 and immune cells through the blood brain barrier 49
Astrocytes 50
Brain Microvascular Endothelial Cells 51
Pericytes 52
Leukocyte Intrusion into the CNS 52
EV Interaction with Host Cell Restriction Factors and HIV 56
Immune Cell-Derived EVs and Antiviral Effects 57
EV-Mediated Enhancement of HIV-1 Infection 58
EVs as Nano-Therapeutics 62

CHAPTER 2 64
Abstract 65
Introduction 65
Material and Methods 68
Caspase-3 Assay 69
XTT Assay 69
Transwell Placental Barrier (PB) Model 69
Generation of exosomes 70
Characterization of EV size distribution and stability 70
Transmission Electron Microscopy (TEM) imaging 70
RNA Extraction and ddPCR 71
Gene Content and miRNA Analysis 71
Analysis of PB permeability and integrity 72
Results 72
ZIKV Envelope protein modulation of neuronal viability 72
ZIKV-Envelope disrupts integrity of in vitro PB model 73
Differential Permissivity to ZIKV infection 75
ZIKV pathogenic strain, FLR induces differential gene expression 77

Discussion 84
Acknowledgements 89

CHAPTER 3 90
Materials and Methods 91
Cell Maintenance 91
HIV Infeti on 91
Morphine Treatment 92
Exosome isolation 92
Characterization of Extracellular Vesicles (EVs) 92
Nanostring 93
Statistical and Bioinformatic Analysis 93
Results 93
Conclusion 102

CHAPTER 4 106
Abstract 107
Introduction 108
Materials and Methods 110
Study Design 110
Study Popula1 on 110
Nef Enzyme Linked Immunosorbant Assay (ELISA) 110
Extracellular Vesicles (EV)/Exosome Isolation 111
Liquid Chromatography-Tandem Mass Spectrometry(LC-MS/MS) 111
Results 112
Cohort Demographics 112
Discussion 121

CHAPTER 5 124
Abstract 125
Introduction 126
Magnetic Nanoparticles (MNPs) 128
Materials and Methods 129
Cell lines 129
HIV Nef-GFP+ reporter virus 130
Exosome isolation 130
MNP Synthesis 131
MNP Characterization 131
M-NEXT Synthesis 133
Characterization of Extracellular Vesicles (EVs) 134
Western Blot 134
Transmission Electron Microscopy (TEM) 135
Blood-Brain-Barrier (BBB) transwell model 136
Cell viability and apoptosis 136
BBB permeability and Transendothelial electrical resistance (TEER) 137
Statistical Analysis 137
Results 138
Characterization of M-NEXT 138
MNP Characterization 139
Effects of M-NEX preparations on neuronal cell viability and BBB integrity 142
M-NEXT effect on BBB 144
M-NEXT protects against gp120/HIV neurotoxicity 145
Conclusions and Discussion 147

REFERENCES 150

VITA 192

LIST OF TABLES

TABLE PAGE

Table 1: ZIKV pathogenic strain, FLR induces differential expression of genes involved in key growth, immune function, viral, apoptosis, cell-cell signaling, and neuronal function, in HVTs..... 82

Table 2: ZIKV pathogenic strain, FLR induces exosomal transport of miRNAs targeting genes involved in key growth, immune function, viral, apoptosis, cell-cell signaling, and neuronal function, in HVT cell-derived EVs. 85

Table 3: HIV differentially modulates miRNA expression of PBMC-derived EVs in the context of opiate exposure 99

Table 4: Summary of Gene Sets: HIV vs NC. 102

Table 5: Summary of Gene Sets: MORPHINE (0.2uM) vs NC. 103

Table 6: Summary of Gene Sets: HIV+ MORPHINE (0.2uM) vs NC. 104

Table 7. Patient demographics for a cohort of 40 patients. 113

Table 8. List of proteins differentially expressed in or on EVs derived from patient serum. 118

LIST OF FIGURES

FIGURE PAGE

Figure 1: Size ranges of EVs and characterization. 2

Figure 2: Comparison of viral and EV biogenesis factors. 5

Figure 3: EV-mediated anti-ZIKV effects 24

Figure 4: A schematic of the HIV-1 virion. 29

Figure 5: A cross-sectional model of the BBB depicting HIV intrusion into the CNS and related. 50

Figure 6: HIV-1 infected cell-derived EV-mediated anti-viral and pro-viral effects. 60

Figure 7: ZIKV E-protein negatively impacts differentiated neurons. 74

Figure 8: ZIKV-Envelope disrupts integrity of *in vitro* PB model. 76

Figure 9: Cells permissive to ZIKV produce higher levels of pathogenic FLR strain. 77

Figure 10: ZIKV pathogenic strain, FLR induces differential gene expression, favoring neuroinflammation, relative to uninfected HVTs. 79

Figure 11: ZIKV pathogenic strain, FLR induces gene expression that favors neuroinflammation relative to MR766.....81

Figure 12: ZIKV pathogenic strain, FLR induces differential gene expression, in HVTs, of genes involved in: key biological processes, cellular components, and molecular functions. 83

Figure 13: FLR induces gene expression that modulates various pathways critical to the immune system, apoptosis, and the anti-viral state, in HVT cells. 83

Figure 14: ZIKV pathogenic strain, FLR induced differential expression of miRNAs in HVT-derived EVs, relative to Untreated HVT-derived EVs.....86

Figure 15: Exosome size was not modulated by viral infection or opiate abuse. 94

Figure 16: HIV-MN and morphine display a trend suggesting potential synergistic effects promoting an increase in HIV-MN replication.....95

Figure 17: HIV-1 and morphine induced differential miRNA expression in PBMC-derived exosomes, relative to the negative control. 96

Figure 18: miRNAs from HIV and/or Morphine treated PBMC-derived EVs are significantly differentially expressed across treatment groups. 97

Figure 19: Differentially altered expression of miRNAs which target key genes involved in viral replication, apoptosis, and neuronal cells. 100

Figure 20: Bioinformatics: GOSlim summary of up-regulated miRNAs. 101

Figure 21: Bioinformatics: GOSlim summary of down-regulated miRNAs. 101

Figure 22: Exosome Characterization. 114

Figure 23. Exosomal EVs containing Nef are elevated in CSF of PLWHAs with neurocognitive impairment. 115

Figure 24. EVs containing Nef may be used to identify HIV-induced NCI. 116

Figure 25: Biomarker of NCI in xEV composition of PLWHAs. 117

Figure 26: HIV induces differential gene expression, varying by NCI status, of EV-derived genes involved in: key biological processes, cellular components, and molecular functions. 120

Figure 27: HIV induces differential gene expression, varying by NCI status, modulating various pathways critical to the immune system, the CNS, and gas-exchange-associated pathways. 121

Figure 28: M-NEXT characterization. 138

Figure 29:Characterization of MNPs via x-ray diffraction (XRD). 140

Figure 30: Iron (Fe) concentration in diluted MNP and M-NEX samples, as measured by x-ray diffraction (XRD) 141

Figure 31: Raman spectrum of citrate-coated Fe_3O_4 MNPs 141

Figure 32: MNP effect on neuronal cell viability 143

Figure 33: M-NEX does not impair BBB 143

Figure 34: M-NEXT Successfully Delivered Across the BBB 145

Figure 35: M-NEXT effect on neuronal cell viability 146

Figure 36: GP120 induces apoptosis in neuronal cell 147

ABBREVIATIONS AND ACRONYMS

HIV	Human Immunodeficiency Virus
AIDS	Acquired Immunodeficiency Syndrome
ZIKV	Zika Virus
HVT	Human Villous Trophoblast
PBMCs	Peripheral Blood Mononuclear Cells
ART	Anti-Retroviral Therapy
PLWHA	People Living with HIV or AIDS
BBB	Blood-Brain Barrier
xEVs	Exosomal Extracellular Vesicles
NCI	Neurocognitive Impairment
HAND	HIV-associated neurocognitive disorders
TDF	Tenofovir disoproxil fumarate
EMT	Emtricitabine

CHAPTER 1

Exosomes and Viral Pathology: An Introduction

Exosomes

EVs formation occurs in most nucleated cells and are evolutionarily conserved [1, 2]. EVs have been detected in bodily fluids, including: saliva, CSF, blood, and urine. EVs were first defined as waste vesicles but have since been described as being integral to intercellular communication and signal transduction [2, 3]. EVs are classified as one of the following: apoptotic bodies, microvesicles, or exosomes (Figure 1). Cells undergoing apoptosis release apoptotic bodies 1–5 µm in diameter and are also capable of releasing smaller EVs such as apoptotic microvesicles (<1 µm) [2, 4]. However, it remains unclear if the formation of apoptotic microvesicles occurs under the same mechanisms responsible for microvesicle generation in healthy cells [2, 4]. Unlike apoptotic bodies, microvesicles and exosomes are derived from healthy cells, have been extensively characterized, and have been shown to be critical in the regulation of the immune response and intercellular communication [2, 4].

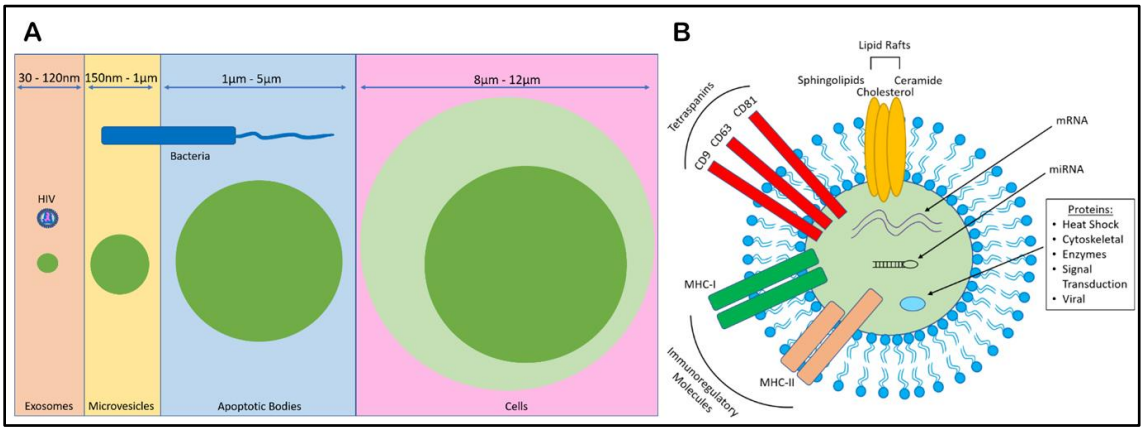

Figure 1: Size ranges of EVs and characterization. (A) Exosomes are defined as vesicles which range from 30-120nm in diameter and are released when an MVB fuses with the PM. Exosomes are similar in size to viruses, increasing the difficulty in isolating exosomes from virus-infected blood. Microvesicles range between 150nm - 1 µm in diameter and are instead generated via shedding/budding from the PM. Apoptotic microvesicles are <1µm and are released from apoptotic bodies, which range from 1µm -

5μm in diameter. (B) Exosomes transport a variety of proteins and genetic material. Lipid raft-derived microdomains form larger domains which are responsible for inducing budding in an ESCRT-independent pathway of lateral cargo segregation. Exosomes are highly enriched with tetraspanins, which play a critical role in the ESCRT-independent pathway of endosomal sorting and function as exosomal biomarkers. Depending on the cell of origin, exosomes may contain differing immunoregulatory molecules, such as MHC-I/II. Lastly, exosomes traffic a variety of host/viral protein, mRNA, and miRNA [2].

Microvesicles range between 150 nm and 1 μm in diameter and are primarily generated via shedding/budding from the plasma membrane (PM) [2, 5]. Microvesicles are also capable of transporting proinflammatory miRNAs and cytokines such as IL-1β thereby initiating the acute inflammatory response and modulating the immune response [5, 6]. Unlike microvesicles, exosomes are intraluminal vesicles (ILVs) ranging from 30 to 120 nm in diameter, are formed during the maturation of multivesicular bodies within the late-endosome via inward budding of the endosomal membrane, and are released into extracellular space when a multivesicular body (MVB) fuses with the PM [1, 7, 8]. However, the ILVs may undergo degradation if the MVB fuses with a lysosome instead of the PM. The process determining the fate of MVB fusion, whether it fuses with the PM releasing exosomes or is destined for lysosomal degradation is not yet fully understood, but is hypothesized to be a result of inhibition of either pathway as lysosome inhibition results in increased EV release [2, 9].

The process of EV release was at first believed to be random; however, studies using different animal models in 1983, found reticulocytes released transferrin receptors within the EVs [10, 11]. It was also demonstrated that EVs with dissimilar protein and lipid profiles potentially associated with cancer invasion and tumor immune escape, may be generated from different variants of lymphoma [12]. After a year had passed, another

study recorded that tumor-derived exosomes (TDEs) presented with antigens comparable to the tumor cells they derived from, and also demonstrated on cytotoxic T-lymphocytes (CTLs), EV-induced anti-tumor effects [13]. Johnstone et al., as a reference for EVs carrying transferrin receptors, coined the term exosomes, in 1987 [3]. The role of exosomes in antigen presentation was demonstrated by Raposo et al. when their study exposed that the specific MHC class II T cell responses were induced by the MHC class II molecules found in exosomes were derived from B lymphocytes [14]. Comparable to cancer, as a result of their ability to transport molecules to target cells in infectious diseases, exosomes function as a double-edged sword, capable of both promoting host immune-response and facilitating viral pathogen dissemination and pathogenesis [15, 16]. Exosomes confer protection against pathogens by trigger immune responses, thus playing a key role in the pathogenesis of infection [15, 16]. This effect is observable in the context of viral infections, given that infected cell-derived exosomes can induce antiviral immune responses and also transport viral content to neighboring cells [17]. A certain hypothesis postulated by Gould et al., labeled the “Trojan exosome” hypothesis, describes the evolutionary similarities between exosomes and viruses in regard to their transmission pathways and biogenesis; this indicates that exosomes may potentially be implemented as a nano-therapeutic for the purpose of vaccination against HIV by hijacking the same exosomal biogenesis pathway which is hijacked and employed by HIV to facilitate viral spread [18, 19]. Overall this data reveal that exosomes can be used in immunotherapeutic strategies, delivery of therapeutic molecules to target cells, vaccine development, and also exploited as biomarkers [16]. The bridging of biogenesis pathways depicts a shared mechanism among EV and virus particles (Figure 2).

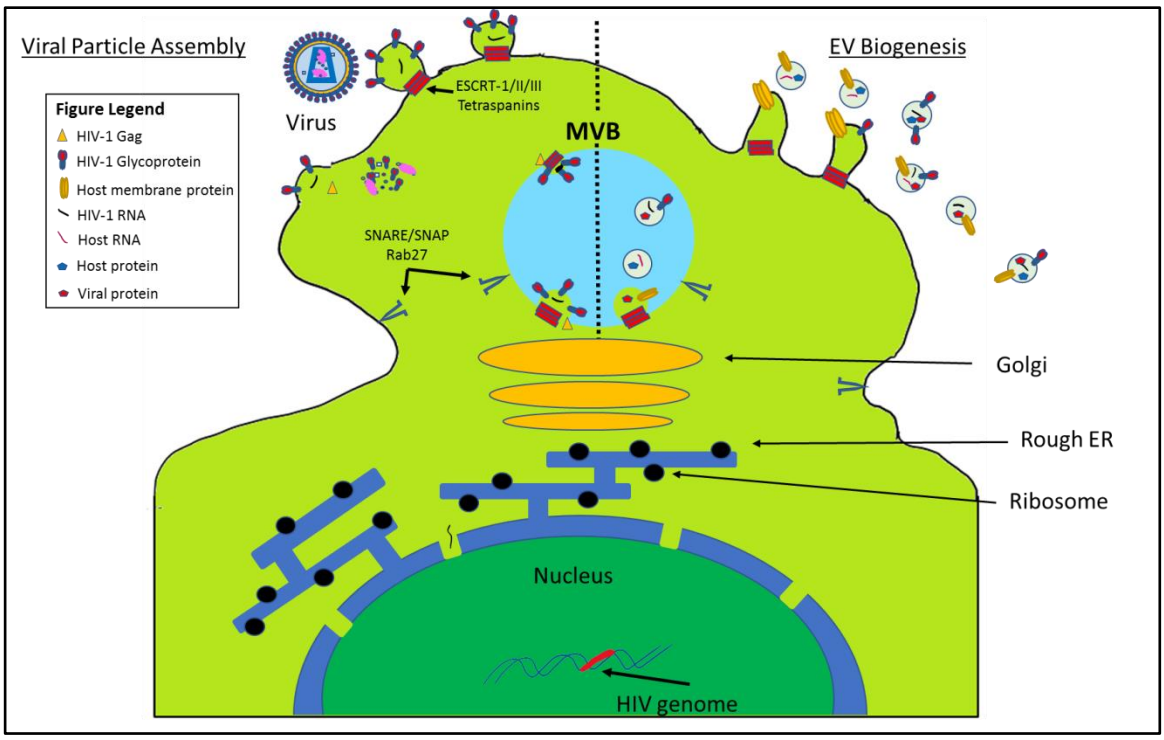

Figure 2: Comparison of viral and EV biogenesis. Infected cells concurrently release EVs and retroviral particles, possessing shared pathways at the MVB and the PM, whilst incorporating SNARE/SNAP Rab27 and tetraspanins, and ESCRT proteins in both pathways. Depicted here is sorting and transport of the exosome-specific proteins to the nascent ILVs, and excision from the MVB, Gag-mediated virion assembly at the PM or the MVB, and EV and virion release [2].

EVs and viral particles are simultaneously released from infected cells [20]. Post-infection, viral RNAs in the cytoplasm, interacting with other viral factors undergo Gag-mediated virion assembly at the PM or close to the MVB [20]. EV or virion-containing MVB employs SNARE/SNAP Rab27 to fuse with the PM, releasing both EVs and virions [20]. Exosome biogenesis requires sorting of the exosome-specific proteins, transport of the exosomal contents to the nascent ILVs, and excision from the MVB [5]. These exosome-specific proteins are guided to the ILVs via a sorting signal consisting of transmembrane proteins with monoubiquitinated cytosolic domains, which are captured by the endosomal sorting complex required for transport (ESCRT) [5]. ESCRT-0,

ESCRT-I, ESCRT-II, and ESCRT-III compose the ESCRT protein machinery required for sorting the ubiquitinated cargo to the ILVs. This sorting is initiated by the interaction of the endosomal protein's (Hrs) double zinc finger domain's binding with phosphatidylinositol 3-phosphate (PtdIns-3-P), permitting ESCRT-0 binding to the endosomal membranes and eventual recruitment cascade of ESCRT-I, which recruits ESCRT-II, resulting in recruitment of ESCRT-III [21]. Of which, all non-ESCRT-III proteins interact with ubiquitylated cargo via their ubiquitin-binding subunits, capturing cargo after it has been concentrated by ESCRT-0 [22]. The captured cargo is then driven into ESCRT-III filament produced invaginations, deubiquitinating the cargo and excising the cargo-filled ILV [22]. Reports describing alternative pathways have been demonstrated. For example, ESCRT-independent EV generation has been observed in oligodendrocytes, where ceramide is released from the breakdown of sphingolipids and promotes domain-induced budding of the ILVs [23]. This proposed ESCRT-independent pathway is dependent on lateral cargo segregation via lipid-raft derived microdomains, which then merge into larger domains, inducing budding [23]. Inhibition of sphingomyelinases, which hydrolyze sphingomyelin into ceramide, have been observed to inhibit exosome release but promote microvesicle secretion from the PM, showcasing that ceramide is critical for exosome formation [2, 24]. Although EVs share a common biogenesis pathway, EV content differs depending upon the cellular source and health status.

Isolation of EVs

Various methods have been employed to isolate EVs: differential ultracentrifugation, immunomagnetic-bead separation, density gradient centrifugation, chromatography, precipitation-based separation, ultrafiltration, nanoplasmon-enhanced scattering (nPES), and on-chip exosome isolation [2, 25]. The gold standard and most commonly used method for exosome separation is differential ultracentrifugation [25-27].

Differential Centrifugation – the Gold Standard

In differential centrifugation (DC), the exosomes are separated from macromolecular proteins, apoptotic bodies, cell debris, and cells as a result of their physical properties and volume, during a series of increasing consecutive centrifugations at 4 °C culminating at an ultracentrifugation at 100,000× *g*[28]. Briefly, samples are pre-cleared by a series of low speed spins, first 300× *g* to pellet cells, then 2000× *g* to pellet debris, and lastly 10,000× *g* to remove the macroparticles within the supernatant. The pre-cleared supernatant is then ultracentrifuged at 100,000× *g* for 70 min resulting in the EV pellet. Given the overlap in the size of exosomes and microvesicles size the EV pellet likely consists of both vesicle types. DC may be effective in isolating exosomal EVs but can be labor-intensive and time-consuming with a low yield. Despite these disadvantages DC is considered the gold standard for exosome isolation [25].

Immunoaffinity

Exosomes can be isolated via immunomagnetic-beads coated with a monoclonal antibody capable of binding tetraspanins, such as CD81, CD9, and CD63, which are

found on the exosome surface [29, 30]. After the sample is incubated with the antibody-labeled magnetic beads, exosome-antibody-bead complexes form, and are retained in the separation column upon application of the magnetic field. This method may compromise the integrity of the captured exosomes but assures highly purified exosomes unlike the DC method [25, 29, 30]. However, this method is not without its disadvantages as separating the beads from the exosomes of interest, once collected, is not an easy task, preventing the use of the isolated exosomes in other subsequent experiments. EVs isolated from plasma require analysis using sophisticated tools and expensive reagents, limiting their use in point-of-care testing in addition to the risk of modulating the exosomal biological activity as a result of the change in salt concentrations and pH which occurs when employing this method [25].

Density Gradient - OptiPrep™

For density gradient centrifugation, the constituents within the culture medium or serum/plasma samples are separated based on the isodensity zone when under a ultracentrifugal force, separating exosomes from the other components within the sample [25, 31-33]. The most commonly used of these methods being either iodixanol (OptiPrep™ STEMCELL Technologies, Vancouver, BC, Canada) or a sucrose density gradient, with samples being layered at the top of a 30% sucrose or iodixonal solution, and then ultracentrifuged, at 100,00× *g* for 16–18 h yielding exosomes at a characteristic banding density zone. This method results in exosome isolations of higher purity as a result of greater separation efficiency. However, the resulting yield, similar to DC is low,

longer centrifugation steps are needed, if not using OptiPrep™ the gradient media must be prepared in advance and is heavily dependent on space-consuming instrumentation [25].

Chromatography

Exosomes uniform in size and of high purity can also be obtained via chromatography, in which the particles within the sample is separated as it is moved through the filtration column at differing rates via centrifugation of the column, separating the particles based on the pore size of the gel [25, 28]. However, this method yields a paltry exosome yield and requires high-priced specialized laboratory equipment.

Precipitation

Precipitation-based exosome extraction methods, such as Exoquick™ (System Biosciences) total exosome isolation (Millipore Sigma, St. Louis, MO, USA), are commercially available, have become popular, and are now commonly used to isolate exosomes from small volume samples [25, 34]. Upon mixing of the sample with the precipitating solution, a polymeric ionic web captures exosomes, which are then pelleted by centrifugation. This method grants extreme ease as it is simple to perform, quick, requires only a simple centrifuge, and provides exosomes uniform in size. However, the exosomes may present with contaminating microvesicles and proteins, impairing their analysis and potential downstream use. For the precipitation reagents, the reagent itself is quite overpriced, with each dose usable only for a small sample size, limiting its use due to the financial strain it places on research funding.

Ultrafiltration

Exosomes may also be separated from EVs using ultrafiltration to isolate exosomes within a sample, as it passes through filters with increasingly small pore size, which traps particles of higher molecular mass and allows exosomes and other nanoparticles to flow through [25, 35]. This method can be accomplished using either ultracentrifugation or stirring, with the latter providing the benefit of a decreased pressure on the exosomes. This allows exosomes to maintain their integrity, is less-time consuming, and results in a higher exosome yield without the risk of exosomal aggregation. However, just as with the other techniques there is likely microvesicle contamination resulting in reduced exosomal sample purity.

Nanoplasmon-Enhanced Scattering (nPES)

With similar properties to an enzyme-linked immunosorbent assay (ELISA), nPES detects and captures exosomes by employing the use of antibodies against exosomal markers, such as CD81. A sensor chip with a silica surface conjugated with anti-tetraspanin antibodies captures the exosomes, which are then bound by antibody-coated gold nanoparticle probes (GNPs), forming complexes of exosomes and GNPs [25, 36]. Exosome quantity can then be measured via dark-field microscopy; however, an analysis may require complex statistical tools and detection of the exosomal protein using this method may be costly. Regardless, nPES is a quick, sensitive, and high-throughput method of detecting even trace amounts of exosomes from samples.

Lab-on-chip Exosome Isolation

Lastly, a lab-on-chip device, such as the exosome total isolation chip (ExoTIC), may be used to extract exosomes via filtration, yielding purified and enriched exosomes [25, 37]. ExoTIC provides a quick, easy to use, scalable, and affordable method of generating a high yield of patient-derived exosomes, which can be employed in downstream applications, in disease diagnosis, and point-of-care testing. Taken together, a multitude of methods are currently available for exosome isolation allowing for different degrees of purity and subsequent downstream application.

EV content and characterization in health and disease

As the exosome research field continues to grow, the exosome isolation techniques will also improve allowing for high yield and purity in exosome isolations. In our studies, we have employed both density gradient and precipitation methods of exosome isolation, namely OptiPrep and Exoquick, respectively. However, our most commonly used method for exosome isolation remains the gold standard, differential centrifugation via ultracentrifugation as described by Théry C. et al., 2006, with an extra filtration step introduced after the 10,000g centrifugation [38]. This extra filtration step is performed by filtering the exosome-containing media through a 0.2µm filter with a sterile disposable syringe with Luer-Lok tips (Fisher Scientific), and further removes any remaining cell debris greater than 0.2µm, providing an exosome sample with a lower average diameter, as determined by dynamic light scattering with a Zetasizer (Malvern Analytical).

Exosomal Content and Characterization

Exosomal EVs are enriched with the protein superfamily consisting of four trans-membrane domains, tetraspanins, which form tetraspanin-enriched microdomains (TEMs) impacting exosome content, EV binding and uptake by target cells, EV biogenesis, and exosome antigen presentation [2, 39]. Tetraspanins, including CD9, CD63, and CD81, are highly enriched within the exosomal membrane of exosomes, which were generated via budding from the plasma membrane, and thus serve as excellent exosomal biomarkers [12]. It is hypothesized that the TEMs assemble the proteins and facilitate the protein–protein interactions required for ILV formation, and therefore offer another ESCRT-independent mechanism of EV generation [40]. Various steps of intracellular vesicular trafficking, such as trafficking and budding of vesicles, vesicle docking, and membrane fusion, are controlled by the RAB family of small GTPase proteins [41]. Endosome-associated RAB GTPases have been observed in exosomes [42]. Inhibition of either RAB35 or RAB11 impaired exosome secretion, in cells bearing the proteolipid protein (PLP) exosome biomarker or the heat shock cognate (Hsc70) chaperone protein, respectively [43, 44]. Additionally, absence of RAB2B, RAB51, RAB9A, RAB27A, or RAB27B in HeLa cells, via knock-out, results in inhibition of exosome secretion, demonstrating that these RAB GTPases are required for exosome biogenesis [45, 46]. There is an inverse relationship between exosome biogenesis and autophagy [46, 47]. Lastly, exosome protein, RNA, and miRNA content differ dependent on the cellular derivation and is modulated in the presence of viral infection [7, 46, 47].

Role of EVs in the Pathogenesis of Viral Infections

EV-mediated modulation of the immune system has been well studied; EVs have the capacity to present antigens, trigger production and release of inflammatory cytokines, and promote cancer metastasis or induce anti-tumor responses [48-53]. There is also data indicating an interaction between EVs and viral infection. For example, EVs may facilitate viral replication and transmission by functioning as carriers of viral genetic elements, viral proteins, or regulatory elements [54]. In order for EV biogenesis to facilitate viral spread the following requirements must be met: (1) Viral proteins or RNA must reach the ILVs; components of Dengue virus (DENV), vesicular stomatitis virus (VSV), and hepatitis C virus (HCV) have all been identified in ILVs [7]. (2) Exosomes must find and bind the target cell releasing their infectious cargo into the recipient cell's cytoplasm upon exosome entry. This is demonstrated by exosomes derived from HCV-infected human hepatoma cells that transport the viral envelope and core proteins alongside a full-length viral RNA [7, 55]. Here we review the role of EVs in the dissemination and pathogenesis of select viral infections in humans [2].

Picornaviridae and Togaviridae

Hundreds to thousands of coxsackievirus, rhinovirus, or poliovirus are packaged within phosphatidylserine (PS) lipid-enriched vesicles, enabling the collective transfer of multiple viral genomes to a single cell, enhancing viral replication and enabling viral quasispecies genetic cooperativity [56, 57]. To spread infection, coxsackievirus B1 must induce host cell lysis [58]. However, given that EVs may carry a replication competent viral genome or proteins, it is possible for coxsackievirus B1 to spread via EVs. Evidence

suggests the intercellular transmission of coxsackievirus B1 via increased release of host cell derived microvesicles as a result of coxsackievirus infection, induced increases in intracellular calcium concentration, resulting in depolymerization of the host's actin cytoskeleton is a possible non-lytic cell–cell strategy to perpetuate infection [58]. Additionally, infectious virions may be transported to adjacent cells via apoptotic bodies, enhancing viral spread [4]. Pharmacologically blocking generation of Chikungunya virus-induced apoptotic bodies, in infected HeLa cells, restricts viral spread to nearby cells, demonstrating the potential of hijacked apoptotic bodies in enhancing viral propagation [4].

Herpesviridae

Viral factors involved in viral spread and transmission are exported as EV cargo. Herpes simplex virus 1 (HSV-1) miRNA and mRNA are transported via exosomes, and potentially suppress viral reactivation effectively in order to facilitate viral transmission to a new host [59]. Epstein–Barr virus (EBV), ubiquitous in humans, is a γ-herpesvirus that is associated with epithelial and lymphoid malignancies, a potential generator of auto-antibodies, and responsible for infectious mononucleosis [60]. Exosomal EVs derived from EBV infected B-lymphocytes, release exosomes carrying MHC II molecules, given the B-cell role in antigen presentation these B-cell-derived EVs could potentially activate CD4+ T-cells [7, 53]. EBV-infected nasopharyngeal carcinoma cell-derived exosomes transport a high quantity of the CD4+ T-cell apoptosis inducer, immunoregulator protein galectin-9, evading the host immune response [7, 61, 62]. Natural killer (NK) cell cytotoxicity, IFN-γ production, and T-lymphocyte activation and

proliferation is known to be inhibited by latent membrane protein 1 (LMP1), a viral oncogene commonly expressed in EBV-associated tumors, which may be found as exosomal cargo and thus further promoting the use of EVs in facilitating viral host-immune response evasion strategy [7, 61, 63, 64].

Filoviridae

Infection with the ssRNA, negative sense Ebola virus (EBOV) results in systemic infection with severe hemorrhagic fever, immune suppression or overactivation, and tissue damage [65-67]. Upon infection EBOV primarily targets dendritic cells, monocytes, and macrophages, potentially facilitating the systemic spread of the virus throughout the host, including the liver and secondary lymphoid organs [68]. Given the aforementioned symptoms and the high mortality rate of 80–90%, rapid identification of Ebola patients is a necessity [69]. A commonly applied technique for diagnosing Ebola patients is detection of VP40, the EBOV matrix protein [67]. VP40 may employ two differing methods to release from cells, independent budding from cells or as exosomal content [67]. This transportation of VP40 into the nucleus facilitates the regulation of EV synthesis via over-transcription of cyclin D1 by binding of VP40 to cyclin D1′s promoter, dysregulating the cell cycle [67]. Additionally, the VP40-laden exosomes exert a dose-dependent decrease in cellular viability of recipient monocytes and T-cells; and these exosomes were also found to contain cytokines, which may contribute to EBOV pathology [67]. Further enhancing EBOV pathology, exosome-bound VP40 could modulate RNAi machinery, such as Dicer and Ago 1, inducing the cell death of recipient naïve cells while upregulating exosome biogenesis [69]. EBOV content release is not

limited to exosomes but extends to microvesicles as well [66]. Microvesicles containing EBOV glycoproteins (GP) have been linked to increased pathogenicity and immune evasion [66].

Paramyxoviridae

As one of the most critical causes of acute respiratory tract infection in the elderly, children, and immunocompromised individuals, respiratory syncytial virus (RSV) results in an estimated 200,000 deaths annually [70]. In an effort to better understand RSV pathology and developing a vaccine, characterization of exosomal cargo during RSV infection was required [70]. Although the exosomes were found to contain RSV components, such as RSV nucleocapsid protein N, they did not contain any infectious viral particles and therefore were unable to establish a productive infection in uninfected cells, but they did exhibit significant changes to RNA composition and the resulting chemokine release [70]. miRNA and piRNA content were found to be increased within exosomes generated from RSV infected cells [70]. Some of this miRNA content was found to be expressed at a significantly higher level within exosomes generated from RSV infected cells than in infected cells [70]. Exposure of PBMC-isolated human monocytes to exosomes derived from RSV infected cells induced the secretion of proinflammatory mediators, such as IP-10, RANTES, and MCP-1 [70]. Additionally, exosome-bound RNA cargo was found to be protected from degradation and the RNA type proportions were found to be significantly modulated by RSV infection; of note, the upregulation and downregulation of miRNAs [70]. RSV infection in patients with cystic fibrosis has been associated with coinfection with the opportunistic pathogen

Pseudomonas aeruginosa [71]. The shift from an acute *P. aeruginosa* infection to a chronic state is dependent on the formation of a biofilm with antibiotic properties, within the lung, which facilitates disease progression [71]. Infection with RSV promoted the secretion of exosome-bound transferrin, an iron-binding protein found in the host, known to promote *P. aeruginosa* biofilm growth [71]. This demonstrates the capacity of RSV to facilitate the persistence of pathogens within the airway epithelium via exosomes [71]. However, exosomes may also facilitate the host immune response upon Influenza A virus (IAV) infection, as human tracheobronchial epithelial cells have been found to traffic components of the innate immune response, such as MUC1, MUC4, and α-2,6-linked sialic acid via exosome-like vesicles [72].

Orthomyxoviridae

Influenza A viruses pose a threat to humans worldwide, causing outbreaks of acute respiratory tract infections and seasonal epidemics [73, 74]. About 36,000 individuals die as a result of flu-associated infections, annually in the US [73]. As previously discussed, intercellular communication via exosomal miRNAs may modulate cell function, alter recipient cell pathways, and facilitate viral persistence [73-76]. IAVs have been found to alter circulating miRNAs within exosomes, potentially promoting viral pathogenesis [77, 78]. For example, IAV-infected human lung adenocarcinoma epithelial A549 cells produced exosomes containing miRNA hsa-miR-1975, which was found to inhibit IAV replication by inducing interferon production [79]. IAV modulation of exosomal cargo is not limited to miRNAs, as autophagy-related proteins including Atg3/7 and antiviral cytokines such as IL6, IL18, and TNF are found in exosomes released from IAV-infected

macrophages [80]. This displays the capacity for IAVs to alter macrophage-dependent innate immune responses and intercellular cell signaling via manipulation of exosomal cargo. Pathogens may also transport viral components within exosomes, such as transportation to the apical side of the membrane of IAV progeny RNA by attaching to Rab11 vesicles, thereby facilitating late stage IAV budding and infection [7, 81]. Applying LC–MS/MS in proteomic studies have discovered that IAVs integrate exosomal proteins or markers such as annexin A3, CD9, CD81, and ICAM1, contributing to the influenza virion structure, viral spread, and implying a shared formation pathway with exosomes [82].

Hepadnaviridae

A major cause of liver fibrosis, hepatitis B virus (HBV), infects human hepatocytes causing hepatocellular carcinoma and cirrhosis [83, 84]. HBV's HBx protein facilitates oncogenic activities via a variety of mechanisms such as host gene stimulation, cell cycle interference, and mitogenic signaling [83]. This HBx protein and mRNA are encapsulated within exosomes and released into the extracellular environment, permitting horizontal transfer of its gene products and expression of the viral protein [83]. Additionally, exosomes generated by cells secreting HBx contain a significantly different cargo, both quantitatively and qualitatively [83]. These altered exosomes have the capacity to promote HBV-associated liver diseases, by inducing proliferative signaling and enhancing exosome biogenesis via increasing neutral sphingomyelinase 2 activity [83]. The natural killer group 2D (NKG2D) receptor recognizes ligands on infected cells, promoting innate immunity and lymphocyte activation to defend the host from infections

[85]. Exosomes generated from HBV infected cells and which contain viral RNA, have been found to induce mRNA expression of the NKG2D ligand in macrophages, implying a role for HBV-infected cell derived exosomes in NK cell activation, confirmed by CD69 upregulation, and induction of IFN-γ production, which was found to degrade viral RNA in hepatocytes [84]. Furthermore, infection with HBV resulted in an increase in immunosuppressive miRNAs: miR-21 and miR-29a, within CD81+ exosomes and EVs, transferred from hepatocytes to macrophages [84]. miR-21 and miR-29a downregulate IL-12p35 and IL-12p40 respectively, potentially inhibiting NK cell activity via IL-12 downregulation and facilitating viral evasion of the host immune response [84]. Another study concluded through a proteomic analysis of exosomes via LC–MS/MS that HBV-infected HepAD38 hepatoblastoma cell line-derived exosomes contain HBV-associated proteins capable of significantly reducing monocyte IL-6 production [86]. A total of 35 exosome-bound proteins were found to have been quantitatively altered as a result of HBV infection in HepAD38 cells, including the increase of five proteasome subunit proteins: PSMD1, PSMD7, PSMD14, PSMC1, and PSMC2, enhancing proteolytic activity [86]. Inhibition of this exosome-dependent proteasomal activity resulted in increased IL-6 production, implying the modulation of proinflammatory molecules by the transport of proteasomal subunit proteins within HepAD38 exosomes [86]. HBV proteins and genetic content can be transferred via exosomes to other cells; HBV proteins and nucleic acids have been found within exosomes, NK cells, and hepatocytes of chronic HBV patients [87]. Uptake of these HBV-laden exosomes impair NK cell production of IFN-γ, NK cell survival and proliferation, cytolytic activity, and NK cell responsiveness to stimulation from poly (I:C) [87]. Exosome activity during an active HBV infection is

not limited to facilitating viral replication, as IFN-α induced HBV antiviral activity has been observed to be transferred from liver nonparenchymal cells (LNPCs) to hepatocytes via exosomes [88].

Flaviviridae

Currently, there is no vaccine against HCV, a +ssRNA flavivirus that is one of the leading causes of liver disease worldwide [89]. HCV-infected patient sera and J6/JFH1-HCV-infected Huh7.5 cell supernatants were found to contain exosomes containing HCV RNA, proteins, and particles [89]. Viral genome packaging is not limited to the Picornaviridae, as HCV-infected hepatocytes release full length genomic HCV RNA laden exosomes with the capacity to activate immune cells and to establish a productive infection in naïve human hepatoma cells, facilitating viral spread [90]. Human Ago2 and miR-122, necessary for HCV RNA accumulation and translation, have been detected within exosomes derived from HCV-infected patient serum or J6/JFH1-HCV-infected Huh7.5 cells, demonstrating the capacity of exosomes to enhance viral spread via transportation of viral regulatory elements [89, 91]. EVs are also capable of transmitting Flaviviruses from arthropod vectors to humans by acting as carriers [46]. Langat virus (LGTV)-infected *Ixodes scapularis* ISE6 tick cells release EVs, which mediate the transmission of viral RNA, envelope protein, and non-structural 1 (NS1) protein from arthropod to human cells [92]. These exosomes transmigrate and infect naïve human skin keratinocytes (HaCaT cells), the barrier that first contacted the tick bites [92]. Arthropod-borne neurotropic encephalitis viruses replicate within the peripheral tissues and blood of a vertebrate host after transmission, cross the blood brain barrier (BBB), and infect the

central nervous system (CNS) [92]. Additionally, LGTV can spread viral components within its vertebrate host, as LGTV infects murine brain endothelial barrier (bEnd.3) cells, of which the BBB is comprised of, and produce exosomes, which transmit infectious RNA and proteins to murine neuronal (N2a) cells [92]. After traversing the BBB, LGTV infects neuronal cells, which can further disseminate the virus across the other neuronal cells via exosomes resulting in neuronal loss and neuropathogenesis [92].

ZIKA

To date few studies have demonstrated that exosomes are integral to the interaction between ZIKV and host cells. ZIKV and Zika viral proteins have been detected in the eyes and semen, months after initial infection, thus creating a need to comprehend how these particles persist and damage neuronal cells. Exosomes can easily cross the endothelial barriers protecting these sites and therefore are a potential antigen source [93]. Additionally, precedence for modulation of EV contents by ZIKV exists, as other flaviviruses have been observed to do so [93]. Here we review the role of EVs in the context of ZIKV infection.

ZIKV has been demonstrated to cross the placental barrier (PB), with detection of ZIKV in the fetal brain and amniotic fluid confirming ZIKV tropism for neuronal tissue [94]. Infection of the fetal brain, with ZIKV, may result in severe congenital malformations, also known as ZIKV fetal syndrome [67-69]. Individuals with ZIKV fetal syndrome may present with several birth defects, including but not limited to: facial disproportionality, microcephaly, hypertonia, cutis gyrata, ventriculomegaly, and a lack of brain tissue [69]. It is believed that after crossing the placenta, ZIKV damages

neuronal cells and induces the immune response [69]. Although, the exact mechanism for ZIKV passage through placental trophoblasts is unknown, ZIKV, like DENV, may employ the placental exosome pathway at the trophoblast ER for this purpose, as it is strongly associated with the process of secretory autophagy [94]. Immature ZIKV viral particles translocate to the trans-Golgi network, from the ER [95]. The viral particles are then packaged into exosomes. However, ZIKV may be vertically transmitted independently of the secretory autophagy pathway as a result of increased permeability due to ZIKV-induced damages and apoptosis of placental cells [94]. Studies indicate a role for autophagy in ZIKV-associated neuropathology, as inhibition of autophagy results in inhibition of ZIKV replication [96].

Uninfected human placental trophoblast (HPT) cells secrete type-III IFNs, IFNλ1 and IFNλ2, conferring anti-ZIKV protection [97]. Syncytiotrophoblasts were found to constitutively generate IFNλ1, providing an antiviral state protecting placental cells in an autocrine manner and non-placental cells in a paracrine manner [97]. Additionally, this protection may be conferred to non-placental cells via exposure to HPT-derived conditioned media (CM) [97]. This data suggests that ZIKV replication within placental syncytiotrophoblasts permitting access to the fetal compartment is not possible without either ZIKV evasion of the IFN type III antiviral properties or bypassing the PB via an unknown pathway, possibly EV-mediated [97].

EV-Mediated Restriction of ZIKV Pathogenesis

Exosomes and microvesicles are released into maternal blood during pregnancy and can be recovered during the 1st and 2nd trimester of pregnancy, increasing in

concentration with the progression of the pregnancy [98]. These exosomes have been found to contain primate specific chromosome 19 cluster (C19MC) miRNAs functioning as antiviral agents, which may be transferred to non-placental cells, conferring protection and upregulating autophagy upon the target cells if delivered via exosomes generated from trophoblasts [98, 99] (Figure 3A). Potent antiviral activity has been documented as a result of target cell exposure to EVs carrying MIR517-3p, MIR16B-5p, and MIR512-3p [98] (Figure 3A). Additionally, HPT-derived exosomes carry miRNAs conferring viral resistance to non-placental recipient cells [99]. C19MC miRNAs have been observed to attenuate ZIKV infection in non-HVT cells; however, they fail to activate IFN-stimulated genes [100]. Together, this data demonstrates the potential anti-ZIKV properties of HPT-derived exosomes, which act in an IFN-independent manner. ZIKV infection of astrocytes leads to a significant rise in EV biogenesis, predominantly composed of microvesicles and exosomes [101]. Additionally, a significant variation of miRNA transcript expression has been observed following permissive replication of ZIKV in HPTs, downregulation of miR-21, known to cause TLR7-mediated neurotoxicity [102, 103] (Figure 3B). This data presents with an apparent anti-ZIKV host cell response transported via exosome-trafficking. ZIKV infection inhibition has been observed by EVs derived from the semen of a ZIKV-infected patient [104]. Although, freshly derived ZIKV-infected patient semen efficiently blocked ZIKV-MR766 infection of Vero E6 cells, the nature of the antiviral component responsible for this inhibition remains unknown [104].

EV-Mediated Enhancement of ZIKV Neuropathology

Upon infection with ZIKV, macrophages, which are permissive to ZIKV infection, are recruited and amplify ZIKV replication [105]. The exosomes generated from the activated macrophages are transported to the human placenta, leading to

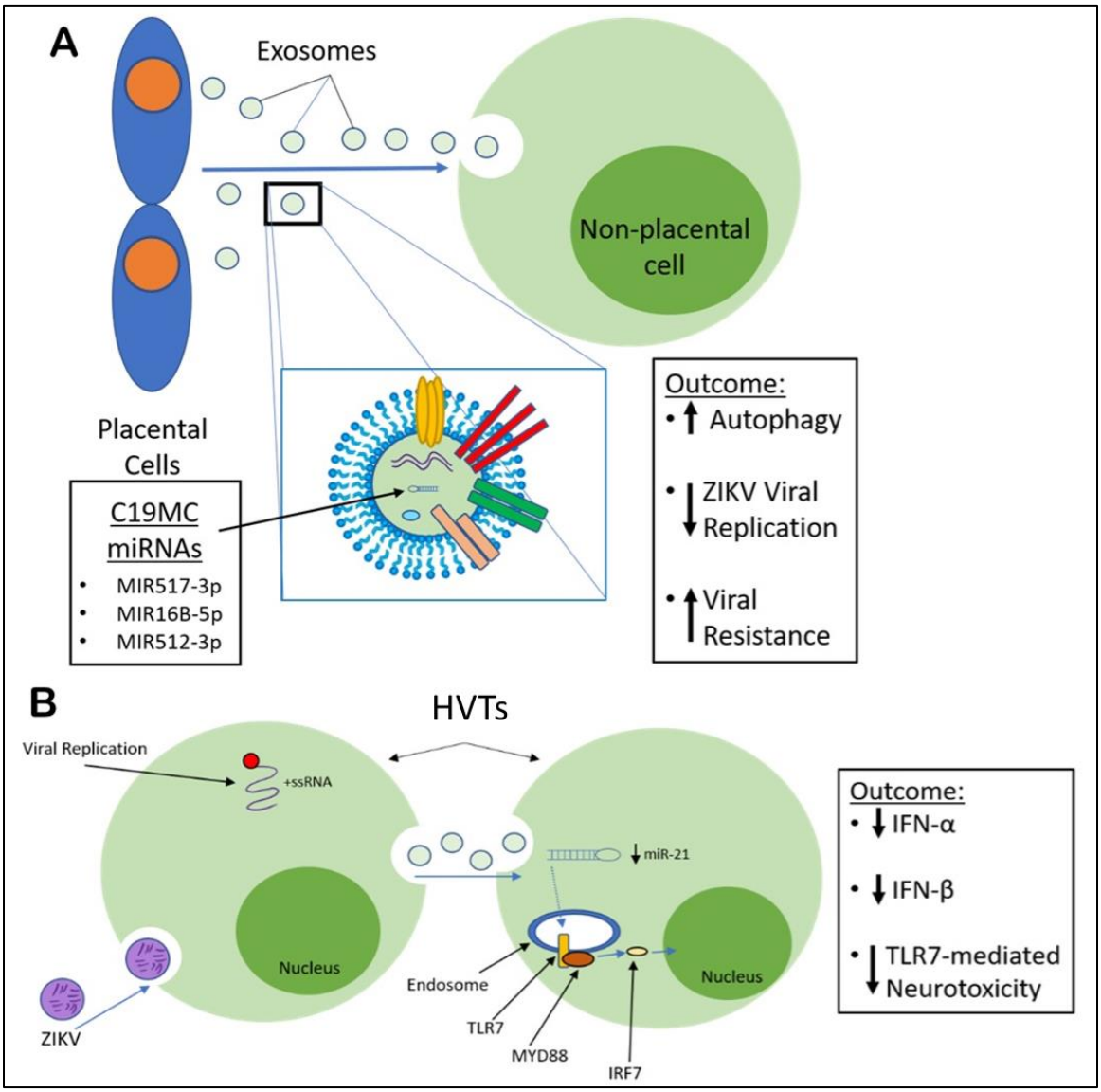

Figure 3: EV-mediated anti-ZIKV effects. (A) HVT cell-derived EVs bound with miRNAs with potent anti-viral properties have been detected. The EVs migrate to non-placental recipient cells conferring anti-ZIKV protection and up-regulating autophagy. (B) ZIKV infection of HPT cells results in an anti-ZIKV host-cell response transported via exosome-trafficking, downregulating miR-21 in uninfected HVTs, reducing TLR7-mediated Neurotoxicity.

the induction of placental proinflammatory cytokine production [106]. In combination with ZIKV NS5-mediated activation of NLRP3, inducing stimulation of human macrophage IL-1β secretion, which results in the host inflammatory response, macrophage recruitment promotes inflammation a major determinant of ZIKV pathogenicity [107].

A murine study has shown that exosomes facilitate transmission of ZIKV across neurons, by functioning as mediators [108]. An increase in exosome biogenesis was recorded in mouse cortical neuronal cell-derived exosomes alongside detection of ZIKV-RNA and envelope (E) protein [108]. Furthermore, neutral sphingomyelinase (nSMase)-2/SMPD3 gene expression and activity was induced by ZIKV [108]. SMPD3 regulates exosome generation and release [108]. A reduced exosome-mediated viral transmission rate and viral burden were observed after silencing of SMPD3 in neuronal cells, a similar effect occurred upon exposure to GW4869, an inhibitor specific to SMPD3 [108]. This study suggests that modulation of SMPD3 activity as a result of ZIKV cortical neuron infection is integral towards viral infection and exosome-mediated transfer resulting in ZIKV-associated neuropathology, such as microcephaly, as a result of severe neuronal death [108]. At this time, not many clinically relevant interactions between EVs and ZIKV are known, research is ongoing. Unlike ZIKV, however, a greater volume of EV-mediated effects on HIV-1 pathogenesis has been studied.

Coronaviridae

Coronaviruses belong to a family of enveloped positive strand RNA viruses encoding a common set of four structural proteins: the small envelope glycoprotein (E), membrane protein (M), nucleocapsid protein (N), and the spike glycoprotein (S) [109-111]. Coronaviruses cause disease in humans and animals. There are four human coronaviruses 229E, NL63, OC43, and HKU1 that cause mild disease similar to the flu with mild systems. However there are three pathogenic strains of coronaviruses that cause an atypical pulmonary disease, known as severe acute respiratory syndrome (SARS), in humans SARS CoV, Middle Eastern respiratory syndrome (MERS-CoV), and now the novel SARS CoV-2 of 2019. The first SARS coronavirus outbreak with SARS CoV was in 2002 and has been contained since 2003. The most recent coronavirus outbreak with SARS CoV-2 is associated with severe respiratory disease called Coronavirus Disease 2019 (COVID-19) and has spread beyond the borders of China, becoming a public health issue and a pandemic in which many lives have been lost [109].

The viral genome of SARS-CoV-2, can be transported to target cells via exosomes [112]. Uptake of these SARS-CoV-2 exosomes by human induced pluripotent stem cell-derived cardiomyocytes (hiPSC-CMs) resulted in an upregulation of genes associated with inflammation in hiPSC-CM [112]. Additionally, viral RNA fragments were detected within the hiPSC-CMs after coincubation with the SARS-CoV-2 gene overexpressing A549-derived EVs [113]. This clearly exhibits how coronaviruses may infect target cardiomyocytes indirectly, without requiring a direct viral infection, instead utilizing

exosomes to deliver viral RNA. This is an excellent example of how coronaviruses may exacerbate pathology by altering the inflammatory state via exosomes.

Human host factor angiotensin-converting enzyme 2 (ACE2) has been identified, during the first coronavirus epidemic, as the receptor for the SARS causing coronavirus [114]. ACE2 and the DC-SIGN family of receptors bind the S protein, mediating coronavirus entry to target cells [109]. Given this most recent outbreak of coronavirus, there is an urgent need for a vaccine against this virus [109]. Given the physiological properties of exosomes, researchers have investigated the potential of exosomal vaccines [109]. Exosomes incorporated with spike S proteins results in the generation of neutralizing antibodies. Furthermore, priming with the S-protein exosome vaccine and subsequent boosting via addition of the adenoviral vector vaccine, yielded neutralizing antibody titers exceeding those of a SARS-convalescent patient serum [109, 115]. This is an excellent example demonstrating the possibilities of exosomes as nanotherapeutics. Vaccines are not the only possibility as already clinical trials using exosomes derived from allogeneic bone marrow mesenchymal stem cells (ExoFlo) have begun[116]. ExoFlo was used to treat 24 patients, testing positive for SARS-CoV-2 via polymerase chain reaction [116]. All of the patients were classified as presenting with severe COVID-19 and moderate to severe acute respiratory distress syndrome (ARDS) [116]. A single dose was administered intravenously, with the 15 mL ExoFlo treatment being evaluated daily for 14 days [116]. Treatment with ExoFlo caused patients' oxygenation and clinical status to improve. These improvements extended to improved neutrophil counts, with a mean reduction of 32%, and increased CD3, CD4, and CD8+ lymphocyte levels, improving patients' lymphopenia [116]. Given its demonstrated ability to restore oxygenation,

downregulate the cytokine storm and its overall safety profile, and reconstitute immune function, ExoFlo is a top candidate as an exosome-based nanotherapeutic for COVID19 [116]. Exosome characteristics make them ideal as therapeutic agents, as they are non-immunogenic, can pass cellular barriers, and their contents can be manipulated. Exosomes can be used as delivery systems to transfer pharmaceutical drugs, proteins, enzymes, antibodies, and other biologically relevant molecules to target cells [117-119]. Since exosomes possess a unique biologic potential for biomedical applications given their <100 nm nanoscale size these EVs have become attractive nanostructures for treatment of viral infection or their associated neuropathologies. [117-119].

Retroviridae

Human Immunodeficiency Virus type 1 (HIV-1)

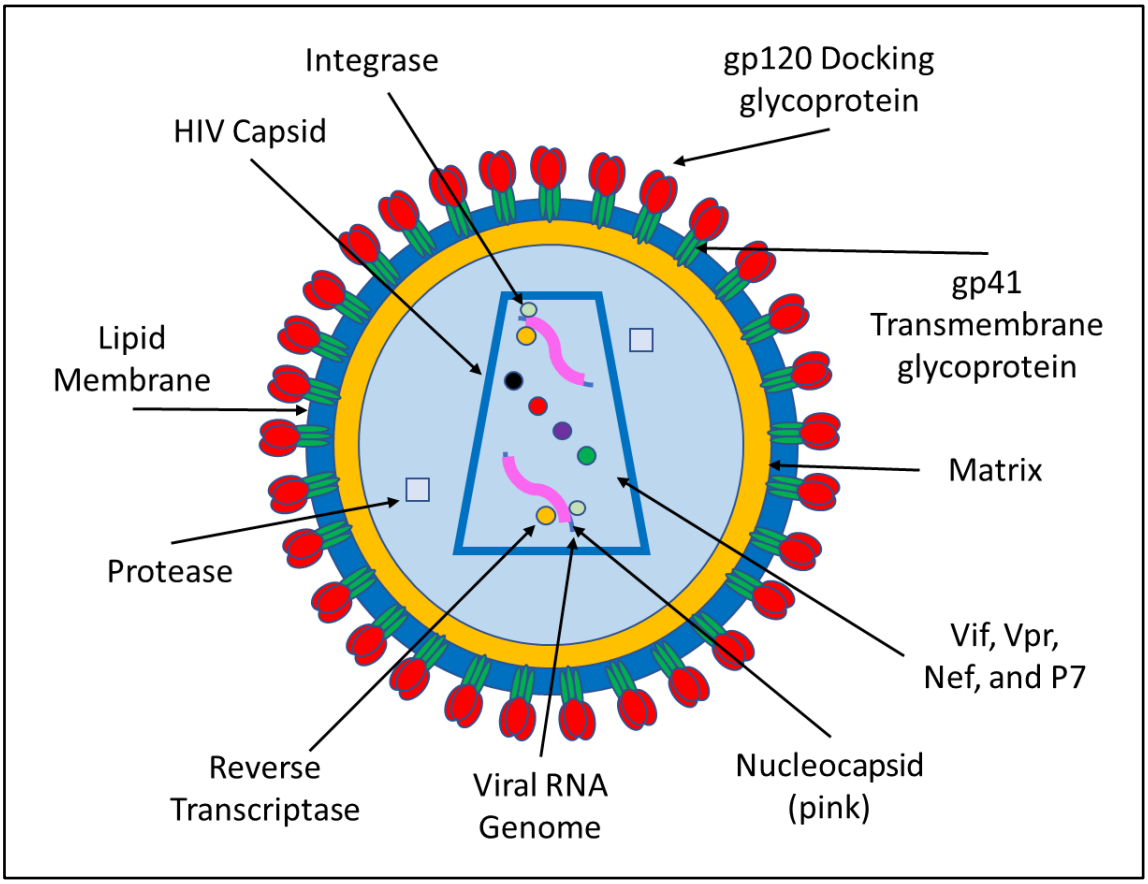

Figure 4: A schematic of the HIV-1 virion. Encoded by the gag gene, the nucleocapsid, capsid, and matrix coat the inner viral core. The pol gene encodes reverse transcriptase which is used in viral replication, protease which cuts viral polyproteins, and integrase which is responsible for the integration of viral DNA into host DNA.The two env proteins are gp120 and gp41, which are needed for binding to the target cell receptor. Nef and vpr are required for efficient infection of HIV. Vif counteracts host anti-viral defenses and vpu enhances viral particle release.

Before we cover the relationship between xEVs and HIV, we must first discuss HIV itself. HIV is the lentivirus within the retroviridae family, responsible for causing Acquired Immune Deficiency Syndrome (AIDS) (Figure 4) [120]. HIV is primarily spread via sexual contact across mucosal surfaces but may also be dispersed via maternal-infant exposure, and by percutaneous inoculation [121]. HIV-1 transmission gives rise to the establishment of a new viral infection, from a single virion [122]. A persistent infection and viremia is produced, as a result of viral replication, in the lymphoid tissue throughout the body [122]. HIV-1 preferentially infects T-cells with a high degree of CD4 surface protein expression and those subsets of T-cells expressing CCR5, particularly memory T cells [122, 123]. The central mediators of the human immune response are CD4+ T-cells which coordinate critical humoral and cellular and immune responses against infections [124]. However, with the onset of immunodeficiency, HIV-1 evolves, infecting new cell types by modulating its tropism, switching from using the CCR5 co-receptor to instead using the CXCR4 co-receptor [122, 123]. As a result, naïve CD4+ T-cells are now included among the population of HIV-1 infected cells [122, 123]. Furthermore, HIV-1 gains the ability to infect monocytes and macrophages, as the virus evolves the ability to infect cells expressing low surface-bound concentrations of CD4 [122, 123]. In order to infect cells, CD4 is required for natural isolates of HIV-1; however, binding to CD4 alone will not lead to HIV viral

particle entry into a cell, a coreceptor is needed as well, namely CCR5 or CXCR4 [122, 123, 125]. As such, only cells expressing CD4 are susceptible to a significant HIV-1 infection [122]. Under normal circumstances, the CD4 receptor functions as a coreceptor in addition to the T-cell receptor employed in MHC Class II binding, which is expressed on antigen presenting cells (APCs) and is responsible for the presentation of heterologous peptides to the CD4+ T helper cell [122]. Overall, HIV isolated from those recently infected, express CCR5 with these R5-tropic HIV variants being detectable throughout the entire course of the HIV infection [125, 126]. HIV variants utilizing CXCR4 are termed X4 variants and, in at least 50% of all patients, are frequently detectible at a late stage of HIV infection [125, 127]. Although both the CCR5 and CXCR4 co-receptors are expressed on leukocytes, they are expressed to different degrees on different T-cell subsets, with CCR5 expression found on primarily on memory T-lymphocytes and CXCR4 expression being presented mostly on resting, naïve T-lymphocytes [125, 128, 129].Consequently, the ideal subset for HIV replication and the primary target are activated CD4+CCR5+ T-lymphocytes [125, 130]. CD4 T-cell count precisely reflects the degree of immunodeficiency in HIV-infected patients, with the progressive depletion of CD4+ T-cells over the course of infection, a hallmark of HIV infection [124]. The rate of AIDS progression varies between patients with some patients able to remain asymptomatic without ART for years after infection by retaining stable CD4 cell counts for prolonged periods of time; these patients have defined as long-term non-progressors (LTNP).[125]. However, without ART treatment, an infected individual will develop AIDS over 90% of the time, within a time span of 10-12 years, facilitating the onset of opportunistic infections by common pathogens which would generally be controlled by a

healthy host [123, 125]. In addition to the aforementioned productive infection and eventual subsequent lysis of most of the CD4+ T-cells, some of the CD4+ T-cells instead establish a latent state, which essentially halts viral replication and prevents the cell from being killed; this latent state is also observed in HIV infected macrophages, however, unlike CD4+ T-cells, productively infected macrophages will not die as a result of HIV-infection [123]. This permits the establishment of HIV-reservoirs in the brain, which will be covered later in this dissertation [123]. Dendritic cells (DCs) function as messengers between the adaptive and innate immune response systems, by binding to foreign particles and presenting this antigen on its cell surface to adaptive immune cells, facilitating their polarization into effector cells [123, 131]. DCs must employ the Sialic acid-binding Immunoglobulin-type Lectin 1 (SIGLEC-1) receptor and the lectin Dendritic Cell Intercellular Adhesion Molecule-3-Grabbing Non-integrin (DC-SIGN) receptor in order to capture and transfer HIV-1 particles to CD4+ T cells [131, 132]. HIV-1 can exploit this to gain access to CD4+ T-cells within the lymph node, establishing a viral reservoir [123]. This dissertation has so far reviewed the cellular targets of HIV; let us briefly explore how HIV replicates by understanding its life cycle.

The life cycle of HIV can be separated into 7 phases: (1) binding, (2) fusion, (3) reverse transcription, (4) integration, (5) replication, (6) assembly, and (7) budding [133]. Binding or attachment of the HIV virion to the target cell followed by membrane fusion is accomplished in four steps. First, HIV Env, which is composed of the gp41 and gp120 subunits, binds to the host cell CD4 [133, 134]. Second, this results in a conformational change in Env, which is partially mediated by the V3 loop of Env, permitting binding to

the coreceptor [133, 134]. The 2nd phase of the HIV life cycle is membrane fusion where the viral lipid bilayers become contiguous with that of a cellular membrane [133, 135]. Third, the fusion peptide of gp41 inserts into the target membrane, initiating the process of membrane fusion [133, 134]. Fourth, membrane fusion is complete via the formation of the six-helix bundle [133, 134]. Upon entering the cell via membrane fusion, the third phase begins with HIV releasing HIV RNA, Tat, protease, integrase, and reverse transcriptase into the cell [133]. Reverse transcriptase then converts HIV RNA into HIV DNA, allowing HIV genetic content to enter the nucleus of the target cell [133]. Once inside the nucleus, the 4th phased commences, integration of the HIV DNA into host DNA through the use of the HIV enzyme, integrase [133]. Once the HIV DNA is integrated with the host DNA, HIV exploits the cell's machinery to produce long chains of viral proteins, which will constitute new virions, this step marks the completion of the 5th phase of the HIV life cycle [133]. These newly produced HIV proteins and RNA will transfer to the cell surface, assembling into non-infectious immature HIV, completing the 6th phase of the life cycle, assembly [133]. The recently generated immature viral particle buds out of the host cell and releasing protease, breaking up long protein chains in the viral particle, thus creating an infectious and mature HIV virion, completing the final 7th phase of the HIV life cycle [133]. Anti-retroviral therapy (ART) targeting different phases of the HIV life cycle exist and have proven efficacious in ameliorating HIV viral load and associated pathology [123, 133, 136]. For example, CCR5 agonists, such as maraviroc, or post-attachment inhibitors such as, ibalizumab-uiyk (brand name: Trogarzo), are entry inhibitors which bind and thus block access to the coreceptor, preventing HIV binding [133, 137]. Fusion inhibitors prevent HIV fusion to target cells

via extracellular actions, as observed with enfuvirtide (T20) which targets the NHR helices, thus preventing the formation of the 6-HB structure [133, 137, 138]. T20 is used in a study detailed in this dissertation and will be reviewed further in that section. Non-Nucleoside Reverse Transcriptase Inhibitors (NNRTIs), such as dovavirine, disrupt reverse transcriptase RNA-dependent and DNA-dependent DNA polymerase activities by directly binding to a site distinct from the nucleoside binding component, thus resulting in an allosteric inhibition of the transcriptase [133, 137, 139]. Nucleoside Reverse Transcriptase Inhibitors (NRTIs), such as emtricitabine and tenofovir disoproxil fumarate, lack, at the 2'-deoxyribosyl moiety, a 3'-hydroxyl group, and as a result of this missing group, the formation of a 3'-5'-phosphodiester bond in the growing DNA chains is blocked, thus averting viral replication [133, 137, 140]. Integrase Strand Transfer Inhibitors (INSTIs), such as raltegravir, inactivate Mg2+ and Mn2+, which are key cofactors required for successful integration, therefore blocking integrase [133, 137, 141]. Lastly, protease inhibitors (PIs), such as atazanavir, bind to the protease active site thus blocking access [133, 137, 142]. Now that this dissertation has reviewed the basics of HIV from contraction to treatment, it is necessary to understand how its diversity may impact patient viral load, immune response, and response to ART.

HIV Phylogeny

For each independent occurrence of a cross-species transmission event of simian immunodeficiency virus (SIV) there is a phylogenetic lineage, Groups M, N, O, and P [143]. However, unlike the other groups, group M was the sole phylogenetic lineage to be spread worldwide as a pandemic [144, 145]. The most recent common ancestor for the

current M group subtype has been proposed to have originated from 1910-1930, according to analysis of HIV-1 viral diversification via mathematical modeling; HIV-1 then spread throughout West Central Africa and eventually the rest of the world [146, 147]. Research on HIV-1 genetic diversity may present with clues on the efficacy of novel interventions, how viral replication is impacted by antiretroviral therapy (ART), and the mechanisms for viral persistence [148]. An extensive genetic diversity which accumulates between and within hosts is a characteristic of HIV-1 infection [148]. As a result of a lack of a proofreading mechanism in the reverse transcriptase (RT) enzyme, a high degree of genetic diversity within the population of HIV-1 in an individual is generated [148]. There are a variety of factors that promotes the buildup of HIV-1 diversity within an infected individual, such as: immune selection for antibody and CD8+ T cell escape variants, a large population size, alterations in the populations of infected cells, a high rate of viral recombination, anatomical compartment microenvironment disparity, and hypermutations mediated by host apolipoprotein B mRNA editing enzyme, catalytic polypeptide-like (APOBEC) [148-162]. The scope of the genetic diversity of HIV-1 is defined by the interactions of these factors and should be reflected upon when analyzing intra-patient HIV-1 phylogenetic data [148]. To better understand the mechanisms sustaining the HIV-1 reservoir, causing ART-interruption induced viral rebound, the study of intra-patient HIV-1 populations, especially for patients undergoing antiretroviral therapy (ART), is needed [148]. In one such study investigating if ART completely suppresses viral replication cycles in individuals on present ART regimens, HIV populations in longitudinal samples were analyzed from a pool of 10 children, classified as HIV-1 RNA positive at birth, that were categorized as having initiated ART

at a time with low viral diversity [163]. Eight of these children displayed suppression of plasma viremia for 7-9 years and started ART at less than ten months of age [163]. On the other hand, for 15 and 30 months, two children presented with uncontrolled viremia respectively, before viremia suppression was observed, thus functioning as positive controls indicative of HIV replication and evolution [163]. Strong evidence of HIV-1 evolution was observed in the two aforementioned children who presented with uncontrolled viremia; however, no evidence of HIV-1 evolution was found in any of the 8 children with viremia suppression on ART after various methods of analysis [163]. The observed patient data displayed no similarity to the recently reported evolutionary rate of HIV-1 on ART of 6 × 10–4 substitutions/site/month simulated with phylogenetic trees [163]. Overall, this data rebuts the hypothesis that the key barrier to curing HIV-1 infection is ongoing HIV-1 replication and that this ongoing replication is expected with ART [163]. With currently available ART treatments, suppressing HIV-1 is possible; however, the elimination of HIV-1 infection remains elusive, as resting memory CD4+ T cells contain a latent reservoir of replication-competent HIV-1 [158, 164]. A closer look at the relationship between ART treatment and HIV-1 replication is needed.

HIV in the ART Era

In regard to HIV-mediated neuropathology, a high HIV viral load within the central nervous system (CNS) is known to lead to HIV-associated neurocognitive disorders (HAND); the establishment of such a high load in the CNS is now significantly reduced since antiretroviral therapy (ART) use became widespread [165]. However, most viral replication cycles will be prevented upon ART initiation, resulting in the death of

most of the infected cells, dropping the cell-free viral load down to clinically undetectable levels [148]. In 2006, HAND was defined and subclassified into three disorders: mild neurocognitive disorder (MCMD), asymptomatic neurocognitive impairment (ANI), and HIV-associated dementia (HAD) [166]. MCMD and ANI are defined by the presenting impairments on neuropsychological tests relative to results from a control population, and complemented with mild interference in daily activities [167]. Before the availability of ART, over 50% of HIV+ individuals suffered from HAD, which presents with memory loss, inability to speak clearly, and lack of motor skills among other neurocognitive impairments (NCI) [165]. However, in the current era of widespread ART use, the prevalence of HAD is only 2-8% according to Saylor, D. et al.[168]; other studies state that 15–55% of PLWHA develop HAND even in the presence of ART, indicating ongoing viral replication [169-172]. Although ART significantly reduced the prevalence of HAD and elevated survival rates of HIV patients, HIV-associated mild cognitive impairment persists, significantly impacting the patient's quality of life (QOL) and mortality, with a persistent rise in HIV+ individuals [165]. Since ART has significantly reduced the prevalence of HAD, the primary HAND disorders observed are MCMD and ANI [166]. With HAND, HIV infects T cells and monocytes, which then migrate to the CNS, infecting brain resident cells and producing pro-inflammatory cytokines such as IL-1β and TNF, which then activate astrocytes and microglia [165]. These activated astrocytes, microglia, and perivascular macrophages, are the primary contributors to neuro-inflammation in HIV infection, releasing cytokines and neurotoxic factors which lead to neuronal dysfunction and death [165]. HIV RNA and DNA have been identified within brain tissues of HIV-infected people on ART, in both

microglia and perivascular macrophages; this implies that these long-lived infected cells may function as viral reservoirs in the CNS [173-178]. Furthermore, viral proteins such as HIV Nef, a profusely expressed accessory protein which promotes viral replication, disrupts host immunity by rerouting cell-surface proteins, and counteracts host immune defenses by employing the secretory or endocytic pathways to degrade or sequester its targets, and HIV Tat, a trans activator of transcription, are generated extracellularly in the CNS of PLWHA, even if they are using ART [179, 180]. HAND in the ART era is significantly different from what was observed in the pre-ART era [181]. In the pre-ART era, the classic description of AIDS–dementia complex was characterized by a pronounced degeneration of motor and cognitive functions in addition to a progressive subcortical dementia [182]. Dissimilarly, in the era of ART, the clinical neuropsychological presentation of HAND, presents with a cortical involvement which is influenced by age and a more refined subcortical association [182]. A comparative analysis investigating pre-ART and post-ART era PLWHA from ascertained that impairments in verbal fluency, motor skills, and cognitive speed were prevalent in the pre-ART era, while in the post-ART era executive function impairments, such as working memory and attention, are the most frequently observed impairments [171]. This creates a problem, in which clinicians may find it difficult to distinguish neurodegenerative disorders as a result of HAND within the now-aging population of HIV-infected individuals from other conditions often seen as a function of age [181]. In our study we employ ART, more specifically, Truvada. Truvada is composed of tenofovir disoproxil fumarate (TDF) and emtricitabine (EMT), both are nucleotide reverse transcriptase inhibitors (NRTIs) [183]. EMT is a synthetic nucleoside analog of cytidine which forms

emtricitabine 5'-triphosphate after being phosphorylated by cellular enzymes [184]. Emtricitabine 5'-triphosphate inhibits HIV-1 reverse transcriptase (RT) activity by being incorporated into nascent viral DNA and thus competing with the natural substrate deoxycytidine 5'-triphosphate, resulting in chain termination [184]. TDF is an acyclic nucleoside phosphonate diester analog of adenosine monophosphate [184]. To convert to tenofovir and form tenofovir diphosphate, TDF first requires diester hydrolysis followed by cellular enzyme-induced phosphorylations [184]. HIV-1 RT activity is inhibited by Tenofovir diphosphate as a result of competition with the natural substrate deoxyadenosine 5′-triphosphate and by DNA chain termination, after incorporation into DNA [184].

A typical daily dosage of Truvada could consist of 200 mg emtricitabine and 300 mg tenofovir disoproxil fumarate, in a single tablet [185, 186]. We first ascertained the optimal dosage of both TDF and EMT after determining the cytotoxic effects of Truvada in a dose-dependent manner. The dosage selected displayed both inhibition of viral replication and manageable cytotoxicity in our *in-vitro* study, 9.44µM final concentration of TDF and 16.17 µM final concentration of EMT. Truvada is one of many drugs which are being employed to treat HIV, usually in combination with other drugs [185, 187]. Additionally, Truvada is also employed as a pre-exposure prophylaxis (PrEP) for adolescents and adults who weigh at least 77 lb (35 kg), to diminish the risk of HIV infection [185, 187]. Based on research performed outside the USA, TDF/EMT has been observed to decrease the risk of contracting HIV, if used daily and alongside a complete strategy for the prevention of HIV, in numerous subgroups of patients [188-190]. A

reduction in the absolute risk of contracting HIV was observed in high-risk MSM, as TDF/EMT treatment decreased the absolute risk from 5.3% to 2.9% [189]. In regions of Botswana with high HIV prevalence, the absolute risk of infection among heterosexual women and men was decreased from 4.3% to 1.6% [190].

HIV Epidemiology

In 2020, there were approximately 37.7 million people worldwide, living with HIV [136]. Of these 37.7 million people, 95.49% or 36 million infected were adults and 4.51% or 1.7 million infected were children from the ages of 0-14 years [136]. Over half (53%) of these 37.7 million people were female [136]. Worldwide HIV incidence for 2020 observed a 31% decline relative to 2010 with an estimated 1.5 million new HIV infections [136]. 1.3 million of these new HIV infections were in individuals aged 15+, with new infections affecting 160,000 children aged 0-14 years [136]. In 2020, approximately 84% of HIV positive individuals worldwide actually knew their HIV status [136]. The remaining 6.0 million people, an estimated 16%, still in need of access to HIV testing services [136]. HIV testing is essential to commence and receive HIV treatment, care, prevention, and support services [136]. As of June 2020, 75% of HIV-infected individuals, about 28.2 million people were using antiretroviral therapy (ART) worldwide [136]. This data means that means 9.5 million people have yet to start ART [136]. Access to HIV treatment is crucial in the global campaign to eradicate AIDS as a threat to public health [136]. Those infected with HIV whom are informed of their HIV status, take prescribed ART medication, and maintain an undetectable viral load pose essentially no risk of transmitting HIV to their HIV-negative partners sexually and may

live healthy and long lives [136]. In 2020, 84% of HIV-infected individuals worldwide knew their HIV status, 73% were using ART, and as a result 66% were virally suppressed [136]. Since 2004, AIDS-related deaths have seen a decline of 64% and a decline of 47% since 2010 [136]. In 2020, an estimated 680,000 people died as a result of AIDS-related illnesses worldwide; this is lower than the number of AIDS-related deaths in 2010, at 1.3 million [136]. Although the number of AIDS-related deaths, individuals on ART, and HIV incidence has improved worldwide, let us focus more locally and observe the epidemiology of HIV infection in the USA. Over 700,000 HIV-positive individuals have died with AIDS, since the beginning of the HIV epidemic in the USA [145]. 52% of all new HIV diagnoses in 2018 originated from 48 US counties, Washington D.C., and Puerto Rico, which constitute only 1.6% of all U.S. counties; most of these counties with a disproportionately high number of diagnoses were located in the southern USA [145]. These observed geographical inconsistencies in regards to new HIV diagnoses are most likely driven by the composition of racial and/or ethnic groups in each county [145]. Compared to individuals who report from other races or ethnicities, the African American population possess unequal access to treatment and prevention services aimed at infected individuals or individuals at-risk of infection, and as a result, a higher burden of HIV infection [145]. Additionally, this higher burden is observed irrespective of sex, as in 2018 the African American women consisted of 58% of new HIV diagnoses in women, and African American men who have sex with men (MSM) constituted 38% of all new diagnoses within the population of MSM, in the USA [145]. On another note, from the period of 2009 – 2018 new HIV diagnoses decreased by 16% [145]. In 2019, the overall rate of new HIV diagnoses was 11.1 per 100,000 people [191]. From 2015-2019 the rate

of HIV diagnoses, among adult and adolescents, decreased for all age groups except those at ages 25-34, in the USA [191]. In 2019, the percent of HIV diagnoses, among adult and adolescents, was 65.6% as a result of male-to-male sexual contact (MMSC), 23.5% due to heterosexual contact, 6.8% due to injection drug use (IDU), and 4% as a result of both IDU and MMSC [191]. Of note, both categories involving IDU have increased since 2015 [191]. In 2019, the overall total prevalence of HIV for adults and adolescents, in the USA and 6 dependent areas, was 379.7 per 100,000 people [191]. By the end of 2019, in the USA and 6 dependent areas, 1,061,482 people were living with HIV; males comprised of 75% of this total [191]. Both the rate and number of HIV-positive individuals, in the USA and dependent areas, increased from 2015-2019 [191]. Given that ART use is widespread in the USA, it is not surprising to see that by the end of 2019, the largest percentage of individuals living with HIV were from ages 55-59 and composed 15% of the total population of HIV-positive individuals within the USA and 6 dependent areas [191]. To further support the aforementioned higher burden of HIV infection in the African American population, 40% of HIV positive individuals in the USA and 6 dependent areas are African American [191]. In 2019, the overall rate of deaths of PLWHA was 5.7 per 100,000 people, within the USA and 6 dependent areas [191]. Both the number and rate of deaths, between 2015-2019, remained stable [191]. 2015-2019 also experienced a decrease in the number and rate of female deaths [191]. Conversely, there was an increase in the rate of deaths for HIV-positive individuals aged 60 or older within the same time-frame; all other age groups experienced a decrease in the rate of death [191]. Only 2 racial/ethnic groups experienced an increase in the rate of deaths within the USA from 2015-2019, Asians (7%) and Native Hawaiian/other Pacific

Islander (86%) [191]. We have now covered the epidemiological data concerning the USA; let us take a closer look at a city with a notoriously high rate of HIV incidence and prevalence, Miami [192]. In 2017, the city of Miami, Florida, in the USA, reportedly had one of the highest rates of HIV incidence in the USA, at 42.9 cases per every 100,000 residents [192]. This rate was more than 2-fold higher than Los Angeles (15.0), New York City (17.9), Washington, DC (18.0), and San Francisco (18.5) [192, 193]. Miami has experienced, since 2004, a decline in HIV incidence across all major categories of HIV transmission: MSM, heterosexual sexual contact, and IDU, with HIV diagnoses dropping from 74.1 per 100,000 people down to 28.4 per 100,000 people [194]. HIV prevalence in 2020 was reported at a total of 27,214 cases of HIV among Miami-Dade County residents and they accounted for 23.16% (27,214/117,477) of all estimated HIV cases in Florida, a drop of 0.74% since 2017 [194]. However, even though there is a trend of decreasing HIV incidence in Miami-Dade County over the past decade, the complex nature of the HIV epidemic in Miami, as a result of the multitude of ethnic, sexually diverse, and racial risk groups present, provides multiple challenges to effective HIV prevention, as no single intervention, whether behavioral, structural, or pharmacological is adequate to eradicate HIV transmission in Miami [192].

Opiate Epidemics in the USA

Opiates have caused medical concern and addiction since the isolation of morphine in 1805, facilitating the treatment of symptoms at the cost of a chronic addiction [195]. The United States of America (USA) is currently in the middle of an opioid epidemic, with opioid deaths quadrupling since 1999 and a 5% increase in drug overdose deaths from

2018 – 2019, with at least 70% of those deaths involving opioids [196]. The USA is currently in the 3rd wave of opiate overdose deaths, with the greater availability of prescription opiates driving the observed increases in opiate overdoses [195, 196]. The escalations of opiate-associated deaths are best illustrated in 3 waves. As a result of over-prescriptions of opioids, the first wave occurred in 1990s and has been increasing since 1999 [196]. The second wave began in 2010 as a result of heroin abuse [196]. Lastly, as a result of the spread of synthetic opioids, such as fentanyl, the third wave of opiate abuse-associated deaths began [196]. Thus, at the moment, the current opioid epidemic is a result of overlapping and inter-related epidemics involving the use of illicitly acquired opiates, misuse of prescriptions, overdoses, and Human Immunodeficiency Virus (HIV) transmission [196, 197]. Studies show that prescription opiate abuse, such as oxycodone, and illegal heroin use are at the forefront of opiate overdoses [195, 198]. The aforementioned overlapping epidemics are primarily occurring in locales already plagued by an unsavory range of conditions, and hence identified as a syndemic, including: under-employment, de-industrialization, poverty, inequality, and HIV spread [199-204]. In 2017 the U.S. Department of Health and Human Services (HHS) declared a public health emergency, stating that the USA is currently in an ongoing opioid epidemic [205, 206]. With over 2.4 million Americans qualifying to be classified as having severe opioid use disorders (OUD) [206]. In 2014 alone, there was 150% additional drug overdose deaths than motor vehicle accident deaths [206, 207]. Opioids generate a potent analgesic affect and are therefore useful in treating the estimated one-third of Americans suffering from chronic pain or trauma-associated pain [208]. Analgesic drugs, such as opioids, play a vital role in pain management, relieving acute severe pain via its action on the μ-opioid

receptor, reducing perceived non-cancer pain by 30% [208, 209]. With a wide variety of opioid analgesics prescribed to manage chronic pain annually, in the USA, opioids have become the most prescribed class of medication [209, 210]. In 2015, the prevalence of opioid misuse in the USA was 21.7–29.3% and the prevalence of addiction was 7.8–11.7% [209]. This differs from the previous epidemic in the 1980s, which was primarily driven by heroin and crack; with the widespread and improper use of opioid analgesics having led to the current opioid epidemic [210]. Opioids interact with multiple systems and organs, including the immune system [208]. Binding of the μ-opioid receptor grants opioids the ability to modulate immune and physiological processes, including addiction, via binding to the opioid receptors, greatly increasing the likelihood of abuse [208]. Recently, there has been an increase in worldwide illicit usage of heroin, fentanyl, and prescription opiates [211]. This abuse tripled since the 1990s and opiate overdose deaths have risen by 200% since 2000, in the USA [211]. The CDC estimates that 130 people die in the USA daily as a result of these opiate overdoses [212]. At the center of this crisis, heroin and fentanyl, a short-acting synthetic opiate 100-fold more potent than heroin, have resulted in deaths due to legal prescription overdoses; with an increase in heroin abuse deaths of 26% and fentanyl abuse by 80% [211]. Opiate abuse increases risk of HIV transmission and exacerbates HIV neuropathology by increasing inflammation, and modulating immune cell function [165, 208, 213, 214].

HIV and Opiates

There is a large body of evidence demonstrating the relationship between opiate abuse and HIV-1 co-exposure, exacerbating and hastening the onset of HIV encephalitis

among other neurodegenerative conditions [215]. Additionally, opiate abuse has been shown to exacerbate HIV transmission and neuropathology [216-220]. Opiate over-consumption and intravenous use significantly contributes to transmission of HIV among opiate abusers [221-223]. Approximately 11% of positive HIV infection diagnoses among adolescents and adults, in 2011, were a result of injection drug users (IDUs) [201]. According to the CDC, this statistic has not changed much as in 2018, adolescents and adult IDUs accounted for 10% of the 37,968 new HIV diagnoses in the USA and dependent areas [224]. Additionally, 37% of new HIV diagnoses in 2018 were specifically male IDUs [224]. Studies demonstrate that IDUs which are HIV positive are economically and socially relegated, confronting life-altering circumstances such as social exclusion, homelessness, addiction, and violence [224]. In addition to facilitating viral spread, opiate abuse may modulate HIV-1 pathogenesis. Alone, opiate abuse increases glial activation, induce neuro-inflammatory pathways, and produce changes in the gene expression and conformation of tight junction proteins [214]. These effects generate Blood Brain Barrier (BBB) dysfunction, increased BBB permeability, and increase the brain's vulnerability to peripheral toxins [214]. Co-exposure of HIV and opiates enhances HIV neuropathogenesis via elevating monocyte entry into the CNS, increasing adhesion of monocytes and Peripheral Blood Mononuclear Cells (PBMCs) to the endothelium, thereby impairing BBB integrity and permeability[225]. Opiates have been demonstrated to activate HIV-1 in microglial cells, which are critical mediators of neuroinflammation and a major contributor in immune defense within the CNS [226]. Given that greater than 50% of all patients positive for HIV-1 develop HIV-1-associated neurocognitive disorder (HAND), and that the cells within the CNS which are

predominantly infected by HIV-1 are microglia; it is probable that infected microglia promote HIV-associated neurotoxicity [227]. Although HIV-1 infects astrocytes and results in EV-bound HIV-Nef-derived vascular dysfunction of endothelial cells, HIV-1 is primarily retained and concentrated within the largest cellular reservoir in the brain, infiltrating macrophages and brain microglia [227-233]. Given this data, neurotoxic viral proteins and virions are primarily found to be produced from microglia and macrophages. HIV-1 infected microglia have been shown to secrete or induce other neuronal cells to generate neurotoxic factors, which may contribute to HAND [234-239]. Some of these microglia-derived neurotoxins include: quinolinic acid, glutamate, platelet activating factor, NTox, arachidonic acid including consequent metabolites, nitric oxide, and pro-inflammatory cytokines such as TNF-α or IL-1β [234-239]. Therefore, it may be possible for opiates to modulate HIV-1-associated neuropathology via altering microglia and macrophages. Although neurons are not susceptible to HIV-1 infection themselves, they suffer injury and sub-lethal neuronal stress as a result of HIV-1 infected cell-derived viral protein release, leading to hyperexcitability [240]. For example, HIV-1 transactivator of transcription (Tat) depolarizes neurons exposed to it, resulting in the aforementioned hyperexcitability and electrophysiological dysfunction via interactions with α-amino-3-hydroxy-5-methyl-4-isoxazolepropionic acid (AMPA) and N-methyl-D-aspartic acid (NMDA) receptors; tat also interacts with opiates activating macrophages, microglia, and enhancing the expression of cytokines, in vitro. [241-248]. In another example, HIV-1 glycoprotein gp120, which is critical for viral entry, causes neurotoxicity and inflammatory effects via binding to HIV co-receptors C-X-C chemokine receptor type 4 (CXCR4) or C-C chemokine receptor type 5 (CCR5) [249-252]. Further supporting the

link between HIV-1 infection and opiate comorbidity is a recent study which investigated the synergism between HIV-1 gp120 and opioids, demonstrating that morphine increased the RNA expression of IL-12p40, CXCL10, CCL2, CCL5, and IFNβ, in immunocompetent gp120tg+ mice [253]. HIV-1 infection and opiate use comorbidity have been linked to an increased severity of HAND [254-257]. This comorbidity is exemplified by communities confronting a rise in the abuse of prescription opiates, such as oxymorphone, a semi-synthetic opioid analgesic, as HIV-1 outbreaks rose as a result of an increase of syringe-sharing [197]. In our studies we used morphine as our opiate of choice, given that heroin, in humans, is rapidly metabolized to 6-acetylmorphine (6-AM), and then further metabolized to morphine and morphine conjugates [258]. In order to determine the concentration of morphine that should be used to investigate potential synergistic effects with HIV-1, studies involving opiate overdoses, resulting in deaths, and average levels of morphine found in the blood of addicts or patients; this data allowed us to then select a potential optimal dose alongside a two more doses, (1) a 10-fold decrease from the dose of interest and (2) a 10-fold increase from the dose of interest. One study investigating the relationship between postmortem morphine concentrations and co-detected psychoactive drugs in fatal overdoses revealed that morphine was present in 159 out of 160 cases with morphine concentration reported to be at a range from as 20ng/ml to 2000ng/ml [259]. Minett et al. found the mean morphine concentration in these overdosed individuals, post-mortem, to be 261.1ng/ml, which equates to a concentration of 915nM [259]. If the lower end of the morphine concentration spectrum is used, the aforementioned 20ng/ml concentration, then a potential lethal dose could be as low as 70nM. Given that these cases are of individuals

who are deceased as a result of opiate-overdose, the observed morphine concentrations may serve to denote a potentially lethal dose of morphine. This data creates a large potential range, as the cases investigated by Minett et al., may have died as a result of a combination of drugs and not just opiates, therefore more studies are necessary before settling on a range of morphine concentrations of interest to investigate [259]. In another study, the concentrations of free-morphine, in overdose deaths and in apprehended drivers, present in the peripheral blood after recent heroin use was investigated [260]. As expected, the median concentration of free-morphine in blood was observed to be higher in autopsy cases (0.24 mg/L, $N = 766$) relative to cases in which the drivers were detained with 6-monoacetyl morphine (MAM) in blood (0.15 mg/L, $N = 124$, $p < 0.05$); additionally, drivers which presented with 6-MAM in urine and none in displayed a large drop in blood-bound morphine (0.03 mg/L, $N = 1,823$, $p < 0.001$) [260]. This equates to a morphine concentration of 841.1nM in overdose cases, 525.68nM for cases in which drivers were arrested, and 105.13nM for the largest grouping of cases, which did not present with 6-MAM in urine [260]. This data further narrows down a potential median value of interest of morphine concentrations to 105nM to 525nM, more data is still needed to further refine this selection. In a study comparing the blood toxicology of current heroin users and heroin-related deaths in south western Sydney found that, among fatal cases, the median blood morphine concentration was 0.35mg/L, which is equivalent to a concentration of 1.22μM [261]. However, the blood morphine levels of current heroin users were found to be 0.09mg/L, equating to 315.4nM. This study further narrowed the median value of interest to the range of 105nM and 315nM. In a study which investigated the blood morphine concentrations, among other opiates and their

derivatives in impaired drivers found that the median concentration of morphine among impaired drivers was 0.03mg/L (N = 2,029) and a mean of 0.046mg/L (N = 2,029), similar to the abovementioned study [262]. This equates to a concentration of 105.13nM and 161.21nM, respectively. With this last data point, we generate a new range containing the median concentration of interest: 161nM – 315nM. The average of these two values is 238nM, however, some of the aforementioned studies reported a greater frequency of individuals possessing blood morphine levels under 200nM, as such the morphine concentration of 200nM was selected as the median value of the morphine dosages of interest, with the other two concentrations used being 20nM and 2µM.

CNS infiltration by HIV-1 and immune cells through the blood brain barrier

Key in the prevention of toxic substances entering the CNS, is the BBB, a brain-specific capillary barrier [263]. The BBB limits the exchange of mediators and inflammatory cells under physiological and pathological conditions [263]. The BBB is mainly formed by astrocytes and pericytes surrounding microvascular endothelial cells (Figure 5) [263]. The vascular aspect of the perivascular space is demarcated by the endothelial basement membrane [263]. However, the parenchymal aspect of the perivascular space is composed of the basement membrane and the glia limitans formed from astrocytic endfoot processes [263]. The physical barriers preventing cellular access to the CNS are the aforementioned glia limitans and the endothelial layer, representing the parenchyma [263]. Additionally, microglial and neuronal processes contribute to the glia limitans [263]. BBB function is enhanced by the interactions between these processes,

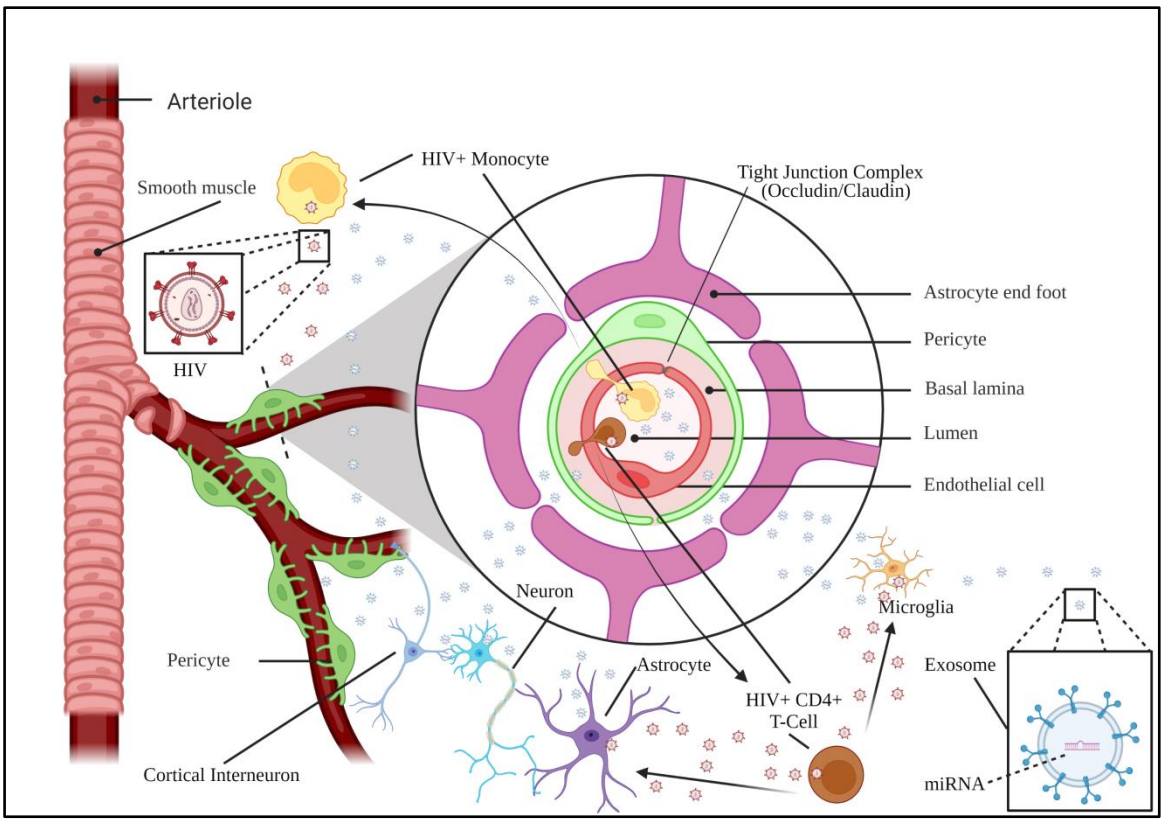

Figure 5: A cross-sectional model of the BBB depicting HIV intrusion into the CNS and related factors. HIV-infected monocytes and CD4+ T-cells cross the BBB via either paracellular or transcellular transmigration. This results in HIV release within the CNS, infecting astrocytes and microglia. Additionally, exosomes are being released from all neighboring cells, transporting miRNAs which may either ameliorate or facilitate HIV-associated neuropathology by silencing target genes. However, HIV will modulate miRNA expression, thus altering expression of genes involved in the immune response, apoptosis, the neuronal system, and membrane trafficking. Figure was created with BioRender.com

surrounding cells, and endothelial cells, resulting in the preservation of proper brain homeostasis [263].First let us examine the three main cellular components of the BBB.

Astrocytes

Separated by only a thin basal membrane, the endfeet processes of astrocytes are essential components of the BBB, with astrocytic endfeet covering 99% of the brain microvessel surface [264]. As a source of vital regulatory factors, astrocytes are capable of supplying

endothelial cells with secreted factors such as: the fibroblast growth factor (FGF), glial-derived neurotropic factor (GDNF), and transforming growth factor-β (TGF-β) [265-268]. It is understood by the scientific community that various characteristics of BBB physiology are regulated by astrocytes regulate with the use of secreted factors, influencing BBB features including: its expression in endothelial cells, formation of tight junctions, and permeability [269].

Brain Microvascular Endothelial Cells

BBB function is directly mediated by brain microvascular endothelial cells (BMVECs) [263]. BMVECs function as mediators between the brain and the blood, BMVECs rest on a basement membrane consisting primarily of proteoglycans, fibronectin, collagen IV, and laminin [270]. BMVECs possess low pinocytic activity, uninterrupted intercellular tight junctions, specialized transport systems, a significant degree of mitochondria, uniform thickness without any transendothelial fenestrations, limited paracellular flux, and the repulsion of compounds carrying a negative charge by a negatively charged luminal surface [263, 271, 272]. Specific transport and carrier systems are responsible for the uptake of crucial molecules [273, 274]. Furthermore, as a result of the adherens junctions and uninterrupted tight junctions present, the paracellular space is nearly fully sealed [273, 275-278]. Of note, the BMVECs may both grant energy and regulate the metabolism and transport of substances across the BBB, from blood to brain, and from the parenchyma to the systemic circulation; this is facilitated by their relatively abundant number, when compared to endothelia in other organs, therefore possessing a greater number and volume of mitochondria [279].

Pericytes

As essential cellular constituents of post-capillary venules and capillaries, Pericytes boast the highest degree of BBB vessel coverage, covering 22–32% of the capillaries in the CNS and sharing with the endothelial cells, the basement membrane [263, 280-282]. Pericytes are responsible for the regulation of various neurovascular functions, including: vascular stability, angiogenesis, clearance of toxic cellular products, capillary blood flow regulation, the formation of the BBB during embryogenesis, and maintenance [283]. By secreting factors such as TGF-β, pericytes are capable of regulating the tight junction molecule expression in endothelial cells [268]. BBB function is enhanced by TGF-β inhibiting endothelial cell proliferation and leukocyte migration [263]. Lastly, critical for the maintenance and recruitment of pericytes on vessels and vascular maturation, is the endothelial cell-secreted platelet-derived growth factor-β (PDGFβ) [284, 285]. The three primary cellular components which compose the BBB have now been reviewed; however, how do immune cells pass through a barrier composed of the abovementioned cells?

Leukocyte Intrusion into the CNS

The full breadth of this topic is beyond the scope of this dissertation, however, we will review the essentials needed to understand immune cell intrusion through the BBB. Additionally, we will note that there are several routes that leukocytes may exploit to cross into CNS, though not all were investigated in our studies, such as: migration into the subarachnoid and Virchow-Robin perivascular spaces through the post-capillary venules at the pial surface, migration into the cerebrospinal fluid via the choroid plexus,

migration into parenchymal perivascular space from microvessel [263, 286-288]. These abovementioned routes comprise the crossing of the blood–spinal cord (BSC) barrier, the blood–cerebrospinal fluid (CSF) barrier, and the BBB [288, 289].

A multi-step process is required for transendothelial leukocyte migration across the BBB and is characterized by a series of tightly controlled and sequential steps [263, 290-293]. In general, there are five steps, which are: (1) rolling: leukocytes weakly adhere to endothelial cells via interactions between selectins and their carbohydrate counter-receptors; (2) activation: chemokine stimulation of G-protein-linked receptors activate leukocytes, leading to the surface adhesion molecule activation; (3) arrest: attachment of leukocytes to the endothelial cells via interactions between integrins associated with endothelial cell-bound cell adhesion molecules (CAMs) and leukocytes; (4) crawling: the targeting of ideal sites of transmigration by leukocytes; (5) and lastly, transmigration: partially driven by chemokine–chemokine receptor interactions, leukocytes migrate across the CNS endothelia entering the perivascular space, advancing across the glia limitans and finally entering the brain parenchyma [263]. Here we will quickly review the next step, in which microglia induce neuroinflammation as a result of chemokine release. Microglia function as both a chief mediator of neuroinflammatory processes and as the primary source of immune defense within the CNS [233]. Microglia have been reported to activate and migrate to the lesion site as a result of insult or neuronal injury, such as unrestrained HIV replication [233]. The primary role of activated microglia is presumably to commence reparative measures of affected areas via the removal of dying cells and debris and/or through the release of immunomodulary and growth factors which

promote neuronal survival [233]. Nonetheless, there is an increasing amount of evidence demonstrating that, if over-activated as a result of a neurodegenerative disease or severe injury, microglia exhibit neurotoxicity potentially leading to the release of an assortment of immune cytokines including IL1β, TNFα, and other neurotoxic factors; this results in neuronal death [233, 294, 295]. For example, in patients presenting with severe HIV encephalopathy, in-vivo PET studies and postmortem examinations and with 11C-PK11195, a ligand selective for the 18 kDa translocator protein (TSPO) isoquinoline site which activated microglial cells express, have demonstrated an increase in microglia activation [296, 297]. In the current post-ART era, postmortem examination of asymptomatic HIV-infected patients has revealed an increased activation of microglia, indicating an ongoing neuroinflammatory process [233]. Overall, microglia activation induces pro-inflammatory marker release and modulation of secondary messengers , cytokine secretion, reactive oxygen species (ROS), and chemokines which result in the activation of signaling pathways which then initiate neuroinflammation [227]. Additionally, inflammation and ROS have key roles in HAND [227]. In fact, chemokines and cytokines which induce cell migration or chemotaxis are produced by microglia, astrocytes, and neurons; such as monocyte chemoattractant protein CCL2/MCP-1 and CX3CL1/Fkn, which has been reported to attract PBMCs to the brain parenchyma from the BBB [298-300]. HIV exploits this in order to cross the BBB, infect the microglia present there, and establish a viral reservoir in the CNS leading to neuroAIDS. For example, chemotaxis of microglia has been reported to be promoted via opiate-induced changes in astrocytes and HIV-1 Tat modulating chemokines and monocyte chemoattractant protein-1 (MCP-1) expression [301]. Additionally, neuroAIDS may be

exacerbated through opiates by promoting microglial activation and macrophage entry accompanied by a buildup of astroglial-derived proinflammatory chemokines at locations key to CNS infection [301]. Studies have demonstrated the capacity of HIV to cross the BBB via infected macrophages and entering the brain resulting in HIV-induced disruption of the BBB from within the brain [227, 302-305]. In another study, striatal neuronal cultures treated with both HIV-1 Tat and morphine were found to interact, increasing intracellular Ca2+ and enhancing mitochondrial dysfunction], therefore implying that HIV and drugs of abuse interact, disturbing brain bioenergetics [227, 306, 307]. In our study, we employed an *in-vitro* BBB Transwell model similar in design to the model described in Stone et al., 2019, but with some noticeable differences [308]. We used primary human brain microvascular endothelial cells (HBMECs), human brain vascular pericytes (HBVPs), and human astrocytes (HAs) as the three primary cell populations which comprise our BBB layer. The HBMECs were seeded on the apical, or blood side, whilst the HBVPs and HAs were seeded upon the basolateral, or brain, side. Seeded below the BBB, on the bottom of the well in the basolateral side was the human neuroblastoma cell line, SH-SY5Y, so that any changes in neuronal function could be ascertained. In addition to investigating the impact of HIV-1 on the integrity and permeability of the BBB, a potential nano-therapeutic capable of crossing the BBB was tested to examine the potential to delivery therapeutic agents across the BBB to ameliorate HIV-associated neuropathology. The nano-carrier selected was an exosome modified with a therapeutic agent and a magnetic nano-particle (MNP) to improve targetability. HIV-1 targets both macrophages and T-lymphocytes via the primary receptor CD4 and coreceptors CCR5 or CXCR4; thus inducing apoptosis of CD4+

receptor T-lymphocytes and weakening the host immune system [309, 310]. With over 75 million infected individuals worldwide, HIV remains an epidemic and one of the greatest causes of morbidity and mortality [310]. Even though antiretroviral therapy (ART) successfully restricts HIV-1 infection often reducing viral loads below detection, challenges continue [46, 310]. Retroviruses are unique in that they have both lytic and latent life cycles. ART is not curative due to either the failure to eliminate latent virus reservoirs, treatment toxicity, viral mutations, or divergent patient responses to HIV infection, therapies, or adherence [46, 310]. Therefore, comprehending the HIV-1 interaction with immune cells is integral to elucidate novel aspects of HIV-1 infection, which could be developed as therapeutic targets [46, 310].

HIV-1 particles and exosomes share some aspects, such as molecular properties, biogenesis and mechanisms for cellular uptake, all of which are beyond the scope of this review [46]. Given the HIV lifecycle, there are critical points in viral assembly that intersect EV biogenesis, therefore exosomal EVs play a critical role in HIV-1 pathogenesis [311]. This indicates a role for exosomes in HIV-1 pathogenesis, which is covered here [46].

EV Interaction with Host Cell Restriction Factors and HIV

EVs contribute to antiviral responses by delivering host-derived restriction factors to nearby cells. For example, in vitro studies demonstrate that the host cell viral restriction factor cellular cytidine deaminase APOBEC3G (A3G) is contained within EVs from CD4+ T-cells. A3G inhibits HIV-1 replication by interfering with HIV-1 reverse transcription in both a deamination-dependent and deamination-independent manner,

catalyzing hypermutation of the viral DNA [312-314]. However, this effect is not observed in vivo, as A3G is depleted post-HIV-1 infection, leaving an insignificant quantity of EV-bound A3G incapable of exhibiting an antiretroviral effect [46, 314].

CD4+ T-lymphocytes release exosomes with CD4 on the surface, thereby competing with cells for binding to HIV-1 virions. The CD4+ EVs can potentially restrict HIV in several ways: acting as a decoy for CD4+ T-cells, neutralizing HIV-1 virions, or protecting neighboring T-cells from infection ultimately inhibiting HIV-1 spread. These effects of CD4+ exosomes can be countered by the HIV-1 accessory protein, Nef, which reduces CD4 expression in T-cells [46, 315]. CD4+ EV effects suggest that CD4+ T-cells utilize exosomes to protect against HIV-1 infection, indicating a role for EVs in antiviral immunity.

Immune Cell-Derived EVs and Antiviral Effects

Similar to CD4+ T-cells, CD8+ T-cells release exosomes that restrict HIV-1 replication. CD8+ T-cell-derived EVs contain an anti-HIV protein moiety that suppresses replication without EV internalization. This indicates that exosome-mediated HIV-1 transcription suppression may comprise of an intracellular signaling pathway [316]. EVs contain components of toll-like receptor (TLR) innate antiviral pathways. For example, exosomes derived from toll-like receptor 3 (TLR3)-activated human brain microvascular endothelial cells (HBMEC) block HIV-1 infection to the CNS via transport of antiviral factors and IFN-stimulated genes (ISGs), transferring anti-HIV protection to macrophages [317]. Macrophage and CD4+ T-cells, enriched in the gastrointestinal system (GI), are protected against HIV-1 by EVs released from TLR3-activated intestinal

epithelial cells (IECs) containing HIV-restriction miRNAs (miRNA-20 and miRNA125b) and ISGs (ISG15, OAS-1, and Viperin) [318]. These mechanisms demonstrate that EVs interact with cellular barriers (BBB/GI) via TLR pathways to promote innate antiviral immunity [317, 318].

EVs are found within most bodily fluids including, blood, breast milk, semen, and vaginal fluids, hindering HIV-1 infection throughout the body [319-323]. Vertical transmission of HIV-1 can be inhibited by breast milk-derived EVs that bind DC-SIGN receptors, thereby preventing HIV-1 from binding, and potentially inhibiting HIV interaction with monocyte-derived dendritic cells (MDDCs) and HIV-1 transfer to CD4+ T-cells [322]. Sexual transmission of HIV-1 is inhibited by EVs derived from uninfected semen or vaginal fluid-derived EVs, negatively affecting reverse transcriptase activity [320, 321]. Heterosexual transmission of HIV-1 is facilitated by vaginal epithelial cells (VECs) uptake of semen-derived EVs, containing functional viral mRNA, facilitating viral spread as evidenced in a murine AIDS model [320]. However, in a human transwell model using VECs, semen-derived EVs inhibited HIV-1 spread [320]. EVs play a dichotomous role in modulating HIV-1 transmission, both restricting and enhancing viral spread [321, 322].

EV-Mediated Enhancement of HIV-1 Infection

EVs also enhance HIV-1 pathogenesis and infection [46]. HIV-1 infection/pathogenesis disrupts the endomembrane system and modulates EV cargo, biogenesis, targeting, and/or release frequency [46]. For example, PBMCs release microvesicular EVs containing CCR5, transporting them to neighboring cells deficient in

CCR5, enhancing cellular susceptibility to HIV-1 [324]. Megakaryocytes release EVs containing CXCR4, delivering the HIV-1 coreceptor to nearby tissues lacking CXCR4 expression, facilitating viral spread [325, 326].

EVs also assist in HIV-1 entry by interacting with HIV-1 virions, which contain high concentrations of phosphatidylserine (PS), a hallmark of apoptosis. PS interacts with T cell immunoglobulin and mucin proteins (TIM-4), which is highly expressed in EVs. TIM-4 binding to HIV-1 PS surface-bound moieties results in increased exosome-mediated trafficking of HIV-1 to immune cells [327, 328]. HIV-1 entry into human T-cell and monocytic cell lines can be enhanced by exosomal tetraspanins CD9 and CD81 [327, 328]. Blocking of TIM-4 or any of these tetraspanins, with antibodies, result in significant blockage of viral entry, supporting an exosome-dependent mechanism for HIV-1 entry [327, 328]. TIM-4 has also been shown to function as an EV and apoptotic cell phagocytic receptor as a result of recognition of the exposed PS moieties [329, 330]. HIV-1 can evade immune surveillance by camouflaging itself within exosome aggregates, facilitating viral spread [331].

Additionally, exosomes derived from HIV-1 infected primary cells are abundant with transactivating response (TAR) element RNA, which has been demonstrated to enhance undifferentiated naïve cell susceptibility to HIV-1 infection [332]. Primary macrophage exposure to these HIV-1 infected cell-derived exosomes promotes macrophage release of proinflammatory cytokines, TNF-β, and IL-6, indicating EV-mediated modulation of proinflammatory cytokine gene expression [332]. EV-mediated enhancement of HIV-1 infection is not restricted to exosomes, as apoptotic bodies generated during HIV infection inhibit the function of dendritic cells (DC), resulting in decreased DC-

dependent cytokine production and T/NK-cell priming, via DC-CD44 receptor binding of apoptotic microvesicles [4]. Taken together, HIV–EV interactions exploit apoptotic clearance mechanisms and facilitate viral replication and host cell viral uptake [46, 329, 330, 333].

Besides facilitating viral entry, EVs transfer active HIV-1-derived molecules to bystander cells, promoting viral infection [334]. HIV-1 infected cells release EVs

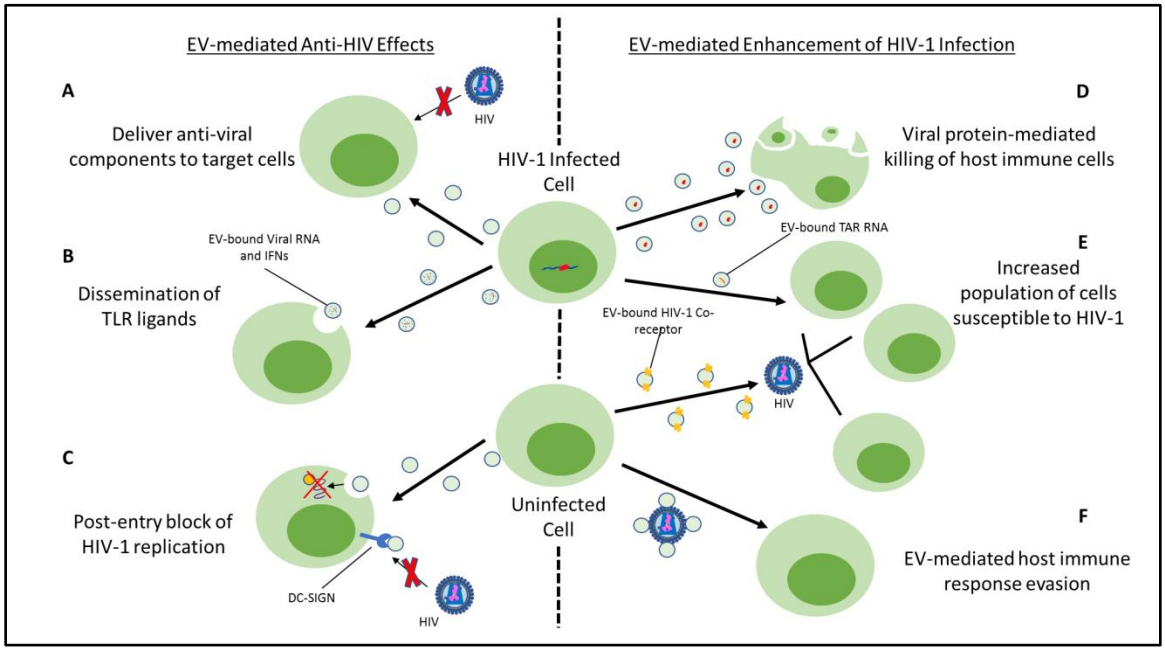

Figure 6: HIV-1 infected cell-derived EV-mediated anti-viral and pro-viral effects. Upon infection with HIV-1, cells release EVs which may modulate HIV-1 pathogenesis, either restricting infection or enhancing it. (A) EVs can deliver anti-viral particles, such as A3G, inhibiting HIV-1 replication. (B) EV-mediate dissemination of TLR ligands, including HIV-restriction miRNAs, ISGs, IFNs, and anti-viral factors transfer anti-HIV protection and alert neighboring cells of ongoing infection. (C) EVs derived from bodily fluids such as breast milk, semen, and vaginal fluids can hinder HIV-1 infection by blocking HIV-1 replication after viral entry or competing with HIV-1 for receptor access. Breast milk-derived EVs compete with HIV-1 binding to the DC-SIGN receptor, preventing vertical transmission. Internalization of either semen or vaginal fluid-derived EVs results in deleterious effects upon HIV-1 reverse transcriptase activity leading to a post-entry block of HIV-1 replication. (D) EV-mediated transport of viral particles, such as HIV-1 Nef protein, triggers viral-mediated apoptosis of anti-viral immune cells. (E)

Transport of HIV-1 chemokine co-receptors CCR5 or CXCR4 via EVs to cells deficient in these receptors, generates new populations of cells which are now susceptible to HIV-1 infection. HIV-1 infected primary cell-derived EVs carry TAR element RNA, enhancing susceptibility to HIV-1 infection in undifferentiated naïve cells. (F) Lastly, EVs may aggregate upon the HIV-1 virion as a result of exploitation of exosomal surface properties, camouflaging HIV-1 and facilitating viral spread to uninfected innate and adaptive immune cells.

containing the HIV-1 envelope (Env) protein (gp120), Gag, and Nef. EVs containing gp120 significantly raise HIV-1 infectivity in lymphoid tissues [334-337]. Nef, an accessory protein responsible for modulation of protein trafficking within host cells and HIV-1 pathogenicity, is known to be released within EVs [338-340]. EVs-containing Nef have been identified at high concentrations in the plasma of HIV-1 infected patients. Nef-containing EVs function to promote EV secretion, increased MVBs within cells, and induces apoptosis within CD4+ T-cells [338-341]. Given that Nef has several functions, Nef-EVs could potentially promote decay of CD4+ T-cell populations, promote CD8+ T-cell activity, CXCR4-mediated apoptosis, and ADAM17 activation increasing CD4+ T-cell permissiveness to HIV-1 [342-346]. Viral components enhancing HIV-1 infection are not limited to viral proteins. Through coevolution with the host, HIV-1 presents with differential miRNA content relative to uninfected cells, facilitating suppression of host RNA interference (RNAi) [347, 348]. EVs from HIV-1 infected macrophages and plasma contain HIV-1-derived miRNAs: vmiR88 and vmiR99, promoting macrophage release of TNF-α via TLR8 activation thus supporting chronic immune activation [349]. Exosomal and cellular miRNA profiles are modulated by the HIV-1 Nef protein, affecting both

HIV-1 pathogenesis and viral replication modulated by host RNAi [350]. EV-encapsulated miRNAs can alter HIV-1 pathology and enhance an infection similar to proteins.

HIV-1 crosses the BBB, enters the CNS, infecting astrocytes and microglia, causing chronic neurologic disease [351]. BBB permeability and integrity are disrupted by microglia-derived Nef-EVs, which reduce zonula occludin-1 (ZO-1), lower tight junction (TJ) protein expression in HBMECs, and increase TLR-induced chemokines and cytokines [352]. This loss of BBB integrity would induce some degree of neuropathology. For example, Nef-EVs are elevated in the plasma of individuals with HIV-1-associated neurocognitive disorders (HANDs), suggesting a role of exosome-encapsulated Nef in HIV-1 neuropathology [338]. Overall EVs enhance and restrict HIV-1 infection through various methods, summarized in (Figure 4).

EVs as Nano-Therapeutics

Potential treatments against viral infections are currently being investigated and range from vaccines to therapeutic drugs [353, 354]. Antiviral agents must be carried across cellular barriers, such as the placental barrier (PB) or the BBB, to reach target cells [354]. Development of EVs as nanocarriers to transport therapeutic agents across the PB may provide a drug/gene delivery system capable of treating a ZIKV infection in-utero or delivering therapeutics across the BBB to treat a neurotropic virus infection of the CNS.

EVs are capable of transporting both hydrophobic and hydrophilic molecules. Hydrophilic compounds stored in the interior and hydrophobic agents embedded within the lipid membrane. However, unlike liposomes, exosomes are not optimized for the

encapsulation of hydrophilic macromolecules [118]. Thus, liposomes can carry both hydrophobic and hydrophilic drugs and molecules to a target site, whereas exosomes will face challenges in encapsulation of hydrophilic agents [118]. Additionally, the loading capacity of the exosomes is low due to the presence of proteins and nucleic acids already within [118]. To improve cell targeting, exosomes may be generated by cells expressing ligands with a high binding affinity to the target cells. However, for liposomes, using a functionalized polymer to coat the liposome, generating a nanobin that improves targeted drug delivery [118]. For neurotropic viruses, EVs could deliver therapeutics across the BBB potentially reducing viral-associated neuropathology [352, 355]. Inhibition of the ESCRT machinery is a promising option for HIV-1 therapeutics since HIV-1 appropriates ESCRT. TSG101 disruption via the small molecule inhibitor FGI-104 could prevent HIV-1 pathogenesis [356]. More research is needed to elucidate both the mechanism of action and potential side effects of FGI-104. Overall, given EV properties, EVs may serve as the next class of antiviral therapeutics, with fewer side effects and greater biocompatibility.

EVs play dichotomous roles in viral infections and pathology. In this dissertation we summarized clinically relevant viruses shown to interact with EVs and EV-mediated effects on viral infection and pathology. Not only are EVs critical for intracellular communication, they may also represent a novel innate antiviral mechanism. Viruses exploit the EV biogenesis pathway to promote: viral infection, replication, spread, and pathology. Aside from promoting their pathology, viruses use EVs to modulate antiviral immune responses.

CHAPTER 2

ZIKV Envelope protein induces apoptosis in primary placental human trophoblast and proliferating neuronal cells

Abstract

Primary human villous trophoblasts (HVTs) are permissible to Zika virus (ZIKV) infection. Similar to neuronal progenitor cells, HVTs undergo apoptosis upon infection by pathogenic strains of ZIKV. HVTs infected with FLR produced a relatively higher titer of ZIKV and underwent apoptosis, whereas MR766 infected HVTs produced lower titers and a lesser degree of apoptosis. ZIKV-EP was found to be cytotoxic to differentiated neuronal cells and was also found to disrupt the integrity and permeability of the placental barrier. In addition to neuronal cells, microglia, PBMCs, and human villous Trophoblasts (HVTs) are also susceptible to ZIKV infection. ZIKV pathogenic strain, FLR, induces differential gene expression and miRNA expression, modulating inflammation and immune function. ZIKV infection of primary placental trophoblast and proliferating neurons by the ZIKV pathogenic strain, FLR, not only promotes gene expression which restricts anti-viral mechanisms but also induce apoptosis. Overall, this study will lead to the understanding of the role of exosomes in ZIKV neuropathology and the development of an exosome-based therapeutic against ZIKV infection *in utero* that could be of great translational significance.

Introduction

Zika virus (ZIKV) is an emerging arborvirus which originated in Uganda, Africa, spread to Asia, French Polynesia, and is now an epidemic in the Americas [357-359]. The primary transmission vector for ZIKV is via the bite of an infected *Aedes aegypti mosquito* [359]. The African strains of ZIKV have been shown to harm the fetus, cause fetal deaths, and be highly virulent; however, they do not cause microcephaly as the

Asian lineage of the virus has been reported to possess a greater degree of neurovirulence [360-362]. It has also been postulated that the primary contributing factor to the sudden spread of ZIKV throughout Asia, and eventually, the Americas, was adaptive mutations permitting more efficient mosquito vector transmission [363], yet another factor differentiating the two lineages. As such, the African strain is considered to be non-pathogenic, while ZIKV Asian strains are considered to be pathogenic.

ZIKV infection, with the Asian lineage of the virus, is associated with congenital microcephaly, Guillain-Barré syndrome, and meningoencephalitis [364-368]. Additionally, ZIKV may be transmissible sexually and even via asymptomatic carriers [369-374]. ZIKV has become a global threat, given: the association of neurological damage inflicted on the fetal brain, that infected individuals not presenting with any symptoms may unknowingly infect others via sexual transmission, in addition to the already vast range of the *Aedes aegypti* mosquito vector.

Extracellular vesicles (EVs) such as exosomes are released from activated or virally infected cells and can modulate immune responses in nearby recipient cells [375-379]. During healthy pregnancy the placenta releases increasing amounts immunomodulatory exosomes during the first trimester into the maternal circulation [380-384]. These exosomes are currently being developed as a biomarker of abnormal placentation related disorders such as pre-eclampsia [385-389]. Thus exosomal extracellular vesicles are potentially pivotal in pregnancy and may play a role in protecting the fetus from poor oxygenation, inflammation, and viral infections. Viruses such as Epstein Barr Virus and Herpes Simplex virus exploit the exosome biogenesis

pathway and cause infected cells to release exosomes containing factors that block antiviral responses in recipient cells [390-399]. Given that Hofbauer cells (HCs), macrophages within the placenta are susceptible to ZIKV infection, we expect exosomes derived from the placental macrophage will enter the fetal compartment and deliver their contents [400-402]. For now, it is unclear how placenta- cell derived exosomes impact anti-ZIKV responses in the host.

Several reports have shown that Neuronal progenitor (NPs) within the fetus are cellular targets of Zika Virus (ZIKV) [403-406]. However, for the virus to enter the fetal compartment, ZIKV must infect a maternal cell and/or cross at the site of maternal-fetus blood exchange [407-410]. Here we show that cells in the periphery as well as placental trophoblasts are permissive to ZIKV infection. Additionally, we investigated whether other cell types were permissive to ZIKV infection and the impact of ZIKV or viral components on cells integral to the placenta/fetus. We hypothesize that ZIKV disrupts exosome-mediated protection during pregnancy and that ZIKV/exosomes negatively impact neuronal cells in the developing fetus by dysregulating cellular functions and/or inducing cell death thereby causing the neuronal loss. Exposure to ZIKV E-protein (EP)(100 ng/ml of) induced apoptosis in neuronal cells. ZIKV-EP was cytotoxic to differentiated neuronal cells and was most effective in the first 24h after exposure. ZIKV EP disrupted the integrity and permeability of the placental barrier. In addition to neuronal cells, microglia, PBMCs, and human villous Trophoblasts (HVTs) are also susceptible to ZIKV infection. Lastly, the ZIKV pathogenic strain, FLR, induces

differential gene expression and miRNA expression, modulating inflammation and immune function.

Material and Methods

Primary human trophoblasts, SH-SY5Y Neuroblastoma Cell Line and Cell culture Human villous trophoblasts (HVTs) were grown in T75 flasks (Corning) for 72 hours within complete growth media, composed of Trophoblast Media (Sciencell) with 10% exosome-depleted fetal bovine serum (XF-FBS) (Gibco) and 1% Penicillin-Streptomycin (PS) (Gibco). The HVT cells will be incubated with virus diluent containing either the non-pathogenic ZIKV-MR766 strain or the pathogenic ZIKV-FLR strain at a multiplicity of infection (MOI) of 0.1 at 37°C for 1 hour. The cells were then washed with PBS and the media was changed back to complete media with XF-FBS. HVT cells were harvested at 3dpi. SH-SY5Y Human Neuroblastoma Cells (ATCC CRL-2266) were grown in complete media consisting of F12 (Gibco) and EMEM (Quality Biological) at a 1:1 ratio with 10% FBS (Gibco) and 1% PS. The neuroblastoma cells were grown as per manufacturer's instructions. Neuroblastoma cells were treated with 100 ng/ml β-NGF, for 72 hours. After 72h, the neuronal cells were treated with increasing dosages of the ZIKV Envelope protein and incubated for 24, 48, or 72 hours. The viability of neurons after β-NGF induced differentiation was assessed via measurement of caspase-3 activity

Caspase-3 Assay

The EnzChek™ Caspase-3 Assay Kit #1, Z-DEVD-AMC substrate (Thermo Fisher Scientific) was employed to ascertain the degree of ZIKV-induced apoptosis. Caspase-3 activity was assayed as per the manufacturer's instructions.

XTT Assay

An XTT assay was performed using XTT sodium salt (Sigma) and Phenazine methosulfate (PMS) (Sigma) as per Thermo Fisher Scientific's protocol. 500µL of sample culture was acquired from each sample after treatment and 100µL of this culture was added in triplicate to a 96-well clear flat-bottom plate (Nunc). After the target cells were treated for a set time, XTT sodium salt was dissolved in 4ml of complete media. PMS was mixed with the XTT solution, at a ratio of 10µL of 10mM PMS with every 4mL of XTT solution. 25 µL of tis XTT/PMS solution was then added to each 100µL of cell culture sample in the 96-well plate. The plate was incubated for 2 hours at 37°C in a CO_2 incubator. The absorbance of the plate was read on a Synergy LX multi-mode reader (Biotek) at 450nm.

Transwell Placental Barrier (PB) Model

HVTs were grown to 90% confluency as previously described. An HTS Transwell 24-well plate (Costar) was acquired, and the basolateral chamber filled with Trophoblast complete media. HVT cells were counted using dual-chambered cell-counting slides (Biorad), trypan blue dye 0.40% (Biorad), and a TC 20 Automated Cell Counter (Biorad). HVTs were seeded apically at 2.0×10^5 cells per well and allowed to adhere for 24h.

Generation of exosomes

These instructions apply to any cell used to generate exosomes or EVs. The media, an estimated 10mls, is collected and centrifuged at 300g for 10 min. Th supernatant is collected, and the resulting pellet discarded. The supernatant is centrifuged once more at 2000g for 10 min. The pellet is again discarded, and the supernatant collected. The supernatant is then centrifuged at 10,000g for 30 min. The resulting supernatant is then filtered via a 0.22µm filter. The supernatant is collected and ultra-centrifuged (UC) (Beckman-Coulter) at 120,000g for 70min in 5ml ultracentrifuge tubes. After the first ultracentrifugation, the majority of the supernatant is carefully removed, leaving an estimated 2mm of supernatant remaining. 4.5ml phosphate buffered saline (PBS) is then added to each UC-tube and they are ultracentrifuged again for 70 min at 120,000g. Lastly, the supernatant is fully removed, and the pellet is resuspended in 160ul PBS.

Characterization of EV size distribution and stability

After re-suspension of the EVs in PBS, the sample's size is characterized using dynamic light scattering (DLS) via a zetasizer (Malvern Panalytical). EV stability was evaluated via zeta potential, also using the zetasizer (Malvern Panalytical). Exosome size and stability I confirmd via hydronamic size and transelcetron microscopy.

Transmission Electron Microscopy (TEM) imaging

EVs were characterized via TEM imaging on a Formvar-Carbon 400-mesh grid to confirm both size and presence. (Allen you need to briefly describe the procedure used

RNA Extraction and ddPCR

Total RNA was isolated from the infected or non-infected cells. The RNA was isolated using the RNeasy Plus Mini Kit (QIAGEN) as per the manufacturer's instructions. The isolated RNA was then quantified using the Take3 Micro-Volume Plate (Biotek) and was converted to cDNA using the High Capacity cDNA Reverse Transcription Kit (applied biosystems) as per manufacturer's instructions. Droplet Digital PCR (ddPCR) was employed to confirm ZIKV infection of the target cells using the following ZIKV NS5 primers, providing absolute quantification of the target gene: FOW: 5' –AARTACACATACCARAACAAAGTGGT-, and REV: 5' – TCCRCTCCCYCTYTGGTCTTG- (Eurofins Genomics). One-Way ANOVA was used to determine statistical significance of ddPCR copy numbers.

Gene Content and miRNA Analysis

Viral-induced changes in gene content were analyzed via the NanoString Neuroinflammation Panel. The sample RNA was used in the panel as described per manufacturer's instructions. A portion of the generated EVs was used to isolate the miRNA using the miRNEasy Mini Kit (QIAGEN). The miRNA was quantified via the Take3 Micro-Volume Plate (Biotek). miRNA content was analyzed via the nanoString nCounter Human v3 miRNA panel using the nCounter SPRINT Profiler (nanoString), allowing for simultaneous analysis of over 800 biologically relevant miRNAs. The sample miRNA was used as described per manufacturer's instructions. This data was then analyzed using both fold change ($2^{-\Delta\Delta Cq}$) and percent difference from control via

one-way ANOVA and graphed using GraphPad Prism 6, generating heat maps, scatter plots, and tables.

Analysis of PB permeability and integrity

Assessment of the permeability of the PB was performed using the EnzChek™ Caspase-3 Assay Kit #1, Z-DEVD-AMC substrate (Invitrogen), as per manufacturer's instructions. Determination of PB integrity was performed by trans-epithelial electrical resistance (TEER) (World Precision Instruments) as per manufacturer's instructions. Statistical significance determined by ANOVA and Dunnett's multiple comparison test. **$p<0.01$, *$p<.05$

Results

ZIKV Envelope protein modulation of neuronal viability

The effect of ZIKV E-protein on β-NGF-induced differentiated neuronal cells was investigated. A schematic for experimental design to test effect of increasing dosages of ZIKV E-protein on developing neuronal cell viability (Figure 7a) demonstrates our experimental workflow. Neuronal cells were allowed to grow and differentiate, after β-NGF treatment, for 72 hours. At which point the neuronal cells were treated with the ZIKV Envelope protein and incubated for 24, 48, or 72 hours. The viability of neurons after β-NGF induced differentiation was assessed via measurement of caspase-3 activity (ThermoFisher) (Figure 7b). Usage of β-NGF to induce neuronal cell differentiation resulted in a significant increase in caspase-3 activity, relative to control (Figure 7b). To ascertain the effect of increasing dosages of ZIKV E-protein on differentiated and

undifferentiated neuronal cell death, an XTT assay was employed (Figure 7c). ZIKV E-protein displayed a significant preference for undifferentiated neuronal cells, relative to control p-value<0.0001 (Figure 7c). 250 ng/ml of ZIKV E-protein was recorded as the optimal concentration of ZIKV E-protein required to elicit neuronal cell death (Figure 7c). XTT assay (ThermoFisher) was performed at 4, 5, or 6 dpt. 100ng/ml of ZIKV-EP was found to have the most cytotoxic effect, relative to the untreated control, after 24h (Figure 7d). The longer the treatment time, the lower the effect of the ZIKV-induced cytotoxicity (Figure 7d). Additionally, increasing the ZIKV-EP dosage to 500ng/ml significantly decreased the cytotoxicity of ZIKV-EP (Figure 7d).

Once we had determined that 100ng/ml is the optimal experimental dose of ZIKV-EP, we then tested for optimal dosage of β-NGF for neuronal differentiation. 100ng of β-NGF was found to be the optimal dose to induce differentiation of the neuronal cells, promoting their growth (Figure 7e). Moreover, co-treatment of β-NGF-induced differentiated neuronal cells with 100ng of ZIKV-EP significantly reduced neuronal cell viability (Figure 7e). These findings demonstrate that ZIKV-EP is cytotoxic to differentiated neuronal cells and is most effective in the first 24h after exposure.

ZIKV-Envelope disrupts integrity of in vitro PB model

The effect of the ZIKV-EP on the placental barrier (PB) was then investigated. In order to investigate this, we employed an *in-vitro* Transwell placental barrier model (Figure 8A). In this model the Human Villous Trophoblasts (HVTs) making up the PB, are layered on the apical side of the membrane, and allowed to adhere and grow in the appropriate

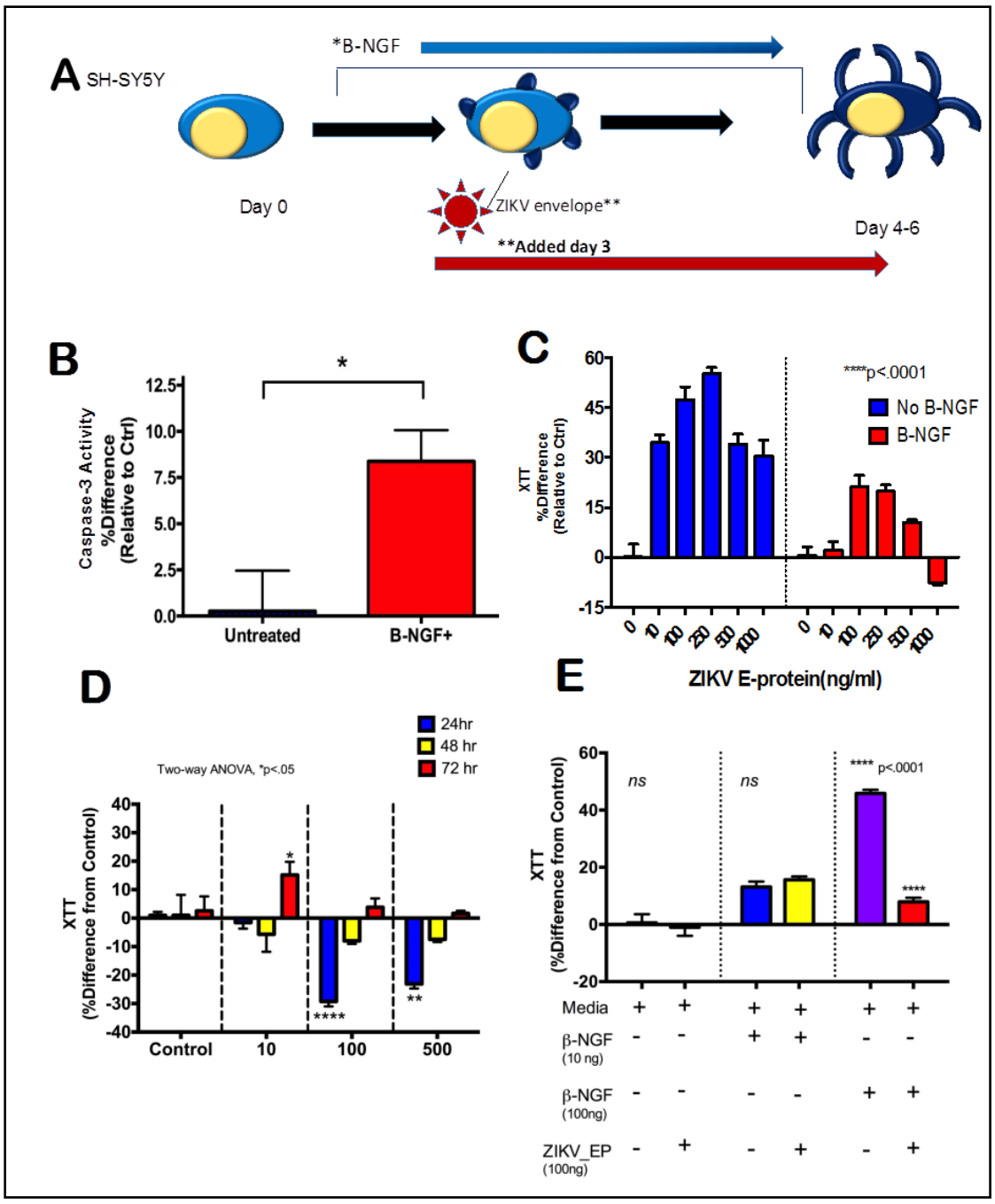

Figure 7: ZIKV E-protein negatively impacts differentiated neurons. (A) SH-SY5Y (ATCC CRL-226) are seeded and permitted to grow for 24h. SH-SY5Y cells are then treated with varying concentrations of β-NGF, promoting differentiation, and ZIKV envelope protein. Cells are harvested 5-7 days after seeding. XTT Assay (ThermoFisher) comparing the impact of various concentrations of ZIKV E-protein on the viability of neuronal cells will be performed. (B) Caspase 3 activity was measured (ThermoFisher) assessing the viability of neurons upon β-NGF-induced differentiation. *p-value <0.05

(C) XTT assay investigating the effect of 100ng of ZIKV E-protein, the most effective dose, on developing neuronal cells. The effect of ZIKV E-protein on β-NGF-induced differentiated neuronal cells. Statistical significance determined by Two-Way ANOVA (Tukey's Multiple Comparison test), ****p-value<0.0001. (D) XTT Assay (ThermoFisher) comparing the impact of various concentrations of ZIKV Env (E) protein on the viability of neuronal cells. *p-value <0.05 (E) XTT assay investigating the effect of 100ng of ZIKV E-protein, the most effective dose, on developing neuronal cells. The effect of ZIKV E-protein on β-NGF-induced differentiated neuronal cells. Statistical significance determined by Two-Way ANOVA (Tukey's Multiple Comparison test), ****p-value<0.0001.

media. The fetal space is defined as the area basolateral to the membrane. ZIKV-EP (100ng/ml) was added on the apical side of the Transwell in presence or absence of anti-ZIKV antibody (1 ug/ml) for 48 hours. Trans-endothelial electrical resistance (TEER) was measured at the 48h time point, to ascertain if the ZIKV-EP exposure induced any changes in PB integrity. No significant difference was found in PB integrity between the treated and untreated samples (Figure 8B). To ascertain if ZIKV-EP modulated PB permeability a Dextran-FITC transport assay was performed. ZIKV-EP significantly increased membrane permeability relative to untreated control (Figure 8C). Addition of the anti-ZIKV-EP antibody significantly reduced membrane permeability back down to control levels (Figure 8C).

Differential Permissivity to ZIKV infection

Next, whether SH-SY5Y, HMC3 (microglia cell line), and relevant primary placental cells were permissive to ZIKV, was investigated. The non-pathogenic strain-MR766 (African lineage) was compared to the pathogneic strain-FLR(Columbian-derived-Asian lineage). In all cell types that we examined the MR766 strain replicated at much lower lower levels than FLR. Significantly, higher levels of FLR was detected in all of the

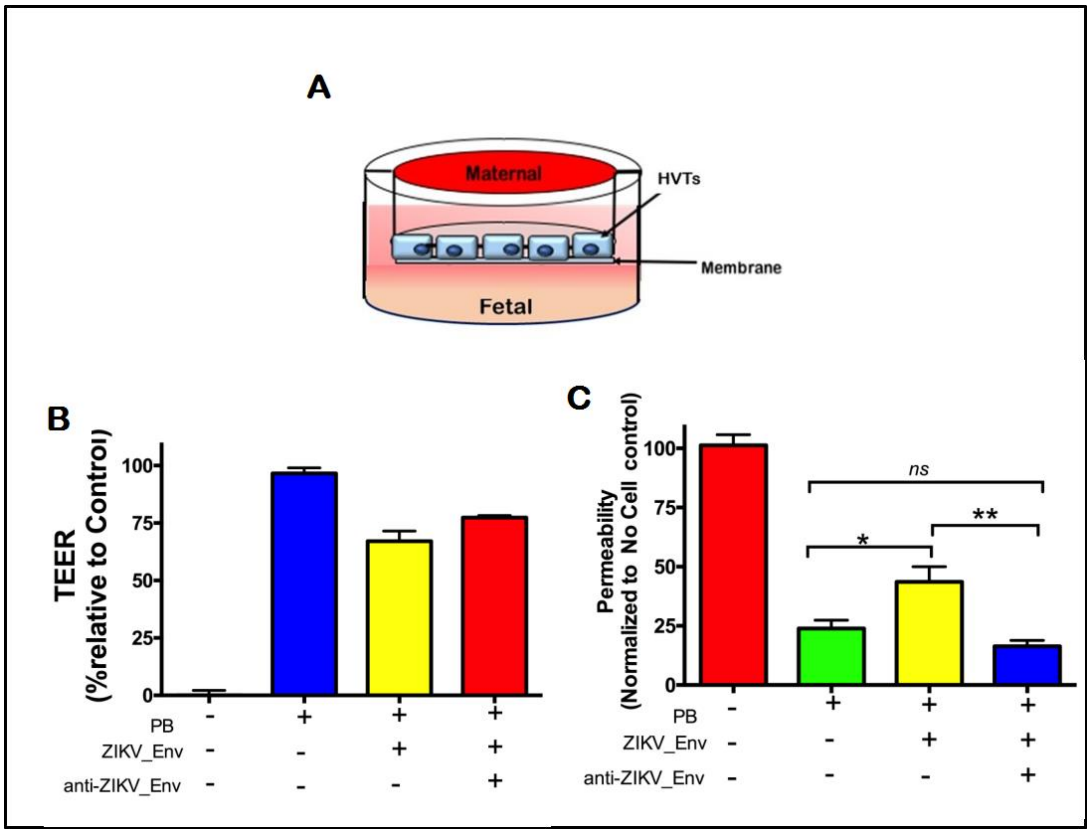

Figure 8: ZIKV-Envelope disrupts integrity of *in vitro* PB model. (A)Schematic of a first-generation placental barrier model. (B) PB was treated with ZIKV-E protein (100 ng/ml) in presence or absence of anti-ZIKV antibody (1 ug/ml) for 48 hours. Trans endothelial electrical resistance (TEER) measured by the REMS auto sampler in triplicate for 15 second intervals. (C) Permeability measured using Dextran-FITC transport assay. Statistical significance determined by ANOVA and Dunnett's multiple comparison test. **p<0.01, *p<.05membrane permeability, without significantly modulating membrane integrity.

infected cells with almost 100 times difference in in the SH-SY5Y and HVTs. Of note, the SH-SY5Y (Figure 9A) and HVTs (Figure 9C) had the highest levels of ZIKV-FLR when compared to the HMC3 microglia cell line (Figure 9B) and PBMCs (Figure 9D). These findings confirm our initial hypothesis that primary placental cells are permissive to ZIKV infection.

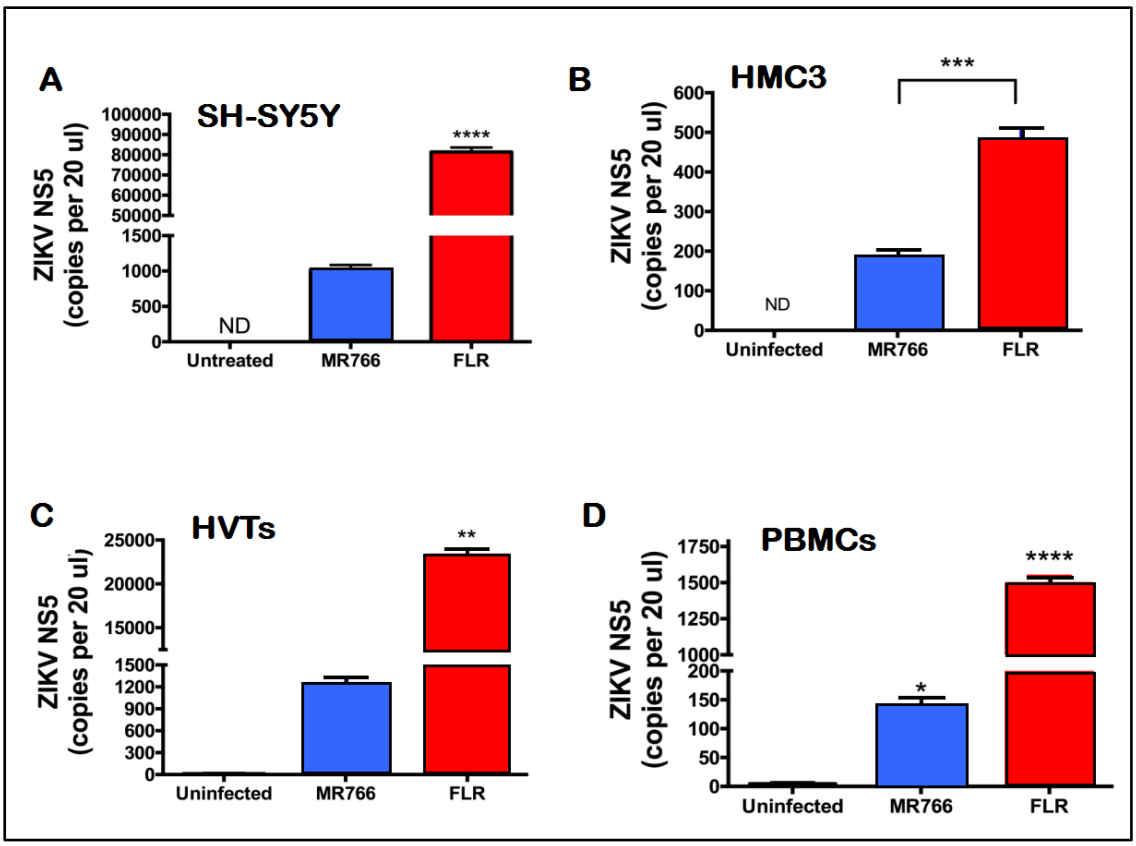

Figure 9: Cells permissive to ZIKV produce higher levels of pathogenic FLR strain. (A) SH-SY5Y, (B) HMC3, (C) HVTs, and (D)peripheral blood mononuclear cells(PBMCs) were each infected with either MR766 (ATCC.org) or FLR (ATCC.org) at a multiplicity of infection (MOI) of 0.1. Cells were harvested 5 days post infection (dpi), RNA isolated (RNeasy, Qiagen.com), cDNA synthesized and digital droplet PCR (ddPCR) EVAgreen absolute quantification (Bio-Rad.com) performed. Primers used for NS5 were adapted from Faye, O. et al 2013, Virology Journal. Statistical significance determined by ANOVA and Dunnett's multiple comparison test. *p<0.05, **p<.001, ***p<.0001 and ****p, 0.00001.

ZIKV pathogenic strain, FLR induces differential gene expression

To ascertain whether there are strain-specific differences in gene modulation post placental cell infection, uninfected, ZIKV-MR766, and ZIKV-FLR infected HVTs were harvested after 72h and its genetic content was analyzed using the NanoString Neuroinflammation panel (Figure 10A). Differential gene expression of HVTs was observed, with the pathogenic ZIKV-FLR strain modulating genes, favoring neuroinflammation. A select

subset of genes involved in: apoptosis suppression (XIAP), neurotransmission and the inflammatory response (NOSTRIN), TLR4 cascade, IL-1/2 pathway, and the TNFR1 pathway (JUN), immune response mediation (PIK3CD), CNS myelination (MYRF), and in the inflammatory response (PTGS2), were found to have their expression be trending towards up-regulation in the HVTs infected with the pathogenic ZIKV-FLR strain, relative to the uninfected HVTs (Figure 10B). Additionally, other genes of note within the aforementioned subset which were also trending towards up-regulation include genes involved in: cell survival and apoptosis (TRAF2), antigen presentation (CD40), and inflammatory and immunoregulatory processes (CCL5) (Figure 10b). However, not all genes of interest were trending towards down-

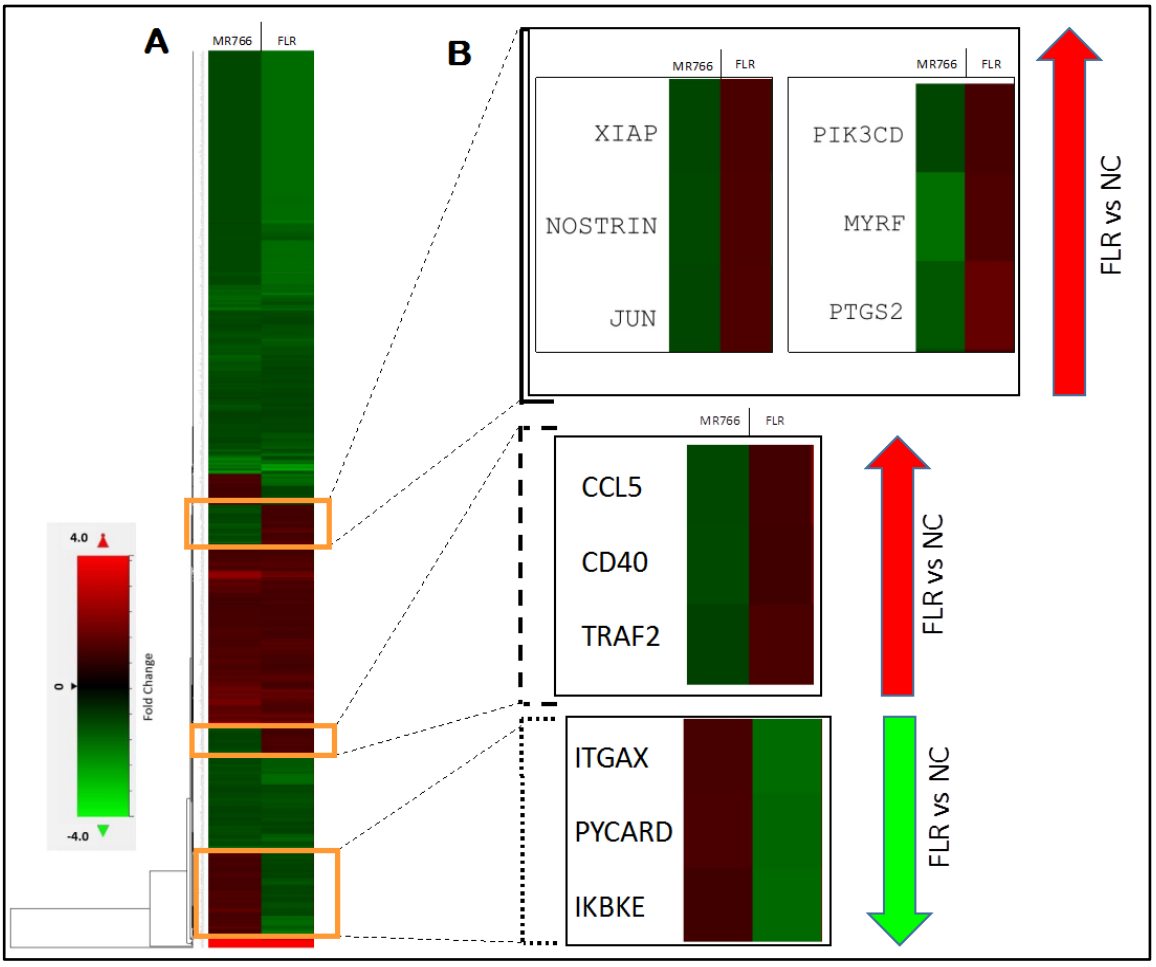

Figure 10: ZIKV pathogenic strain, FLR induces differential gene expression, favoring neuroinflammation, relative to uninfected HVTs. (A) A heat map depicting the ratio of ZIKV-infected HVTs vs uninfected HVTs fold change using the nCounter Human Neuroinflammation Panel. The ratio of MR766 vs NC is depicted in the leftmost column. The ratio of FLR vs NC is depicted in the rightmost column. RNA was isolated using the RNeasy Mini Kit (QIAGEN). (B) A heat map of a subset of genes selected from the aforementioned expression panel performed using NanoString. The selected genes were selected for possessing a differential gene expression relative to each sample ratio. Trends in the modulation of gene expression for the selected subset of genes is expressed as arrows (on the right), depicting a trend favoring upregulation or downregulation of FLR vs NC. Heat map legend depicting fold change based on a color gradient. Fold change was scaled from -4 to 4.

regulation. Such down-regulated genes are involved in: mediation of cell-cell interactions during inflammatory responses (ITGAX), mediation of inflammation and caspase-mediated apoptosis (PYCARD), and regulation of anti-viral signaling pathways (IKBKE) (Figure 10b).

ZIKV-FLR up-regulated XIAP, which encodes an apoptotic suppressor protein, which also regulates inflammatory signaling and immunity. Pathogenic ZIKV-FLR strain also up-regulated PIK3CD activating signaling cascades involved in survival, cell growth, motility, proliferation, and morphology. PIK3CD additionally mediates immune responses, is required for B-cell receptor (BCR) signaling, B-cell development and proliferation, is involved in antigen presentation function of B-cells, is required for T-cell receptor (TCR) signaling and T-cell signaling, among other immune-related functions. Lastly, the ZIKV-FLR strain also up-regulated MYRF, encoding for a protein required for central nervous system (CNS) myelination. This data demonstrates that the pathogenic ZIKV-FLR strain modulates the expression of genes critical to inflammation, the immune response, and myelination. We compared gene expression of HVTs infected with the pathogenic FLR strain to expression of cells infected with the non-pathogenic

Ugandan strain (Figure 11a). Using the same neuroinflammation panel as in (figure 10), trends can be observed. Trending towards up-regulation, genes involved in: inflammation and immune function (NFKB2), apoptosis (HRK), immune system regulation (PILRB), multiple immune system functions (AXL), regulation of apoptosis (BAK1), and innate immunity and apoptosis (LCN2) (Figure 11b). However, it may also be observed that there are a few select genes that are trending towards down-regulation, instead. Genes involved in: the regulation of gene expression during embryonic development (JARID2), inhibition of axonal regeneration (LINGO1), the innate immune response and inflammation (IL1RL2) (Figure 11b). (Table 1) depicts all of the significantly modulated genes induced by the ZIKV-FLR strain, relative to the MR766 strain, in fold change. Using the WEB-based GEne SeT AnaLysis Toolkit (Webgestalt), a high-level functional classification of the significant differentially expressed genes was acquired (Figure 12). This classification classified the significantly expressed genes within different biological processes, cellular components, or molecular functions. A Bar chart depicting modulated pathways as a result of ZIKV-infection, relative to NC, is shown in (Figure 13). Although, the pathways modulated between the pathogenic vs the non-pathogenic strain are mostly similar, the pathogenic FLR strain has a slightly increased relationship with the modulation of IFN-related pathways or genes.

ZIKV pathogenic strain, FLR induces differential expression of miRNAs. Strain-specific differences in miRNA expression of ZIKV-infected placental trophoblast was assessed via NanoString multiplexed mRNA array (Figure 14a). A subset of these miRNAs, believed to be critical to the growth of neuronal cells, immune response, and/or the anti-

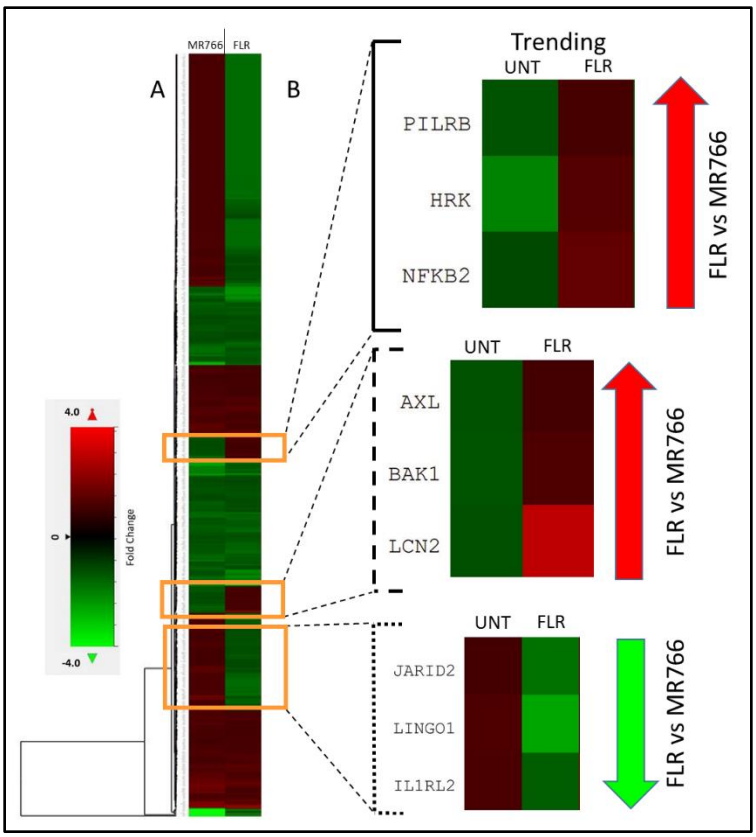

Figure 11: ZIKV pathogenic strain, FLR induces gene expression that favors neuroinflammation relative to MR766 (A) A heat map depicting the ratio of uninfected HVTs or ZIKV FLR-infected HVTs vs ZIKV MR766-infected HVTs, as fold change, using the nCounter Human Neuroinflammation Panel. The ratio of MR766 vs NC is depicted in the leftmost column. The ratio of FLR vs NC is depicted in the rightmost column. RNA was isolated using the RNeasy Mini Kit (QIAGEN). (B) A heat map of a subset of genes selected from the aforementioned expression panel performed using NanoString. The selected genes were selected for possessing a differential gene expression relative to each sample ratio. Trends in the modulation of gene expression for the selected subset of genes is expressed as arrows (on the right), depicting a trend favoring upregulation or downregulation of FLR vs MR766. Heat map legend depicting fold change based on a color gradient. Fold change was scaled from -4 to 4.

viral state are depicted (Figure 14b). (Table 2) depicts the biological processes, cellular component, and molecular function GO analyses of select up/down-regulated miRNAs differentially modulated by ZIKV-FLR.

Gene	Fold Change (FLR vs MR766)
TM4SF1	-3.64
S1PR3	-2.91
TMEM100	-2.41
LINGO1	-2.32
OLFML3	-2.26
AGT	-2.19
TNFSF13B	-2.14
SIGLEC1	-2.13
GPR183	-2.12
OAS1	-2.11
C3AR1	-2.07
SLC2A5	-2.06
TMEM119	-2.06
HSD11B1	-2.02
RSAD2	-2.02
GADD45G	-2.01
IL1R2	-2.01
TNFRSF1B	-2
KDM4B	2.03
MYRF	2.15
PTGS2	2.18
EGR1	2.22
PILRA	2.56
LCN2	2.95

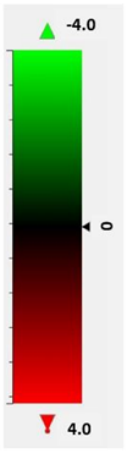

Table 1: ZIKV pathogenic strain, FLR induces differential expression of genes involved in key growth, immune function, viral, apoptosis, cell-cell signaling, and neuronal function, in HVTs. (A) A table depicting the differential expression of genes induced by the ZIKV-FLR strain, relative to the MR766 strain, in fold change. The genes listed in

this table are all the genes significantly modulated by ZIKV-FLR infection of HVTs. Fold change values acquired via the nCounter Human Neuroinflammation Panel and nSolver software.

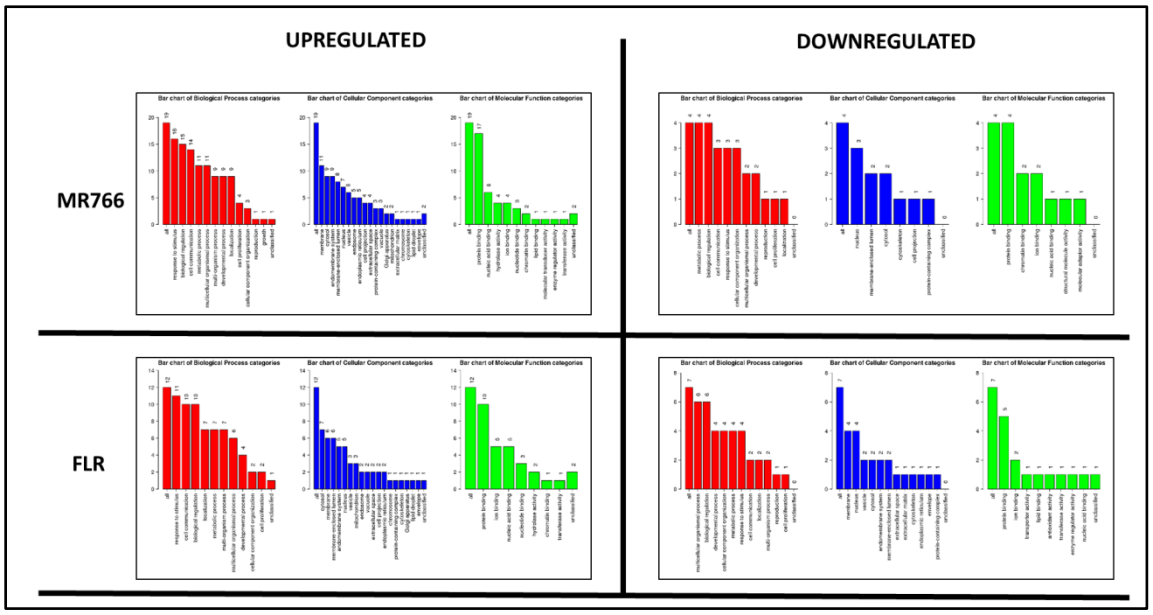

Figure 12: ZIKV pathogenic strain, FLR induces differential gene expression, in HVTs, of genes involved in: key biological processes, cellular components, and molecular functions. (A) A GO Slim classification of the up or downregulated genes within each subset ratio of ZIKV-infected HVTs vs NC, providing a high-level functional classification of the significant differentially expressed genes. GO Slim was analyzed and acquired via the WEB-based GEne SeT AnaLysis Toolkit (Webgestalt).

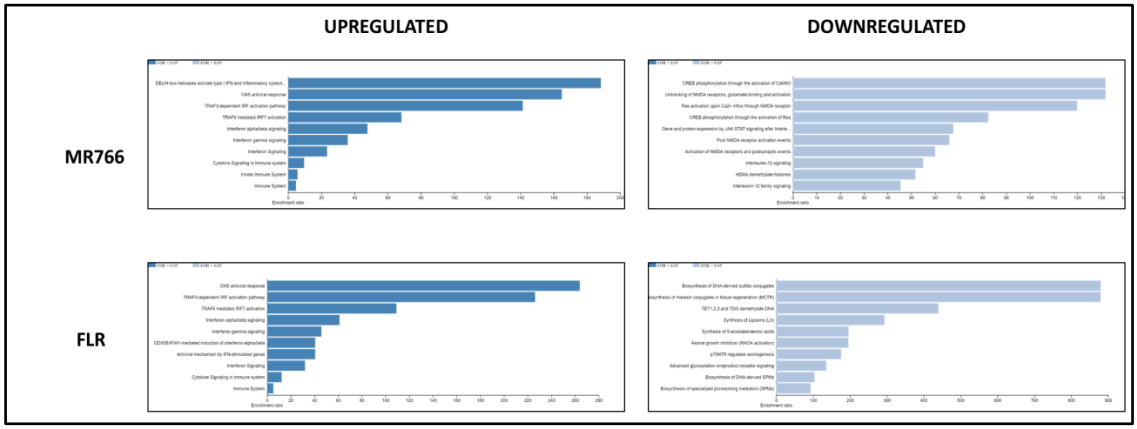

Figure 13: FLR induces gene expression that modulates various pathways critical to the immune system, apoptosis, and the anti-viral state, in HVT cells. (A) Bar charts depicting modulated pathways as a result of ZIKV-infection, relative to NC. Data was analyzed via the WebGestalt online tool using a complementary method for enrichment analysis, over-representation analysis (ORA), with the Reactome functional database for pathway analyses.

Discussion

ZIKV envelope protein displayed an increase in caspase-3 activity when deployed against differentiating neuronal cells, significantly increasing neuronal apoptosis. Additionally, as expected, ZIKV E-protein also displayed a greater impact on cell viability against β-

NGF induced differentiated neuronal cells. This lends further credence to published data associating ZIKV infection, congenital microcephaly, the presence of ZIKV in the fetal brain, and development of ZIKV-associated neuropathology. ZIKV infects radial glial cells, spinal and neocortical neuro-epithelial stem cells. This results in supernumerary centrosomes, structural disorganization, disrupted mitoses, and cell death. Analysis shows that ZIKV infection of radial glial cells and neuro-epithelial stem cells results in mitochondrial sequestration of phospho-TBK1 during mitosis and centrosomal depletion. Sequestering TBK1, which is needed for the organization of cell division to the mitochondria, facilitating immune response initiation, results in cell death and a lack of the

A

Up-Regulated miRNAs

GO Category	p-value	#genes	#miRNAs
cellular protein modification process	5.91E-39	523	5
gene expression	2.20E-23	142	5
neurotrophin TRK receptor signaling pathway	1.83E-16	69	5
protein binding transcription factor activity	2.14E-14	120	5
viral process	2.34E-13	103	5
response to stress	9.70E-10	416	5
Fc-epsilon receptor signaling pathway	5.01E-09	39	5
post-translational protein modification	4.49E-08	41	5
cell death	1.97E-07	179	5
cell-cell signaling	6.37E-07	134	5
synaptic transmission	7.34E-07	90	5
epidermal growth factor receptor signaling pathway	7.11E-06	48	5
phosphatidylinositol-mediated signaling	6.08E-05	35	5
platelet activation	0.000106607	43	5
activation of signaling protein activity involved in unfolded protein response	0.000703045	17	5
axon guidance	0.001033821	94	5
transmembrane transporter activity	0.002025594	188	5
leukocyte migration	0.002220989	27	5
cell motility	0.005874102	104	5
platelet degranulation	0.013051627	16	5
protein targeting to Golgi	0.020077151	12	4
Fc-gamma receptor signaling pathway involved in phagocytosis	0.025312119	14	5
toll-like receptor TLR1:TLR2 signaling pathway	0.027025714	13	4
toll-like receptor TLR6:TLR2 signaling pathway	0.027025714	13	4
protein targeting	0.032056851	55	5
regulation of Ras GTPase activity	0.033117626	7	4
toll-like receptor 10 signaling pathway	0.041768744	12	4
toll-like receptor 9 signaling pathway	0.041768744	14	4
immune system process	0.044948575	256	5

B

Down-Regulated miRNAs

GO Category	p-value	#genes	#miRNAs
cellular protein modification process	5.29E-42	438	7
gene expression	6.76E-20	114	7
protein binding transcription factor activity	2.01E-18	110	6
post-translational protein modification	1.02E-14	46	7
viral process	2.80E-14	89	7
nucleic acid binding transcription factor activity	3.86E-13	172	7
neurotrophin TRK receptor signaling pathway	5.44E-13	54	6
Fc-epsilon receptor signaling pathway	4.51E-11	37	7
cellular component assembly	1.15E-10	205	7
post-Golgi vesicle-mediated transport	5.02E-07	18	3
phosphatidylinositol-mediated signaling	1.31E-05	31	5
cell death	1.31E-05	137	7
response to stress	0.000176956	298	7
leukocyte migration	0.000211614	25	6
synaptic transmission	0.000456042	65	6
fibroblast growth factor receptor signaling pathway	0.000580876	35	5
cellular component disassembly involved in execution phase of apoptosis	0.001457459	11	6
axon guidance	0.007463985	72	6
activation of MAPKK activity	0.00996537	20	5
transcription initiation from RNA polymerase II promoter	0.011223048	36	7
platelet activation	0.012976263	30	6
transforming growth factor beta receptor signaling pathway	0.019837778	34	6
negative regulation of epidermal growth factor receptor signaling pathway	0.039936591	12	4
insulin receptor signaling pathway	0.042626843	28	5
negative regulation of extrinsic apoptotic signaling pathway	0.044415113	17	3
RNA polymerase II core promoter proximal region sequence-specific DNA binding transcription factor activity involved in positive regulation of transcription	0.044881114	48	5
generation of neurons	0.046290255	10	4

Table 2: ZIKV pathogenic strain, FLR induces exosomal transport of miRNAs targeting genes involved in key growth, immune function, viral, apoptosis, cell-cell signaling, and neuronal function, in HVT cell-derived EVs. (A) A table depicting the biological processes, cellular component, and molecular function GO analyses of select up-regulated miRNAs differentially modulated by FLR. MicroT-CDS algorithm employed with GO analysis using MirPath v.3 of DIANA Tools. (B) A table depicting the biological processes, cellular component, and molecular function GO analyses of select down-regulated miRNAs differentially modulated by FLR. MicroT-CDS algorithm employed with GO analysis using MirPath v.3 of DIANA Tools.

protein required for cell division, preventing the formation of new brain cells, and thus resulting in microcephaly [411]. Additionally, the CDC has confirmed that ZIKV infection during pregnancy causes microcephaly [412]. Within a 24-hour period, ZIKV E-protein significantly impacted neuronal viability resulting in a near 30% decrease, relative to

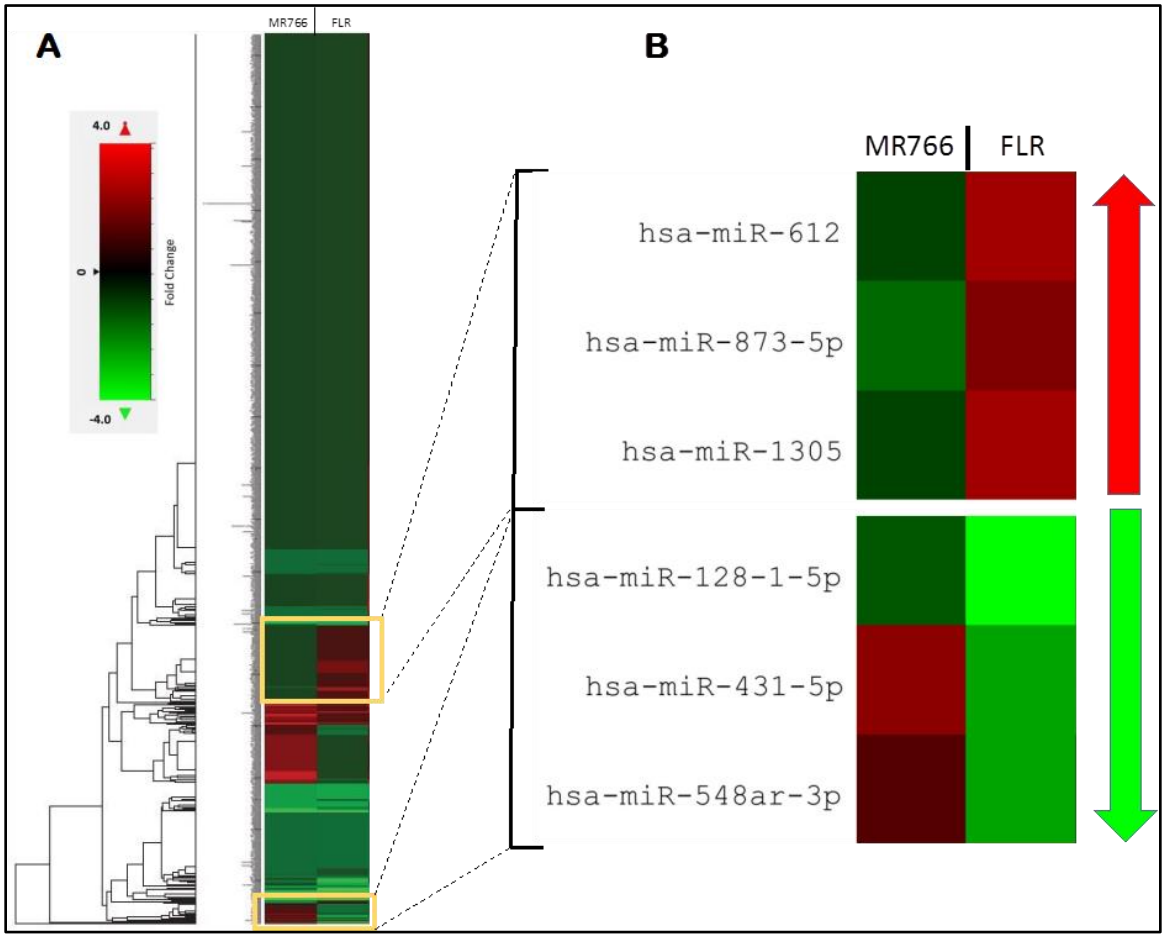

Figure 14: ZIKV pathogenic strain, FLR induced differential expression of miRNAs in HVT-derived EVs, relative to Untreated HVT-derived EVs. (A) A heat map depicting the comparison of the ratio of ZIKV-infected HVTs vs uninfected HVTs as fold-change for all the miRNAs in the nCounter Human v3 miRNA Expression assay. miRNA isolated using miRNeasy Mini Kit (QIAGEN). (B) A heat map of a subset of genes selected from the aforementioned expression panel performed using NanoString. Heat map legend depicting fold change based on a color gradient.

control. A trend demonstrating a ZIKV E-Protein dose-dependent decrease in neuronal cell viability could be observed in differentiated neuronal cells. This data demonstrates that 100ng/ml of ZIKV EP is the optimal dosage. A decrease in PB integrity as a result of ZIKV E-protein exposure and subsequent rescue upon treatment with anti-ZIKV E-protein antibody was observed. This demonstrates that ZIKV E-protein may impair the integrity of the PB membrane, facilitating its transportation across the PB and eventually the fetal brain space. A significant rise in PB permeability is recorded via the dextran-FITC transport assay. Additionally, upon treatment with the anti-ZIKV EP antibody in conjunction with the ZIKV EP, permeability levels return to baseline thus suggesting, with this rescue, that ZIKV EP was responsible for that increase in PB permeability. It has been previously demonstrated, that ZIKV infections disrupts the PB by using the proteasomal degradation pathway to disrupt cellular tight junctions [413]. Neuroblastoma cell line SH-SY5Y, microglia cell line HMC3, primary HVTs and primary PBMCs were permissive to ZIKV infection, and generated higher levels of the ZIKV pathogenic FLR strain, relative to the non-pathogenic MR766 strain. Additionally, the ZIKV-FLR strain induced changes in the expression of genes, supporting neuroinflammation. These changes will most likely yield an increase in: apoptosis, as XIAP and TRAF2, were up-regulated. Most importantly, the immune response would be modulated by ZIKV, as

NOSTRIN, JUN, PIK3CD, PTGS2, CD40, and CCL5 were all found to be up-regulated, significantly in some cases. Additionally, the CNS would be affected as well, as NOSTRIN, and MYRF were found to have their expression be trending towards up-regulation in the HVTs infected with the pathogenic ZIKV-FLR strain, relative to the uninfected HVTs. In the opposite spectrum, mediation/regulation of inflammation, anti-viral pathways, and apoptosis was found to be down-regulated by ZIKV infection, via downregulation of PYCARD, IKBKE, and ITGAX. This data also shows that ZIKV-FLR specific differential gene expression modulates inflammation and immune function through up-regulation of NFKB2, PILRB, AXL, and LCN2. Apoptosis was altered via up-regulation of HRK, BAK1, and LCN2. Furthermore, unlike the aforementioned up-regulation in immune function gene expression, down-regulation of IL1RL2 demonstrates a potential ZIKV-induced modulation to increase its likelihood of propagation and immune evasion via altering the innate immune response and inflammation. Lastly, ZIKV-FLR differentially modulated JARID2 and LINGO1, down-regulating the regulation of gene expression during embryonic development and the inhibition of axonal regeneration, respectively. WebGestalt analysis demonstrated a differential categorization of biological processes, cellular components, and molecular functions modulated by ZIKV-FLR. ZIKV-FLR differentially modulated genes involved in cell communication, as a greater percentage of significantly modulated genes were involved in cell communication, relative to significantly modulated genes in ZIKV-MR766 infected HVTs. Additionally, within both the up and down-regulated gene list, fewer genes were involved in cell proliferation in ZIKV-FLR infected HVTs, relative to MR766 infected HVTs. This suggests that the pathogenic strain ZIKV-FLR induces a

greater rate of apoptosis, as indicated by the aforementioned up-regulated genes. This category classification ranked lower than that of MR766. Additionally, within the subset of significantly down-regulated genes, ZIKV-FLR induced down-regulation of multiple genes classified as affecting vesicles, at a greater ratio than MR766. ZIKV-FLR infection resulted in the up-regulation of genes, of which many were involved in IFN signaling, IFN-induced anti-viral mechanisms, or the OAS antiviral response. However, multiple genes which were down-regulated as a result of ZIKV-MR766 infection of HVTs, were involved in several different N-methyl-D-aspartate (NMDA) receptor pathways. This data implies that ZIKV-MR766 may impact synaptic plasticity and learning [414]. Additionally, infection with ZIKV-FLR induced differential expression of HVT-derived miRNAs. ZIKV-FLR infection of HVTs resulted in the release of EVs containing and up-regulated concentration of hsa-mir-612, hsa-mir-873-5p, and hsa-mir-1305. Of note, hsa-mir-612 targets genes involved in the neurotrophin signaling pathway. hsa-mir-873-5p targets genes involved in synaptic transmission, cell-cell signaling, viral process, and the neurotrophin signaling pathway. hsa-mir-1305 targets genes involved in a myriad of pathways, from cell death and viral process to response to stress and cell-cell signaling. These EVs also contained a concentration of down-regulated miRNAs hsa-mir-128-1-5p, hsa-mir-431-5p, hsa-mir-548ar-3p. hsa-mir-128-1-5p targets genes involved in the neurotrophin TRK receptor signaling pathway, positive regulation of type I interferon, and post-translational protein modification. hsa-mir-431-5p targets genes involved with the neurotrophin TRK receptor signaling pathway and the Fc-epsilon receptor signaling pathway. hsa-mir-548ar-3p targets genes involved in a myriad of functions and pathways, from viral process and response to stress, to axon guidance, synaptic transmission and

cell death. Overall, these findings suggests that differentiated neuronal cells are permissive to ZIKV infection, pathogenic ZIKV strain FLR disrupts the integrity and permeability of the PB, infection FLR strain induced differential expression of genes and the infected cells released EV-encapsulated miRNAs, that target genes critical to the immune response, apoptosis, and neuronal cell growth.

Acknowledgements

This work was supported in part by the Herbert Wertheim College of Medicine Foundation Pilot Grant and the Florida Department of Health Zika Research grant.

CHAPTER 3

HIV-1 and Opiate Modulation of Extracellular Vesicle (EV) miRNA Content Establishes a Potential Biomarker Profile of HIV-infection and Opiate Use

Materials and Methods

Cell Maintenance

Peripheral blood mononuclear cells (PBMCs) were isolated from the blood of anonymous healthy donors using Ficoll-Paque gradient centrifugation and then expanded in medium containing RPMI 1640 medium with 10% FBS, 100 units/mL penicillin, and 100 units/mL streptomycin at 37°C in humidified air with 5% CO_2. The PBMCs were incubated with phytohemagglutinin-P (PHA-P) for 72 hours at a final concentration of 3µg/ml. After 72h, the PBMCs were centrifuged at 1,500rpm in a 50ml conical tube, a pellet was acquired and the cells were resuspended in 5ml of fresh media. Polybrene was added to the resuspended cells at a final concentration of 2 µg/ml; the PBMCs were then incubated at 37°C in humidified air with 5% CO_2 for 30 minutes.

HIV Infection

After the cells were incubated in polybrene for 30 mins, HIV-MN (X4-strain) was added to the samples slated for HIV-1 infection, at a concentration of HIV-1 of 20ng/10 million cells, as previously tittered by P24 ELISA. The HIV-infected cells were incubated at 37°C in humidified air with 5% CO_2 for 2 hours. The PBMCs were centrifuged again at 1,500rpm generating a pellet of PBMCs. The PBMC media was discarded carefully, so as to not disturb the pellet, and the cells were washed with sterile PBS and centrifuged again at 1,500rpm. Once a pellet was acquired, the cells were placed in 10ml of fresh complete media and IL-2 at a concentration of 20U/ml.

Morphine Treatment

Once infected, the cells were treated with various concentrations of morphine diluted in PBS. The concentrations used in this study were 0.02µM, 0.2 µM, and 2 µM. This treatment was repeated every 48h. RNA was isolated from the cells (QIAGEN) to examine HIV-1 viral titer via ddPCR. The supernatant was also collected after 7days post-infection for the purpose of exosome isolation.

Exosome isolation

Culture media of the PBMCs, an estimated 10mls, was collected and centrifuged at 300g for 10 min to remove cells. Supernatant was collected, and the resulting pellet discarded. The supernatant was centrifuged once more at 2000g for 10 min for removal of dead cells and debris. The pellet was discarded, the supernatant collected and centrifuged at 10,000g for 30 min to remove smaller debris. The resulting supernatant was sterile filtered via a 0.22µm filter (Fisher Scientific). The filtered supernatant was ultra-centrifuged (UC) (Beckman Coulter/ Optima MAX-XP) at 100,000g for 70min using a swing bucket rotor (Beckman Coulter/ MLS-50). The supernatant was discarded and 4.5ml of PBS was then added to the pellet remaining in the UC tube. The UC tubes were ultra-centrifuged again for 70 min at 100,000g. Lastly, the supernatant was removed, and the pellet was resuspended in 160µl PBS.

Characterization of Extracellular Vesicles (EVs)

EV size and stability was characterized using dynamic light scattering (DLS) via a zetasizer (Malvern Panalytical).

Nanostring

miRNA was isolated through the use of the miRNEasy kit (QIAGEN). Isolated miRNA was concentrated via the use of a vacufuge to at least a concentration of 33.33ng/µl. The concentrated miRNA was then delivered to Nanostring for analysis. The Nanostring miRNA Expression Panel was used to detect the expression of over 800 different miRNAs simultaneously.

Statistical and Bioinformatic Analysis

Experiments were performed in triplicates. Data was analyzed and graphed using GraphPad Prism 6. Statistical significance (p-value <0.05) and was determined via ANOVAs (One- and two-way) with post-hoc test (Kruskal-Wallis test) or (Tukey's multiple comparisons test). Bioinformatic analysis was performed using the functional enrichment analysis web tool Web-based Gene SeT AnaLysis Toolkit (WebGestalt) to perform Over-Representation Analysis (ORA), determining the Gene Ontology (GO) categories with significantly enriched gene numbers. The enriched Kyoto Encyclopedia of Genes and Genomes (KEGG) pathways were employed via the WebGestalt software.

Results

To determine if either morphine or HIV infection would alter EV size, DLS was used to ascertain both EV diameter and PDI. Neither exosome size nor PDI was found to be modulated by viral infection or opiate abuse (Figure 15). To determine the impact of opiate use in the context of HIV-1 infection, the total copy number of the HIV-1 LTR was ascertained per sample via ddPCR. Analysis of the cellular RNA, via droplet digital

PCR (ddPCR), confirmed HIV-1 replication in HIV+ samples, in addition to a visible trend suggesting an increase in HIV-1 replication when HIV is in the presence of morphine, displaying a higher copy number, relative to HIV without morphine (Figure 16). Samples treated with ART presented with diminished HIV-1 viral copy numbers, relative to the un-treated infected samples (Figure 16). The ART treatment presents with a trend demonstrating a decrease in viral replication approximating the values observed in the negative control (Figure 16). Morphine presence did not appear to significantly impact the anti-retroviral effects of ART, which was composed of TDF (9.44µM) and EMT (16.17µM).

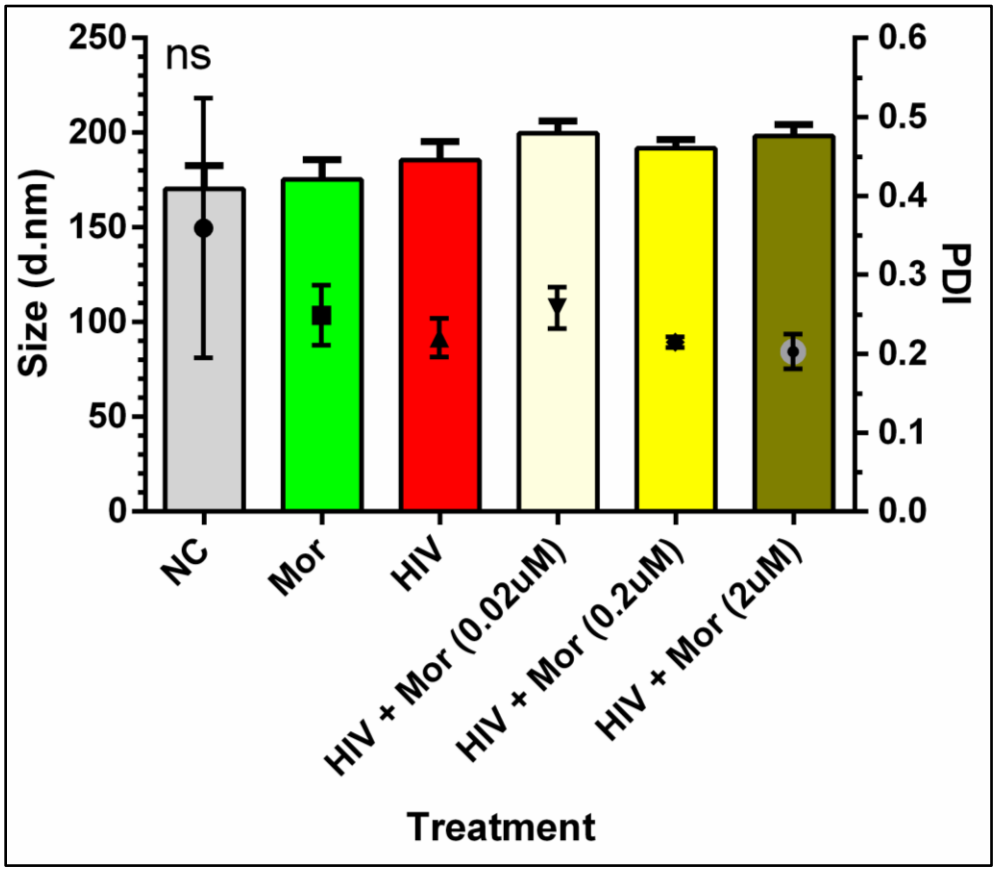

Figure 15: Exosome size was not modulated by viral infection or opiate abuse. Depicted here is a column graph displaying both the average exosome diameter per treatment and

the exosome polydispersity index (PDI), as measured via dynamic light scattering (DLS) on a Zetasizer (Malvern Panalytical)

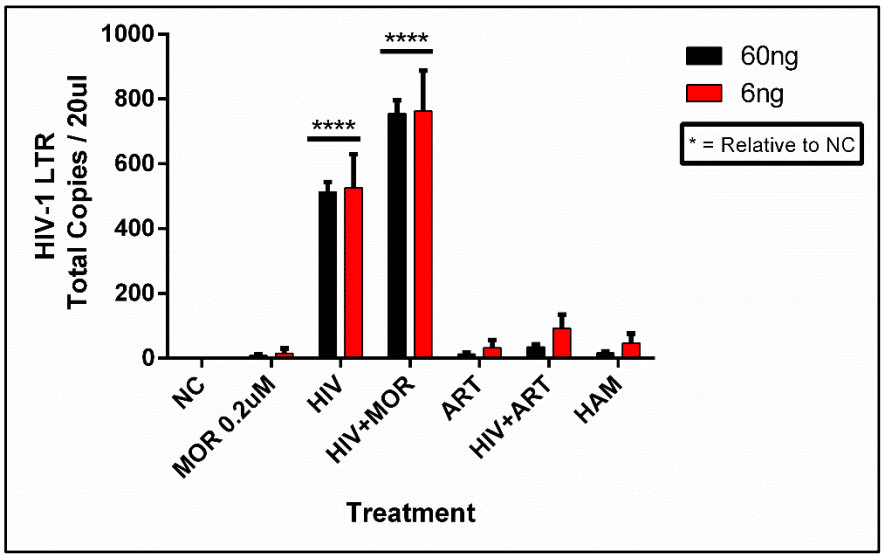

Figure 16: HIV-MN and morphine display a trend suggesting potential synergistic effects promoting an increase in HIV-MN replication. The two groups, 60ng and 6ng, are the selected quantities of RNA used to generate the cDNA used to analyze HIV-1 LTR copy number. (****p-value <0.0001).

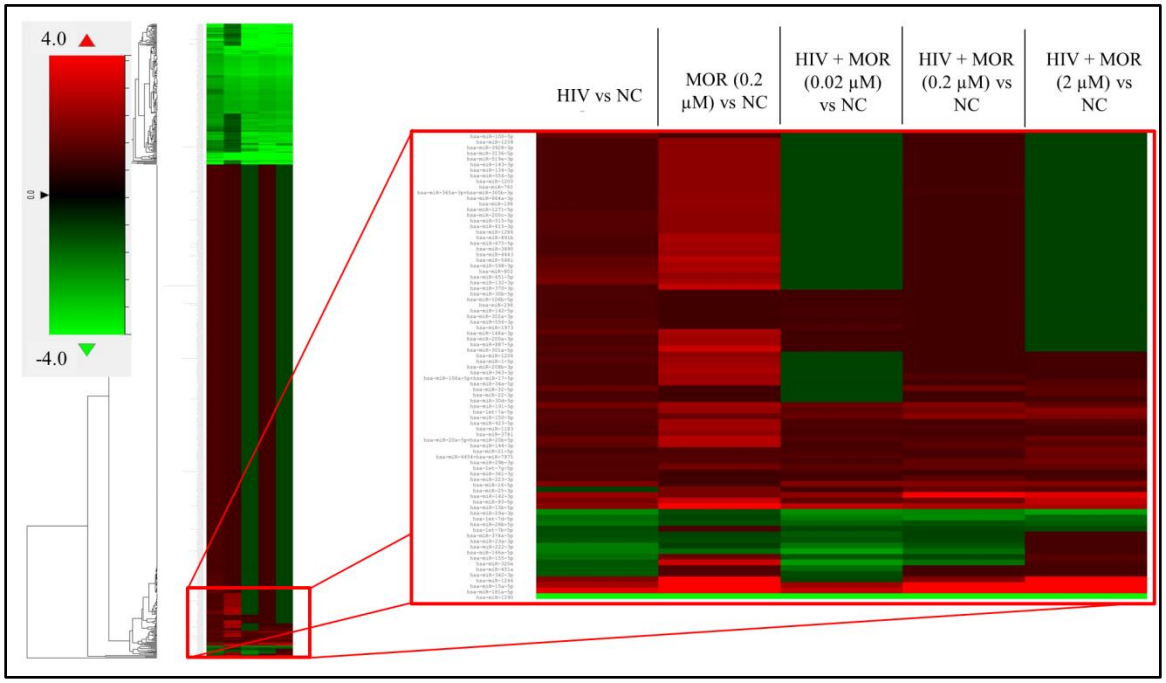

Figure 17: HIV-1 and morphine induced differential miRNA expression in PBMC-derived exosomes, relative to the negative control. This is a heat map displaying the HIV and/or morphine induced miRNA alterations within PBMC-derived exosomes. On the far left is the fold change key, which illustrates the difference in fold-change, relative to control, in a color-dependent format. Cells highlighted in red are upregulated, whereas cells presenting with green are downregulated.

To determine if the miRNA profile of PBMC-derived EVs was altered as a result of HIV-infection or opiate use, a heat map was generated using the miRNA panel data acquired from Nanostring. Infection with HIV-MN strain and/or morphine treatment resulted in PBMC-derived EVs containing a unique miRNA profile that seems to be treatment-dependent, as a result of differential expression of miRNA (Figure 17). The lower portion of the heat map was selected for bioinformatic analysis for its highly varied region (Figure 17). In order to ascertain if there are shared groups of miRNAs among the different treatment groups, the (Figure 17) heat map data was analyzed further. Analysis of the heat map which consisted of a total 797 miRNAs, yielded that HIV significantly modulates 164 miRNAs, morphine significantly alters the expression of 151 miRNAs, and the combination of both HIV-1 and morphine modify 188 (Figure 18). Of note, all 164 miRNAs that HIV alters, are the exact same miRNAs also altered by the combination of HIV and morphine (Figure 18). This means that there are no miRNAs which HIV uniquely modulates, when compared to HIV and morphine, as all 164 miRNAs are also differentially expressed in HIV+MOR (Figure 18). There are 24 miRNAs unique to HIV+MOR when compared to just HIV (Figure 18). However, there are 66miRNAs unique to HIV, when compared to MOR (Figure 18). There are 107 miRNAs which are modulated as result of either HIV+MOR or MOR alone (Figure 18). Lastly, there are 97 miRNAs which all three treatment groups share (Figure 18).

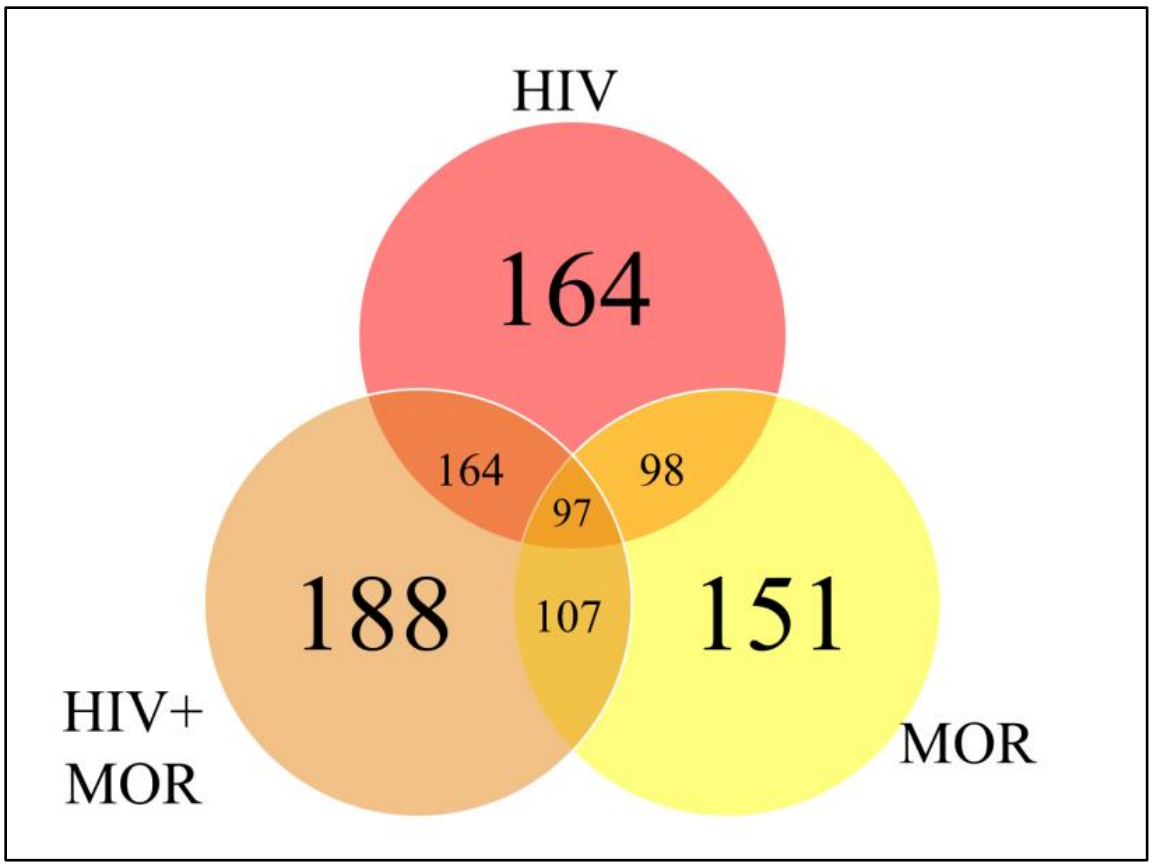

Figure 18: miRNAs from HIV and/or Morphine treated PBMC-derived EVs are significantly differentially expressed across treatment groups. Shown here is a venn diagram depicting the miRNAs which are shared/ or in common between the varying treatment groups, HIV, HIV+MOR (0.2μM), and MOR (0.2μM), all relative to the NC.

In order to ascertain if there were any significant differences, among the treatment groups, in the expression of EV- bound miRNAs, a selection of miRNAs were selected based on the perceived fold change differences in expression as a result of the varied treatment groups (Table 3). From this data set (Table 3) the miRNAs with a either a combination of targeting genes of interest or presenting with a great difference in expression, as a result of the exposed treatment, were selected for potential miRNA mimic or CRISPR experiments downstream (Figure 19). Hsa-miR-1246 presents with a 12-fold up-regulation when in the presence of morphine, solely (Figure 19). However,

this drops when in combination with HIV, reducing as low as -1.09 fold change for the HIV+MOR (0.02μM) treatment. On the other end of the spectrum, has-miR-1290 presents with large fold change modulations, however, they are all in the negative (Figure 19). The MOR treatment alone resulted in a -4.6 fold decrease of has-miR-1290. However, the combination of HIV+MOR at 0.2μM dropped miR-1290 expression even lower, down to -13.95 fold change relative to control (Figure 19). According to the GOSLim summary, across all treatment groups, modulated miRNAs primarily target genes involved in biological regulation and response to stimulus (Figure 20-21). miRNAs targeting the membrane where among the most modulated as a result of HIV and/or MOR treatment (Figure 20-21). Protein and ion binding were among the 2 molecular functions most targeted by the miRNAs altered as a result of HIV-1 and/or morphine treatment (Figure 20-21). In order to determine the pathways which would most likely be affected as a result of the transport and release of EVs derived from morphine and/or HIV-infection of PBMCs, enriched pathway data was acquired through WebGestalt's Over-Representation Analysis (Tables 4-6). Here the targets of the miRNAs, DNA, are grouped by gene set (Tables 4-6). A gene set is a group of genes which share a particular function. This function could be a pathway, a trait such as morphine addiction, or a molecular function such as Renin secretion. Relative to the NC, HIV-induced changes in PBMC-derived EV cargo yield miRNAs targeting: the cholinergic/dopaminergic Synapse, neuroactive ligand-receptor interaction, the neuronal system, K+ Channels, membrane trafficking, vesicle-mediated Transport, apoptosis, and RNA degradation (Table 4). On the other hand, morphine (0.2μM) modulates EV cargo, such that EV-bound miRNAs target: morphine addiction, NF-K-Beta signaling pathway, T-Cell

receptor signaling pathway, neuroactive ligand-receptor interaction, stem cell pluripotency signaling pathways, TNF signaling pathway, and cellular senescence (Table 5). The combination of HIV and morphine (0.2μM) alter PBMC-derived EV content, to yield EVs transporting miRNAs targeting: morphine addiction, neuroactive ligand-receptor interaction, cytokine-cytokine receptor interaction, SNARE interactions in vesicular transport, axon guidance, TNF signaling pathway, TLR- signaling pathway, neurotropin signaling pathway (Table 6).

Probe Name	HIV vs. NC Fold Change	HIV + MOR (0.2 uM) vs. NC	MOR (0.2 uM) vs. NC
hsa-miR-1290	-8.19	-13.95	-4.6
hsa-miR-1253	-5.6	-7.21	-2.11
hsa-miR-371a-5p	-5.36	-8.92	-2.15
hsa-miR-502-5p	-4.85	-5.56	-5.53
hsa-miR-603	-4.85	-7.87	-2.05
hsa-miR-4536-5p	-4.75	-5.45	-1.9
hsa-miR-627-5p	-4.67	-8.71	-1.09
hsa-miR-570-3p	-4.66	-5.35	-5.32
hsa-miR-548aa+hsa-miR-548t-3p	-4.48	-5.14	-2.3
hsa-miR-4531	-4.39	-5.03	-5
hsa-miR-411-5p	-4.12	-5.08	-1.64
hsa-miR-644a	-4.02	-4.62	-1.52
hsa-miR-1246	2.07	2.1	12
hsa-miR-15b-5p	2.24	2.72	4
hsa-miR-142-3p	2.42	4	1.89
hsa-miR-15a-5p	2.62	4.22	4.33
hsa-miR-181a-5p	3.65	4.09	4.98

Table 3: HIV differentially modulates miRNA expression of PBMC-derived EVs in the context of opiate exposure.

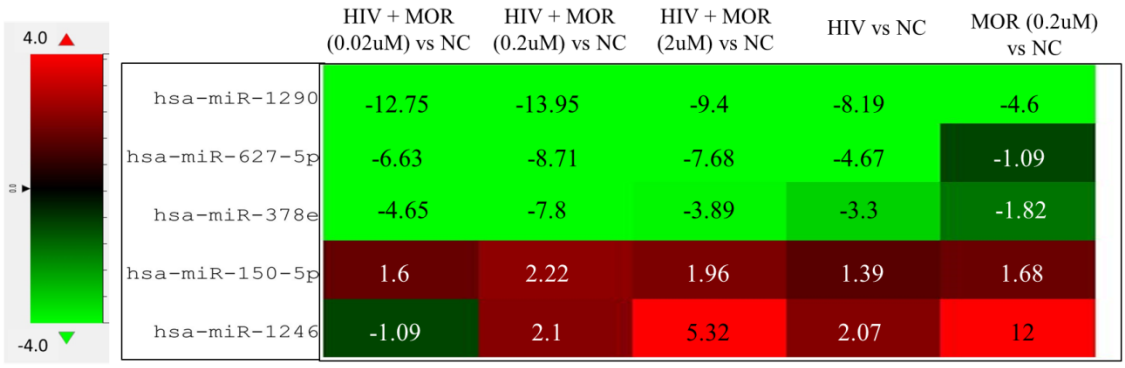

Figure 19: Differentially altered expression of miRNAs which target key genes involved in viral replication, apoptosis, and neuronal cells. The numbers listed within each cell is the fold change as a result of the listed treatment/infection.

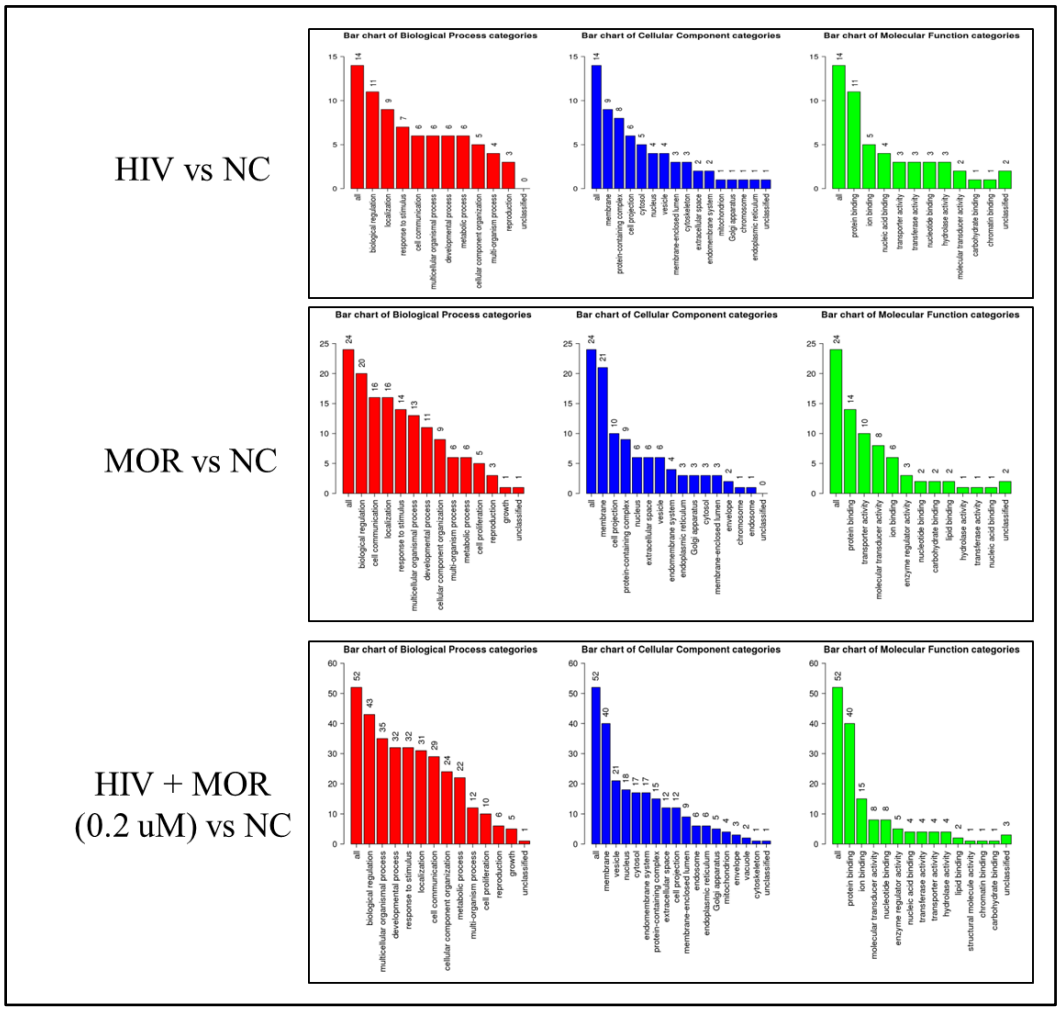

Figure 20: Bioinformatics: GOSlim summary of up-regulated miRNAs. Each Biological Process, Cellular Component and Molecular Function category is represented by a red, blue and green bar, respectively. The height of the bar represents the number of IDs in the user list and also in the category. The numbers on top are the number of target DNAs inputed that are in that category.

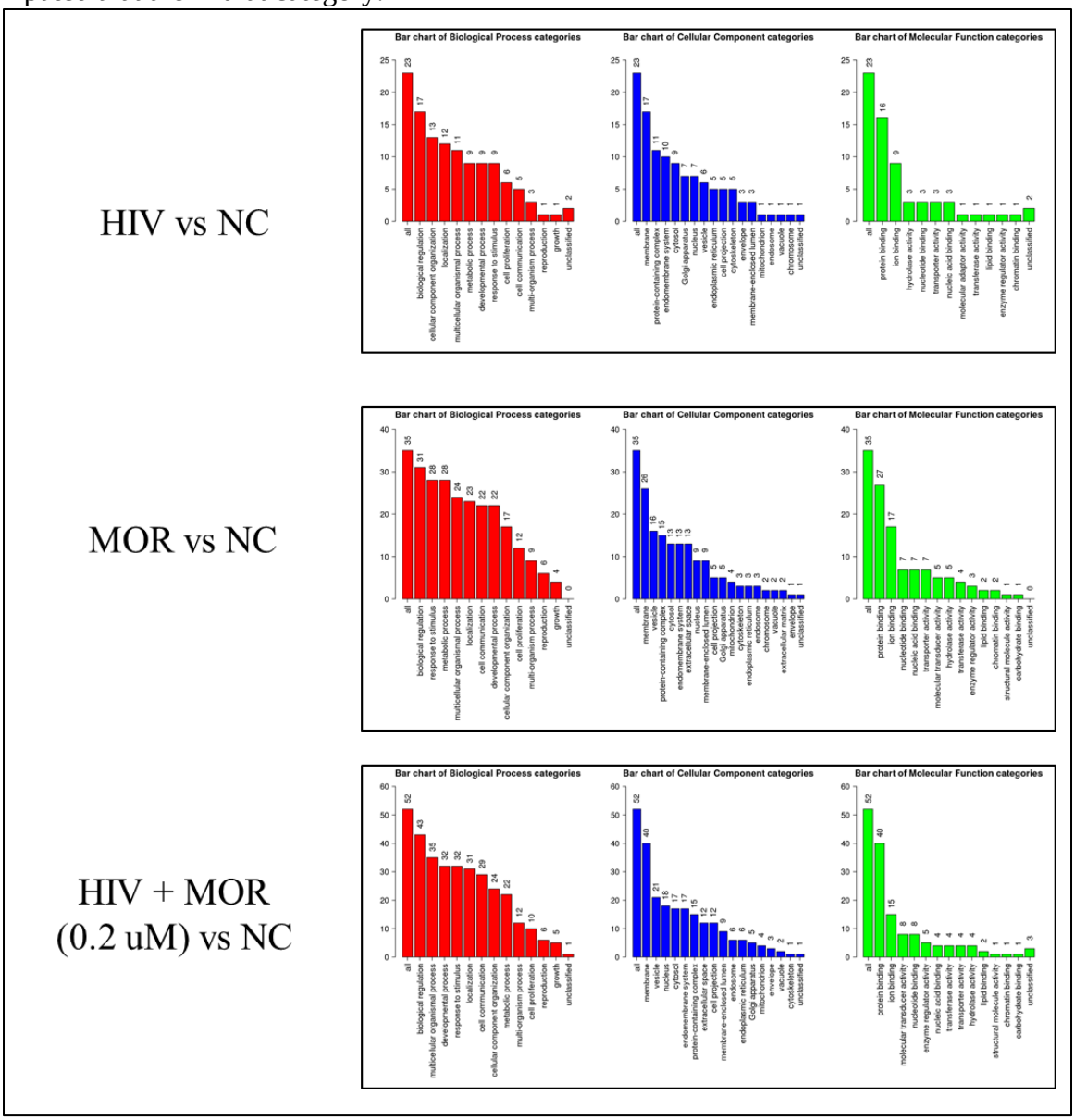

Figure 21: Bioinformatics: GOSlim summary of down-regulated miRNAs. Each Biological Process, Cellular Component and Molecular Function category is represented by a red, blue and green bar, respectively. The height of the bar represents the number of IDs in the user list and also in the category. The numbers on top are the number of target DNAs inputed that are in that category.

Upregulated miRNAs

Gene Set	Description	Size	Expect	Ratio	P Value	↑ FDR
hsa05168	Herpes simplex infection	185	0.099076	20.186	0.0035431	1
hsa04710	Circadian rhythm	31	0.016602	60.234	0.016502	1
hsa04520	Adherens junction	72	0.038559	25.934	0.038013	1
hsa04725	Cholinergic synapse	112	0.059981	16.672	0.058657	1
hsa04728	Dopaminergic synapse	131	0.070157	14.254	0.068346	1
hsa04514	Cell adhesion molecules (CAMs)	144	0.077119	12.967	0.074932	1
hsa04080	Neuroactive ligand-receptor interaction	277	0.14835	6.7410	0.14032	1

Downregulated miRNAs

Gene Set	Description	Size	Expect	Ratio	P Value	↑ FDR
R-HSA-112316	Neuronal System	368	0.48816	8.1941	0.0011025	1
R-HSA-204626	Hypusine synthesis from eIF5A-lysine	4	0.0053060	188.46	0.0052962	1
R-HSA-6794362	Protein-protein interactions at synapses	87	0.11541	17.330	0.0057319	1
R-HSA-1296071	Potassium Channels	99	0.13132	15.229	0.0073654	1
R-HSA-199991	Membrane Trafficking	628	0.83305	4.8016	0.0076943	1
R-HSA-5653656	Vesicle-mediated transport	667	0.88478	4.5209	0.0095028	1
R-HSA-1296052	Ca2+ activated K+ channels	9	0.011939	83.762	0.011880	1
R-HSA-8963888	Chylomicron assembly	9	0.011939	83.762	0.011880	1
R-HSA-8963898	Plasma lipoprotein assembly	18	0.023877	41.881	0.023629	1
R-HSA-388844	Receptor-type tyrosine-protein phosphatases	20	0.026530	37.693	0.026222	1

Table 4: Summary of Gene Sets: HIV vs NC. The table concisely summarizes the enriched functional categories with their statistics. Ratio of enrichment equals the number of observed divided by the number of expected genes from each GO or KEGG category in the gene list

Conclusion

It is good to observe that there are no changes in exosome diameter as a result of either HIV infection or morphine treatment, as an increase in size could have meant a lower concentration of exosomes. Treatment with ART (Truvada) successfully reduced viral replication, including in the presence of morphine. Given the data acquired from the Nanostring miRNA panel, it may be possible to generate an miRNA biomarker profile capable of identifying HIV-1 infected individuals or opiate drug abusers.

Upregulated miRNAs

Gene Set	Description	Size	Expect	Ratio	P Value	↑ FDR
hsa04672	Intestinal immune network for IgA production	49	0.091846	32.663	0.000091816	0.030208
hsa04924	Renin secretion	65	0.12184	16.415	0.0063441	0.52354
hsa04742	Taste transduction	83	0.15558	12.855	0.010181	0.52354
hsa05166	Human T-cell leukemia virus 1 infection	255	0.47798	6.2765	0.010827	0.52354
hsa05032	Morphine addiction	91	0.17057	11.725	0.012148	0.52354
hsa04064	NF-kappa B signaling pathway	95	0.17807	11.232	0.013189	0.52354
hsa04080	Neuroactive ligand-receptor interaction	277	0.51921	5.7780	0.013555	0.52354
hsa04660	T cell receptor signaling pathway	101	0.18932	10.564	0.014821	0.52354
hsa04625	C-type lectin receptor signaling pathway	104	0.19494	10.260	0.015669	0.52354
hsa04060	Cytokine-cytokine receptor interaction	294	0.55108	5.4439	0.015913	0.52354

Downregulated miRNAs

Gene Set	Description	Size	Expect	Ratio	P Value	↑ FDR
hsa04917	Prolactin signaling pathway	70	0.23430	17.072	0.000077145	0.013451
hsa04550	Signaling pathways regulating pluripotency of stem cells	139	0.46526	10.747	0.000081767	0.013451
hsa04380	Osteoclast differentiation	128	0.42844	9.3362	0.00078749	0.072406
hsa05213	Endometrial cancer	58	0.19414	15.453	0.00090536	0.072406
hsa05223	Non-small cell lung cancer	66	0.22091	13.58	0.0013192	0.072406
hsa05224	Breast cancer	147	0.49203	8.1295	0.0013205	0.072406
hsa04218	Cellular senescence	160	0.53555	7.469	0.0018058	0.084870
hsa01521	EGFR tyrosine kinase inhibitor resistance	79	0.26443	11.345	0.0022152	0.091102
hsa04933	AGE-RAGE signaling pathway in diabetic complications	99	0.33137	9.0533	0.0042044	0.15369
hsa04668	TNF signaling pathway	110	0.36819	8.148	0.0056467	0.16400

Table 5: Summary of Gene Sets: MORPHINE (0.2uM) vs NC. The table concisely summarizes the enriched functional categories with their statistics. Ratio of enrichment equals the number of observed divided by the number of expected genes from each GO or KEGG category in the gene list.

More research is needed in this field as this is not conclusive data. Of the miRNAs of interest, has-miR-1290 has been reported to contribute to HIV-1 latency, targeting the HIV-1 3′ UTR and suppressing viral expression. Significant downregulation of this miRNA could result in increased viral replication. miR-1290 affects pathways such as, binding and uptake of ligands by scavenger receptors and phagocytosis of microbes, Akt signaling, STAT3 pathway, TNF superfamily, and NF-kappaB Signaling.

Upregulated miRNAs

Gene Set	Description	Size	Expect	Ratio	P Value	↑ FDR
hsa04672	Intestinal immune network for IgA production	49	0.11809	16.937	0.0060330	1
hsa05110	Vibrio cholerae infection	50	0.12050	16.598	0.0062755	1
hsa04520	Adherens junction	72	0.17352	11.526	0.012690	1
hsa04742	Taste transduction	83	0.20003	9.9987	0.016634	1
hsa05032	Morphine addiction	91	0.21931	9.1197	0.019790	1
hsa04080	Neuroactive ligand-receptor interaction	277	0.66756	4.4940	0.027249	1
hsa04060	Cytokine-cytokine receptor interaction	294	0.70853	4.2341	0.031776	1
hsa04514	Cell adhesion molecules (CAMs)	144	0.34703	5.7631	0.046162	1
hsa04130	SNARE interactions in vesicular transport	34	0.081939	12.204	0.078930	1
hsa05330	Allograft rejection	38	0.091579	10.920	0.087819	1

Downregulated miRNAs

Gene Set	Description	Size	Expect	Ratio	P Value	↑ FDR
hsa04514	Cell adhesion molecules (CAMs)	144	0.48199	12.448	0.0000060576	0.0019930
hsa04668	TNF signaling pathway	110	0.36819	8.148	0.0056467	0.92888
hsa04010	MAPK signaling pathway	295	0.98741	4.0510	0.015655	1
hsa04360	Axon guidance	175	0.58575	5.1216	0.019914	1
hsa04912	GnRH signaling pathway	93	0.31129	6.4249	0.038219	1
hsa04640	Hematopoietic cell lineage	97	0.32468	6.16	0.041261	1
hsa05142	Chagas disease (American trypanosomiasis)	102	0.34141	5.8580	0.045188	1
hsa04620	Toll-like receptor signaling pathway	104	0.34811	5.7454	0.046797	1
hsa04722	Neurotrophin signaling pathway	119	0.39831	5.0212	0.059516	1
hsa04060	Cytokine-cytokine receptor interaction	294	0.98407	3.0486	0.073329	1

Table 6: Summary of Gene Sets: HIV+ MORPHINE (0.2uM) vs NC. The table concisely summarizes the enriched functional categories with their statistics. Ratio of enrichment equals the number of observed divided by the number of expected genes from each GO or KEGG category in the gene list.

Has-miR-627-5p is of interest primarily as a result of both the pathways involved and the potential synergistic downregulation observed. miR-627-5p targets genes involved in Activated TLR4 signaling, IL-2 Pathway, TNF Signaling, toll-like receptor signaling pathway, activation of cAMP-Dependent PKA and neuropathic pain-signaling in dorsal horn neurons, axon guidance, neurotransmitter clearance in the synaptic cleft, Rho GTPase cycle and signal transduction and signaling by Rho GTPases. Similary has-

miR-378e is also of interest as a result of potential synergistic effects driving downregulation and the pathways that may be altered as a result of miRNA-mediated gene silencing. miR-378e may modulate EVs targeting: nuclear receptor transcription pathway, P38 MAPK signaling pathway, gene expression, innate immune system, neutrophil degranulation, membrane trafficking, vesicle-mediated transport, AMPK signaling pathway, muscle/cardiac contraction, neuroactive ligand-receptor interaction, signaling by GPCR, peptide ligand-binding receptors. Although, there does not appear to be any significant difference between treatment groups, in regards to has-miR-150-5p, this particular miRNA has been reported in multiple studies to be modulated by HIV-infection. miR-150-5p was found to be down-regulated in patients with HAART-resistance, which has also been demonstrated to target the HIV-1 RNA genome limiting viral expression. On the other hand, has-miR-1246 is primarily of interest as a result of the experimental data acquired, although it has been previously reported to be upregulated 7.4-fold in HIV+ group relative to control group. Overall, HIV-1 and morphine induced differential miRNA expression in PBMC-derived exosomes, which, may potentially impact multiple pathways by altering EV-bound miRNA cargo, resulting in the potential modulation of genes involved in the neuronal system, cell-cell communication, TNF signaling pathway, morphine addiction, NF-K-Beta signaling pathway, autophagy, and apoptosis.

CHAPTER 4

Exosomal extracellular vesicles containing Nef are indicative of HIV-associated Neurocognitive Impairment status

Abstract

The HIV Negative factor (Nef) protein is detected in exosomal extracellular vesicles(xEVs) of serum and cerebrospinal fluid (CSF)of aviremic people living with HIV/AIDS(PLWHA). The role xEV-Nef plays in HIV infection and pathology is unknown. But may play a role in the neurocognitive impairment that some PLWHAs develop despite successful anti-retroviral therapy. Here we performed a cross-sectional study to determine whether the content of xEVs derived from serum or CSF-derived xEVs and Nef-containing-xEVs of PLWHAs correlates with the neurocognitive status of PLWHAs. Using cryopreserved serum and matched CSF from a sub-cohort of AIDS clinical trial group (ACTG)-5811 PLWHAs within the exosomal EVs were isolated from using differential ultracentrifugation. The xEVs size and protein content were characterized via Zetasizer analysis and LC- MS/MS, respectively. Nef was detected by anti-Nef ELISA in both serum and the CSF. Exosomal EVs containing Nef were found to be elevated in the CSF of PLWHAs with neurocognitive impairment. Additionally, the xEV-Nef level correlated with CD T-cell count. EV-bound proteins were profiled, providing a means by which the NCI status of a PLWHA may be ascertained. A decreased expression of TLN2 and DLGAP1 are indicative of MCMD. Whereas increased expression of SCUBE2 and ARID4A is indicative of ANI. MCND samples, displayed a greater modulation of CNS-associated pathways, such as: neurexins and neuroligins, protein-protein interactions at synapses, the glutamatergic synapse, and the neuronal system.

Introduction

Despite successful suppression of HIV viral loads by anti-retroviral therapy (ART) to undetectable levels, many aviremic HIV-infected individuals still develop neurocognitive deficits. Mechanism(s) of HIV-associated neurocognitive disorder (HAND) in aviremic patients is still unclear. Currently there are no therapeutic methods or monitoring systems that directly address the causes of neurocognitive impairment (NCI) in aviremic HIV+ subjects. We predict that extracellular vesicles (EVs) released from neuronal cells and/or immune cells within the central nervous system/periphery of aviremics may play a role in neurocognitive impairment (NCI).

Of the three classes of EVs – exosomes, microvesicles, and apoptotic bodies. Exosomal extracellular vesicles (xEVs) are the smallest ranging in size from 30-150 nm vesicles and are derived from the plasma membrane that are capable of invagination and encapsulation of cell material such as proteins, RNA, and DNA. These vesicles can then fuse with the plasma membrane and be released into the extracellular space. These exosomes can then be internalized in a juxtracrine, paracrine, or endocrine manner, resulting in transfer of the cell material to a recipient cell. Once internalized, the exosomal content can alter the recipient cell's molecular profile by various mechanisms (alterations in transcription, translation, protein modification, signaling cascades, etc.). These xEVs are hypothesized to play a large role in cell-to-cell communication. xEVs were initially identified in cells of hematopoietic lineage but have since been identified in a variety of cells including neurons, tumor cells, and epithelial cells. xEVs have been observed in body fluids such as blood, urine, and cerebrospinal fluid. It has been

determined that HIV+ individuals (viremic and aviremic) possess higher concentrations of xEVs than non-infected individuals.

HIV and other retroviruses are capable of inducing the release of xEVs from xEV-producing cells and then utilize these xEVs for viral dissemination and pathogenesis. HIV-specific proteins, such as Nef, have been identified in the xEVs, indicating that xEVs secreted from HIV-infected cells transport viral components throughout host fluids and tissues. It is hypothesized that viral dissemination and pathogenesis via xEV transport may be involved in the development of HAND in aviremic patients. HAND encompasses deficits in memory, concentration, attention, motor abilities, and other neurocognitive skills in HIV+ patients that cannot be better explained by the presence of another medical illness/condition. The National Institute of Health updated HAND criteria in 2007. HAND now includes three levels of progressively worsening neurocognitive impairments – asymptomatic neurocognitive impairment (ANI), minor cognitive motor disorder (MCMD), and HIV-associated dementia (HAD). The mechanism of HAND in aviremic patients is still unclear and currently there are no therapeutic methods or monitoring systems that directly address the causes of neurocognitive impairment in aviremic HIV+ subjects. These neurocognitive impairments can vary in severity and clinical presentation and can negatively impact the quality of life in aviremic HIV+ subjects. Daily activities such as medication adherence, driving, workplace tasks, etc. can be affected by the neurocognitive impairment. It is estimated that 50-60% of the HIV+ population is affected by HAND and, therefore, methods to monitor, diagnose, and treat HAND are needed. We hypothesize that the

exosomal extracellular vesicles (xEVs) released in the peripheral blood and/or the cerebrospinal fluid (CSF) of aviremic HIV+ subjects contribute to the development of HAND. To date no studies have examined the role of xEVs in HIV neuropathogenesis. Some PLWHAs develop neurocognitive impairment (NCI) despite undetectable viral loads. Nef is associated with HIV pathogenesis we predict that xEV-Nef correlates NCI in aviremic PLWHAs. Here we performed a cross-sectional study in which we aimed to determine whether xEVs and/or Nef-containing-xEVs in serum and/or CSF of PLWHAs correlate with the neurocognitive status of PLWHAs.

Materials and Methods

Study Design.

Clinical specimens were acquired from the ACTGC repository. Cryopreserved serum and matching CSF specimens were acquired from 30 participants. Protein cargo of exosomes derived from the CSF and/or plasma of patients diagnosed with ANI, HAND, or HAD were compared (Table 7).

Study Population

Specimens collected from demographically matched individuals without neurocognitive impairment and individual diagnosed with either ANI, MCMD, or HAD, primarily males.

Nef Enzyme Linked Immunosorbant Assay (ELISA)

Nef ELISA Nef concentration was measured using a commercially available anti-Nef ELISA kit (Immunodx, Woburn, MA). Briefly, the Nef reference was diluted 1:1

with 150 ul of diluent buffer and then 3x-serial dilution performed. Exosomes lysate were diluted 1:2 in component C and placed on the 96 well plate coated with anti-Nef monoclonal antibody. The plate was covered and incubated at room temperature (RT) for 1 hour. The plate contents removed, the plate washed three times with wash buffer (Component B), and then patted dry. Detector reagent (Component E), 100 ul was added to each well and the plate incubated at RT for 1 hour in the dark. Plates were washed and tapped dry as previously described. TMB substrate (Component F) was added to each well and blue color developed within 5-10 minutes. The reaction was stopped by adding 50 ul of Stop solution (Component G). After reaction stopped the color changed to yellow and was read at 450 nm on spectrometer (Biotek).

Extracellular Vesicles (EV)/Exosome Isolation

EVs were isolated from serum/CSF samples using standard precipitation procedures previously described (ref). Briefly, 500 ul of plasma was mixed with ExoQuick solution, incubated on ice for 30 minutes, and then centrifuged at 1500 g. Pellet was resuspended in PBS (I ml) and then filtered (.2 uM). EV were either used immediately or stored at 4 C prior to use.

Liquid Chromatography-Tandem Mass Spectrometry(LC-MS/MS)

Proteins from exosomal lysates were prepared for LC-MS/MS by using in-solution digest(ThermoScientific.com). LC-MS/MS analysis was conducted on a Brunker Tims-TOF instrument operated in positive (+) ion mode in the mass range from 300 – 2100. Chromatography separation was conducting utilizing a 46 minute long LC method with Optima grade water (0.1% Formic acid) as the aqueous phase and Optima Grade

Acetonitrile with 0.1 % Formic as the organic phase. The in-solution digested extracts were diluted 1:5 in 50:50 MeOH:Water (0.1% formic acid) and stored in silanized glass inserts placed inside a sampling vial and then loaded on to a Shimadzu Prominence HPLC autosampler. Thereafter, 20 ul aliquots were loaded into the HPLC for separation prior to MS analysis. Mass spectrometry was calibrated with TuneMixture(Agilent.com) utilizing 6 calibration points between 322 and 2121 with a reported standard deviation <1 ppm. Peptide fragmentation was conducted with Collision Induced Dissociation of the 25 most abundant precursors. Post data acquisition, the raw mass spectrometry data was processed with Peaks Studio 8.5 for protein identification and peptide sequencing.

Results

Cohort Demographics

In order to determine whether xEVs and/or Nef-containing-xEVs in serum and/or the CSF of PLWHAs correlate with the neurocognitive status of PLWHAs, cryopreserved serum of PLWHA was acquired. The study population was comprised of 40 individuals whom are primarily white (not of Hispanic origin) MSMs ranging from age 40-59. The majority of the population did not use IV drugs; however, some of the members of the cohort presented with neurocognitive impairments of some variety, as denoted in Table 7.

Figures, Tables and Schemes

In order to explore the relationship between Nef-contained EVs and the neurocognitive status of PLWHA, EVs must be isolated and characterized. Exosomes were isolated via differential ultracentrifugation (UC) and exosomal

markers were detected via western blot. Exosome size was ascertained via dynamic light scattering (DLS) using the Malvern Zetasizer Nano. Exosomal marker Alix was found to be expressed indifferently of NCI status (Figure 22A).

DEMOGRAPHICS	(n=36)
Age	
30-39	4 (11%)
40-49	17 (47%)
50-59	11 (31%)
60-69	4 (11%)
Race	
Black	6 (17%)
Other	4 (11%)
White	26 (72%)
Ethnicity	
Hispanic/Latino	11(31%)
Not Hispanic/Not Latino	25 (69%)
IV Drug Use	
Yes	5 (14%)
No	31 (86%)
Men who have sex with men (MSM)	
Yes	29 (81%)
No	7 (19%)
Clinical Diagnosis	
No significant impairment on NP Testing	16 (44%)
Neuropsychological impairment- does not meet criteria for syndromic disorder	2 (6%)
Asymptomatic Neurocognitive Impairment (ANI)	5 (14%)
Minor Cognitive Motor Disorder (MCMD)	7 (19%)
HIV-Associated Dementia (HAD)	4 (11%)
Neuropsychological impairment or dementia due to other cause	1 (3%)
Unknown	1 (3%)

Table 7. Patient demographics for a cohort of 40 patients. The cryopreserved patient serum and the demographics were acquired from the AIDS clinical trial group (ATCG) group.

Additionally, isolated exosomes were also characterized by their size. Both individuals with and without neurocognitive impairment presented with EVs within the expected size range of 30-120nm in diameter (Figure 22B). However, the average EV size was found to be greater in individuals with NCI. However, exosomal marker CD9 expression was significantly downregulated in NCI patient serum (Figure 22A). To determine whether there is a variance in the concentration of xEVs and/or Nef-containing-xEVs, in serum or CSF; ex-vivo data using plasma from ACTG was collected

via an Exocet ELISA. Total EVs isolated from patient serum and CSF were tallied and compared. A significantly greater concentration of EVs was present within patient CSF, relative to patient serum (Figure 23A).

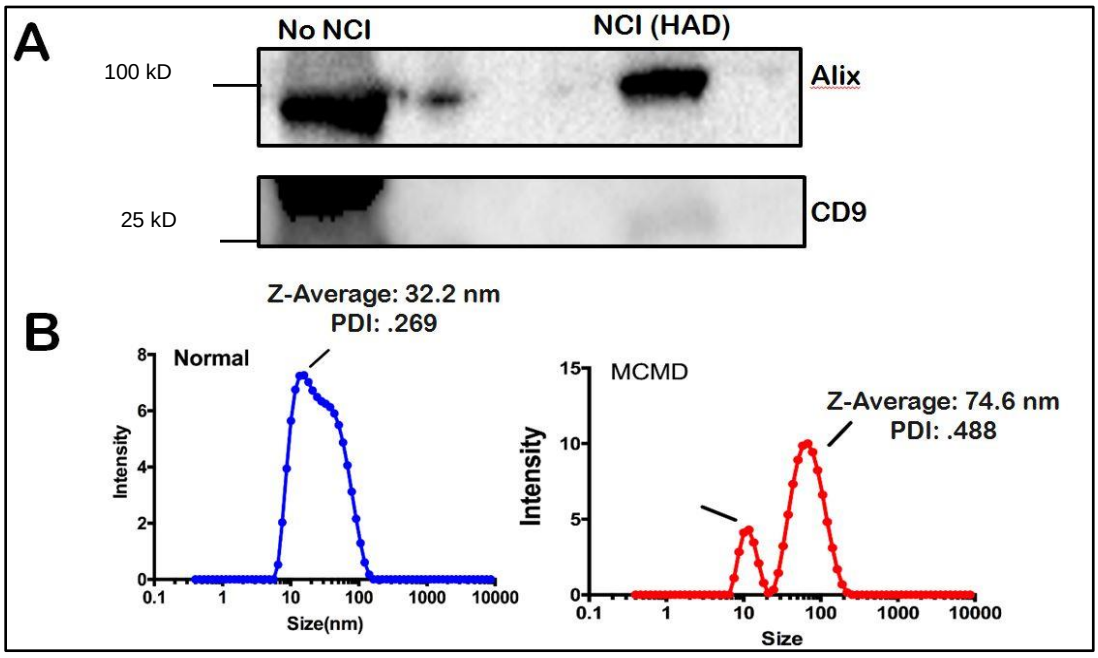

Figure 22: Exosome Characterization. xEV characterization and size (A) Western Blot representative sample of exosomal markers Alix (96 kDa) and CD9 (25 kDa) (B). Size determination of serum exosomal preparations.

An elevated concentration of EVs was detected in CSF in patients presenting with NCI, relative to asymptomatic HIV-infected patients (Figure 23B). To ascertain if Nef-containing EVs are predominant within the EV population in PLWHA presenting with NCI, the number of EVs containing Nef was attained via an anti-Nef ELISA. There was no significant difference found between individuals with NCI versus those without, within patient CSF (Figure 23C). However, there was a trend of increasing Nef-containing EVs within the serum of NCI presenting patients. This data suggests that EV concentration may function as a biomarker for NCI, as a greater presence of EVs may be found within the CSF of PLWHA presenting with NCI.

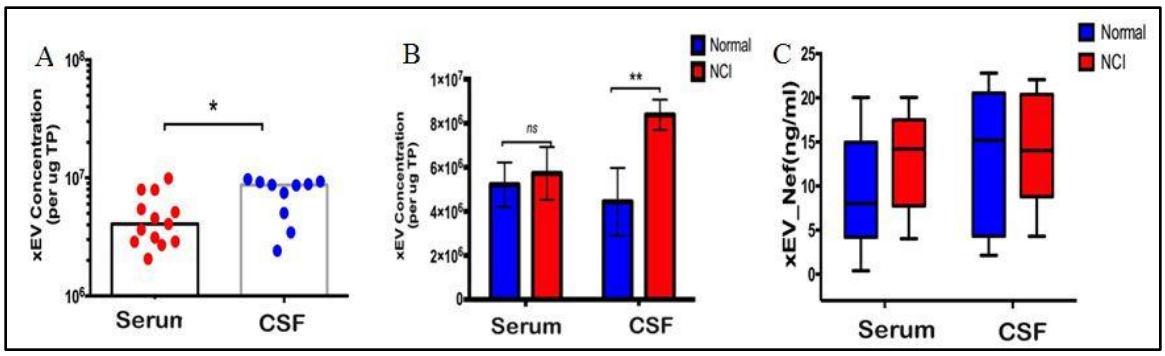

Figure 23. Exosomal EVs containing Nef are elevated in CSF of PLWHAs with neurocognitive impairment. (A) Total xEVs isolated from serum (n=13) or CSF (n=10) using Exoquick^{TM} followed by Ultra-centrifugation were enumerated via Exocet ELISA (System Biosciences). (B) xEVs from the plasma (n=13) and CSF (n=9) of PLWHAs with NCI compared to donors that did not have NCI Samples form plasma and CSF of PLWHAs (C) Nef-levels in serum- and CSF-derived xEVs from normal or NCI PLWHAs was measured via anti-Nef ELISA. Statistical significance determined using Unpaired t-Test or Two-Way ANONA; post-hoc analysis – Sidak's test. *p<.05, **p<.01, and ns=not significant.

In order to ascertain if there is any correlation between Nef-containing EVs and HIV-induced NCI, xEV-Nef concentration was compared to the Total Lymphocyte Count of CD4+ T-cells (TLC-CD4). No correlation was found between xEV-Nef concentration and TLC-CD4 in serum (Figure 24A); However, a positive correlation was observed in patient CSF (Figure 24B) and when grouped by NCI (Figure 24C). This data suggests that Nef-contained EVs may have a role in NCI development in PLWHA.

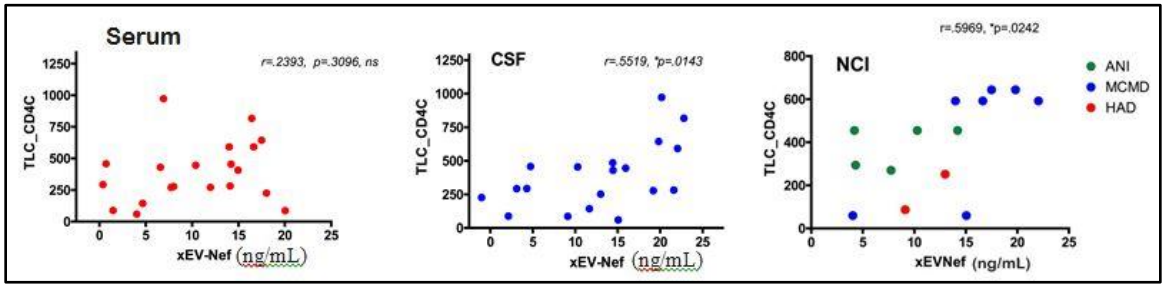

Figure 24. EVs containing Nef may be used to identify HIV-induced NCI. xEV-Nef level correlates with CD T-cell count xEV-Nef concentration in (A)serum(n=20, XY pairs) and (B) CSF(n=19, XY pairs) was correlated with TLCCD4-C independent of compartment. (C)Correlation of xEV and CD4-C in PLWHAs with NCI. Statistical significance determined using parametric analysis Pearson, r and *p<.05

In order to ascertain if EVs may serve as biomarkers of NCI for PLWHA, serum-derived EV protein content was compared to that of CSF via mass spectrometry (LC-MS/MS). In order to determine if EV-bound proteins may be employed as biomarkers capable of identifying the NCI status of a PLWHA, EV protein content was isolated from both serum and CSF patient samples and then analyzed via mass spectrometry (LC-MS/MS). The data shows that there is some differential expression of protein, dependent on NCI status (Figure 25). First, all differences observed are from serum-derived samples, as there is no significant difference in protein content between NCI groups in CSF-derived EVs. These differences in protein expression may be exploited to generate an exosomal protein profile, serving as a biomarker. The genes encoding the proteins observed to be upregulated relative to the control, for both MCMD patients in serum, are: PELP1, FGG, HBB, IGHV1-69-2, FGB, A2M, HP, and IGKV2D-28 (Table 8). However, only two proteins were found to be differentially downregulated, relative to the NC, for the MCMD patients: TLN2 and DLGAP1 (Table 8). There were no proteins found to be significantly upregulated in the ANI group relative to the NC. However, multiple proteins were found to be downregulated in the ANI group, relative to the NC: ALB, SERPINA1, IGHM, APOA1, GC, SLC12A3, NNT, TLN2, DLGAP1, IGHA1, IGKV3-20, IGLV1-47, FGA, APOC1, LRIG1, APCS, IGHV3-73, C3, TF IGKC, MYO7A, UPB1, ANKDD1A, and IGKV3D-7 (Table 8). To better develop a

profile of EV-bound protein dependent on NCI status, A GO Slim classification of the up or downregulated proteins was generated. Patients presenting with MCMD had a higher concentration of EV-bound proteins involved in biological processes including response to stimulus, biological regulation, localization, and metabolic processes (Figure 26). MCMD patient samples also presented with a downregulation of proteins primarily involved in cellular component organization, within the biological process category (Figure 26).

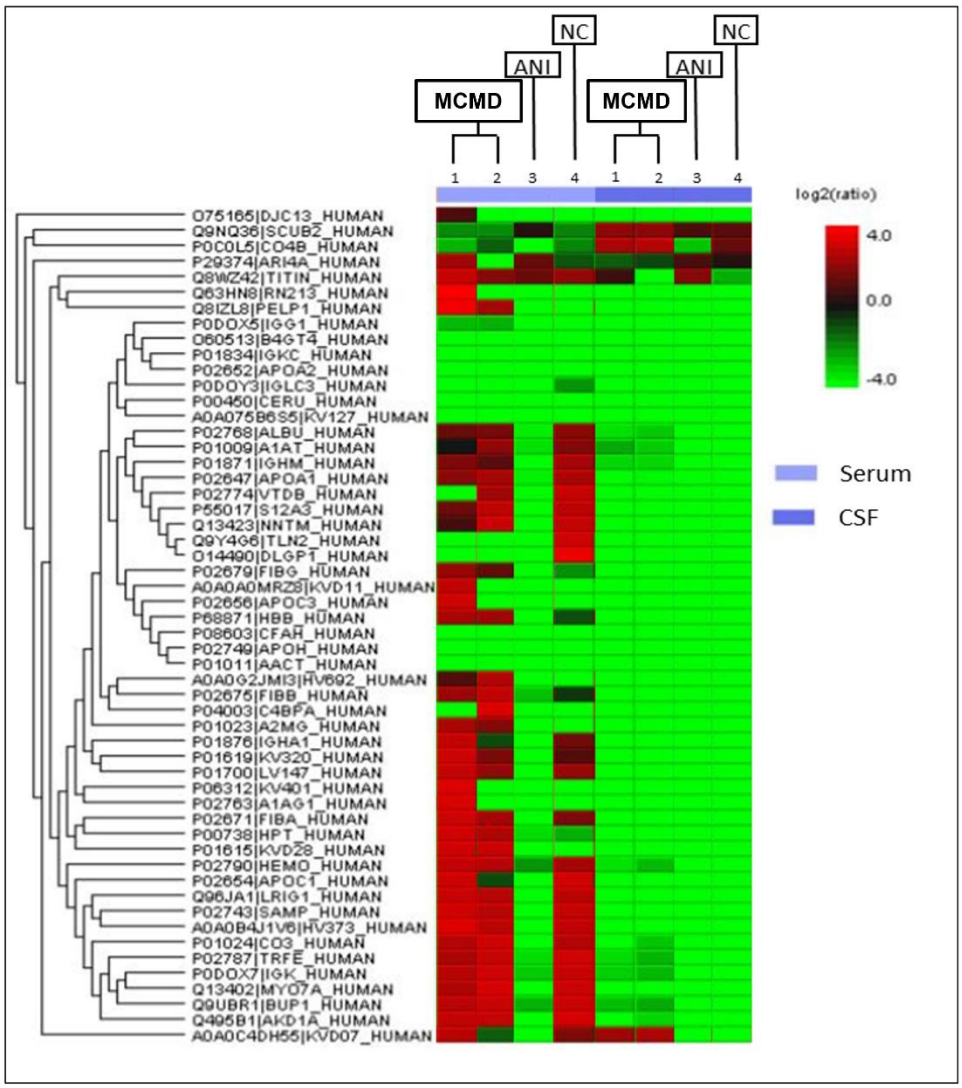

Figure 25: Biomarker of NCI in xEV composition of PLWHAs. Protein content of xEVs isolated from serum and matched CSF sample were analyzed via mass spectrometry (LC-MS/MS). Samples representative of either ANI or MCMD NCI were compared to respective non-NCI control (Normal). Depicted here is the protein content of 4 patients, patients 1 and 2 present with MCMD and are HIV+. Patient 3 presents with ANI and is HIV+. And patient 4 is an HIV+ patient without NCI. (Cell color represents the log2(ratio) to the average area across different samples)

MCMD		ANI	
Upregulated	Downregulated	Upregulated	Downregulated
PELP1	TLN2	SCUBE2	ALB
FGG	DLGAP1	ARID4A	SERPINA1
HBB			IGHM
IGHV1-69-2			APOA1
FGB			GC
A2M			SLC12A3
HP			NNT
IGKV2D-28			TLN2
			DLGAP1
			IGHA1
			IGKV3-20
			IGLV1-47
			FGA
			APOC1
			LRIG1
			APCS
			IGHV3-73
			C3
			TF
			IGKC
			MYO7A
			UPB1
			ANKDD1A
			IGKV3D-7

Table 8: List of proteins differentially expressed in or on EVs derived from patient serum. The proteins listed here are listed using the most up-to-date gene symbol, according to GeneCards the Human Gene Database (genecards.org). The proteins listed in Figure 4 were compared group-wise, by NCI status against the NC. On the left column, are listed proteins which were found to be upregulated in both of the MCMD patients versus NC. In the middle column, are listed the two proteins found to be downregulated in MCMD patient serum-derived EVs, relative to NC. Lastly, or the right column are listed proteins observed to be downregulated in ANI patients, relative to NC.

ANI samples demonstrated a similar set of modulated biological processes, including: biological regulation, metabolic process, and localization among the top 4 biological processes categories for both groups (Figure 26). Of note, ANI samples had at least twice as many proteins involved in the extracellular space, the vesicle, membrane, and transporter activity (Figure 26). In order to ascertain which pathways are affected by these modulated proteins, an over-representation analysis (ORA) using the Reactome and KEGG functional database for pathway analyses, was performed. The protein upregulated within the MCMD samples demonstrated a modulation of proteins involved in: the scavenging of heme from plasma, MAPK signaling, TLR regulation, fibrin clot formation, integrin alpha beta 3 signaling, complement and coagulation cascades, platelet degranulation and response to an elevated platelet cytosolic calcium level (Figure 27). In contrast, the downregulated proteins, within the MCMD samples, are much more involved in the CNS, involved in pathways such as: neurexins and neuroligins, protein-protein interactions at synapses, the glutamatergic synapse, and the neuronal system (Figure 27). Of note, ANI samples-derived protein modulates some pathways also modulated by MCMD's upregulated proteins, such as: complement and coagulation cascades, platelet degranulation, and scavenging of heme from plasma (Figure 27). However, a few differences may be observed between the pathways modulated by ANI and MCMD's upregulated proteins, such as: HDL remodeling, post-translational protein phosphorylation, platelet activation, signaling and aggregation (Figure 27).

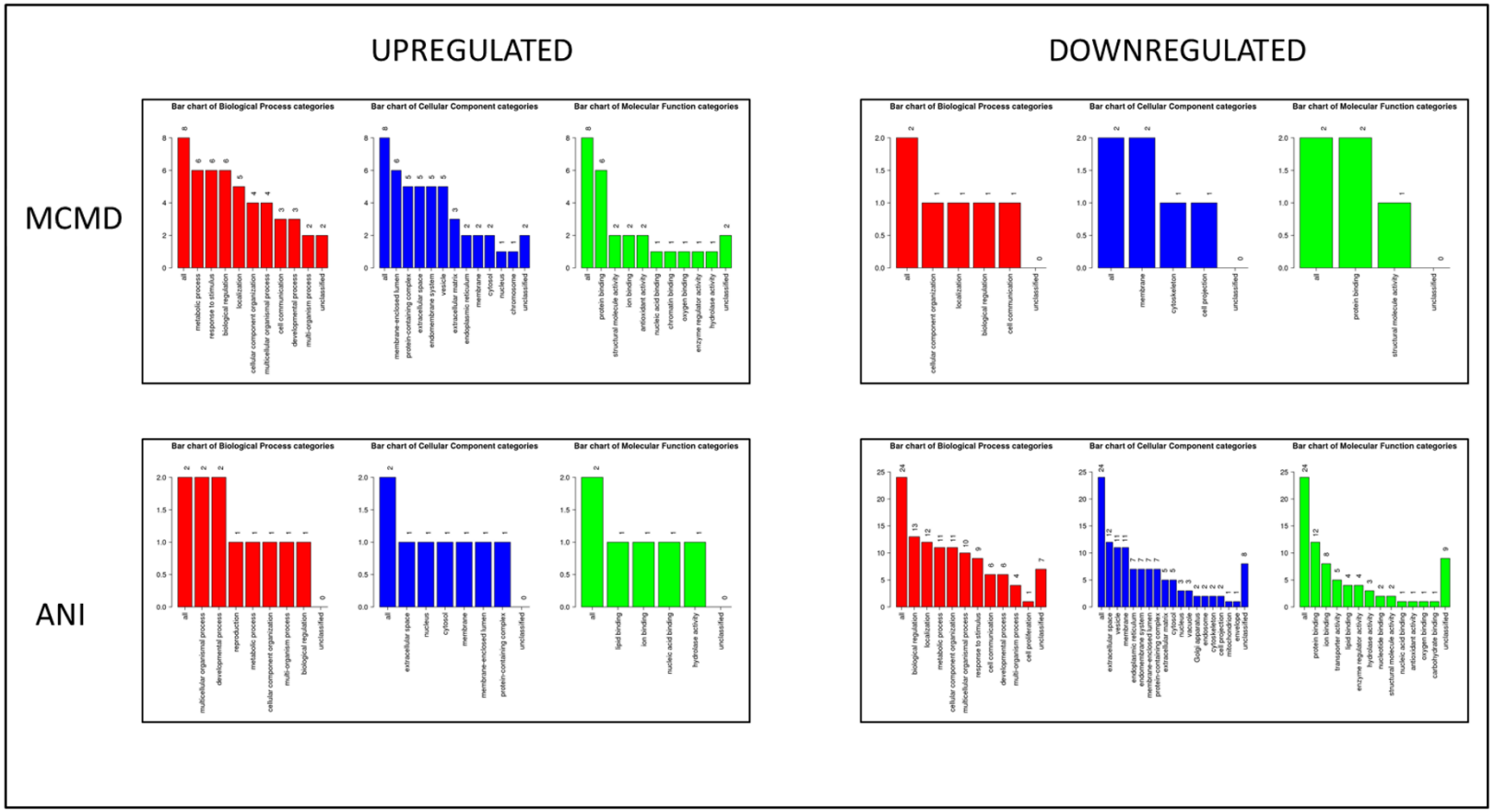

Figure 26: HIV induces differential gene expression, varying by NCI status, of EV-derived genes involved in: key biological processes, cellular components, and molecular functions. (A) A GO Slim classification of the up or downregulated proteins within each subset ratio of HIV-infected patient serum vs Uninfected patient serum, providing a high-level functional classification of the significant differentially expressed genes. GO Slim was analyzed and acquired via the WEB-based GEne SeT AnaLysis Toolkit (Webgestalt).

Figure 27: HIV induces differential gene expression, varying by NCI status, modulating various pathways critical to the immune system, the CNS, and gas-exchange-associated pathways. (A) Bar charts depicting modulated pathways as a result of HIV-induced NCI, relative to NC. Data was analyzed via the WebGestalt online tool using a complementary method for enrichment analysis, over-representation analysis (ORA), with the Reactome and KEGG functional database for pathway analyses.

Discussion

Exosomes characterized from patient serum were found to be within the expected size range for exosomes, at 32.2nm and 74.6nm in Z-Average, for normal patients and patients presenting with MCMD, respectively (Figure 22). Additionally, exosomal marker, Alix, was found to be present in both control and NCI samples (Figure 22). However, there was a notable decrease in CD9

expression, a known exosomal biomarker, in EVs derived from NCI patient serum (Figure 1). This data confirms that the isolated EVs were composed primarily of exosomes. EV concentration with respect to NCI status was then investigated, and exosomal EVs containing Nef were found to be elevated in the CSF of PLWHAs with NCI (Figure 23c). Additionally, exosome concentration was found to be elevated in the CSF of individuals presenting with NCI (Figure 23a-b). This data implies a relationship between EV-bound Nef and patient neurocognitive status. Nef has been previously observed to be transported via EVs to recipient cells [415]. This EV-bound secreted Nef is also known to enhance its own export from infected cells by increasing exosome production [416]. Studies show that Nef-EVs also initiates activation-induced apoptosis in resting CD4+ T- lymphocytes suggesting that it may be involved in the notable loss of CD4+ T-cells observed in AIDS [416]. EV-bound Nef has previously been found to rearrange lipid rafts, by re-localizing an amplifier of the innate immune response and a critical inflammatory receptor, TREM1 and TLR4 respectively, and modulate cholesterol metabolism, resulting in Nef-EVs potentiating the inflammatory response [417]. Our data shows that EV-Nef concentrations, in the CSF, correlate with CD4+ T-Cell count (Figure 24b). Additionally, EV-Nef Concentration was positively correlated with NCI status in PLWHA (Figure 24c). Altogether, these studies and this data strongly suggest a potential link between EV-bound Nef and NCI in PLWHA. This study also demonstrates the capacity of EVs derived from PLWHA to be employed as biomarkers capable of identifying the NCI status of PLWHA (Figure 25). There are also several differentially expressed proteins present on EVs derived from PLWHA dependent on NCI status, MCND or ANI (Figure 25). These proteins may be separated into groups detailing their

expression relative to a non-NCI control (Table 8). Based on this data, these protein groups may potentially serve as biomarkers of MCND or ANI. Furthermore, a profile of EV-bound protein dependent on NCI status was generated based on biological processes, cellular components, and molecular functions of the aforementioned protein groups (Figure 26). Individuals presenting with ANI could be more easily classified as they presented with at least twice as many proteins involved in the extracellular space, the vesicle, membrane, and transporter activity (Figure 26). On the other hand, MCMD may be more easily profiled by ascertaining which pathways were modulated (Figure 27). MCND samples, displayed a greater modulation of CNS-associated pathways, such as: neurexins and neuroligins, protein-protein interactions at synapses, the glutamatergic synapse, and the neuronal system (Figure 27). The establishment of an exosomal protein profile of PLWHA may aid in the identification of HIV-associated NCIs, such as MCMD or ANI.

CHAPTER 5

Magnetic Nanoparticle and Exosomal Therapeutic (M-NEXT) effects on HIV-associated Neurotoxicity.

Abstract

The Human immunodeficiency virus (HIV) envelope glycoprotein protein 120 (gp120) induces neurotoxicity associated with HIV-associated neurocognitive disorders (HAND). Mechanism of Gp120-mediated neurotoxicity is primarily apoptosis. Currently, there are no therapeutics that address gp120 neurotoxicity. A biocompatible, efficacious therapeutic that easily cross the blood-brain-barrier (BBB) is needed to treat neuronal toxicity observed in HIV-infected individuals. Magnetic nanoparticles (MNPs) have successfully delivered anti-HIV agents across *in-vitro* BBB transwell model. However, MNPs at high doses may damage cells. Exosomal extracellular vesicles (xEVs) are endogenous nanocarriers capable of crossing the BBB. Unlike MNPs, xEVs interact with cells in a paracrine or juxtracrine manner, lacking long-range site specificity. Here we investigated the efficacy of an MNP and xEV-coupled therapeutic: magnetic nanoparticle and exosomal therapeutic (M-NEXT) as a nanocarrier for targeted delivery of anti-HIV fusion agent across the BBB to inhibit HIV-gp120 associated neuropathology. M-NEXT consisting of MNPs encapsulated within xEV carrying T20 peptide on the surface was synthesized and characterized via zeta potential, dynamic light scattering, and TEM imaging. Preliminary efficacy studies using SH-SY5Y co-cultured with the *in-vitro* BBB model showed that the M-NEXT-T20-fusion peptide protected neurons from HIV gp120-mediated neurotoxicity. Additionally, BBB integrity and permeability assessed via trans-endothelial resistance (TEER) and a Dextran-FITC transport assay was unaffected. SH-SY5Y viability measured by XTT assay was not significantly modulated by M-NEXT. In

summary, preliminary findings support M-NEXT as effective nanocarriers for delivery of anti-HIV gp120 associated neurotoxicity agents.

Introduction

Human Immunodeficiency Virus (HIV), a retrovirus is the causative agent of acquired immunodeficiency syndrome (AIDS) targets cells of both the immune and nervous system [418-426]. Untreated, HIV leads to a progressive depletion of CD4+ T-cells, via induction of apoptosis, onset of infections by opportunistic pathogens, neurocognitive disorders, and eventual death [427]. The envelope glycoprotein gp120 of HIV induces human and murine neuronal cell apoptosis and/or injury accompanied by a rise in intracellular calcium levels, associated with delayed-onset neuronal injury [428-430]. This mechanism may involve the enhancement of 4-Aminopyridine-senstive outward potassium (K+) currents, exploitation of the CXCR4-NADPH oxidase-superoxide-NSMase-ceramide pathway, or mediation by the CXCR4 chemokine receptor [431-433]. However, the other mechanism of action for gp120—mediated neurotoxicity is primarily apoptosis [434]. Further evidence suggests a critical role for gp120 in HIV associated neurocognitive disorders (HAND) development, via the modulation of mitochondrial dynamics [435-437]. Currently, there are no FDA approved therapeutics to treat HIV gp120-associated neurotoxicity. Therefore, a treatment to ameliorate HIV gp120-mediated neurotoxicity is needed. However, any therapeutic employed must be capable of crossing the blood-brain barrier (BBB). The BBB is an essential diffusion barrier, composed of endothelial cells, pericytes and astrocytes, which maintains brain homeostasis by inhibiting the passage of substances from the blood to the brain. This

restriction of the diffusion of small molecules, proteins, and water-soluble substances by the BBB prevents the entry of most drugs and reduces the number of small molecule drugs capable of crossing, thereby preventing most anti-viral therapeutic compounds from crossing the BBB [438]. Given the variance in penetrative capacity among the CNS-targeting drugs, an index reflecting the capacity of a drug to penetrate the brain has been developed, the CNS penetration effectiveness (CPE) [439]. Higher HIV viral loads within the CSF correlate with a lower CPE rank [439]. Less than 2% of US Food and Drug Agency (FDA) approved small molecule drugs are able to cross the BBB intact [440]. Thus, the development of a non-immunogenic and bio-compatible nanocarrier is necessary to transport drugs or molecular agents to treat HIV neuropathology [118, 441-445]. A promising nanocarrier candidate is extracellular vesicles (EVs), specifically exosomes. EVs are membrane vesicles containing various proteins, nucleic acids, enzymes, and signaling molecules are released by most hematopoietic cells and found in bodily fluids. The transport of xEVs across cells facilitates intercellular communication, amplification of cellular responses, and modulation of the immune response and alteration of viral pathogenicity. EVs are able to cross most physiological barriers and are non-immunogenic, and capable of transporting viral content across immunological barriers such as the BBB [446]. Although EVs are an excellent therapeutic nanocarrier candidate they lack targetability. Encapsulation of magnetic nanoparticles (MNPs) within exosomes should provide enhanced targetability for the delivery of any exosome-bound cargo.[447, 448] Therefore, exosomes are an excellent candidate as a targeted drug delivery vehicle of therapeutic agents against neurotropic-virus-associated pathology. To reduce HIV gp120-mediated neurotoxicity, delivery of T20, a viral fusion inhibitor to a

site of gp120-mediated neuronal cell death should reduce gp120-mediated neuropathology [449-451]. Here we generated an exosome and MNP hybrid that effectively delivered the anti-fusion agent, T20, across the BBB, to reduce HIV gp120-mediated apoptosis in neuronal cells.

Magnetic Nanoparticles (MNPs)

In biomedicine, one of the nanoparticles most frequently used is magnetite (Fe_3O_4), primarily as a result of its specific surface properties and biocompatibility [452]. These magnetic nanoparticles react with an external magnetic field, displaying distinctive magnetic field-dependent properties [448]. Contingent on physical parameters including: a field gradient, susceptibility of particles, and particle volume, magnetic force is exerted upon magnetic nanoparticles [448]. The delivery of therapeutic agents to a site of interest is improved by this magnetic force. Magnetic nanoparticles (MNPs) of varying sizes have been investigated for targeted delivery of therapeutics and disease diagnosis [452]. Recently, a hybridization strategy where MNPs are encapsulated within exosomes, forming M-NEX, has emerged as a potential solution. An MNP-based nanotherapeutic possesses several advantages [453]. One such advantage is its inherent superparamagnetic property, providing the means to direct the MNPs to target cells of interest via its property of magnetization [453]. Thus, by utilizing a non-invasive magnetic force, the bound therapeutic agent may be transported to specific sites of interest, such as to the brain, across the BBB [453]. As a result of advances in MNP synthesis techniques, 10nm super paramagnetic MNPs capable of crossing the BBB without negatively impacting BBB integrity can be developed [454]. Additionally,

studies have demonstrated that MNPs encapsulated into liposomes, forming magnetoliposomes, may be employed for drug delivery across the BBB [455]. These now magnetized nano-carriers, M-NEXT, function the same as non-encapsulated MNPs, with similar movement and speed [453]. In this study citrate-coated magnetite MNPs are encapsulated within xEVs and linked with a therapeutic agent of choice via carbodiimide crosslinking chemistry, developing a nanotherapeutic capable of crossing the BBB and ameliorating HIV-associated neuropathology.

Materials and Methods

Cell lines

All cell lines used were cultured in respective growth media containing 10% FBS, 100 units/mL penicillin, and 100 units/mL streptomycin at 37°C in humidified air with 5% CO_2. Human embryonic kidney (HEK-293T) cells were cultured in DMEM (Gibco) supplemented with 10%FBS in T75 flasks. SH-SY5Y cells cultured at a 1:1 ratio with ATCC-formulated Eagle's Minimum Essential Medium (EMEM) (ATCC) and F12 (ATCC) media, supplemented with 10%FBS in T75 flasks and differentiated with retinoic acid (RA) until ~80% confluent. The SH-SY5Y cells were seeded unto 24-well plates. Primary cells and associated media were purchased from ScienCell; human astrocytes (HA) grown in astrocyte media (AM), human brain vascular pericytes (HBVPs) cultured in pericyte medium (PM), and human brain microvascular endothelial cells (HBMECs) cultured in endothelial cell media (ECM).

HIV Nef-GFP+ reporter virus

The plasmid for Nef-GFP+ reporter virus was acquired from the NIH AIDS reagent program and pseudotyped with VSV-G (Addgene.com). For the co-expression of eGFP and Nef from a single bicistronic RNA, Nef was cloned into an HIV-1 (NL4-3 based) proviral vector. Expression of Nef in this reporter virus is mediated by the HIV-1 LTR promoter. Co-expression of Nef and eGFP can be detected in cells infected with these reporter viruses by fluorescence microscopy.[456] HEK293T were used to package the HIV reporter virus. Briefly, HEK293T cells were seeded in 10cm dishes and cultured until 90% confluency. HEK293T cells were co-transfected with 5μg pBR43IeG-nef+ (cat#11349, Aidsreagent.org) and 5μg p-VSV (Addgene) using Lipofectamine reagent (Invitrogen) according to the manufacturer's instructions. Culture supernatant containing the reporter virus was collected 72 hours post-transfection and centrifuged 3,000 rpm for 10 min. The pellet was discarded and the cleared supernatant aliquoted and stored at -80 C. Prior to use the reporter virus was tittered using a p24 ELISA (Zeptomatrix).

Exosome isolation

Culture media of HEK 293T cells, an estimated 10mls, was collected and centrifuged at 300g for 10 min to remove cells. Supernatant was collected, and the resulting pellet discarded. The supernatant was centrifuged once more at 2000g for 10 min for removal of dead cells and debris. The pellet was discarded, the supernatant collected and centrifuged at 10,000g for 30 min to remove smaller debris. The resulting supernatant was sterile filtered via a 0.22µm filter (Fisher Scientific). The filtered supernatant was ultra-centrifuged (UC) (Beckman Coulter/ Optima MAX-XP) at

120,000g for 70min using a swing bucket rotor (Beckman Coulter/ MLS-50). The supernatant was discarded and 4.5ml of phosphate buffered saline (PBS) was then added to the pellet remaining in the UC tube. The UC tubes were ultra-centrifuged again for 70 min at 120,000g. Lastly, the supernatant was removed, and the pellet was resuspended in 160µl PBS.

MNP Synthesis

The citrate-coated MNPs used in this study were a gift from Dr. Asahi Tomitaka. These MNPs were synthesized as described in Tomitaka A, et al., 2017 [448]. Additionally, the MNPs possessed a citrate coating which was added unto the MNPs as described in Tomitaka A, et al., 2017 [448].

MNP Characterization

Size and Stability

MNP size and stability was characterized using dynamic light scattering (DLS) and zeta potential via a zetasizer (Malvern Panalytical), respectively.

Transmission Electron Microscopy (TEM)

MNP morphology was characterized via TEM imaging on a Formvar-Carbon 400-mesh grid as directed by Thery et al., 2006 [457]. Briefly, MNPs were fixed with 2% PFA, resuspended on formvar-carbon coated EM grids, and fixed with 1% glutaraldehyde. The grids were then exposed to diluted UAR-EMS stain (Electron Microscopy Sciences), as an as alternative negative stain to uranyl acetate, for 30 mins at

RT, as per manufacturer instruction. The grids were dried and then observed under the TEM at 80 kV.[457]

Inductively coupled plasma mass spectrometry (ICP/MS)

MNPs were transferred from a stock solution at 13mg/ml in a 15ml conical tube to a 2ml Eppendorf tube at a quantity of 130µg and 13 µg. Additionally, M-NEX was prepared as well at a quantity of 3.25 µg and 325ng of MNPs. Aqua regia was prepared with nitric acid (70%) and hydrochloric acid (37%), at a 1:3 ratio to digest non-tissue samples (MNPs). 400µl of aqua regia was added to the dried MNPs. The above-mentioned MNPs were then mixed with 400 µl of aqua regia. The samples were allowed to digest overnight at room temperature, in a closed 2ml Eppendorf tube. After 16 hours, the digest was transferred to a 15ml conical tube. The original 2ml Eppendorf tube was rinsed thrice with de-ionized (DI) water and the rinse solution was added to the 15ml conical tuber containing the sample. The digest solution was then brought up to 10ml with DI water. ICP-MS analysis was performed using an Agilent 7700X ICP/MS at the Trace Evidence Analysis Facility at FIU. ICP RF power was set at 1550. Nebulizer gas flow was set to 0.9 L/min. Plasma gas flow was set to 15 L/min. Collision mode(He) flow was set to 4.3 mL/min. Optima grade nitric acid was used to prepare the calibration curve and standards. The calibration curve was prepared at 0, 1, 5, 20, 50, 100, and 200 ppb. Good linearity was obtained for Fe (r2 better than 0.99). Quality control standards were prepared at concentrations of 20 ppb and 100 ppb and analyzed at the beginning and end of the analytical sequence. Each sample was analyzed in 3 replicates. Additional 1:50 dilutions were applied for the MNP samples.

X-Ray Diffraction (XRD)

400µl of MNPs at 13mg/ml, diluted in water, were placed on a glass microscope slide. The slide was then placed on a hot plate at 45°C for 2 hours, until the sample was dried. Structural conformation of MNPs was determined by x-ray diffraction using a RIGAKU Smartlab II run at 40 KV & 40 mA with a Cu alfa tube.

RAMAN Spectroscopy

MNPs were dried via heated centrifugation on a Savant SPD1010-115 SpeedVac Concentrator at 45°C for 4 hours at a vacuum pressure of 5.1 Vac, a dry black powder was obtained. Raman analyses were carried out in a home build Raman system, with excitation using a 514 nm laser at 5mW of power and a laser spot size 0.05 mm. The spectrum was measured for 10 minutes.

M-NEXT Synthesis

First step was to form M-NEX, which included just the encapsulation of MNPs within EVs. For these experiments MNPs previously synthesized at (FIU) were used [448]. Two differing methods of encapsulating MNPs within EVs were explored: incubation and sonication. Both methods involved mixing the resuspended EVs and the MNPs at a 1:40 ratio, respectively. The incubation method for MNP-EV mix involved incubation at 37°C for 1h followed by shaking at 500 rpm. For the sonication method, the MNPs were first sonicated in a water bath sonicator for 5 min, before mixed with EVs at the aforementioned 1:40 ratio. The MNP-EV mix is then probe sonicated, on ice at a low amplitude of 20% with 6 pulse cycles. Each pulse cycle consisted of 30sec on and 30sec off, for 3 min per cycle, with 2min cooling in between cycles. Sonicated samples were

then incubated for 1h at 37°C, without shaking (M-NEX). The M-NEX product was then bound to T20 peptide via amide crosslinking to EV carboxylates using N-hydroxysulfosuccinimide (Sulfo-NHS) and 1-ethyl-3-(3-dimethylaminopropyl) carbodiimide (EDC/ Thermoscientific), which yielded a stable Sulfo-NHS ester that reacted with the primary amine group on the T20 peptide. M-NEXT generated by combination of 100µl of M-NEX, 40µl of 10mg/ml EDC, 110µl of 10mg/ml Sulfo-NHS, and 50µl of 1mg/ml T20 according to manufacturer's instructions to generate M-NEXT. M-NEXT solution was placed against a magnet for 10min, supernatant removed during this period, and the remaining pellet was resuspended in 300µl PBS. The resuspension was centrifuged for 5 min at 5,000g and the resulting pellet discarded. M-NEXT formulation was contained in the supernatant and was stored at 4 C until use.

Characterization of Extracellular Vesicles (EVs)

EV size and stability was characterized using dynamic light scattering (DLS) and zeta potential via a zetasizer (Malvern Panalytical), respectively.

Western Blot

HEK-293T-derived exosome samples were washed with PBS and lysed with RIPA buffer (ThermoFisher Scientific) with protease inhibitor (Halt™, ThermoFisher Scientific) as per manufacturer's instructions. Exosome lysate protein concentration was determined via the DC protein assay (Biorad) as per manufacturer's instructions. Briefly, western blot performed as follows: Sample lysates (5-20µg) were diluted in Laemmli sample buffer, heated for 5 min at 95°, and then loaded on a Mini-Protean TGX Precast

Protein Gel (Bio-Rad). Samples were electrophoresed at 100V for 1 hour (h). Proteins were transferred to a polyvinylidene fluoride membrans (PVDF) (Bio-Rad) for 1h at 100V. PVDF membrane was then blocked with either 5% BSA or 5% milk in Tris-Buffered Saline (TBS) (Bio-Rad) with 0.1% Tween-20 (Sigma-Aldrich)(TBS-T) for 1 hour and then incubated overnight at 4°C with either anti-CD63 (1:1000, Abcam ab216130), or anti-Alix (1:500, Santa Cruz Biotechnology SC-99010) antibody. After incubation the membrane was washed with TBST and incubated with goat anti-rabbit IgG horseradish peroxidase (1:50,000, ThermoFisher Scientific) for 1 hour at room temperature (RT). The membrane was washed with TBS-T, incubated with SuperSignal West Femto (ThermoFisher Scientific) for 5 minutes and developed on CL-XPosure™ Film (ThermoFisher Scientific).

Transmission Electron Microscopy (TEM)

EVs were characterized via TEM imaging on a Formvar-Carbon 400-mesh grid to confirm size, presence, and encapsulation of MNPs as directed by Thery et al., 2006 [457]. Briefly, exosomes were fixed with 2% PFA, resuspended on formvar-carbon coated EM grids, and fixed with 1% glutaraldehyde. The grids were then exposed to diluted UAR-EMS stain (Electron Microscopy Sciences), as an as alternative negative stain to uranyl acetate, for 30 mins at RT, as per manufacturer instruction. The grids were dried and then observed under the TEM at 80 kV.[457]

Blood-Brain-Barrier (BBB) transwell model

An *in vitro* BBB transwell model was prepared as previously described [458-460]. Using HTS Transwell 24-well permeable support system (Corning), the basolateral (brain side) of the BBB was formed by layering a mix of human astrocytes (HA) and human brain vascular pericytes (HBVPs), at a 1:1 ratio on the under-face of the transwell membrane for a total cell number of $5x10^5$ per well and incubated for up to 1 hour. After incubation the transwell was placed in a well containing complete HA-PM media. HBMECs were then added to the apical (blood side) of the membrane and the mixed cell BBB model cultured at 37°C for 5 days prior to use in M-NEXT efficacy studies. The Trans Human neuroblastoma SH-SY5Y (ATCC) cell line was cultured separately in a 24-well plate which was later combined with the cultured BBB transwell plate to generate the BBB transwell model. M-NEXT formulations were added on the apical side of the BBB transwell model, placed on a magnet, and incubated overnight. Nef-GFP virus was added basolateral (brain-side) to select wells simultaneously. After 72h, cell viability was assayed as described below and the basolateral media was collected and dispensed unto a 96-well black flat-bottom plate to ascertain T20 transport via fluorescence at 485/20 excitation, and 528/20 emission using the Synergy LX Multi-Mode Reader (BioTek Instruments).

Cell viability and apoptosis

Cell viability was determined using an XTT assay (ThermoFisher) as per manufacturer's instructions. Briefly, PMS (N-methyl dibenzopyrazine methyl sulfate) was mixed with the XTT reagent at a 1:50 ratio. The XTT labeling mixture was added to the neuronal

cells and incubated for 2h at 37°C and 5% CO_2. The spectrophotometrical absorbance of the samples were measured with a microplate reader at a wavelength of 450nm using the Synergy LX Multi-Mode Reader (BioTek Instruments).

Caspase-3 activity as measured by the EnzChek Caspase-3 Assay Kit #1 (ThermoFisher Scientific) as per manufacturer instructions. Briefly, to assay caspase-3 activation, the samples were lysed, centrifuged, and pre-cleared supernatant collected. Standard and samples were placed in a 96-well plate, substrate solution added to each well, and the plate incubated for 30min at RT. Fluorescence was read at 485/20,528/20 using the Synergy LX Multi-Mode Reader (BioTek Instruments).

BBB permeability and Transendothelial electrical resistance (TEER)

The BBB integrity was ascertained by measuring TEER via the Automated Tissue Resistance Measuring System (REMS) (World Precision Instruments), an indicator for two parameters of interest: barrier tightness and strength. The permeability of the BBB membrane was determined via a Dextran-FITC transport assay as previously described.

Statistical Analysis

Experiments were performed in triplicates. Data was analyzed and graphed using GraphPad Prism 6. Statistical significance (p-value <0.05) and was determined via ANOVAs (One- and two-way) with post-hoc test (Kruskal-Wallis test) or (Tukey's multiple comparisons test). Origin 2022 was used to normalize the XRD data set from 0-100 and to both create a polynomial baseline and subtract it.

Results

Characterization of M-NEXT

Exosomes derived from XF-HEK-293T cells were characterized prior to the sonication step of the M-NEXT formulation. Exosomal biomarkers: Alix and CD63 were detected in EV preparation confirming that the population of isolated EVs contained exosomes (Fig. 28B). TEM imaging confirmed that the size and morphology of the EVs

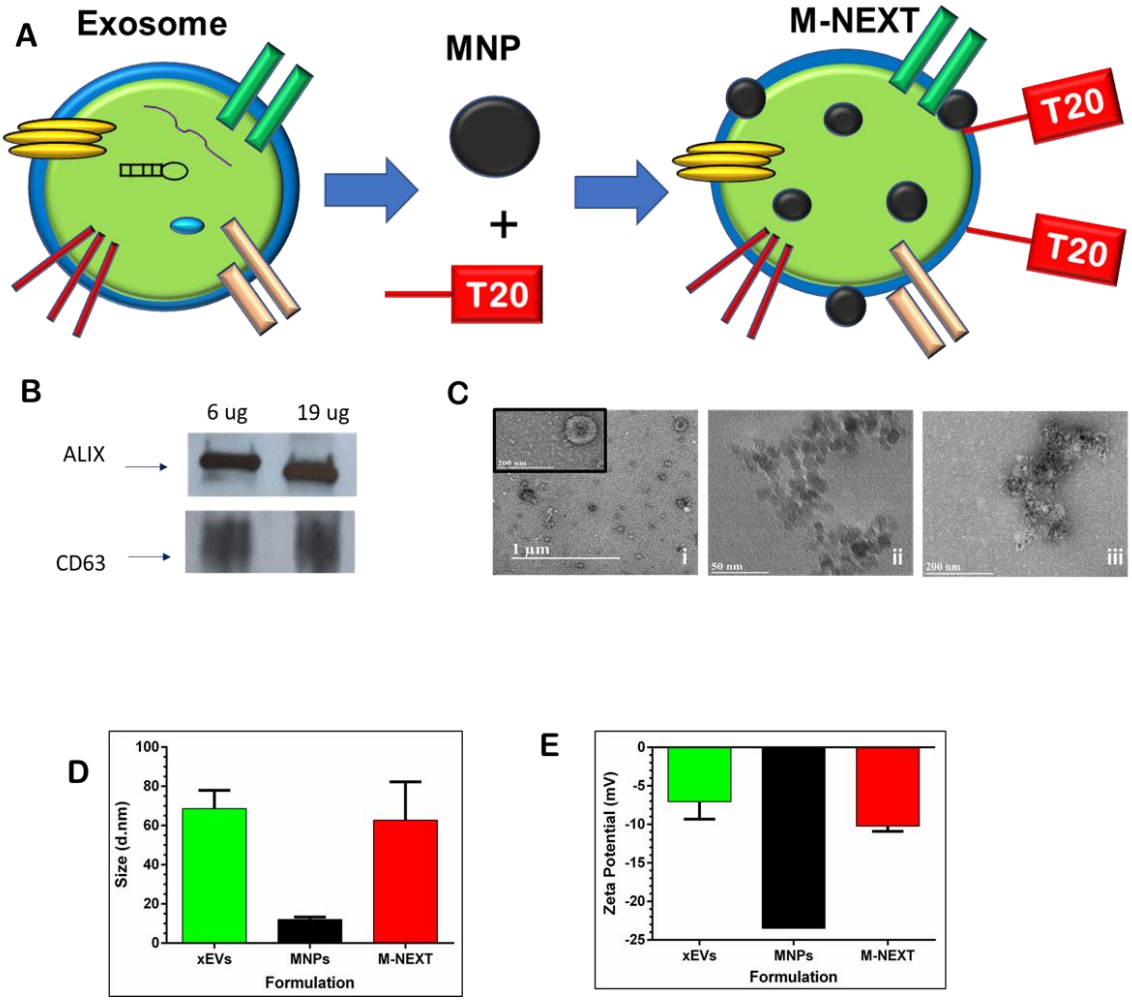

Figure 28: M-NEXT characterization. (A) Schematic of M-NEXT (B) Detection of exosomal biomarker, Alix (top) (Sigma-Aldrich) and CD63 (bottom) (abcam) via western blot of HEK-293T cells in exosome free (XF) media. (C) TEM images of xEVs (left) MNPs (middle) and M-NEXT (right). (D) Particle size of varying formulations determined by measuring a random subset of the formulations acquired via TEM

imaging. (E) Zeta potential of xEVs, as determined by Zetasizer (Malvern). Statistical significance determined by One-Way ANOVA (Kruskal-Wallis test), *p-value<.05, ns – not significant.

were within the expected range of 30-120nm (Fig. 28C-D). The stability of both the EVs and M-NEXT formulation was determined via zetasizer and deemed to be within an acceptable range (Fig. 28E). Synthesis and characterization of the MNPs used in this study were previously described (Tomitaka et al., 2017) [448].

MNP Characterization

MNP morphology and size were ascertained via TEM and DLS (Fig. 28C-D). MNP stability was determined by examining its zeta potential using the Zetasizer (Fig. 28E). Additionally, MNPs were characterized via X-Ray Diffraction (XRD), Raman spectroscopy, and ICP/MS (Fig. 29-31). The structure of the synthesized MNPs were established by X-ray diffraction spectroscopic measurement (Fig. 29A). The XRD spectra was normalized, from 0-100 and the baseline subtracted (Fig. 29B). The X-ray spectrum consisted of magnetite-specific peaks similar to those previously reported by Ding et al., 2014 and Loh et al., 2008 [452, 461]. Furthermore, ICP/MS was employed to ascertain the percentage of iron (Fe) in the MNPs in addition to quantifying the percentage of MNPs successfully loaded as measured by Fe concentration (Fig. 30). 130 µg of MNPs were found to contain 8,082 µg/L of Fe. This means that every 1µg contains 62.17 µg/L of Fe. We attempted to load 32.5 µg of MNPs in 100 µl of xEVs, this should equate to an expected Fe concentration of 2,020.5 µg/L. However, the M-NEX sample was found to contain 159 µg/L of Fe in a small sample that contained 3.25 µg of MNPs. Therefore, in a sample containing a 10-fold greater MNP quantity, such as the amount we attempted to load with EVs, there is an Fe concentration of 1,590 µg/L. This concentration equates to

78.7% of the expected concentration of the total loaded material. Thus, 25.58 µg of out of 32.5 µg of MNPs were successfully loaded, unto xEVs via sonication, as measured by ICP/MS.

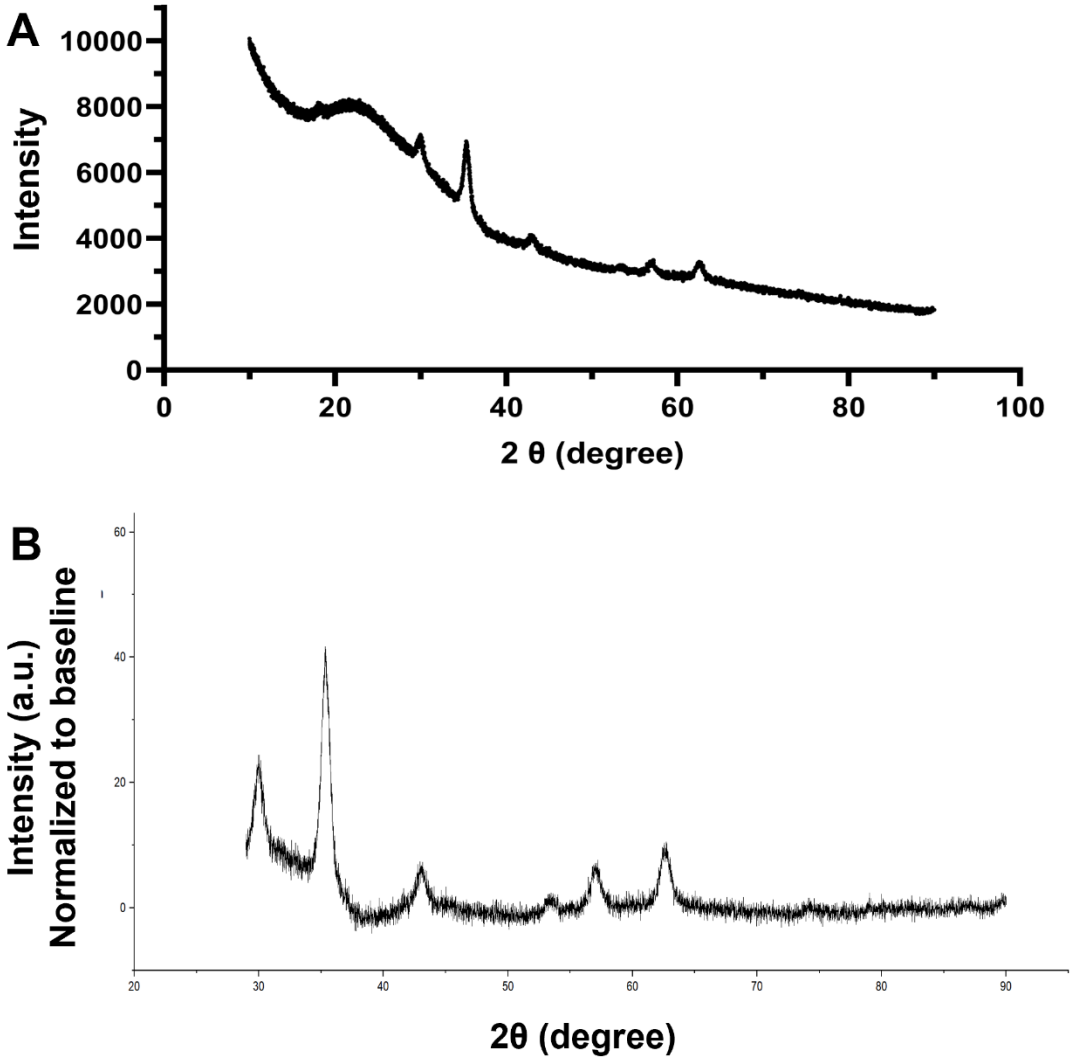

Figure 29: Characterization of MNPs via x-ray diffraction (XRD). (A) XRD spectra raw output plotted. (B) XRD spectra normalized from 0-100 and the baseline subtracted.

Displayed in Figure 31 is the Raman spectra of the citrate-coated Fe_3O_4 MNPs. Figure 31 depicts a broad peak at 610 cm-1. Additionally, 2 smaller peaks are visible at 254 cm-1 and 308 cm-1 (Fig. 31).

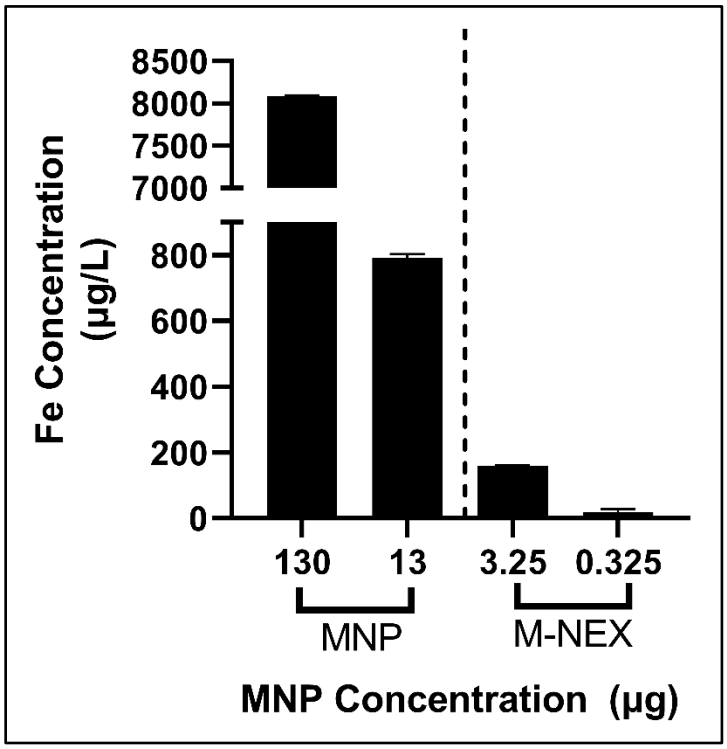

Figure 30: Iron (Fe) concentration in diluted MNP and M-NEX samples, as measured by x-ray diffraction (XRD).

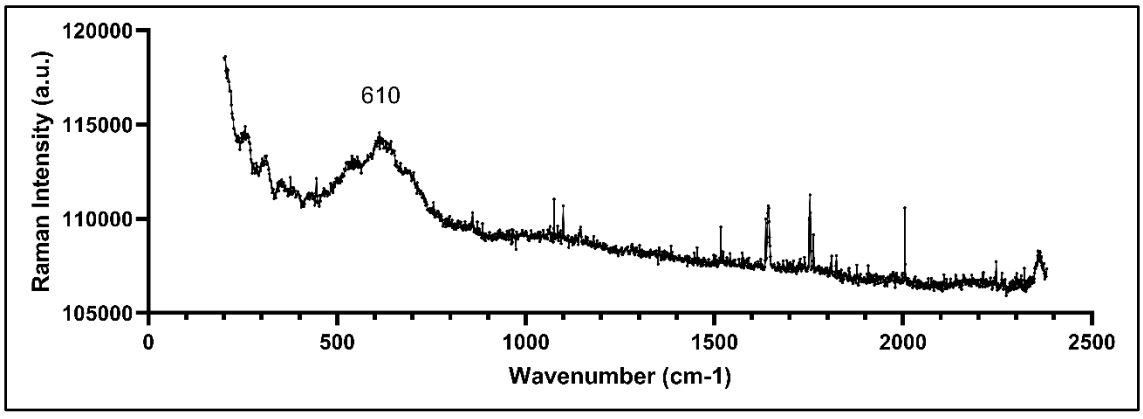

Figure 31: Raman spectrum of citrate-coated Fe_3O_4 MNPs.

Effects of M-NEX preparations on neuronal cell viability and BBB integrity

MNPs were encapsulated within the EVs via sonication prior to loading the exosomal nanocarrier with the T20 peptide. The resulting exosome-MNP hybrid was labeled M-NEX. Afterwards, the therapeutic T20 peptide was bound to the M-NEX via carbodiimide crosslinking chemistry, the complete product M-NEXT was formed. To determine the functional effects, if any, of the M-NEX formulations on their ability to ameliorate HIV-gp120 -associated neuropathology; various formulations of EVs and MNPs were generated with increasing concentrations of MNPs but a constant amount of EVs per formulation, and their effect on neuronal cell viability examined via XTT assay. Exposure of loose MNPs upon neuronal cells were found to significantly impact neuronal cell viability at a concentration of 100µg/ml of MNPs (Fig. 32A). MNPs encapsulated via sonication within EVs (M-NEX) did not significantly alter neuronal cell viability (Fig. 32B). M-NEX prepared via incubation significantly altered neuronal cell viability at an MNP concentration of 10 µg/ml (Fig. 32C). Encapsulation of MNPs within EVs was

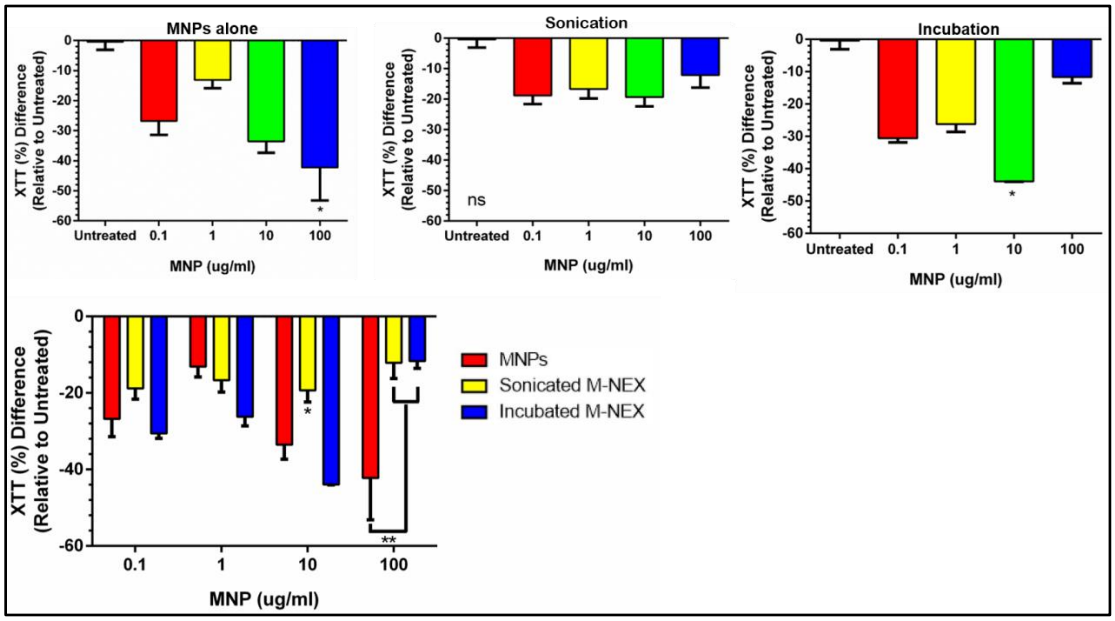

Figure 32: MNP effect on neuronal cell viability. Neuronal cell (SH-SY5Y cell line) viability as measured by XTT assay 24-hour exposure to different preparations - (A) MNPs alone, M-NEX by (B) Sonication (C) Incubation. (D) Comparison of the cell viability relative to MNPs alone. Statistical significance determined by One-Way ANOVA (post hoc test Kruskal-Wallis test), *p-value<0.05, **p-value<.01 ns – not significant. Two-Way ANOVA (Tukey's multiple comparisons test), **p=.0057, *p=.0052

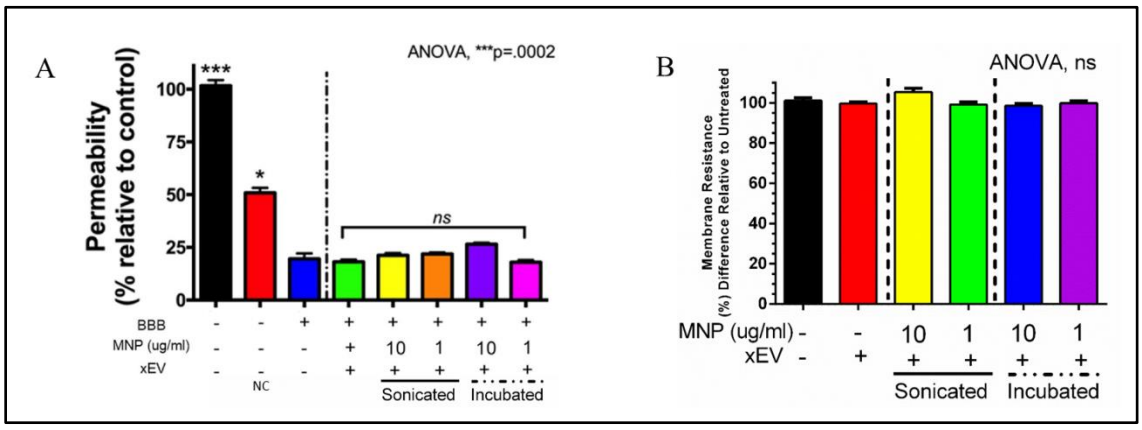

Figure 33: M-NEX does not impair BBB. (A) Permeability of the BBB transwell system 24h post-exposure to M-NEX nanoformulations measured via dextran-FITC transport. Data relative to the untreated control. (B) BBB integrity as measured by trans-endothelial electrical resistance (TEER) is modulated by M-NEX. Statistical significance determined by One-Way ANOVA (Kruskal-Wallis test), *p-value<0.05, ***p=.0002, ns – not significant.

found to significantly reduce the negative impact of MNPs on neuronal cell viability at an MNP concentration of 100µg/ml (Fig. 32D). The effect of M-NEX formulations on BBB integrity and permeability was examined using a BBB transwell model. The black bar from the left is the positive control, in which dextran-FITC was added directly to the outer chamber. The red bar next to the black bar represents passive diffusion of Dextran-FITC in complete media across a membrane without a BBB layer. M-NEX formulations did not significantly dysregulate BBB membrane permeability relative to the control, regardless of MNP concentration or encapsulation method used, as measured via dextran-FITC permeability assay (Fig. 33A). M-NEX formulations did not significantly alter BBB membrane integrity, relative to untreated control, as measured by TEER (Fig. 33B).

M-NEXT effect on BBB

To determine whether the M-NEXT formulations significantly impacted BBB integrity in the context of Nef-GFP reporter virus infection, the efficacy and the impact of M-NEXT formulations on BBB integrity, permeability, and T-20 transport across the barrier were tested using an *in-vitro* BBB transwell model (Fig. 34A). M-NEXT did not significantly modulate the integrity of the BBB membrane, as measured by TEER. Instead, M-NEXT protected against HIV-mediated loss of BBB integrity as the TEER values were not altered in wells receiving both M-NEXT and Nef-GFP virus (Fig. 34B). The BBB permeability was assessed using dextran-FITC transport assay. The HIV-Nef-GFP reporter virus alone increased permeability 30% (Fig. 34C). But in the presence of M-NEXT the viral-mediated changes in permeability were prevented and permeability was similar to the untreated control (Fig. 34C). Thus, M-NEXT protected against HIV-gp120 mediated changes in BBB permeability. Next, we assessed M-NEXT transport by measuring T-20 peptide as detected by fluorescence in media collected from the basolateral chambers. T20 peptide was mixed with exosomal protein content at a 1:10 ratio using a weight-based method previously established for click chemistry [462]. First the 3.83 µg of the fluorescent T-20 peptide was loaded unto the exosomes. Fluorescence measurements of internal controls confirmed that of the 3.83 ug of T-20 peptide incubated with M-NEX, 42.73% of the 3.83µg of T20 peptide successfully loaded unto the M-NEX formulation via carbodiimide crosslinking chemistry, thereby forming the M-NEXT. Approximately, 18% -31% of the T-20 peptide loaded M-NEXT successfully crossed the BBB in experimental samples. The experimental controls (orange and black

bars without cells) show that 42% of the T-20 peptide bound in the M-NEXT formulation compared to T20 stock solution (Fig. 34D). Taken together this data provide evidence that M-NEXT may protect against BBB damage induced by HIV.

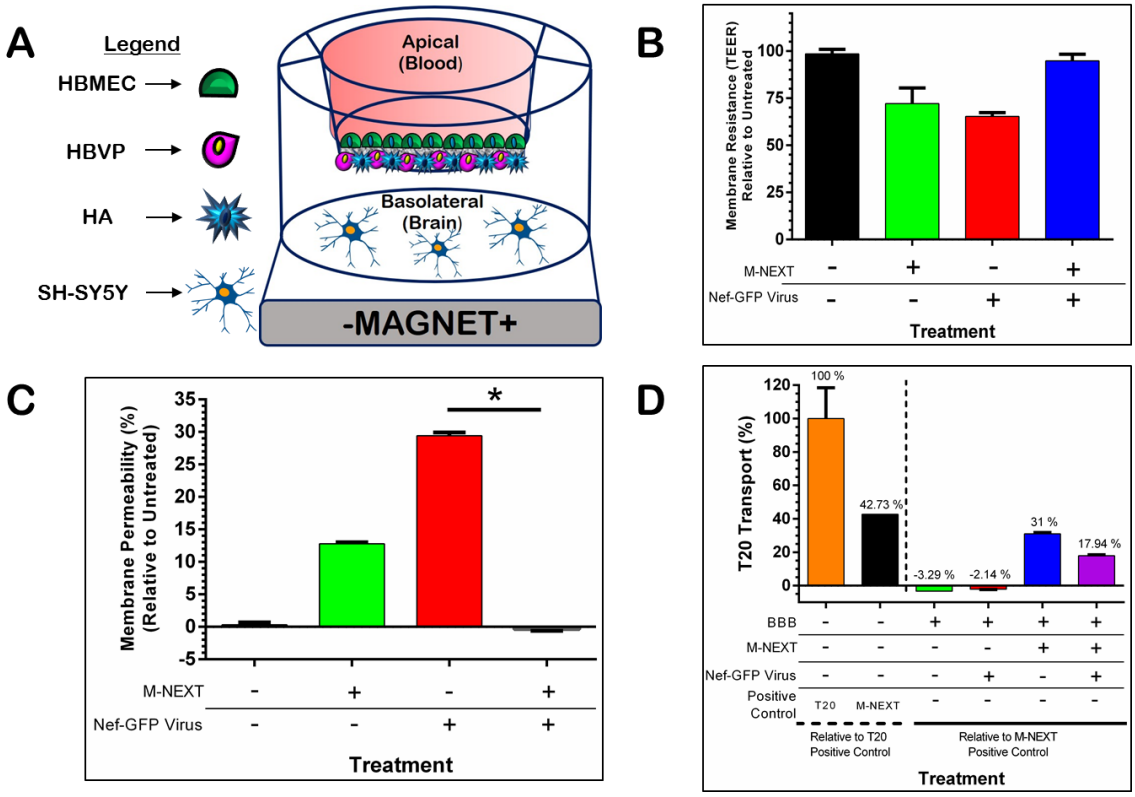

Figure 34: M-NEXT Successfully Delivered Across the BBB. (A) Schematic of In-vitro transwell model of the BBB. (B) BBB integrity as measured by trans-endothelial electrical resistance (TEER) was not significantly modulated by M-NEXT. (C) Permeability of the BBB transwell system 24h post-exposure to xEV and M-NEXT nanoformulations measured via dextran-FITC transport. (D) M-NEXT transport across BBB measured via fluorescence at 485/20,528/20. Statistical significance determined by One-Way ANOVA (post hoc analysis Kruskal-Wallis test), *p-value<0.05, ***p=.0002, ns – not significant.

M-NEXT protects against gp120/HIV neurotoxicity

To ascertain whether the M-NEXT formulations could reduce HIV gp120-medeated neurotoxicity, XTT and Caspase-3 assays were performed. SH-SY5Y viability as measured by XTT assay was reduced almost 20% upon exposure to HIV-Nef-GFP+

virus while M-NEXT pre-treatment blocked the reporter virus impact on cells and increased cell viability by 30% (Fig. 35). HIV gp120-mediated neuronal apoptosis was confirmed via caspase-3 activation. SH-SY5Y exposed to increasing concentrations of GP120 for 24, 48, and 72 hours exhibited elevated caspase-3 activation (Fig. 36A).

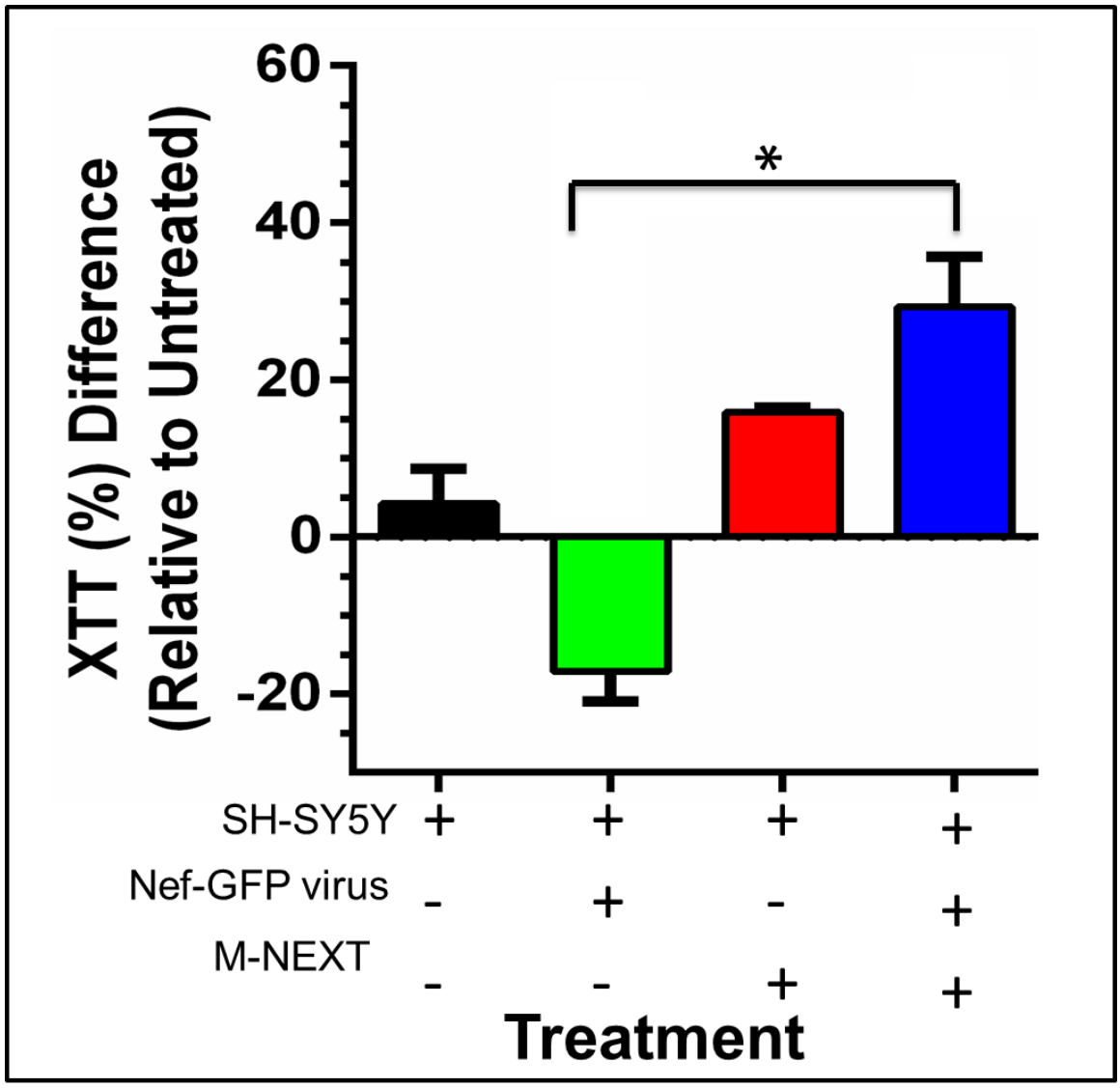

Figure 35: M-NEXT effect on neuronal cell viability. Neuronal cell viability as measured by XTT Assay (Thermo Fisher). Statistical significance determined by One-Way ANOVA (Kruskal-Wallis test), *p-value<0.05 (relative to untreated and uninfected control).

Pre-treatment with the T-20 peptide, moderately reduced caspase-3 activation in SH-SY5Y exposed to gp120 (0.6 ug) for 24 hours. Pre-treatment with T-20 peptide had a protective trend in which less caspase-3 is activated in SH-SY5Y exposed to recombinant gp120 (Fig. 36B).

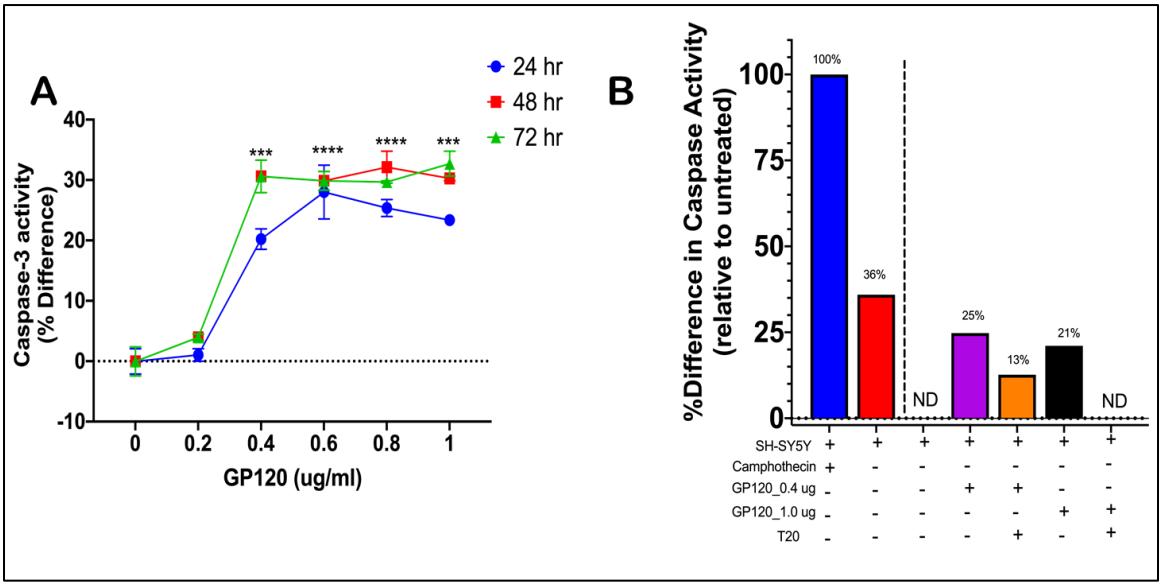

Figure 36: GP120 induces apoptosis in neuronal cells. (A) Caspase-3 activation by gp120 dose-response at 24, 48, and 72 hours (hr). (B) T20 (6 ug/ml) pre-treatment of gp120 (0.4 ug/ml) or (1.0 ug/ml) exposed neuronal cells modulated caspase-3 activity as measured by the EnzChek Caspase-3 Assay Kit #1 (ThermoFisher Scientific). Data is shown as percent difference from untreated control. Statistical significance determined by Two-Way ANOVA (post hoc Tukey's Muliple comparison test), *p-value<0.05 (relative to untreated control).

Conclusions and Discussion

This study demonstrated the feasibility an exosomal-based nanocarrier capable of crossing the BBB to deliver an agent that disrupted HIV-associated neuropathology. Here we started by showing successful exosome isolation and subsequent encapsulation of MNPs within EVs, Sonication proved to be the least damaging method for EV

encapsulation of MNPs. To ascertain the nature of the iron oxide core (magnetite), Raman spectroscopy was used, in which the Raman effect is caused by the variation in the light wavelength which occurs upon the deflection of a beam of light by molecules [463]. Additionally, magnetite is known for presenting with weak Raman scattering, particularly when using lasers at lower power levels, resulting in a lack of phase transformations induced by the laser [463]. Li Y.S et al., 2012, examined magnetite Raman spectrum peaks, in which the peak at 670 cm-1 was identified as a characteristic band [463, 464]. This study found a broad peak at 610 cm-1, close to the expected wavelength. The fact that the exposure of MNPs alone upon neuronal cells significantly reduced cell viability is noteworthy. This suggests that any MNPs bound to the EV surface and not necessarily encapsulated may cause a reduction in neuronal cell viability. However, preparation of M-NEX via either sonication or incubation was a significant improvement in the viability of the neuronal cells relative to the effects of non-encapsulated MNPs, providing further evidence supporting the use of sonication for encapsulation. Additionally, both the M-NEX and M-NEXT formulations did not negatively impact the permeability and integrity of the BBB membrane, demonstrating that it is safe to use, regardless of encapsulation method, in that regard. M-NEXT treatment protected against HIV-Nef-GFP+ reporter virus induced reduction in membrane permeability. Of note, over 42% of the T20 peptide incubated with M-NEX successfully conjugated. Loading efficiency was about 9% higher than in previous experiments (data not shown) with 31% of the M-NEXT added on the apical (blood side) successfully crossing the *in vitro* BBB . Thus, only 13.25% of the T20 dosage bound to M-NEXT and crossed the BBB.

HIV Nef-GFP+ virus alone negatively impacted neuronal viability. However, M-NEXT pre-treatment protected the neuronal cell line from the loss of viability exhibited by cells treated with Nef-GFP+ virus alone, suggesting that the nanocarrier hybrid M-NEXT can effectively protect against virion associated gp120 induced toxicity. Overall, this study demonstrated a potential EV-based nanotherapeutics to combat HIV-induced apoptosis. Other studies have used the properties of magnetism to isolate and characterize exosomes, whereas here we explored the use of magnetism for enhanced targeting of the EV to cells [465]. Unlike other studies, which focused on MNP-based viral detection using flow cytometry to detect HIV-1 gp120, this study focused on combating gp120-mediated neuronal apoptosis [466]. Although MNPs have been investigated for target-specific drug delivery, there has been a lack of progress in the application of MNPs for drug delivery across the BBB [467]. This study explored employing an exosome-based nanotherapeutic with an MNP enhanced targeting feature. Preliminary findings showed M-NEXT to be efficacious in an *in vitro* BBB model. MNPs have been previously employed for the following: (1) the electrochemical characterization and detection of exosomes, (2) exosomal protein analysis via MNP-labeling of exosomal protein or surface markers, and (3) amelioration of the exosomal Nef-mediated functional effects upon the BBB, by adsorbing a myristoylated Nef peptide [460, 468-470]. This work provides a proof-of-concept of an exosome/MNP hybrid therapeutic with the capacity for targeted safe delivery of a therapeutic agent across the BBB that can ameliorate HIV-associated induction of neuronal apoptosis. Future studies will investigate M-NEXT efficacy in the reduction of HIV-1 and/or gp120- associated neuropathology *in vivo* models.

REFERENCES

1. van Niel, G., G. D'Angelo, and G. Raposo, *Shedding light on the cell biology of extracellular vesicles.* Nat Rev Mol Cell Biol, 2018. **19**(4): p. 213-228.

2. Caobi, A., M. Nair, and A.D. Raymond, *Extracellular Vesicles in the Pathogenesis of Viral Infections in Humans.* Viruses, 2020. **12**(10): p. 1200.

3. Johnstone, R.M., et al., *Vesicle formation during reticulocyte maturation. Association of plasma membrane activities with released vesicles (exosomes).* J Biol Chem, 1987. **262**(19): p. 9412-20.

4. Caruso, S. and I.K.H. Poon, *Apoptotic Cell-Derived extracellular vesicles: More Than Just Debris.* Frontiers in Immunology, 2018. **9**.

5. Robbins, P.D. and A.E. Morelli, *Regulation of immune responses by extracellular vesicles.* Nat Rev Immunol, 2014. **14**(3): p. 195-208.

6. MacKenzie, A., et al., *Rapid Secretion of Interleukin-1β by Microvesicle Shedding.* Immunity, 2001. **15**(5): p. 825-835.

7. Alenquer, M. and M.J. Amorim, *Exosome Biogenesis, Regulation, and Function in Viral Infection.* Viruses, 2015. **7**(9): p. 5066-83.

8. Camussi, G., et al., *Exosome/microvesicle-mediated epigenetic reprogramming of cells.* Am J Cancer Res, 2011. **1**(1): p. 98-110.

9. Eitan, E., et al., *Impact of lysosome status on extracellular vesicle content and release.* Ageing Res Rev, 2016. **32**: p. 65-74.

10. Harding, C. and P. Stahl, *Transferrin recycling in reticulocytes: pH and iron are important determinants of ligand binding and processing.* Biochemical and Biophysical Research Communications, 1983. **113**(2): p. 650-658.

11. Pan, B.-T. and R.M. Johnstone, *Fate of the transferrin receptor during maturation of sheep reticulocytes in vitro: Selective externalization of the receptor.* Cell, 1983. **33**(3): p. 967-978.

12. Barz, D., et al., *Characterization of cellular and extracellular plasma membrane vesicles from a non-metastasizing lymphoma (Eb) and its metastasizing variant (ESb).* Biochimica et Biophysica Acta (BBA) - Biomembranes, 1985. **814**(1): p. 77-84.

13. Schirrmacher, V. and D. Barz, *Characterization of cellular and extracellular plasmamembrane vesicles from a low metastatic lymphoma (Eb) and its high metastatic variant (ESb): inhibitory capacity in cell-cell interaction systems.* Biochimica et Biophysica Acta (BBA) - Biomembranes, 1986. **860**(2): p. 236-242.

14. Raposo, G., et al., *B lymphocytes secrete antigen-presenting vesicles.* The Journal of experimental medicine, 1996. **183**(3): p. 1161-1172.

15. Schorey, J.S. and C.V. Harding, *Extracellular vesicles and infectious diseases: new complexity to an old story.* The Journal of clinical investigation, 2016. **126**(4): p. 1181-1189.

16. Santos, P. and F. Almeida, *Exosome-Based Vaccines: History, Current State, and Clinical Trials.* Frontiers in immunology, 2021. **12**: p. 711565-711565.

17. Martins, S.d.T. and L.R. Alves, *Extracellular Vesicles in Viral Infections: Two Sides of the Same Coin?* Frontiers in cellular and infection microbiology, 2020. **10**: p. 593170-593170.

18. Gould, S.J., A.M. Booth, and J.E.K. Hildreth, *The Trojan exosome hypothesis.* Proceedings of the National Academy of Sciences of the United States of America, 2003. **100**(19): p. 10592-10597.

19. Teow, S.-Y., et al., *Exosomes in Human Immunodeficiency Virus Type I Pathogenesis: Threat or Opportunity?* Advances in virology, 2016. **2016**: p. 9852494-9852494.

20. Nolte-'t Hoen, E., et al., *Extracellular vesicles and viruses: Are they close relatives?* Proc Natl Acad Sci U S A, 2016. **113**(33): p. 9155-61.

21. Stuffers, S., et al., *Multivesicular endosome biogenesis in the absence of ESCRTs.* Traffic, 2009. **10**(7): p. 925-37.

22. Raiborg, C. and H. Stenmark, *The ESCRT machinery in endosomal sorting of ubiquitylated membrane proteins.* Nature, 2009. **458**(7237): p. 445-52.

23. Trajkovic, K., et al., *Ceramide triggers budding of exosome vesicles into multivesicular Endosomes.* Science, 2008. **319**(5867): p. 1244-1247.

24. Menck, K., et al., *Neutral sphingomyelinases control extracellular vesicles budding from the plasma membrane.* J Extracell Vesicles, 2017. **6**(1): p. 1378056.

25. Yu, L.L., et al., *A Comparison of Traditional and Novel Methods for the Separation of Exosomes from Human Samples.* Biomed Res Int, 2018. **2018**: p. 3634563.

26. Livshits, M.A., et al., *Corrigendum: Isolation of exosomes by differential centrifugation: Theoretical analysis of a commonly used protocol.* Sci Rep, 2016. **6**: p. 21447.

27. Jeppesen, D.K., et al., *Comparative analysis of discrete exosome fractions obtained by differential centrifugation.* J Extracell Vesicles, 2014. **3**: p. 25011.

28. Szatanek, R., et al., *Isolation of extracellular vesicles: Determining the correct approach (Review).* Int J Mol Med, 2015. **36**(1): p. 11-7.

29. Konadu, K.A., et al., *Isolation of Exosomes from the Plasma of HIV-1 Positive Individuals.* J Vis Exp, 2016(107).

30. Tauro, B.J., et al., *Comparison of ultracentrifugation, density gradient separation, and immunoaffinity capture methods for isolating human colon cancer cell line LIM1863-derived exosomes.* Methods, 2012. **56**(2): p. 293-304.

31. Whiteside, T.L., *The potential of tumor-derived exosomes for noninvasive cancer monitoring: an update.* Expert Rev Mol Diagn, 2018. **18**(12): p. 1029-1040.

32. Kamerkar, S., et al., *Exosomes facilitate therapeutic targeting of oncogenic KRAS in pancreatic cancer.* Nature, 2017. **546**(7659): p. 498-503.

33. Lobb, R.J., et al., *Optimized exosome isolation protocol for cell culture supernatant and human plasma.* J Extracell Vesicles, 2015. **4**: p. 27031.

34. Alvarez, M.L., et al., *Comparison of protein, microRNA, and mRNA yields using different methods of urinary exosome isolation for the discovery of kidney disease biomarkers.* Kidney Int, 2012. **82**(9): p. 1024-32.

35. Bhattacharjee, C. and M. Singh, *Studies on the applicability of artificial neural network (ANN) in continuous stirred ultrafiltration.* Chemical Engineering & Technology, 2002. **25**(12): p. 1187-1192.

36. Rojalin, T., et al., *Nanoplasmonic Approaches for Sensitive Detection and Molecular Characterization of Extracellular Vesicles.* Front Chem, 2019. **7**: p. 279.

37. Liu, F., et al., *The Exosome Total Isolation Chip.* ACS Nano, 2017. **11**(11): p. 10712-10723.

38. Théry, C., et al., *Isolation and characterization of exosomes from cell culture supernatants and biological fluids.* Curr Protoc Cell Biol, 2006. **Chapter 3**: p. Unit 3.22.

39. Andreu, Z. and M. Yanez-Mo, *Tetraspanins in extracellular vesicle formation and function.* Front Immunol, 2014. **5**: p. 442.

40. Akers, J.C., et al., *Biogenesis of extracellular vesicles (EV): exosomes, microvesicles, retrovirus-like vesicles, and apoptotic bodies.* J Neurooncol, 2013. **113**(1): p. 1-11.

41. Kowal, J., M. Tkach, and C. Thery, *Biogenesis and secretion of exosomes.* Curr Opin Cell Biol, 2014. **29**: p. 116-25.

42. Thery, C., et al., *Proteomic analysis of dendritic cell-derived exosomes: a secreted subcellular compartment distinct from apoptotic vesicles.* J Immunol, 2001. **166**(12): p. 7309-18.

43. Hsu, C., et al., *Regulation of exosome secretion by Rab35 and its GTPase-activating proteins TBC1D10A-C.* J Cell Biol, 2010. **189**(2): p. 223-32.

44. Savina, A., et al., *Rab11 promotes docking and fusion of multivesicular bodies in a calcium-dependent manner.* Traffic, 2005. **6**(2): p. 131-43.

45. Ostrowski, M., et al., *Rab27a and Rab27b control different steps of the exosome secretion pathway.* Nat Cell Biol, 2010. **12**(1): p. 19-30; sup pp 1-13.

46. Dias, M.V.S., C.S. Costa, and L.L.P. daSilva, *The Ambiguous Roles of Extracellular Vesicles in HIV Replication and Pathogenesis.* Front Microbiol, 2018. **9**: p. 2411.

47. Baixauli, F., C. Lopez-Otin, and M. Mittelbrunn, *Exosomes and autophagy: coordinated mechanisms for the maintenance of cellular fitness.* Front Immunol, 2014. **5**: p. 403.

48. Bretz, N.P., et al., *Body fluid exosomes promote secretion of inflammatory cytokines in monocytic cells via Toll-like receptor signaling.* J Biol Chem, 2013. **288**(51): p. 36691-702.

49. Buzas, E.I., et al., *Emerging role of extracellular vesicles in inflammatory diseases.* Nat Rev Rheumatol, 2014. **10**(6): p. 356-64.

50. Clayton, A., et al., *Analysis of antigen presenting cell derived exosomes, based on immuno-magnetic isolation and flow cytometry.* J Immunol Methods, 2001. **247**(1-2): p. 163-74.

51. Kahlert, C. and R. Kalluri, *Exosomes in tumor microenvironment influence cancer progression and metastasis.* J Mol Med (Berl), 2013. **91**(4): p. 431-7.

52. Melo, S.A., et al., *Cancer exosomes perform cell-independent microRNA biogenesis and promote tumorigenesis.* Cancer Cell, 2014. **26**(5): p. 707-21.

53. Raposo, G., et al., *B lymphocytes secrete antigen-presenting vesicles.* J Exp Med, 1996. **183**(3): p. 1161-72.

54. Chahar, H.S., X.Y. Bao, and A. Casola, *Exosomes and Their Role in the Life Cycle and Pathogenesis of RNA Viruses.* Viruses-Basel, 2015. **7**(6): p. 3204-3225.

55. Ramakrishnaiah, V., et al., *Exosome-mediated transmission of hepatitis C virus between human hepatoma Huh7.5 cells.* Proceedings of the National Academy of Sciences of the United States of America, 2013. **110**(32): p. 13109-13113.

56. Altan-Bonnet, N., *Extracellular vesicles are the Trojan horses of viral infection.* Curr Opin Microbiol, 2016. **32**: p. 77-81.

57. Chen, Y.H., et al., *Phosphatidylserine vesicles enable efficient en bloc transmission of enteroviruses.* Cell, 2015. **160**(4): p. 619-630.

58. Inal, J.M. and S. Jorfi, *Coxsackievirus B transmission and possible new roles for extracellular vesicles.* Biochemical Society Transactions, 2013. **41**: p. 299-302.

59. Kalamvoki, M., T. Du, and B. Roizman, *Cells infected with herpes simplex virus 1 export to uninfected cells exosomes containing STING, viral mRNAs, and microRNAs.* Proc Natl Acad Sci U S A, 2014. **111**(46): p. E4991-6.

60. Gutzeit, C., et al., *Exosomes derived from Burkitt's lymphoma cell lines induce proliferation, differentiation, and class-switch recombination in B cells.* J Immunol, 2014. **192**(12): p. 5852-62.

61. Keryer-Bibens, C., et al., *Exosomes released by EBV-infected nasopharyngeal carcinoma cells convey the viral latent membrane protein 1 and the immunomodulatory protein galectin 9.* BMC Cancer, 2006. **6**: p. 283.

62. Klibi, J., et al., *Blood diffusion and Th1-suppressive effects of galectin-9-containing exosomes released by Epstein-Barr virus-infected nasopharyngeal carcinoma cells.* Blood, 2009. **113**(9): p. 1957-66.

63. Dukers, D.F., et al., *Direct immunosuppressive effects of EBV-encoded latent membrane protein 1.* J Immunol, 2000. **165**(2): p. 663-70.

64. Flanagan, J., J. Middeldorp, and T. Sculley, *Localization of the Epstein-Barr virus protein LMP 1 to exosomes.* J Gen Virol, 2003. **84**(Pt 7): p. 1871-9.

65. Baseler, L., et al., *The Pathogenesis of Ebola Virus Disease.* Annual Review of Pathology: Mechanisms of Disease, 2017. **12**(1): p. 387-418.

66. Nehls, J., et al., *Release of Immunomodulatory Ebola Virus Glycoprotein-Containing Microvesicles Is Suppressed by Tetherin in a Species-Specific Manner.* Cell Rep, 2019. **26**(7): p. 1841-1853 e6.

67. Pleet, M.L., et al., *Ebola Virus VP40 Modulates Cell Cycle and Biogenesis of Extracellular Vesicles.* J Infect Dis, 2018. **218**(suppl_5): p. S365-S387.

68. Messaoudi, I., G.K. Amarasinghe, and C.F. Basler, *Filovirus pathogenesis and immune evasion: insights from Ebola virus and Marburg virus.* Nature reviews. Microbiology, 2015. **13**(11): p. 663-676.

69. Pleet, M.L., et al., *Ebola VP40 in Exosomes Can Cause Immune Cell Dysfunction (vol 7, 1765, 2016).* Frontiers in Microbiology, 2018. **9**.

70. Chahar, H.S., et al., *Respiratory Syncytial Virus Infection Changes Cargo Composition of Exosome Released from Airway Epithelial Cells.* Sci Rep, 2018. **8**(1): p. 387.

71. Bomberger, J., et al., *Exosome-Associated Iron Release during Respiratory Virus Co-Infection Enhances Pseudomonas aeruginosa Biofilm Growth.* The FASEB Journal, 2016. **30**(1_supplement): p. 1223.23-1223.23.

72. Kesimer, M., et al., *Characterization of exosome-like vesicles released from human tracheobronchial ciliated epithelium: a possible role in innate defense.* FASEB journal : official publication of the Federation of American Societies for Experimental Biology, 2009. **23**(6): p. 1858-1868.

73. Nadmdari, H., et al., *Evaluation of Antibody and Cytokines Responses in Intranasally and Intramuscularly Administrated BALB/C Mice With Influenza Virus-Like Particle.* Acta Med Iran, 2017. **55**(10): p. 604-611.

74. Deriu, E., et al., *Influenza Virus Affects Intestinal Microbiota and Secondary Salmonella Infection in the Gut through Type I Interferons.* PLoS pathogens, 2016. **12**(5): p. e1005572-e1005572.

75. Cheng, L., et al., *Exosomes provide a protective and enriched source of miRNA for biomarker profiling compared to intracellular and cell-free blood.* Journal of extracellular vesicles, 2014. **3**: p. 10.3402/jev.v3.23743.

76. Keshavarz, M., et al., *miRNA-based strategy for modulation of influenza A virus infection.* Epigenomics, 2018. **10**(6): p. 829-844.

77. Loveday, E.-K., et al., *Temporal- and strain-specific host microRNA molecular signatures associated with swine-origin H1N1 and avian-origin H7N7 influenza A virus infection.* Journal of virology, 2012. **86**(11): p. 6109-6122.

78. Tambyah, P.A., et al., *microRNAs in circulation are altered in response to influenza A virus infection in humans.* PloS one, 2013. **8**(10): p. e76811-e76811.

79. Liu, Y.M., et al., *Exosome-delivered and Y RNA-derived small RNA suppresses influenza virus replication.* J Biomed Sci, 2019. **26**(1): p. 58.

80. Cypryk, W., et al., *Proteomic and Bioinformatic Characterization of Extracellular Vesicles Released from Human Macrophages upon Influenza A Virus Infection.* J Proteome Res, 2017. **16**(1): p. 217-227.

81. Bruce, E.A., P. Digard, and A.D. Stuart, *The Rab11 pathway is required for influenza A virus budding and filament formation.* Journal of virology, 2010. **84**(12): p. 5848-5859.

82. Hutchinson, E.C., et al., *Conserved and host-specific features of influenza virion architecture.* Nature communications, 2014. **5**: p. 4816-4816.

83. Kapoor, N.R., et al., *The HBx gene of hepatitis B virus can influence hepatic microenvironment via exosomes by transferring its mRNA and protein.* Virus Research, 2017. **240**: p. 166-174.

84. Kouwaki, T., et al., *Extracellular Vesicles Including Exosomes Regulate Innate Immune Responses to Hepatitis B Virus Infection.* Front Immunol, 2016. **7**: p. 335.

85. Spear, P., et al., *NKG2D ligands as therapeutic targets.* Cancer immunity, 2013. **13**: p. 8-8.

86. Jia, X., et al., *Label-free Proteomic Analysis of Exosomes Derived from Inducible Hepatitis B Virus-Replicating HepAD38 Cell Line.* Molecular & Cellular Proteomics, 2017. **16**(4 suppl 1): p. S144-S160.

87. Yang, Y., et al., *Exosomes mediate hepatitis B virus (HBV) transmission and NK-cell dysfunction.* Cell Mol Immunol, 2017. **14**(5): p. 465-475.

88. Yao, Z., et al., *Exosomes Exploit the Virus Entry Machinery and Pathway To Transmit Alpha Interferon-Induced Antiviral Activity.* Journal of Virology, 2018. **92**(24): p. e01578-18.

89. Bukong, T.N., et al., *Exosomes from Hepatitis C Infected Patients Transmit HCV Infection and Contain Replication Competent Viral RNA in Complex with Ago2-miR122-HSP90.* Plos Pathogens, 2014. **10**(10).

90. Cosset, F.L. and M. Dreux, *HCV transmission by hepatic exosomes establishes a productive infection.* J Hepatol, 2014. **60**(3): p. 674-5.

91. Wilson, J.A., et al., *Human Ago2 Is Required for Efficient MicroRNA 122 Regulation of Hepatitis C Virus RNA Accumulation and Translation.* Journal of Virology, 2011. **85**(5): p. 2342-2350.

92. Zhou, W.S., et al., *Exosomes serve as novel modes of tick-borne flavivirus transmission from arthropod to human cells and facilitates dissemination of viral RNA and proteins to the vertebrate neuronal cells.* Plos Pathogens, 2018. **14**(1).

93. Anderson, M.R., F. Kashanchi, and S. Jacobson, *Exosomes in Viral Disease.* Neurotherapeutics, 2016. **13**(3): p. 535-546.

94. Zhang, Z.W., Z.L. Li, and S. Yuan, *The Role of Secretory Autophagy in Zika Virus Transfer through the Placental Barrier.* Frontiers in Cellular and Infection Microbiology, 2017. **6**.

95. Wang, L., et al., *From Mosquitos to Humans: Genetic Evolution of Zika Virus.* Cell Host Microbe, 2016. **19**(5): p. 561-5.

96. Klase, Z.A., et al., *Zika Fetal Neuropathogenesis: Etiology of a Viral Syndrome.* PLoS Negl Trop Dis, 2016. **10**(8): p. e0004877.

97. Bayer, A., et al., *Type III Interferons Produced by Human Placental Trophoblasts Confer Protection against Zika Virus Infection.* Cell Host Microbe, 2016. **19**(5): p. 705-12.

98. Chiramel, A.I. and S.M. Best, *Role of autophagy in Zika virus infection and pathogenesis.* Virus Res, 2018. **254**: p. 34-40.

99. Delorme-Axford, E., et al., *Human placental trophoblasts confer viral resistance to recipient cells.* Proc Natl Acad Sci U S A, 2013. **110**(29): p. 12048-53.

100. Bayer, A., et al., *Chromosome 19 microRNAs exert antiviral activity independent from type III interferon signaling.* Placenta, 2018. **61**: p. 33-38.

101. Huang, Y.L., et al., *Zika virus propagation and release in human fetal astrocytes can be suppressed by neutral sphingomyelinase-2 inhibitor GW4869.* Cell Discovery, 2018. **4**.

102. Aagaard, K.M., et al., *Primary Human Placental Trophoblasts are Permissive for Zika Virus (ZIKV) Replication.* Sci Rep, 2017. **7**: p. 41389.

103. Yelamanchili, S.V., et al., *MiR-21 in Extracellular Vesicles Leads to Neurotoxicity via TLR7 Signaling in SIV Neurological Disease.* PLoS Pathog, 2015. **11**(7): p. e1005032.

104. Muller, J.A., et al., *Semen inhibits Zika virus infection of cells and tissues from the anogenital region.* Nat Commun, 2018. **9**(1): p. 2207.

105. Ngono, A.E. and S. Shresta, *Immune Response to Dengue and Zika.* Annu Rev Immunol, 2018. **36**: p. 279-308.

106. Holder, B., et al., *Macrophage Exosomes Induce Placental Inflammatory Cytokines: A Novel Mode of Maternal-Placental Messaging.* Traffic, 2016. **17**(2): p. 168-78.

107. Wang, W.B., et al., *Zika virus infection induces host inflammatory responses by facilitating NLRP3 inflammasome assembly and interleukin-1 beta secretion.* Nature Communications, 2018. **9**.

108. Zhou, W.S., et al., *Exosomes mediate Zika virus transmission through SMPD3 neutral Sphingomyelinase in cortical neurons.* Emerging Microbes & Infections, 2019. **8**(1): p. 307-326.

109. Kuate, S., et al., *Exosomal vaccines containing the S protein of the SARS coronavirus induce high levels of neutralizing antibodies.* Virology, 2007. **362**(1): p. 26-37.

110. Lai, M.M., *Coronavirus: organization, replication and expression of genome.* Annu Rev Microbiol, 1990. **44**: p. 303-33.

111. Spaan, W., D. Cavanagh, and M.C. Horzinek, *Coronaviruses: Structure and Genome Expression.* Journal of General Virology, 1988. **69**(12): p. 2939-2952.

112. Kwon, Y., et al., *Exosomes Facilitate Transmission of SARS-CoV-2 Genome into Human Induced Pluripotent Stem Cell-Derived Cardiomyocytes.* bioRxiv, 2020: p. 2020.05.14.093583.

113. Kwon, Y., et al., *Detection of Synthetic Viral RNA Fragments in Human iPSC-Cardiomyocytes following Treatment with Precipitated Extracellular Vesicles from SARS-CoV-2 Coding-Sequence-Overexpressing Lung Epithelial Cells.* bioRxiv, 2020: p. 2020.05.14.093583.

114. Giannessi, F., et al., *The Role of Extracellular Vesicles as Allies of HIV, HCV and SARS Viruses.* Viruses, 2020. **12**(5).

115. Kang, J.-S., *Chapter 20 - The potential of exosomes as theragnostics in various clinical situations*, in *Exosomes*, L. Edelstein, et al., Editors. 2020, Academic Press. p. 467-486.

116. Vikram Sengupta, S.S., Angel Lazo, Peter Woods, Anna Nolan, and Nicholas Bremer, *Exosomes Derived from Bone Marrow Mesenchymal Stem Cells as Treatment for Severe COVID-19.* Stem Cells and Development, 2020. **29**(12): p. 747-754.

117. Paliwal, R., R.J. Babu, and S. Palakurthi, *Nanomedicine scale-up technologies: feasibilities and challenges.* AAPS PharmSciTech, 2014. **15**(6): p. 1527-34.

118. McMillan, J., E. Batrakova, and H.E. Gendelman, *Cell delivery of therapeutic nanoparticles.* Prog Mol Biol Transl Sci, 2011. **104**: p. 563-601.

119. Agrahari, V., V. Agrahari, and A.K. Mitra, *Nanocarrier fabrication and macromolecule drug delivery: challenges and opportunities.* Ther Deliv, 2016. **7**(4): p. 257-78.

120. Johnson, N.M., et al., *HIV-based lentiviral vectors: Origin and sequence differences.* Molecular Therapy - Methods & Clinical Development, 2021. **21**: p. 451-465.

121. Shaw, G.M. and E. Hunter, *HIV transmission.* Cold Spring Harbor perspectives in medicine, 2012. **2**(11): p. a006965.

122. Swanstrom, R. and J. Coffin, *HIV-1 pathogenesis: the virus.* Cold Spring Harbor perspectives in medicine, 2012. **2**(12): p. a007443-a007443.

123. Hung Y. Fan, R.F.C., Luis P. Villarreal, *AIDS Science and Society*. 6th ed. 2011, Studbury, Massachusetts: Jones and Bartlett Publishers.

124. Vidya Vijayan, K.K., et al., *Pathophysiology of CD4+ T-Cell Depletion in HIV-1 and HIV-2 Infections.* Frontiers in Immunology, 2017. **8**.

125. Meijerink, H., et al., *The number of CCR5 expressing CD4+ T lymphocytes is lower in HIV-infected long-term non-progressors with viral control compared to normal progressors: a cross-sectional study.* BMC Infectious Diseases, 2014. **14**(1): p. 683.

126. Schuitemaker, H., et al., *Monocytotropic human immunodeficiency virus type 1 (HIV-1) variants detectable in all stages of HIV-1 infection lack T-cell line tropism and syncytium-inducing ability in primary T-cell culture.* J Virol, 1991. **65**(1): p. 356-63.

127. Brumme, Z.L., et al., *Molecular and clinical epidemiology of CXCR4-using HIV-1 in a large population of antiretroviral-naive individuals.* J Infect Dis, 2005. **192**(3): p. 466-74.

128. Loetscher, P., B. Moser, and M. Baggiolini, *Chemokines and their receptors in lymphocyte traffic and HIV infection.* Adv Immunol, 2000. **74**: p. 127-80.

129. Bleul, C.C., et al., *The HIV coreceptors CXCR4 and CCR5 are differentially expressed and regulated on human T lymphocytes.* Proc Natl Acad Sci U S A, 1997. **94**(5): p. 1925-30.

130. McCune, J.M., *The dynamics of CD4+ T-cell depletion in HIV disease.* Nature, 2001. **410**(6831): p. 974-9.

131. Martin-Gayo, E. and X.G. Yu, *Role of Dendritic Cells in Natural Immune Control of HIV-1 Infection.* Frontiers in Immunology, 2019. **10**.

132. Izquierdo-Useros, N., et al., *HIV-1 Capture and Transmission by Dendritic Cells: The Role of Viral Glycolipids and the Cellular Receptor Siglec-1.* PLOS Pathogens, 2014. **10**(7): p. e1004146.

133. (NIH), N.I.o.H., *The HIV Life Cycle*. 2021.

134. Wilen, C.B., J.C. Tilton, and R.W. Doms, *HIV: cell binding and entry.* Cold Spring Harbor perspectives in medicine, 2012. **2**(8): p. a006866.

135. Doms, R.W. and J.P. Moore, *HIV-1 membrane fusion: targets of opportunity.* The Journal of cell biology, 2000. **151**(2): p. F9-F14.

136. HIV.gov, *The Global HIV/AIDS Epidemic*. 2021.

137. (NIH), N.I.o.H., *FDA-Approved HIV Medicines*. 2021.

138. Ding, X., et al., *Enfuvirtide (T20)-Based Lipopeptide Is a Potent HIV-1 Cell Fusion Inhibitor: Implications for Viral Entry and Inhibition.* Journal of virology, 2017. **91**(18): p. e00831-17.

139. Scholar, E., *HIV Non-Nucleoside Reverse Transcriptase Inhibitors*, in *xPharm: The Comprehensive Pharmacology Reference*, S.J. Enna and D.B. Bylund, Editors. 2007, Elsevier: New York. p. 1-3.

140. Zulfiqar, P.H.P.H., *Reverse Transcriptase Inhibitor*. 2022, StatPearls Publishing LLC.: Treasure Island, FL.

141. Fan, X., et al., *Design of HIV-1 integrase inhibitors targeting the catalytic domain as well as its interaction with LEDGF/p75: a scaffold hopping approach using salicylate and catechol groups.* Bioorganic & medicinal chemistry, 2011. **19**(16): p. 4935-4952.

142. Farady, C.J. and C.S. Craik, *Mechanisms of macromolecular protease inhibitors.* Chembiochem : a European journal of chemical biology, 2010. **11**(17): p. 2341-2346.

143. D'arc, M., et al., *Origin of the HIV-1 group O epidemic in western lowland gorillas.* Proceedings of the National Academy of Sciences, 2015. **112**(11): p. E1343-E1352.

144. Takebe, Y., S. Kusagawa, and K. Motomura, *Molecular epidemiology of HIV: Tracking AIDS pandemic.* Pediatrics International, 2004. **46**(2): p. 236-244.

145. Sullivan, P.S., et al., *Epidemiology of HIV in the USA: epidemic burden, inequities, contexts, and responses.* The Lancet, 2021. **397**(10279): p. 1095-1106.

146. Worobey, M., et al., *Direct evidence of extensive diversity of HIV-1 in Kinshasa by 1960.* Nature, 2008. **455**(7213): p. 661-664.

147. Korber, B., et al., *Timing the ancestor of the HIV-1 pandemic strains.* Science, 2000. **288**(5472): p. 1789-96.

148. Bale, M.J. and M.F. Kearney, *Review: HIV-1 phylogeny during suppressive antiretroviral therapy.* Current opinion in HIV and AIDS, 2019. **14**(3): p. 188-193.

149. Woodland, D.L., *Viral Epitope Escape in Acute HIV-1 Infection.* Viral Immunol, 2018. **31**(7): p. 485.

150. Pollack, R.A., et al., *Defective HIV-1 Proviruses Are Expressed and Can Be Recognized by Cytotoxic T Lymphocytes, which Shape the Proviral Landscape.* Cell host & microbe, 2017. **21**(4): p. 494-506.e4.

151. Lorenzo-Redondo, R., et al., *Persistent HIV-1 replication maintains the tissue reservoir during therapy.* Nature, 2016. **530**(7588): p. 51-56.

152. Oliveira, M.F., et al., *Early Antiretroviral Therapy Is Associated with Lower HIV DNA Molecular Diversity and Lower Inflammation in Cerebrospinal Fluid but Does Not Prevent the Establishment of Compartmentalized HIV DNA Populations.* PLoS Pathog, 2017. **13**(1): p. e1006112.

153. Chaillon, A., et al., *HIV Trafficking Between Blood and Semen During Early Untreated HIV Infection.* J Acquir Immune Defic Syndr, 2017. **74**(1): p. 95-102.

154. Nolan, D.J., et al., *The Spleen Is an HIV-1 Sanctuary During Combined Antiretroviral Therapy.* AIDS Res Hum Retroviruses, 2018. **34**(1): p. 123-125.

155. Wagner, T.A., et al., *HIV latency. Proliferation of cells with HIV integrated into cancer genes contributes to persistent infection.* Science (New York, N.Y.), 2014. **345**(6196): p. 570-573.

156. Maldarelli, F., et al., *HIV latency. Specific HIV integration sites are linked to clonal expansion and persistence of infected cells.* Science (New York, N.Y.), 2014. **345**(6193): p. 179-183.

157. Reeves, D.B., et al., *A majority of HIV persistence during antiretroviral therapy is due to infected cell proliferation.* Nature communications, 2018. **9**(1): p. 4811-4811.

158. Rosenbloom, D.I.S., et al., *Re-evaluating evolution in the HIV reservoir.* Nature, 2017. **551**(7681): p. E6-E9.

159. Hosmane, N.N., et al., *Proliferation of latently infected CD4(+) T cells carrying replication-competent HIV-1: Potential role in latent reservoir dynamics.* The Journal of experimental medicine, 2017. **214**(4): p. 959-972.

160. Bruner, K.M., et al., *Defective proviruses rapidly accumulate during acute HIV-1 infection.* Nature medicine, 2016. **22**(9): p. 1043-1049.

161. Hu, W.-S. and S.H. Hughes, *HIV-1 reverse transcription.* Cold Spring Harbor perspectives in medicine, 2012. **2**(10): p. a006882.

162. Batorsky, R., et al., *Estimate of effective recombination rate and average selection coefficient for HIV in chronic infection.* Proceedings of the National Academy of Sciences of the United States of America, 2011. **108**(14): p. 5661-5666.

163. Van Zyl, G.U., et al., *No evidence of HIV replication in children on antiretroviral therapy.* The Journal of clinical investigation, 2017. **127**(10): p. 3827-3834.

164. Maldarelli, F., et al., *ART suppresses plasma HIV-1 RNA to a stable set point predicted by pretherapy viremia.* PLoS pathogens, 2007. **3**(4): p. e46-e46.

165. Hong, S. and W.A. Banks, *Role of the immune system in HIV-associated neuroinflammation and neurocognitive implications.* Brain, behavior, and immunity, 2015. **45**: p. 1-12.

166. Clifford, D.B. and B.M. Ances, *HIV-associated neurocognitive disorder.* The Lancet. Infectious diseases, 2013. **13**(11): p. 976-986.

167. Gisslén, M., R.W. Price, and S. Nilsson, *The definition of HIV-associated neurocognitive disorders: are we overestimating the real prevalence?* BMC Infectious Diseases, 2011. **11**(1): p. 356.

168. Saylor, D., et al., *HIV-associated neurocognitive disorder--pathogenesis and prospects for treatment.* Nature reviews. Neurology, 2016. **12**(4): p. 234-248.

169. Harezlak, J., et al., *Persistence of HIV-associated cognitive impairment, inflammation, and neuronal injury in era of highly active antiretroviral treatment.* AIDS (London, England), 2011. **25**(5): p. 625-633.

170. Heaton, R.K., et al., *Neurocognitive Change in the Era of HIV Combination Antiretroviral Therapy: The Longitudinal CHARTER Study.* Clinical Infectious Diseases, 2014. **60**(3): p. 473-480.

171. Heaton, R.K., et al., *HIV-associated neurocognitive disorders before and during the era of combination antiretroviral therapy: differences in rates, nature, and predictors.* Journal of NeuroVirology, 2011. **17**(1): p. 3-16.

172. Cysique, L.A. and B.J. Brew, *Prevalence of non-confounded HIV-associated neurocognitive impairment in the context of plasma HIV RNA suppression.* Journal of NeuroVirology, 2011. **17**(2): p. 176-183.

173. Churchill, M.J., et al., *Use of laser capture microdissection to detect integrated HIV-1 DNA in macrophages and astrocytes from autopsy brain tissues.* Journal of Neurovirology, 2006. **12**(2): p. 146-152.

174. Ko, A., et al., *Macrophages but not Astrocytes Harbor HIV DNA in the Brains of HIV-1-Infected Aviremic Individuals on Suppressive Antiretroviral Therapy.* Journal of Neuroimmune Pharmacology, 2019. **14**(1): p. 110-119.

175. Gisolf, E.H., et al., *Increasing cerebrospinal fluid chemokine concentrations despite undetectable cerebrospinal fluid HIV RNA in HIV-1-infected patients receiving antiretroviral therapy.* Journal of acquired immune deficiency syndromes (1999), 2000. **25**(5): p. 426-433.

176. Edén, A., et al., *HIV-1 Viral Escape in Cerebrospinal Fluid of Subjects on Suppressive Antiretroviral Treatment.* The Journal of Infectious Diseases, 2010. **202**(12): p. 1819-1825.

177. Oliveira, M.F., et al., *Early Antiretroviral Therapy Is Associated with Lower HIV DNA Molecular Diversity and Lower Inflammation in Cerebrospinal Fluid but Does Not Prevent the Establishment of Compartmentalized HIV DNA Populations.* PLOS Pathogens, 2017. **13**(1): p. e1006112.

178. Dahl, V., et al., *Low levels of HIV-1 RNA detected in the cerebrospinal fluid after up to 10 years of suppressive therapy are associated with local immune activation.* AIDS (London, England), 2014. **28**(15): p. 2251-2258.

179. Rice, A.P., *The HIV-1 Tat Protein: Mechanism of Action and Target for HIV-1 Cure Strategies.* Current pharmaceutical design, 2017. **23**(28): p. 4098-4102.

180. Buffalo, C.Z., et al., *How HIV Nef Proteins Hijack Membrane Traffic To Promote Infection.* J Virol, 2019. **93**(24).

181. Alford, K. and J.H. Vera, *Cognitive Impairment in people living with HIV in the ART era: A Review.* British Medical Bulletin, 2018. **127**(1): p. 55-68.

182. Guha, A., et al., *Topographies of Cortical and Subcortical Volume Loss in HIV and Aging in the cART Era.* Journal of acquired immune deficiency syndromes (1999), 2016. **73**(4): p. 374-383.

183. Brüning, A., et al., *The HIV reverse transcriptase inhibitor tenofovir induces cell cycle arrest in human cancer cells.* Investigational New Drugs, 2012. **30**(4): p. 1389-1395.

184. Birnkrant, D., *TRUVADA® (emtricitabine/tenofovir disoproxil fumarate) tablets*. 2008, Gilead Sciences.

185. clinicalinfo.hiv.gov, *Drug Database: Emtricitabine / Tenofovir Disoproxil Fumarate*. 2022.

186. Coutinho, B. and R. Prasad, *Emtricitabine/tenofovir (Truvada) for HIV prophylaxis.* Am Fam Physician, 2013. **88**(8): p. 535-40.

187. Prevention, C.f.D.C.a., *Truvada Medication Information Sheet*. 2022.

188. Baeten, J.M., et al., *Antiretroviral Prophylaxis for HIV Prevention in Heterosexual Men and Women.* New England Journal of Medicine, 2012. **367**(5): p. 399-410.

189. Grant, R.M., et al., *Preexposure Chemoprophylaxis for HIV Prevention in Men Who Have Sex with Men.* New England Journal of Medicine, 2010. **363**(27): p. 2587-2599.

190. Thigpen, M.C., et al., *Antiretroviral Preexposure Prophylaxis for Heterosexual HIV Transmission in Botswana.* New England Journal of Medicine, 2012. **367**(5): p. 423-434.

191. *HIV Surveillance Report, 2019*, N.C.f.H. Division of HIV Prevention, Viral Hepatitis, STD, and TB Prevention, Editor. 2021, Centers for Disease Control and Prevention.

192. Escudero, D.J., et al., *Progress and Challenges in "Getting to Zero" New HIV Infections in Miami, Florida.* Journal of the International Association of Providers of AIDS Care, 2019. **18**: p. 2325958219852122-2325958219852122.

193. Prevention, C.f.D.C.a., *HIV Surveillance Report, 2017*. 2018.

194. Florida Department of Health, D.o.P.H.S.a.P.M. *HIV Diagnoses*. 2020; Available from: https://www.flhealthcharts.gov/ChartsReports/rdPage.aspx?rdReport=HIVAIDS.DataViewer&cid=471.

195. Unick, G.J., et al., *Intertwined epidemics: national demographic trends in hospitalizations for heroin- and opioid-related overdoses, 1993-2009.* PloS one, 2013. **8**(2): p. e54496-e54496.

196. Centers for Disease Control and Prevention, N.C.f.I.P.a.C. *Understanding the Opioid Overdose Epidemic*. 2021 [cited 2022; Available from: https://www.cdc.gov/opioids/basics/epidemic.html.

197. Conrad, C., et al., *Community Outbreak of HIV Infection Linked to Injection Drug Use of Oxymorphone--Indiana, 2015.* MMWR. Morbidity and mortality weekly report, 2015. **64**(16): p. 443-444.

198. *Vital signs: overdoses of prescription opioid pain relievers---United States, 1999--2008.* MMWR Morb Mortal Wkly Rep, 2011. **60**(43): p. 1487-92.

199. McLean, K., *"There's nothing here": Deindustrialization as risk environment for overdose.* Int J Drug Policy, 2016. **29**: p. 19-26.

200. Friedman, S.R., et al., *Income inequality, drug-related arrests, and the health of people who inject drugs: Reflections on seventeen years of research.* Int J Drug Policy, 2016. **32**: p. 11-6.

201. Mizuno, Y., et al., *Syndemic vulnerability, sexual and injection risk behaviors, and HIV continuum of care outcomes in HIV-positive injection drug users.* AIDS Behav, 2015. **19**(4): p. 684-93.

202. Storr, C.L., C.Y. Chen, and J.C. Anthony, *"Unequal opportunity": neighbourhood disadvantage and the chance to buy illegal drugs.* Journal of epidemiology and community health, 2004. **58**(3): p. 231-237.

203. Singer, M., *Drugging the Poor: Legal and Illegal Drugs and Social Inequality*. 2008, Illinois, USA: Waveland Press, Inc.

204. Singer, M. and S. Clair, *Syndemics and public health: reconceptualizing disease in bio-social context.* Med Anthropol Q, 2003. **17**(4): p. 423-41.

205. Services, U.S.D.o.H.a.H. *What is the U.S. Opioid Epidemic?* About the Epidemic 2019; Available from: https://www.hhs.gov/opioids/about-the-epidemic/index.html.

206. Vashishtha, D., M.L. Mittal, and D. Werb, *The North American opioid epidemic: current challenges and a call for treatment as prevention.* Harm Reduction Journal, 2017. **14**(1): p. 7.

207. Rudd, R.A., et al., *Increases in Drug and Opioid Overdose Deaths--United States, 2000-2014.* MMWR Morb Mortal Wkly Rep, 2016. **64**(50-51): p. 1378-82.

208. Liang, X., et al., *Opioid System Modulates the Immune Function: A Review.* Translational perioperative and pain medicine, 2016. **1**(1): p. 5-13.

209. National Academies of Sciences, E., and Medicine, in *Pain Management and the Opioid Epidemic: Balancing Societal and Individual Benefits and Risks of Prescription Opioid Use*, J.K. Phillips, M.A. Ford, and R.J. Bonnie, Editors. 2017: Washington (DC).

210. Volkow, N.D. and A.T. McLellan, *Opioid Abuse in Chronic Pain — Misconceptions and Mitigation Strategies.* New England Journal of Medicine, 2016. **374**(13): p. 1253-1263.

211. Ostling, P.S., et al., *America's Opioid Epidemic: a Comprehensive Review and Look into the Rising Crisis.* Current Pain and Headache Reports, 2018. **22**(5): p. 32.

212. Centers for Disease Control and Prevention, N.C.f.I.P.a.C. *Opioid Overdose*. 2018 December 19, 2018; Available from: https://www.cdc.gov/drugoverdose/epidemic/index.html.

213. Ratycz, M.C., T.J. Papadimos, and A.A. Vanderbilt, *Addressing the growing opioid and heroin abuse epidemic: a call for medical school curricula.* Med Educ Online, 2018. **23**(1): p. 1466574.

214. Kousik, S., T.C. Napier, and P. Carvey, *The Effects of Psychostimulant Drugs on Blood Brain Barrier Function and Neuroinflammation.* Frontiers in Pharmacology, 2012. **3**(121).

215. Fitting, S., et al., *Interactive Comorbidity between Opioid Drug Abuse and HIV-1 Tat: Chronic Exposure Augments Spine Loss and Sublethal Dendritic Pathology in Striatal Neurons.* The American Journal of Pathology, 2010. **177**(3): p. 1397-1410.

216. Meyer, J.P., S.A. Springer, and F.L. Altice, *Substance abuse, violence, and HIV in women: a literature review of the syndemic.* Journal of women's health (2002), 2011. **20**(7): p. 991-1006.

217. Mustanski, B., et al., *Psychosocial health problems increase risk for HIV among urban young men who have sex with men: preliminary evidence of a syndemic in need of attention.* Annals of behavioral medicine : a publication of the Society of Behavioral Medicine, 2007. **34**(1): p. 37-45.

218. Balinang, J.M., et al., *Productive infection of human neural progenitor cells by R5 tropic HIV-1: opiate co-exposure heightens infectivity and functional vulnerability.* AIDS (London, England), 2017. **31**(6): p. 753-764.

219. Chilunda, V., et al., *The impact of substance abuse on HIV-mediated neuropathogenesis in the current ART era.* Brain Research, 2019. **1724**: p. 146426.

220. Wang, X., et al., *Heroin Abuse and/or HIV Infection Dysregulate Plasma Exosomal miRNAs.* Journal of Neuroimmune Pharmacology, 2019.

221. Singh, K., et al., *Association of History of Injection Drug Use with External Cause-Related Mortality Among Persons Linked to HIV Care in an Urban Clinic, 2001–2015.* AIDS and Behavior, 2019. **23**(12): p. 3286-3293.

222. Chen, X., et al., *Burmese injecting drug users in Yunnan play a pivotal role in the cross-border transmission of HIV-1 in the China-Myanmar border region.* Virulence, 2018. **9**(1): p. 1195-1204.

223. Degenhardt, L., et al., *Global prevalence of injecting drug use and sociodemographic characteristics and prevalence of HIV, HBV, and HCV in people who inject drugs: a multistage systematic review.* Lancet Glob Health, 2017. **5**(12): p. e1192-e1207.

224. *HIV and People Who Inject Drugs*. 2022 [cited 2022; Available from: https://www.cdc.gov/hiv/group/hiv-idu.html.

225. Murphy, A., et al., *The Effects of Opioids on HIV Neuropathogenesis.* Frontiers in Immunology, 2019. **10**(2445).

226. Garvey, L.J., et al., *Increased microglia activation in neurologically asymptomatic HIV-infected patients receiving effective ART.* AIDS, 2014. **28**(1).

227. Borrajo, A., et al., *Important role of microglia in HIV-1 associated neurocognitive disorders and the molecular pathways implicated in its pathogenesis.* Annals of Medicine, 2021. **53**(1): p. 43-69.

228. Gu, C.-J., et al., *EcoHIV infection of mice establishes latent viral reservoirs in T cells and active viral reservoirs in macrophages that are sufficient for induction of neurocognitive impairment.* PLOS Pathogens, 2018. **14**(6): p. e1007061.

229. Gong, Y., et al., *An Elvitegravir Nanoformulation Crosses the Blood–Brain Barrier and Suppresses HIV-1 Replication in Microglia.* Viruses, 2020. **12**(5): p. 564.

230. Ramirez, S.H., et al., *Extracellular Microvesicles Released From Brain Endothelial Cells are Detected in Animal Models Of HIV-1 Signifying Unresolved Inflammation.* Journal of Neuroimmune Pharmacology, 2021. **16**(4): p. 785-795.

231. Chelvanambi, S., et al., *HIV-Nef Protein Transfer to Endothelial Cells Requires Rac1 Activation and Leads to Endothelial Dysfunction Implications for Statin Treatment in HIV Patients.* Circulation Research, 2019. **125**(9): p. 805-820.

232. Lutgen, V., et al., *HIV infects astrocytes in vivo and egresses from the brain to the periphery.* PLOS Pathogens, 2020. **16**(6): p. e1008381.

233. Garvey, L.J., et al., *Increased microglia activation in neurologically asymptomatic HIV-infected patients receiving effective ART.* AIDS, 2014. **28**(1): p. 67-72.

234. Adamson, D.C., et al., *Immunologic NO synthase: elevation in severe AIDS dementia and induction by HIV-1 gp41.* Science, 1996. **274**(5294): p. 1917-21.

235. Jiang, Z.G., et al., *Glutamate is a mediator of neurotoxicity in secretions of activated HIV-1-infected macrophages.* J Neuroimmunol, 2001. **117**(1-2): p. 97-107.

236. Giulian, D., et al., *Study of receptor-mediated neurotoxins released by HIV-1-infected mononuclear phagocytes found in human brain.* J Neurosci, 1996. **16**(10): p. 3139-53.

237. Heyes, M.P., et al., *Quinolinic acid in cerebrospinal fluid and serum in HIV-1 infection: relationship to clinical and neurological status.* Ann Neurol, 1991. **29**(2): p. 202-9.

238. Nottet, H.S., et al., *A regulatory role for astrocytes in HIV-1 encephalitis. An overexpression of eicosanoids, platelet-activating factor, and tumor necrosis factor-alpha by activated HIV-1-infected monocytes is attenuated by primary human astrocytes.* J Immunol, 1995. **154**(7): p. 3567-81.

239. Gelbard, H.A., et al., *Platelet-activating factor: a candidate human immunodeficiency virus type 1-induced neurotoxin.* J Virol, 1994. **68**(7): p. 4628-35.

240. Barbour, A.J., et al., *HIV and opiates dysregulate K+- Cl− cotransporter 2 (KCC2) to cause GABAergic dysfunction in primary human neurons and Tat-transgenic mice.* Neurobiology of Disease, 2020. **141**: p. 104878.

241. Ru, W. and S.-J. Tang, *HIV-1 gp120Bal down-Regulates Phosphorylated NMDA Receptor Subunit 1 in Cortical Neurons via Activation of Glutamate and Chemokine Receptors.* Journal of Neuroimmune Pharmacology, 2016. **11**(1): p. 182-191.

242. Khodr, C.E., et al., *Combined chronic blockade of hyper-active L-type calcium channels and NMDA receptors ameliorates HIV-1 associated hyper-excitability of mPFC pyramidal neurons.* Neurobiology of Disease, 2016. **94**: p. 85-94.

243. Krogh, K.A., et al., *HIV-1 protein Tat produces biphasic changes in NMDA-evoked increases in intracellular Ca2+ concentration via activation of Src kinase and nitric oxide signaling pathways.* Journal of Neurochemistry, 2014. **130**(5): p. 642-656.

244. Fitting, S., et al., *Interactive HIV-1 Tat and morphine-induced synaptodendritic injury is triggered through focal disruptions in Na^+ influx, mitochondrial instability, and Ca^{2+} overload.* The Journal of neuroscience : the official journal of the Society for Neuroscience, 2014. **34**(38): p. 12850-12864.

245. El-Hage, N., et al., *Synergistic increases in intracellular Ca2+, and the release of MCP-1, RANTES, and IL-6 by astrocytes treated with opiates and HIV-1 Tat.* Glia, 2005. **50**(2): p. 91-106.

246. Bruce-Keller, A.J., et al., *Morphine causes rapid increases in glial activation and neuronal injury in the striatum of inducible HIV-1 Tat transgenic mice.* Glia, 2008. **56**(13): p. 1414-1427.

247. Bokhari, S.M., et al., *Morphine enhances Tat-induced activation in murine microglia.* Journal of neurovirology, 2009. **15**(3): p. 219-228.

248. Wodarski, R., et al., *Reduced intraepidermal nerve fibre density, glial activation, and sensory changes in HIV type-1 Tat-expressing female mice: involvement of Tat during early stages of HIV-associated painful sensory neuropathy.* Pain reports, 2018. **3**(3): p. e654-e654.

249. Tamamis, P. and C.A. Floudas, *Molecular Recognition of CCR5 by an HIV-1 gp120 V3 Loop.* PLOS ONE, 2014. **9**(4): p. e95767.

250. Smith, L.K., et al., *Direct interaction of HIV gp120 with neuronal CXCR4 and CCR5 receptors induces cofilin-actin rod pathology via a cellular prion protein- and NOX-dependent mechanism.* PLOS ONE, 2021. **16**(3): p. e0248309.

251. Velasquez, S., et al., *Pannexin1 Channels Are Required for Chemokine-Mediated Migration of CD4⁺ T Lymphocytes: Role in Inflammation and Experimental Autoimmune Encephalomyelitis.* The Journal of Immunology, 2016. **196**(10): p. 4338.

252. Kaul, M., et al., *HIV-1 coreceptors CCR5 and CXCR4 both mediate neuronal cell death but CCR5 paradoxically can also contribute to protection.* Cell Death & Differentiation, 2007. **14**(2): p. 296-305.

253. Canonico, D., et al., *Effects of Morphine on Gp120-induced Neuroinflammation Under Immunocompetent Vs. Immunodeficient Conditions.* Journal of Neuroimmune Pharmacology, 2022.

254. Byrd, D.A., et al., *Neurocognitive impact of substance use in HIV infection.* Journal of acquired immune deficiency syndromes (1999), 2011. **58**(2): p. 154-162.

255. Carrico, A.W., *Substance use and HIV disease progression in the HAART era: Implications for the primary prevention of HIV.* Life Sciences, 2011. **88**(21): p. 940-947.

256. Smith, D.B., P. Simmonds, and J.E. Bell, *Brain viral burden, neuroinflammation and neurodegeneration in HAART-treated HIV positive injecting drug users.* Journal of NeuroVirology, 2014. **20**(1): p. 28-38.

257. Kim, S., et al., *A central role for glial CCR5 in directing the neuropathological interactions of HIV-1 Tat and opiates.* Journal of Neuroinflammation, 2018. **15**(1): p. 285.

258. Gottås, A., et al., *Levels of heroin and its metabolites in blood and brain extracellular fluid after i.v. heroin administration to freely moving rats.* British journal of pharmacology, 2013. **170**(3): p. 546-556.

259. Minett, W.J., et al., *Concentrations of Opiates and Psychotropic Agents in Polydrug Overdoses: A Surprising Correlation Between Morphine and Antidepressants.* Journal of Forensic Sciences, 2010. **55**(5): p. 1319-1325.

260. Jones, A.W., A. Holmgren, and J. Ahlner, *Concentrations of free-morphine in peripheral blood after recent use of heroin in overdose deaths and in apprehended drivers.* Forensic Science International, 2012. **215**(1): p. 18-24.

261. Darke, S., et al., *A comparison of blood toxicology of heroin-related deaths and current heroin users in Sydney, Australia.* Drug Alcohol Depend, 1997. **47**(1): p. 45-53.

262. Jones, A.W., A. Holmgren, and F.C. Kugelberg, *Driving under the influence of opiates: concentration relationships between morphine, codeine, 6-acetyl morphine, and ethyl morphine in blood.* J Anal Toxicol, 2008. **32**(4): p. 265-72.

263. Takeshita, Y. and R.M. Ransohoff, *Inflammatory cell trafficking across the blood-brain barrier: chemokine regulation and in vitro models.* Immunological reviews, 2012. **248**(1): p. 228-239.

264. Hawkins, B.T. and T.P. Davis, *The blood-brain barrier/neurovascular unit in health and disease.* Pharmacol Rev, 2005. **57**(2): p. 173-85.

265. Mi, H., H. Haeberle, and B.A. Barres, *Induction of astrocyte differentiation by endothelial cells.* The Journal of neuroscience : the official journal of the Society for Neuroscience, 2001. **21**(5): p. 1538-1547.

266. Reuss, B., R. Dono, and K. Unsicker, *Functions of fibroblast growth factor (FGF)-2 and FGF-5 in astroglial differentiation and blood-brain barrier permeability: evidence from mouse mutants.* The Journal of neuroscience : the official journal of the Society for Neuroscience, 2003. **23**(16): p. 6404-6412.

267. Igarashi, Y., et al., *Glial cell line-derived neurotrophic factor induces barrier function of endothelial cells forming the blood-brain barrier.* Biochem Biophys Res Commun, 1999. **261**(1): p. 108-12.

268. Dohgu, S., et al., *Brain pericytes contribute to the induction and up-regulation of blood-brain barrier functions through transforming growth factor-beta production.* Brain Res, 2005. **1038**(2): p. 208-15.

269. Alvarez, J.I., R. Cayrol, and A. Prat, *Disruption of central nervous system barriers in multiple sclerosis.* Biochim Biophys Acta, 2011. **1812**(2): p. 252-64.

270. Calabria, A.R. and E.V. Shusta, *A genomic comparison of in vivo and in vitro brain microvascular endothelial cells.* Journal of cerebral blood flow and metabolism : official journal of the International Society of Cerebral Blood Flow and Metabolism, 2008. **28**(1): p. 135-148.

271. de Boer, A.G. and P.J. Gaillard, *Blood-brain barrier dysfunction and recovery.* J Neural Transm (Vienna), 2006. **113**(4): p. 455-62.

272. Chaudhuri, J.D., *Blood brain barrier and infection.* Med Sci Monit, 2000. **6**(6): p. 1213-22.

273. Kniesel, U. and H. Wolburg, *Tight junctions of the blood-brain barrier.* Cell Mol Neurobiol, 2000. **20**(1): p. 57-76.

274. Gloor, S.M., et al., *Molecular and cellular permeability control at the blood-brain barrier.* Brain Res Brain Res Rev, 2001. **36**(2-3): p. 258-64.

275. Harhaj, N.S. and D.A. Antonetti, *Regulation of tight junctions and loss of barrier function in pathophysiology.* Int J Biochem Cell Biol, 2004. **36**(7): p. 1206-37.

276. Vorbrodt, A.W. and D.H. Dobrogowska, *Molecular anatomy of intercellular junctions in brain endothelial and epithelial barriers: electron microscopist's view.* Brain Res Brain Res Rev, 2003. **42**(3): p. 221-42.

277. Wolburg, H. and A. Lippoldt, *Tight junctions of the blood-brain barrier: development, composition and regulation.* Vascul Pharmacol, 2002. **38**(6): p. 323-37.

278. Schulze, C. and J.A. Firth, *Immunohistochemical localization of adherens junction components in blood-brain barrier microvessels of the rat.* J Cell Sci, 1993. **104 (Pt 3)**: p. 773-82.

279. Zheng, W., M. Aschner, and J.-F. Ghersi-Egea, *Brain barrier systems: a new frontier in metal neurotoxicological research.* Toxicology and applied pharmacology, 2003. **192**(1): p. 1-11.

280. Armulik, A., A. Abramsson, and C. Betsholtz, *Endothelial/pericyte interactions.* Circ Res, 2005. **97**(6): p. 512-23.

281. Dore-Duffy, P., *Pericytes: pluripotent cells of the blood brain barrier.* Curr Pharm Des, 2008. **14**(16): p. 1581-93.

282. Bagley, R.G., et al., *Pericytes and endothelial precursor cells: cellular interactions and contributions to malignancy.* Cancer Res, 2005. **65**(21): p. 9741-50.

283. Winkler, E.A., R.D. Bell, and B.V. Zlokovic, *Central nervous system pericytes in health and disease.* Nature neuroscience, 2011. **14**(11): p. 1398-1405.

284. Levéen, P., et al., *Mice deficient for PDGF B show renal, cardiovascular, and hematological abnormalities.* Genes Dev, 1994. **8**(16): p. 1875-87.

285. Lindahl, P., et al., *Pericyte loss and microaneurysm formation in PDGF-B-deficient mice.* Science, 1997. **277**(5323): p. 242-5.

286. Ransohoff, R.M., P. Kivisäkk, and G. Kidd, *Three or more routes for leukocyte migration into the central nervous system.* Nat Rev Immunol, 2003. **3**(7): p. 569-81.

287. Engelhardt, B., *Regulation of immune cell entry into the central nervous system.* Results Probl Cell Differ, 2006. **43**: p. 259-80.

288. Engelhardt, B. and R.M. Ransohoff, *The ins and outs of T-lymphocyte trafficking to the CNS: anatomical sites and molecular mechanisms.* Trends Immunol, 2005. **26**(9): p. 485-95.

289. Ubogu, E.E., M.B. Cossoy, and R.M. Ransohoff, *The expression and function of chemokines involved in CNS inflammation.* Trends Pharmacol Sci, 2006. **27**(1): p. 48-55.

290. Engelhardt, B., *T cell migration into the central nervous system during health and disease: Different molecular keys allow access to different central nervous system compartments.* Clinical and Experimental Neuroimmunology, 2010. **1**(2): p. 79-93.

291. Ley, K., et al., *Getting to the site of inflammation: the leukocyte adhesion cascade updated.* Nat Rev Immunol, 2007. **7**(9): p. 678-89.

292. Greenwood, J., et al., *Review: leucocyte-endothelial cell crosstalk at the blood-brain barrier: a prerequisite for successful immune cell entry to the brain.* Neuropathol Appl Neurobiol, 2011. **37**(1): p. 24-39.

293. Man, S., E.E. Ubogu, and R.M. Ransohoff, *Inflammatory cell migration into the central nervous system: a few new twists on an old tale.* Brain pathology (Zurich, Switzerland), 2007. **17**(2): p. 243-250.

294. Melton, L.M., et al., *Chronic glial activation, neurodegeneration, and APP immunoreactive deposits following acute administration of double-stranded RNA.* Glia, 2003. **44**(1): p. 1-12.

295. Wilms, H., et al., *Intrathecal synthesis of monocyte chemoattractant protein-1 (MCP-1) in amyotrophic lateral sclerosis: further evidence for microglial activation in neurodegeneration.* J Neuroimmunol, 2003. **144**(1-2): p. 139-42.

296. Fischer-Smith, T., et al., *Macrophage/microglial accumulation and proliferating cell nuclear antigen expression in the central nervous system in human immunodeficiency virus encephalopathy.* Am J Pathol, 2004. **164**(6): p. 2089-99.

297. Anthony, I.C., et al., *Influence of HAART on HIV-related CNS disease and neuroinflammation.* J Neuropathol Exp Neurol, 2005. **64**(6): p. 529-36.

298. Boehme, S.A., et al., *The chemokine fractalkine inhibits Fas-mediated cell death of brain microglia.* J Immunol, 2000. **165**(1): p. 397-403.

299. Antinori, A., et al., *Updated research nosology for HIV-associated neurocognitive disorders.* Neurology, 2007. **69**(18): p. 1789-99.

300. Gras, G. and M. Kaul, *Molecular mechanisms of neuroinvasion by monocytes-macrophages in HIV-1 infection.* Retrovirology, 2010. **7**(1): p. 30.

301. El-Hage, N., et al., *HIV-1 Tat and opiate-induced changes in astrocytes promote chemotaxis of microglia through the expression of MCP-1 and alternative chemokines.* Glia, 2006. **53**(2): p. 132-146.

302. Cai, Y., et al., *Multiple Faceted Roles of Cocaine in Potentiation of HAND.* Curr HIV Res, 2016. **14**(5): p. 412-416.

303. Mangus, L.M., et al., *Neuroinflammation and virus replication in the spinal cord of simian immunodeficiency virus-infected macaques.* J Neuropathol Exp Neurol, 2015. **74**(1): p. 38-47.

304. Churchill, M.J., et al., *Extensive astrocyte infection is prominent in human immunodeficiency virus-associated dementia.* Ann Neurol, 2009. **66**(2): p. 253-8.

305. Rahimy, E., et al., *Blood-Brain Barrier Disruption Is Initiated During Primary HIV Infection and Not Rapidly Altered by Antiretroviral Therapy.* J Infect Dis, 2017. **215**(7): p. 1132-1140.

306. Natarajaseenivasan, K., et al., *Astrocytic metabolic switch is a novel etiology for Cocaine and HIV-1 Tat-mediated neurotoxicity.* Cell Death Dis, 2018. **9**(4): p. 415.

307. Fitting, S., et al., *Interactive HIV-1 Tat and morphine-induced synaptodendritic injury is triggered through focal disruptions in Na^+ influx, mitochondrial instability, and Ca^{2+} overload.* J Neurosci, 2014. **34**(38): p. 12850-64.

308. Stone, N.L., T.J. England, and S.E. O'Sullivan, *A Novel Transwell Blood Brain Barrier Model Using Primary Human Cells.* Frontiers in Cellular Neuroscience, 2019. **13**.

309. Chun, T.W. and A.S. Fauci, *HIV reservoirs: pathogenesis and obstacles to viral eradication and cure.* AIDS, 2012. **26**(10): p. 1261-8.

310. Deeks, S.G., et al., *HIV infection.* Nat Rev Dis Primers, 2015. **1**: p. 15035.

311. Madison, M.N. and C.M. Okeoma, *Exosomes: Implications in HIV-1 Pathogenesis.* Viruses-Basel, 2015. **7**(7): p. 4093-4118.

312. Ebrahimi, D., et al., *Genetic and mechanistic basis for APOBEC3H alternative splicing, retrovirus restriction, and counteraction by HIV-1 protease.* Nat Commun, 2018. **9**(1): p. 4137.

313. Miyagi, E., et al., *Enzymatically active APOBEC3G is required for efficient inhibition of human immunodeficiency virus type 1.* J Virol, 2007. **81**(24): p. 13346-53.

314. Holmes, M., F.W. Zhang, and P.D. Bieniasz, *Single-Cell and Single-Cycle Analysis of HIV-1 Replication.* Plos Pathogens, 2015. **11**(6).

315. de Carvalho, J.V., et al., *Nef neutralizes the ability of exosomes from CD4+ T cells to act as decoys during HIV-1 infection.* PLoS One, 2014. **9**(11): p. e113691.

316. Tumne, A., et al., *Noncytotoxic suppression of human immunodeficiency virus type 1 transcription by exosomes secreted from CD8+ T cells.* J Virol, 2009. **83**(9): p. 4354-64.

317. Sun, L., et al., *Exosomes contribute to the transmission of anti-HIV activity from TLR3-activated brain microvascular endothelial cells to macrophages.* Antiviral Res, 2016. **134**: p. 167-171.

318. Guo, L., et al., *Human Intestinal Epithelial Cells Release Antiviral Factors That Inhibit HIV Infection of Macrophages.* Front Immunol, 2018. **9**: p. 247.

319. Smith, J.A. and R. Daniel, *Human vaginal fluid contains exosomes that have an inhibitory effect on an early step of the HIV-1 life cycle.* AIDS, 2016. **30**(17): p. 2611-2616.

320. Madison, M.N., P.H. Jones, and C.M. Okeoma, *Exosomes in human semen restrict HIV-1 transmission by vaginal cells and block intravaginal replication of LP-BM5 murine AIDS virus complex.* Virology, 2015. **482**: p. 189-201.

321. Madison, M.N., R.J. Roller, and C.M. Okeoma, *Human semen contains exosomes with potent anti-HIV-1 activity.* Retrovirology, 2014. **11**: p. 102.

322. Naslund, T.I., et al., *Exosomes from breast milk inhibit HIV-1 infection of dendritic cells and subsequent viral transfer to CD4+ T cells.* AIDS, 2014. **28**(2): p. 171-80.

323. Admyre, C., et al., *Exosomes with immune modulatory features are present in human breast milk.* J Immunol, 2007. **179**(3): p. 1969-78.

324. Mack, M., et al., *Transfer of the chemokine receptor CCR5 between cells by membrane-derived microparticles: a mechanism for cellular human immunodeficiency virus 1 infection.* Nat Med, 2000. **6**(7): p. 769-75.

325. Rozmyslowicz, T., et al., *Platelet- and megakaryocyte-derived microparticles transfer CXCR4 receptor to CXCR4-null cells and make them susceptible to infection by X4-HIV.* AIDS, 2003. **17**(1): p. 33-42.

326. Flaumenhaft, R., A.T. Mairuhu, and J.E. Italiano, *Platelet- and megakaryocyte-derived microparticles.* Semin Thromb Hemost, 2010. **36**(8): p. 881-7.

327. Sims, B., et al., *Tetraspanin blockage reduces exosome-mediated HIV-1 entry.* Arch Virol, 2018. **163**(6): p. 1683-1689.

328. Sims, B., et al., *Role of TIM-4 in exosome-dependent entry of HIV-1 into human immune cells.* Int J Nanomedicine, 2017. **12**: p. 4823-4833.

329. Feng, D., et al., *Cellular internalization of exosomes occurs through phagocytosis.* Traffic, 2010. **11**(5): p. 675-87.

330. Miyanishi, M., et al., *Identification of Tim4 as a phosphatidylserine receptor.* Nature, 2007. **450**(7168): p. 435-9.

331. Kadiu, I., et al., *Biochemical and biologic characterization of exosomes and microvesicles as facilitators of HIV-1 infection in macrophages.* J Immunol, 2012. **189**(2): p. 744-54.

332. Sampey, G.C., et al., *Exosomes from HIV-1-infected Cells Stimulate Production of Pro-inflammatory Cytokines through Trans-activating Response (TAR) RNA.* J Biol Chem, 2016. **291**(3): p. 1251-66.

333. Birge, R.B., et al., *Phosphatidylserine is a global immunosuppressive signal in efferocytosis, infectious disease, and cancer.* Cell Death Differ, 2016. **23**(6): p. 962-78.

334. Arakelyan, A., et al., *Extracellular Vesicles Carry HIV Env and Facilitate Hiv Infection of Human Lymphoid Tissue.* Sci Rep, 2017. **7**(1): p. 1695.

335. Booth, A.M., et al., *Exosomes and HIV Gag bud from endosome-like domains of the T cell plasma membrane.* J Cell Biol, 2006. **172**(6): p. 923-35.

336. Cabezas, S.C. and M. Federico, *Sequences within RNA coding for HIV-1 Gag p17 are efficiently targeted to exosomes.* Cellular Microbiology, 2013. **15**(3): p. 412-429.

337. Fang, Y., et al., *Higher-order oligomerization targets plasma membrane proteins and HIV gag to exosomes.* PLoS Biol, 2007. **5**(6): p. e158.

338. Raymond, A.D., et al., *HIV Type 1 Nef Is Released from Infected Cells in CD45(+) Microvesicles and Is Present in the Plasma of HIV-Infected Individuals.* Aids Research and Human Retroviruses, 2011. **27**(2): p. 167-178.

339. Campbell, T.D., et al., *HIV-1 Nef protein is secreted into vesicles that can fuse with target cells and virions.* Ethn Dis, 2008. **18**(2 Suppl 2): p. S2-14-9.

340. Lenassi, M., et al., *HIV Nef is Secreted in Exosomes and Triggers Apoptosis in Bystander CD4(+) T Cells.* Traffic, 2010. **11**(1): p. 110-122.

341. Stumptner-Cuvelette, P., et al., *Human immunodeficiency virus-1 Nef expression induces intracellular accumulation of multivesicular bodies and major histocompatibility complex class II complexes: potential role of phosphatidylinositol 3-kinase.* Mol Biol Cell, 2003. **14**(12): p. 4857-70.

342. Sevilya, Z., et al., *Killing of Latently HIV-Infected CD4 T Cells by Autologous CD8 T Cells Is Modulated by Nef.* Front Immunol, 2018. **9**: p. 2068.

343. Jacob, R.A., et al., *The interaction between HIV-1 Nef and adaptor protein-2 reduces Nefmediated CD4+ T cell apoptosis.* Virology, 2017. **509**: p. 1-10.

344. James, C.O., et al., *Extracellular Nef protein targets CD4+ T cells for apoptosis by interacting with CXCR4 surface receptors.* J Virol, 2004. **78**(6): p. 3099-109.

345. Lee, J.H., et al., *HIV-Nef and ADAM17-Containing Plasma Extracellular Vesicles Induce and Correlate with Immune Pathogenesis in Chronic HIV Infection.* Ebiomedicine, 2016. **6**: p. 103-113.

346. Arenaccio, C., et al., *Exosomes from Human Immunodeficiency Virus Type 1 (HIV-1)-Infected Cells License Quiescent CD4(+) T Lymphocytes To Replicate HIV-1 through a Nef- and ADAM17-Dependent Mechanism.* Journal of Virology, 2014. **88**(19): p. 11529-11539.

347. Roth, W.W., et al., *Micro RNA in Exosomes from HIV-Infected Macrophages.* Int J Environ Res Public Health, 2015. **13**(1): p. ijerph13010032.

348. de Vries, W. and B. Berkhout, *RNAi suppressors encoded by pathogenic human viruses.* Int J Biochem Cell Biol, 2008. **40**(10): p. 2007-12.

349. Bernard, M.A., et al., *Novel HIV-1 MiRNAs Stimulate TNF alpha Release in Human Macrophages via TLR8 Signaling Pathway.* Plos One, 2014. **9**(9).

350. Aqil, M., et al., *The HIV Nef protein modulates cellular and exosomal miRNA profiles in human monocytic cells.* J Extracell Vesicles, 2014. **3**.

351. Boisse, L., M.J. Gill, and C. Power, *HIV infection of the central nervous system: clinical features and neuropathogenesis.* Neurol Clin, 2008. **26**(3): p. 799-819, x.

352. Raymond, A.D., et al., *Microglia-derived HIV Nef plus exosome impairment of the blood-brain barrier is treatable by nanomedicine-based delivery of Nef peptides.* Journal of Neurovirology, 2016. **22**(2): p. 129-139.

353. Wahid, B., et al., *Current status of therapeutic and vaccine approaches against Zika virus.* European Journal of Internal Medicine, 2017. **44**: p. 12-18.

354. Griffiths, S.K. and J.P. Campbell, *Placental structure, function and drug transfer.* Bja Education, 2015. **15**(2): p. 84-89.

355. Ha, D., N.N. Yang, and V. Nadithe, *Exosomes as therapeutic drug carriers and delivery vehicles across biological membranes: current perspectives and future challenges.* Acta Pharmaceutica Sinica B, 2016. **6**(4): p. 287-296.

356. Kinch, M.S., et al., *FGI-104: a broad-spectrum small molecule inhibitor of viral infection.* American Journal of Translational Research, 2009. **1**(1): p. 87-98.

357. Henderson, A.D., et al., *Zika seroprevalence declines and neutralizing antibodies wane in adults following outbreaks in French Polynesia and Fiji.* eLife, 2020. **9**: p. e48460.

358. Luo, X.S., N. Imai, and I. Dorigatti, *Quantifying the risk of Zika virus spread in Asia during the 2015-16 epidemic in Latin America and the Caribbean: A modeling study.* Travel Medicine and Infectious Disease, 2020. **33**: p. 101562.

359. McAllister, J.C., et al., *Mosquito Control Activities during Local Transmission of Zika Virus, Miami-Dade County, Florida, USA, 2016.* Emerging infectious diseases, 2020. **26**(5): p. 881-890.

360. Nakayama, E., et al., *Neuroinvasiveness of the MR766 strain of Zika virus in IFNAR-/- mice maps to prM residues conserved amongst African genotype viruses.* PLoS Pathog, 2021. **17**(7): p. e1009788.

361. Lambrechts, L., *Did Zika virus attenuation or increased virulence lead to the emergence of congenital Zika syndrome?* Journal of Travel Medicine, 2021. **28**(5).

362. Jaeger, A.S., et al., *Zika viruses of African and Asian lineages cause fetal harm in a mouse model of vertical transmission.* PLoS neglected tropical diseases, 2019. **13**(4): p. e0007343-e0007343.

363. Liu, J., et al., *Emergence of Zika virus: Role of founder effects, drift and mutational reversions in spread to the Americas.* bioRxiv, 2020: p. 2020.06.29.179150.

364. Li, C., et al., *Chloroquine, a FDA-approved Drug, Prevents Zika Virus Infection and its Associated Congenital Microcephaly in Mice.* EBioMedicine, 2017. **24**: p. 189-194.

365. Brasil, P., et al., *Zika Virus Infection in Pregnant Women in Rio de Janeiro.* New England Journal of Medicine, 2016. **375**(24): p. 2321-2334.

366. Driggers, R.W., et al., *Zika Virus Infection with Prolonged Maternal Viremia and Fetal Brain Abnormalities.* New England Journal of Medicine, 2016. **374**(22): p. 2142-2151.

367. Araujo, L.M., M.L. Ferreira, and O.J. Nascimento, *Guillain-Barré syndrome associated with the Zika virus outbreak in Brazil.* Arq Neuropsiquiatr, 2016. **74**(3): p. 253-5.

368. Rasmussen, S.A., et al., *Zika Virus and Birth Defects — Reviewing the Evidence for Causality.* New England Journal of Medicine, 2016. **374**(20): p. 1981-1987.

369. Hills SL, R.K., Hennessey M, et al., *Transmission of Zika Virus Through Sexual Contact with Travelers to Areas of Ongoing Transmission - Continental United States, 2016.* , C.f.D.C.a. Prevention, Editor. 2016: Informe Semanal de Morbilidad y Mortalidad (MMWR) 2016. p. 215-216.

370. D'Ortenzio, E., et al., *Evidence of Sexual Transmission of Zika Virus.* New England Journal of Medicine, 2016. **374**(22): p. 2195-2198.

371. Tang, W.W., et al., *A Mouse Model of Zika Virus Sexual Transmission and Vaginal Viral Replication.* Cell Reports, 2016. **17**(12): p. 3091-3098.

372. Fréour, T., et al., *Sexual transmission of Zika virus in an entirely asymptomatic couple returning from a Zika epidemic area, France, April 2016.* Eurosurveillance, 2016. **21**(23): p. 30254.

373. Duggal, N.K., et al., *Frequent Zika Virus Sexual Transmission and Prolonged Viral RNA Shedding in an Immunodeficient Mouse Model.* Cell Reports, 2017. **18**(7): p. 1751-1760.

374. Pletnev, A.G., et al., *Epididymal epithelium propels early sexual transmission of Zika virus in the absence of interferon signaling.* Nature Communications, 2021. **12**(1): p. 2469.

375. Bedford, J.G., et al., *Airway Exosomes Released During Influenza Virus Infection Serve as a Key Component of the Antiviral Innate Immune Response.* Frontiers in Immunology, 2020. **11**(887).

376. Wang, J., et al., *Exosomes Released from Rabies Virus-Infected Cells May be Involved in the Infection Process.* Virologica Sinica, 2019. **34**(1): p. 59-65.

377. Chahar, H.S., et al., *Respiratory Syncytial Virus Infection Changes Cargo Composition of Exosome Released from Airway Epithelial Cells.* Scientific Reports, 2018. **8**(1): p. 387.

378. Nanbo, A., et al., *Infection of Epstein–Barr Virus in Type III Latency Modulates Biogenesis of Exosomes and the Expression Profile of Exosomal miRNAs in the Burkitt Lymphoma Mutu Cell Lines.* Cancers, 2018. **10**(7): p. 237.

379. Chen, L., et al., *Exosomes derived from HIV-1-infected cells promote growth and progression of cancer via HIV TAR RNA.* Nature Communications, 2018. **9**(1): p. 4585.

380. Nair, S. and C. Salomon, *Extracellular vesicles and their immunomodulatory functions in pregnancy.* Seminars in Immunopathology, 2018. **40**(5): p. 425-437.

381. Kshirsagar, S.K., et al., *Immunomodulatory molecules are released from the first trimester and term placenta via exosomes.* Placenta, 2012. **33**(12): p. 982-990.

382. Nakahara, A., et al., *Circulating Placental Extracellular Vesicles and Their Potential Roles During Pregnancy.* Ochsner Journal, 2020. **20**(4): p. 439-445.

383. Favaro, R.R., et al., *Immunomodulatory properties of extracellular vesicles in the dialogue between placental and immune cells.* American Journal of Reproductive Immunology, 2021. **85**(2): p. e13383.

384. Gall, A.R., et al., *Placental mediated mechanisms of perinatal brain injury: Evolving inflammation and exosomes.* Experimental Neurology, 2022. **347**: p. 113914.

385. Orozco, A.F., et al., *Placental Release of Distinct DNA-associated Micro-particles into Maternal Circulation: Reflective of Gestation Time and Preeclampsia.* Placenta, 2009. **30**(10): p. 891-897.

386. Lok, C.A.R., et al., *Changes in Microparticle Numbers and Cellular Origin During Pregnancy and Preeclampsia.* Hypertension in Pregnancy, 2008. **27**(4): p. 344-360.

387. Goswami, D., et al., *Excess syncytiotrophoblast microparticle shedding is a feature of early-onset pre-eclampsia, but not normotensive intrauterine growth restriction.* Placenta, 2006. **27**(1): p. 56-61.

388. Salomon, C., et al., *Placental Exosomes as Early Biomarker of Preeclampsia: Potential Role of Exosomal MicroRNAs Across Gestation.* The Journal of Clinical Endocrinology & Metabolism, 2017. **102**(9): p. 3182-3194.

389. Jia, R., et al., *Comparative Proteomic Profile of the Human Umbilical Cord Blood Exosomes between Normal and Preeclampsia Pregnancies with High-Resolution Mass Spectrometry.* Cellular Physiology and Biochemistry, 2015. **36**(6): p. 2299-2306.

390. Hinata, M., et al., *Exosomes of Epstein-Barr Virus-Associated Gastric Carcinoma Suppress Dendritic Cell Maturation.* Microorganisms, 2020. **8**(11): p. 1776.

391. Nachmani, D., et al., *Diverse Herpesvirus MicroRNAs Target the Stress-Induced Immune Ligand MICB to Escape Recognition by Natural Killer Cells.* Cell Host & Microbe, 2009. **5**(4): p. 376-385.

392. Stern-Ginossar, N., et al., *Host Immune System Gene Targeting by a Viral miRNA.* Science, 2007. **317**(5836): p. 376-381.

393. Albanese, M., et al., *MicroRNAs of Epstein-Barr Virus Control Innate and Adaptive Antiviral Immunity.* Journal of Virology, 2017. **91**(16): p. e01667-16.

394. Kalamvoki, M. and T. Deschamps, *Extracellular vesicles during Herpes Simplex Virus type 1 infection: an inquire.* Virology Journal, 2016. **13**(1): p. 63.

395. Sadeghipour, S. and R.A. Mathias, *Herpesviruses hijack host exosomes for viral pathogenesis.* Seminars in Cell & Developmental Biology, 2017. **67**: p. 91-100.

396. Dogrammatzis, C., et al., *Biogenesis of Extracellular Vesicles during Herpes Simplex Virus 1 Infection: Role of the CD63 Tetraspanin.* Journal of Virology, 2019. **93**(2): p. e01850-18.

397. Bello-Morales, R. and J.A. López-Guerrero, *Extracellular Vesicles in Herpes Viral Spread and Immune Evasion.* Frontiers in Microbiology, 2018. **9**(2572).

398. Flanagan, J., J. Middeldorp, and T. Sculley, *Localization of the Epstein–Barr virus protein LMP 1 to exosomes.* Journal of General Virology, 2003. **84**(7): p. 1871-1879.

399. Naqvi, A.R., et al., *Viral miRNAs Alter Host Cell miRNA Profiles and Modulate Innate Immune Responses.* Frontiers in Immunology, 2018. **9**(433).

400. Simoni, M.K., et al., *Zika virus infection of Hofbauer cells.* American Journal of Reproductive Immunology, 2017. **77**(2): p. e12613.

401. Schwartz, D.A., *Viral infection, proliferation, and hyperplasia of Hofbauer cells and absence of inflammation characterize the placental pathology of fetuses with congenital Zika virus infection.* Archives of gynecology and obstetrics, 2017. **295**(6): p. 1361-1368.

402. Rosenberg, A.Z., et al., *Placental Pathology of Zika Virus: Viral Infection of the Placenta Induces Villous Stromal Macrophage (Hofbauer Cell) Proliferation and Hyperplasia.* Archives of Pathology & Laboratory Medicine, 2016. **141**(1): p. 43-48.

403. Souza, B.S.F., et al., *Zika virus infection induces mitosis abnormalities and apoptotic cell death of human neural progenitor cells.* Scientific Reports, 2016. **6**(1): p. 39775.

404. Ferraris, P., et al., *Zika virus differentially infects human neural progenitor cells according to their state of differentiation and dysregulates neurogenesis through the Notch pathway.* Emerging Microbes & Infections, 2019. **8**(1): p. 1003-1016.

405. Wells, M.F., et al., *Genetic Ablation of AXL Does Not Protect Human Neural Progenitor Cells and Cerebral Organoids from Zika Virus Infection.* Cell Stem Cell, 2016. **19**(6): p. 703-708.

406. Ghezzi, S., et al., *Heparin prevents Zika virus induced-cytopathic effects in human neural progenitor cells.* Antiviral Research, 2017. **140**: p. 13-17.

407. Quicke, Kendra M., et al., *Zika Virus Infects Human Placental Macrophages.* Cell Host & Microbe, 2016. **20**(1): p. 83-90.

408. Coyne, C.B. and H.M. Lazear, *Zika virus — reigniting the TORCH.* Nature Reviews Microbiology, 2016. **14**(11): p. 707-715.

409. Arumugasaamy, N., et al., *Biomimetic Placenta-Fetus Model Demonstrating Maternal–Fetal Transmission and Fetal Neural Toxicity of Zika Virus.* Annals of Biomedical Engineering, 2018. **46**(12): p. 1963-1974.

410. Olagnier, D., et al., *Mechanisms of Zika Virus Infection and Neuropathogenesis.* DNA and Cell Biology, 2016. **35**(8): p. 367-372.

411. Onorati, M., et al., *Zika Virus Disrupts Phospho-TBK1 Localization and Mitosis in Human Neuroepithelial Stem Cells and Radial Glia.* Cell Reports, 2016. **16**(10): p. 2576-2592.

412. *Microcephaly & Other Birth Defects*, N.C.f.E.a.Z.I.D.N. Centers for Disease Control and Prevention, Division of Vector-Borne Diseases (DVBD), Editor. 2019, U.S. Department of Health & Human Services.

413. Chiu, C.-F., et al., *The Mechanism of the Zika Virus Crossing the Placental Barrier and the Blood-Brain Barrier.* Frontiers in Microbiology, 2020. **11**(214).

414. Blanke ML, V.A., *Activation Mechanisms of the NMDA Receptor.*, in *Biology of the NMDA Receptor.*, V. AM, Editor. 2009, CRC Press/Taylor & Francis: Boca Raton (FL).

415. McNamara, R.P., et al., *Nef Secretion into Extracellular Vesicles or Exosomes Is Conserved across Human and Simian Immunodeficiency Viruses.* mBio, 2018. **9**(1): p. e02344-17.

416. Lenassi, M., et al., *HIV Nef is secreted in exosomes and triggers apoptosis in bystander CD4+ T cells.* Traffic (Copenhagen, Denmark), 2010. **11**(1): p. 110-122.

417. Mukhamedova, N., et al., *Exosomes containing HIV protein Nef reorganize lipid rafts potentiating inflammatory response in bystander cells.* PLOS Pathogens, 2019. **15**(7): p. e1007907.

418. Gallo, R.C. and L. Montagnier, *The Discovery of HIV as the Cause of AIDS.* New England Journal of Medicine, 2003. **349**(24): p. 2283-2285.

419. Montagnier, L., *25 years after HIV discovery: prospects for cure and vaccine.* Virology, 2010. **397**(2): p. 248-54.

420. Gallo, R., et al., *Frequent detection and isolation of cytopathic retroviruses (HTLV-III) from patients with AIDS and at risk for AIDS.* Science, 1984. **224**(4648): p. 500-503.

421. Gallo, R.C. and L. Montagnier, *AIDS in 1988.* Scientific American, 1988. **259**(4): p. 40-51.

422. Spudich, S.S., *Immune activation in the central nervous system throughout the course of HIV infection.* Current opinion in HIV and AIDS, 2016. **11**(2): p. 226-233.

423. Balcom, E.F., et al., *HIV-1 persistence in the central nervous system: viral and host determinants during antiretroviral therapy.* Current Opinion in Virology, 2019. **38**: p. 54-62.

424. Prusiner, S.B., *Discovering the Cause of AIDS.* Science, 2002. **298**(5599): p. 1726-1726.

425. Chan, P. and J. Ananworanich, *Perspective on potential impact of HIV central nervous system latency on eradication.* AIDS, 2019. **33**.

426. Rojas-Celis, V., et al., *New Challenges of HIV-1 Infection: How HIV-1 Attacks and Resides in the Central Nervous System.* Cells, 2019. **8**(10).

427. Buchacz, K., et al., *Incidence of AIDS-Defining Opportunistic Infections in a Multicohort Analysis of HIV-infected Persons in the United States and Canada, 2000–2010.* The Journal of Infectious Diseases, 2016. **214**(6): p. 862-872.

428. Lipton, S.A., et al., *Synergistic effects of HIV coat protein and NMDA receptor-mediated neurotoxicity.* Neuron, 1991. **7**(1): p. 111-118.

429. Lipton, S.A., *HIV-Related Neurotoxicity.* Brain Pathology, 1991. **1**(3): p. 193-199.

430. Kaul, M. and S.A. Lipton, *Chemokines and activated macrophages in HIV gp120-induced neuronal apoptosis.* Proceedings of the National Academy of Sciences, 1999. **96**(14): p. 8212-8216.

431. Jana, A. and K. Pahan, *Human immunodeficiency virus type 1 gp120 induces apoptosis in human primary neurons through redox-regulated activation of neutral sphingomyelinase.* The Journal of neuroscience : the official journal of the Society for Neuroscience, 2004. **24**(43): p. 9531-9540.

432. Hesselgesser, J., et al., *Neuronal apoptosis induced by HIV-1 gp120 and the chemokine SDF-1 alpha is mediated by the chemokine receptor CXCR4.* Curr Biol, 1998. **8**(10): p. 595-8.

433. Chen, L., et al., *HIV-1gp120 Induces Neuronal Apoptosis through Enhancement of 4-Aminopyridine-Senstive Outward K+ Currents.* PLOS ONE, 2011. **6**(10): p. e25994.

434. Bardi, G., et al., *Human immunodeficiency virus gp120-induced apoptosis of human neuroblastoma cells in the absence of CXCR4 internalization.* Journal of neurovirology, 2006. **12**(3): p. 211-218.

435. Fields, J.A., et al., *HIV alters neuronal mitochondrial fission/fusion in the brain during HIV-associated neurocognitive disorders.* Neurobiology of Disease, 2016. **86**: p. 154-169.

436. Teodorof-Diedrich, C. and S.A. Spector, *Human Immunodeficiency Virus Type 1 gp120 and Tat Induce Mitochondrial Fragmentation and Incomplete Mitophagy in Human Neurons.* Journal of Virology, 2018. **92**(22): p. e00993-18.

437. Avdoshina, V., et al., *The HIV Protein gp120 Alters Mitochondrial Dynamics in Neurons.* Neurotoxicity Research, 2016. **29**(4): p. 583-593.

438. Garrido, C. and D.M. Margolis, *Translational challenges in targeting latent HIV infection and the CNS reservoir problem.* Journal of neurovirology, 2015. **21**(3): p. 222-226.

439. Letendre, S., et al., *Validation of the CNS Penetration-Effectiveness rank for quantifying antiretroviral penetration into the central nervous system.* Archives of neurology, 2008. **65**(1): p. 65-70.

440. Mikitsh, J.L. and A.-M. Chacko, *Pathways for small molecule delivery to the central nervous system across the blood-brain barrier.* Perspectives in medicinal chemistry, 2014. **6**: p. 11-24.

441. Kerza-Kwiatecki, A.P. and S. Amini, *CNS as an HIV-1 reservoir; BBB and Drug Delivery.* Journal of Neurovirology, 1999. **5**(2): p. 113-114.

442. Berger, J.R. and M. Avison, *The blood brain barrier in HIV infection.* Front Biosci, 2004. **9**: p. 2680-5.

443. Martins, C., et al., *Using microfluidic platforms to develop CNS-targeted polymeric nanoparticles for HIV therapy.* European Journal of Pharmaceutics and Biopharmaceutics, 2019. **138**: p. 111-124.

444. Wallace, D.R., *HIV neurotoxicity: potential therapeutic interventions.* Journal of biomedicine & biotechnology, 2006. **2006**(3): p. 65741-65741.

445. Ha, D., N. Yang, and V. Nadithe, *Exosomes as therapeutic drug carriers and delivery vehicles across biological membranes: current perspectives and future challenges.* Acta Pharm Sin B, 2016. **6**(4): p. 287-96.

446. Aryani, A. and B. Denecke, *Exosomes as a Nanodelivery System: a Key to the Future of Neuromedicine?* Molecular neurobiology, 2016. **53**(2): p. 818-834.

447. Tomitaka, A., et al., *Dynamic magnetic characterization and magnetic particle imaging enhancement of magnetic-gold core–shell nanoparticles.* Nanoscale, 2019. **11**(13): p. 6489-6496.

448. Tomitaka, A., et al., *Development of magneto-plasmonic nanoparticles for multimodal image-guided therapy to the brain.* Nanoscale, 2017. **9**(2): p. 764-773.

449. Moseri, A., et al., *The C4 region as a target for HIV entry inhibitors – NMR mapping of the interacting segments of T20 and gp120.* The FEBS Journal, 2015. **282**(24): p. 4643-4657.

450. Qi, Q., et al., *HIV-1 gp41-targeting fusion inhibitory peptides enhance the gp120-targeting protein-mediated inactivation of HIV-1 virions.* Emerging Microbes & Infections, 2017. **6**(1): p. 1-7.

451. Huang, L., L. Zhang, and C.H. Chen, *Potential drug targets on the HIV-1 envelope glycoproteins, gp120 and gp41.* Curr Pharm Des, 2003. **9**(18): p. 1453-62.

452. Ding, H., et al., *Enhanced blood-brain barrier transmigration using a novel transferrin embedded fluorescent magneto-liposome nanoformulation.* Nanotechnology, 2014. **25**(5): p. 055101-055101.

453. Nair, M., et al., *Getting into the brain: Potential of nanotechnology in the management of NeuroAIDS.* Advanced Drug Delivery Reviews, 2016. **103**: p. 202-217.

454. Kong, S.D., et al., *Magnetic targeting of nanoparticles across the intact blood–brain barrier.* Journal of Controlled Release, 2012. **164**(1): p. 49-57.

455. Saiyed, Z.M., N.H. Gandhi, and M.P.N. Nair, *Magnetic nanoformulation of azidothymidine 5'-triphosphate for targeted delivery across the blood-brain barrier.* International journal of nanomedicine, 2010. **5**: p. 157-166.

456. Schindler, M., et al., *Nef-mediated suppression of T cell activation was lost in a lentiviral lineage that gave rise to HIV-1.* Cell, 2006. **125**(6): p. 1055-67.

457. Thery, C., et al., *Isolation and characterization of exosomes from cell culture supernatants and biological fluids.* Curr Protoc Cell Biol, 2006. **Chapter 3**: p. Unit 3 22.

458. Stone, N.L., T.J. England, and S.E. O'Sullivan, *A Novel Transwell Blood Brain Barrier Model Using Primary Human Cells.* Frontiers in cellular neuroscience, 2019. **13**: p. 230-230.

459. Pilakka-Kanthikeel, S., et al., *Targeted brain derived neurotropic factors (BDNF) delivery across the blood-brain barrier for neuro-protection using magnetic nano carriers: an in-vitro study.* PloS one, 2013. **8**(4): p. e62241-e62241.

460. Raymond, A.D., et al., *Microglia-derived HIV Nef+ exosome impairment of the blood–brain barrier is treatable by nanomedicine-based delivery of Nef peptides.* Journal of NeuroVirology, 2016. **22**(2): p. 129-139.

461. Loh, K.-S., et al., *Use of Fe_3O_4 Nanoparticles for Enhancement of Biosensor Response to the Herbicide 2,4-Dichlorophenoxyacetic Acid.* Sensors (Basel, Switzerland), 2008. **8**(9): p. 5775-5791.

462. Smyth, T., et al., *Surface functionalization of exosomes using click chemistry.* Bioconjugate chemistry, 2014. **25**(10): p. 1777-1784.

463. Cp, P.P.B., *Raman Spectroscopy of Iron Oxide of Nanoparticles (Fe3O4).* Journal of Material Science & Engineering, 2015. **5**(1).

464. Li, Y.-S., J.S. Church, and A.L. Woodhead, *Infrared and Raman spectroscopic studies on iron oxide magnetic nano-particles and their surface modifications.* Journal of Magnetism and Magnetic Materials, 2012. **324**(8): p. 1543-1550.

465. Lim, J., et al., *Direct isolation and characterization of circulating exosomes from biological samples using magnetic nanowires.* Journal of nanobiotechnology, 2019. **17**(1): p. 1-1.

466. Arakelyan, A., et al., *Nanoparticle-based flow virometry for the analysis of individual virions.* J Clin Invest, 2013. **123**(9): p. 3716-27.

467. Sagar, V., et al., *Magnetic nanotherapeutics for dysregulated synaptic plasticity during neuroAIDS and drug abuse.* Molecular Brain, 2016. **9**(1): p. 57.

468. Ko, J., et al., *Combining Machine Learning and Nanofluidic Technology To Diagnose Pancreatic Cancer Using Exosomes.* ACS Nano, 2017. **11**(11): p. 11182-11193.

469. Shao, H., J. Chung, and D. Issadore, *Diagnostic technologies for circulating tumour cells and exosomes.* Bioscience Reports, 2016. **36**(1).

470. Zhou, Y.-G., et al., *Interrogating Circulating Microsomes and Exosomes Using Metal Nanoparticles.* Small, 2016. **12**(6): p. 727-732.

VITA

ALLEN CAOBI

Born, Miami, Florida

2006-2012	B.A., Biology Florida International University Miami, Florida
2013-2016	Research Technician Florida International University Miami, Florida
2016-2020	Ph.d Student, Biomedical Sciences Florida International University Miami, Florida
2018-2020	Teaching Assistant Florida International University Miami, Florida
2020 -2022	Doctoral Candidate Florida International University Miami, Florida

PUBLICATIONS

1. Tiwari, S., Lapierre, J., Ojha, C. R., Martins, K., Parira, T., Dutta, R. K., Caobi, A., Garbinski, L., Ceyhan, Y., Esteban-Lopez, M., & El-Hage, N. (2018). Signaling pathways and therapeutic perspectives related to environmental factors associated with multiple sclerosis. *Journal of neuroscience research*, *96*(12), 1831–1846. https://doi.org/10.1002/jnr.24322
2. Chayaratanasin, P., Caobi, A., Suparpprom, C., Saenset, S., Pasukamonset, P., Suanpairintr, N., Barbieri, M. A., & Adisakwattana, S. (2019). *Clitoria ternatea* Flower Petal Extract Inhibits Adipogenesis and Lipid Accumulation in 3T3-L1 Preadipocytes by Downregulating Adipogenic Gene Expression. *Molecules (Basel, Switzerland)*, *24*(10), 1894. https://doi.org/10.3390/molecules24101894

3. Gonzalez, B. A., Perez-Nevarez, M., Mirza, A., Perez, M. G., Lin, Y. M., Hsu, C. D., Caobi, A., Raymond, A., Gomez Hernandez, M. E., Fernandez-Lima, F., George, F., & Ramaswamy, S. (2020). Physiologically Relevant Fluid-Induced Oscillatory Shear Stress Stimulation of Mesenchymal Stem Cells Enhances the Engineered Valve Matrix Phenotype. *Frontiers in cardiovascular medicine*, *7*, 69. https://doi.org/10.3389/fcvm.2020.00069
4. Caobi, A., Dutta, R. K., Garbinski, L. D., Esteban-Lopez, M., Ceyhan, Y., Andre, M., Manevski, M., Ojha, C. R., Lapierre, J., Tiwari, S., Parira, T., & El-Hage, N. (2020). The Impact of CRISPR-Cas9 on Age-related Disorders: From Pathology to Therapy. *Aging and disease*, *11*(4), 895–915. https://doi.org/10.14336/AD.2019.0927
5. Miles, J., Andre, M., Caobi, A., Ruiz, M., Nair, M., & Raymond, A. D. (2020). Bioengineered Exosomal Extracellular Vesicles in Cancer Therapeutics. *Critical reviews in biomedical engineering*, *48*(3), 177–187. https://doi.org/10.1615/CritRevBiomedEng.2020034847
6. Caobi, A., Nair, M., & Raymond, A. D. (2020). Extracellular Vesicles in the Pathogenesis of Viral Infections in Humans. *Viruses*, *12*(10), 1200. https://doi.org/10.3390/v12101200
7. Caobi, A., Andre, M., Miles, J., Tomitaka, A., Nikkhah-Moshaie, R., Hernandez, A., Nair, M., & Raymond, A. D. (2020). Magnetic Nanoparticle and Exosomal Therapeutic (M-NEXT) Effects on HIV-Associated Neurotoxicity. *Critical reviews in biomedical engineering*, *48*(3), 189–198. https://doi.org/10.1615/CritRevBiomedEng.2020034629.
8. Andre, M., Caobi, A., Miles, J.M., Tran, D., Suthumphong, C., Ruiz, M., and Raymond, A.D. Exosomal extracellular vesicle cargo as multifaceted biomarkers in Oncology. *The Oncologist.* Submitted, 2022, Under Review, EMID:e2e19972d6fcfffe.
9. Allen Caobi, Rachel Fields, Mario Gomez , Jana Miles , Mickensone Andre, Adriana Yndart , Francisco Lima-Hernandez , Madhavan Nair , and Andrea D. Raymond. Exosomal extracellular vesicles containing Nef are indicative of HIV-associated Neurocognitive Impairment status. *Cells*. Submitted, 2022.
10. Caobi A., Miles J., Andre M., Tomitaka A., Nikkhah-Moshaie R., Hernandez A., Nair M., and Raymond AD. Development of Magnetic Exosomal Therapeutic (M-NEXT) to reduce HIV-associated Neurotoxicity. 2019. The 6th Society for Personalized NanoMedicine Symposium. Miami, FL.

*Ran out of space to add 5 more posters.